

The Mechanics of Lipid Bilayer and Fiber-reinforced Composite Sheet

by

Wenhao Yao

A thesis submitted in partial fulfillment of the requirements for the degree of

Doctor of Philosophy

Department of Mechanical Engineering
University of Alberta

© Wenhao Yao, 2024

Abstract

The thesis delves into the mechanics of hyperelastic materials, specifically lipid bilayers and fiber-reinforced composites (FRC). The primary objective is to achieve an advanced understanding of cell physiology from the aspect of lipid membrane mechanics and provide qualitative analysis of the mechanical properties of fiber-reinforced composites by elucidating the continuum models of lipid membrane and fiber-reinforced composites, respectively. Due to the commonly observed abnormal morphology of cells in current literature, the study emphasizes investigating the non-uniform morphogenesis of lipid membranes subjected to interaction forces and lateral pressure to enhance our understanding of membrane-protein interactions and membrane inflammation. The highlight of the thesis has been given to developing the three-dimensional theory of FRC sheets within the context of lipid membrane theory, unveiling the concurrent three-dimensional deformation of FRC and the embedded meshwork.

To accomplish these objectives, first, we derive the Euler equations within the variational framework of the Canham-Helfrich model by accounting for the non-uniform (coordinate-dependent) strain energy distributions of lipid membranes. Then, the corresponding partial differential equations (PDEs) are obtained by projecting the equilibrium equations on the polar and Cartesian coordinate systems and numerical cases are applied to demonstrate the capability of describing lipid membrane morphology. In cases of membrane-protein interactions and membrane inflammation, the resulting homogeneous and inhomogeneous PDEs are solved numerically or/and analytically, where the obtained results reasonably describe the circumferentially and radially non-uniform membrane properties, providing quantitative proofs for under-

standing the cell membrane morphology in the pathological research of cell.

In the proceeding efforts of studying lipid membrane morphology, emphasis is placed on uncovering the effects of intra-surface viscous flow on membrane morphologies and surface dilatation, particularly in the scenarios involving membrane-protein interactions and cell membrane inflammation. Within the variational framework, we derive and solve equilibrium equations by accommodating the viscous stress into the equilibrium equations, where the viscous stress is considered to be induced by intra-surface viscous flow, and the viscous effects on membrane surface dilatation are unveiled. In particular, our findings from continuum models are theoretically evidenced by the results of molecular dynamics simulation, illustrating that the protein-membrane interaction forces can induce local bending effects on the membrane, leading to surface compressions near the substrate-interaction boundaries. Notably, the proposed continuum model offers quantitative descriptions of highly curved membrane morphologies and associated thickness reductions, especially when nuclear pore complexes (NPCs) interact with the nuclear envelope.

More importantly, a three-dimensional model for analyzing the concurrent three-dimensional performance of FRC sheets is proposed based on the theory of lipid membrane. This involves modeling the FRC by incorporating the Neo-Hookean strain energy model for the matrix material and computing the strain energy of fiber meshwork by accounting for the stretching, bending, and twisting of fibers. To elucidate the three-dimensional deformation of the FRC, we derive the Euler equations and admissible boundary conditions via the surface coordinate configurations and solve the model numerically in the Cartesian coordinate system. The numerical results reasonably indicate the microstructural kinematics of fiber (for instance, bending, twisting, and stretching of fibers within the matrix material) determines the overall deformation of FRC. In particular, the concurrent three-dimensional deformations of FRC provide a reasonable understanding of the damage patterns in the FRC used in the construction sector, the formation of hemispherical domes in bamboo poly (lactic)

acid (PLA) composites, and out-of-plane deformations in woven fabrics. This work offers quantitative and qualitative contributions to the design and analysis of FRC in terms of the deformation profiles, stress-strain responses, strain distributions, and deformations of fiber meshwork.

Preface

This thesis is an original work by Wenhao Yao as a section of research projects supervised by Professor Chun Il Kim. The contents presented in Chapters 3, 4, and 5 are respectively published in different journals, and Chapter 6 has been submitted to the journal “International Journal of Engineering Science”.

Chapter 3 of this thesis has been published in the journal “Mathematics and Mechanics of Solids” named “An Analysis of Lipid Membrane Morphology in the Presence of Coordinate-dependent Non-uniformity”.

Chapter 4 has been published in the journal “Mathematics and Mechanics of Complex Systems” entitled “Deformation Analysis of Non-uniform Lipid Membrane Subjected to Local Inflammations”.

Chapter 5 has been published in the journal “Continuum Mechanics and Thermodynamics” under the title “A Lipid Membrane Morphology Subjected to Intramembrane Viscosity and Membrane Thickness Dilation”.

Chapter 6 under the name “The Mechanics of Elastomeric Sheet Reinforced with Bi-directional Fiber Mesh under Lateral Pressure” has been submitted to the journal “International Journal of Engineering Science”.

“Excellence is never an accident. It is always the result of high intention, sincere effort, and intelligent execution; it represents the wise choice of many alternatives - choice, not chance, determines your destiny.”

-Aristotle

*To my parents, and to the memory of my grandfather, **Qiren Yao** (1932 ~ 2008)
and **Hongen Wang** (1929 ~ 2012).*

Acknowledgements

I would like to express my heartfelt gratitude to Dr. Chun il Kim for his invaluable guidance, continuous support, and unwavering patience throughout my Ph.D. program. I extend special thanks to Professor David Steigmann for his invaluable and inspirational advice in my research endeavors, as well as for laying the theoretical foundations in hyperelasticity materials. Additionally, my sincere appreciation goes to Professor Peter Schiavone for delivering exceptional courses and providing steadfast support in his classes. I also wish to acknowledge and thank my talented colleagues Mr. Zhe Liu, Mr. Seyed Ehsan Seyed Bolouri, Dr. Suprabha Islam, and Mr. Md Hafijur Rahman for generously sharing their experiences and expertise with me. I must express my gratitude to Dr. Wenhui Li, with whom I collaborated closely on a research project and who provided invaluable assistance with simulations. I expand my thanks to all the dedicated staff and volunteers at the Project Adult Literacy Society, and it is their selfless commitment and support that have made my academic journey and life in Edmonton truly enriching. Last but not least, I am deeply appreciative of the relentless support and belief in me from the rest of my family.

Table of Contents

1	Introduction	1
1.1	Lipid Membrane	2
1.1.1	Lipid membrane curvature	3
1.1.2	Lipid membrane-protein interaction	4
1.1.3	Non-uniform morphology of lipid membrane and surface dilata- tion	6
1.1.4	Lipid membrane viscosity	7
1.1.5	Lipid membrane inflammation	7
1.1.6	Lipid membrane thickness	9
1.2	Elastomeric Materials	9
1.3	Objectives and Overview of Dissertation	11
	References	15
2	General Formulation and Preliminaries	23
2.1	Differential Geometry	23
2.2	Canham–Helfrich Theory	25
2.3	Neo-Hookean Hyperelastic Model	25
2.4	Notation	26
	References	28
3	An Analysis of Lipid Membrane Morphology in the Presence of Co- ordinate Dependent Non-uniformity	29
3.1	Introduction	30
3.2	Non-uniform Membrane Shape Equation	33
3.2.1	Formulations under Monge parametric representation	36
3.2.2	Linear model for non-uniform membranes	39
3.2.3	Example 1: Circumferentially non-uniform membranes	41
3.2.4	Example 2: Radially non-uniform membranes	45
	References	53

4	Deformation Analysis of Non-uniform Lipid Membrane Subjected to Local Inflammations	57
4.1	Introduction	58
4.2	Membrane Shape Equation	61
4.2.1	Monge parametric representation	63
4.2.2	Superposed incremental deformations	66
4.3	Explanation on Inflammation from the Non-uniform Lipid Membrane morphology	67
4.3.1	A rectangular membrane patch subjected to lateral pressures	68
4.3.2	Inflammations of circumferentially non-uniform membranes	76
4.3.3	Inflammations of radially non-uniform membranes	81
4.4	Conclusion	85
	References	87
5	A Lipid Membrane Morphology Subjected to Intra-membrane Viscosity and Membrane Thickness Dilation	91
5.1	Introduction	92
5.2	Energy Potential of Lipid Membrane	94
5.3	Distension Induced Lipid Membrane Equilibria	96
5.4	Intra-membrane Viscosity	100
5.5	Boundary Conditions	103
5.6	Monge Parametrization	104
5.7	Numerical Analysis and Discussion	105
5.7.1	Coarse-grained MD simulation	106
5.7.2	Local inflammation of a rectangular membrane patch	108
5.7.3	Membrane-protein interactions	113
5.7.4	Effects of intra-membrane viscous flow and interaction forces on lipid membrane	119
5.7.5	Experimental comparison	120
5.8	Conclusion	123
	References	125
6	The Mechanics of Elastomeric Sheet Reinforced with Bi-directional Fiber Mesh under Lateral Pressure	129
6.1	Introduction	130
6.2	Kinematics	134
6.3	Equilibrium	139

6.3.1	Variational formulation	139
6.3.2	Euler equilibrium equation	141
6.4	Model implementation and Boundary condition	145
6.5	Results and Discussion	147
6.5.1	Matrix material deformation	148
6.5.2	Fiber meshwork deformation	152
6.5.3	Fiber-reinforced composite deformation	159
6.6	Conclusion	164
	References	167
7	Conclusions and Future Work	173
7.1	Conclusions	173
7.2	Future Work	180
	Bibliography	181

List of Figures

1.1	Schematic of cell membrane structure [17], where the use of the image was admitted by Encyclopaedia Britannica, Inc. ©2007.	2
1.2	The structure of a lipid molecule (phosphatidylcholine), where (a) schematical structure, (b) formula structure, (c) space-filling model, and (d) symbol representation. The kink resulting from the cis-double bond is exaggerated for emphasis [20].	3
1.3	The illustration of the flexible surface model (FSM) in explaining the interaction between lipid membrane and protein [44]: (a) local bending and compression, (b) flat profile, and (c) alternative of local bending and compression in (a).	5
2.1	Schematic of surface configurations: surface vectors to the specific trajectories in referential (Ω) and current configurations (ω), respectively.	24
3.1	Transverse deflections of lipid membrane subjected to different α when: $\lambda + \phi = \alpha\theta^2$	44
3.2	Transverse deflections of circumferentially non-uniform membranes: linear vs non-linear solutions.	44
3.3	(a) The assimilation of the echinocyte formation: when $\phi + \lambda = \alpha[\cos(8\theta) + \pi]$, (b, c) the echinocyte formation of the cell membrane [41].	46
3.4	The assimilation of the off-centered non-uniform morphology: (a) when $\phi + \lambda = \alpha(\cos(\theta) + \pi)$, (b) the off-centered non-uniform morphology of red blood cell [35].	46
3.5	Transverse deflections of lipid membrane subjected to different α : when $\phi + \lambda = \alpha\sqrt{r}$	48
3.6	Transverse deflections of radially non-uniform membrane: Linear VS Non-linear solutions.	49

3.7	(a) The image of discocyte-stomatocyte morphology in sequential stages [45]; (b, c) The sequence of deformation mapping when $\phi + \lambda = \alpha r^n$ where α and n are adjusted to achieve the transitioning membrane morphology.	50
3.8	Deformation of combined radially and circumferentially non-uniform membrane when $\phi + \lambda = \alpha(\cos(\theta) + \pi) + \alpha\sqrt{r}$	51
3.9	(a) The off-centered deformation of lipid membrane characterized by the potential of $\phi(\theta, r) = \alpha \cos(r - 1)\theta $, in which r is treated as non-dimensional coordinate with r/R_{ext} , in which $R_{ext} = 1$ with the same spacial configuration of r ; (b) The scanning electron images of long-stored RBCs [36].	51
3.10	(a) The multiple peak deformation of lipid membrane characterized by the function $\phi(\theta, r) = -\alpha \cos(r) \cos(\theta) \cos(r - 1) \cos(\theta - \beta\pi)$, where the r is treated as non-dimensional coordinate with r/R_{ext} , where $R_{ext} = 1$ with the same spacial configuration of r ; (b) The scanning electron microscope (SEM) image of cell membranes with different morphological configurations of stomatocytosis and echinocytosis [37].	52
4.1	Deformation contour of non-uniform lipid membrane subjected to uniform pressure $P = 1$: (a) double-peak morphology, (b) single-peak morphology.	73
4.2	Transverse deflections of the lipid membrane with respect to different α when $P = 1$	74
4.3	Transverse deflections of uniform lipid membrane under increasing lateral pressure P	75
4.4	(a) The transverse deflection of circumferentially non-uniform lipid membrane with respect to increasing lateral pressure P ; (b) The transverse deflection of circumferentially non-uniform lipid membrane with respect to increasing α	79
4.5	(a, b, d): The morphologies and cross-section image of the lecithin-treated cell [36]; (c): The deformation of circumferentially non-uniform membrane when $\tilde{\theta}(\theta) = \cos(8\theta) + \pi$	80
4.6	(a) The simulation result of the off-centered non-uniform morphology when $\phi + \lambda = \cos(\theta) + \pi$; (b) The off-centered biconcave discoid morphology of red blood cell [35].	81

4.7	(a) The transverse deflection of radially non-uniform lipid membrane subjected to increasing lateral pressure P ; (b) The transverse deflection of radially non-uniform lipid membrane with respect to different α	83
4.8	(a) The discocyte-stomatocyte morphology of red blood cell [44]; (b, c) The deformation contour mappings with $\lambda(\theta^\alpha) + \phi(\theta^\alpha) = \alpha r^{-2}$, where the α is adjusted to obtain the transitioning morphology from (b) to (c).	84
4.9	The deformation contour achieved by superimposing the radial and circumferential non-uniform distribution potential when $\lambda(\theta^\alpha) + \phi(\theta^\alpha) = \alpha(\cos(8\theta) + \pi) + \alpha r^{-2}$	84
5.1	Schematic view of the computational model: (a) 40nm×40nm lipid membrane, (b) illustration of membrane-water system.	107
5.2	Formation of membrane morphology subjected to lateral pressure and viscous flow: (a) continuum model results at $t = 3.4s$, (b) at $t = 3.6s$, (c) at $t = 3.8s$, and (d) at $t = 4.0s$	109
5.3	Formation of membrane morphology subjected to lateral pressure and viscous flow: (a) MD simulation results at $t = 2.95ns$, (b) $t = 3.00ns$, (c) $t = 3.05ns$, and (d) $t = 3.10ns$	110
5.4	Membrane deformation subjected to lateral pressure and viscous flow: (a) comparison between continuum model result at $t = 4.0s$ and MD simulation result at $t = 2ns$, (b) cross-section of MD simulation result at $t = 2ns$	111
5.5	Membrane thickness distension subjected to lateral pressure and viscous flow: (a) continuum model results ($\nu = 40$) at $t = 0s$, (b) at $t = 0.16s$, (c) at $t = 0.32s$, and (d) at $t = 0.48s$	112
5.6	Membrane thickness distension subjected to lateral pressure and viscous flow: (a) MD simulation results at $t = 3.00ns$, (b) at $t = 3.02ns$, (c) at $t = 3.04ns$, and (d) at $t = 3.06ns$	113
5.7	Formation of membrane morphology subjected to lateral pressure and various viscosity at $t = 4s$: (a) $\nu = 20$, (b) $\nu = 80$, (c) $\nu = 140$, (d) $\nu = 200$	114
5.8	Thickness distension of lipid membrane subjected to lateral pressure and different viscosity at $t = 4s$: (a) $\nu = 20$, (b) $\nu = 80$, (c) $\nu = 140$, (d) $\nu = 200$	115
5.9	Formation of membrane morphology subjected to interaction force and viscous flow: (a) continuum model results at $t = 0.002s$, (b) $t = 0.003s$, (c) $t = 0.004s$, (d) $t = 0.005s$	116

5.10	Formation of membrane morphology subjected to interaction force and viscous flow: (a) MD simulation results at $t = 1.75\text{ns}$, (b) at $t = 1.85\text{ns}$, (c) at $t = 1.95\text{ns}$, (d) at $t = 2.05\text{ns}$	117
5.11	Membrane morphological transition (diagonal cross-section) subjected to lateral pressure and viscous flow: (a) comparison between continuum model result at $t=0.004\text{s}$ and MD simulation result at $t = 2\text{ns}$, (b) cross-section of MD simulation result.	118
5.12	Membrane thickness distension subjected to interaction force and viscous flow: (a) results of continuum model at $t = 0\text{s}$ and (b) at $t = 0.001\text{s}$	118
5.13	Membrane thickness distension subjected to interaction force and viscous flow: (a) MD simulation results at $t = 0.2\text{ns}$, (b) at $t = 2.05\text{ns}$. .	119
5.14	Membrane thickness distribution subjected to interaction force and viscous flow: (a) continuum model result at $t = 4\text{s}$, (b) MD simulation result at $t = 1.1\text{ns}$	120
5.15	Experimental results of lipid membrane morphology transition: (a) fluorescence microscopy images of the membrane subjected to the increasing pH values, (b) quantitative results of membrane deformation in (a); black, $t = 0\text{s}$; red, $t = 0.8\text{s}$; blue, $t=1.2\text{s}$; green, $t=2.8\text{s}$ [39]. . .	121
5.16	Continuum modeling results of membrane inflammation at different time steps.	122
5.17	Comparison between simulation result and experimental result: (a) continuum modeling result of membrane inflammation subject to viscous flow at $t = 4\text{s}$, (b) scanning electron microscope (SEM) images of long-stored red blood cells [33].	122
5.18	Comparison between simulation result and experimental result: (a) simulation result of substrate interaction subjected to viscous flow at $t = 0.005\text{s}$, (b) electron-tomographic slice of Hela cells, in which the highly curved pore-membrane deformation is induced as the NPCs are inserted into the nuclear envelope. ONM, outer nuclear membrane; INM, inner nuclear membrane [40].	123
6.1	Schematic of surface configurations: surface vectors to the specific trajectories in referential (Ω) and current configurations (ω), respectively.	135
6.2	Schematic of fiber kinematics: unit tangents to the trajectories of the fibers in reference (\mathbf{L} and \mathbf{M}) and current configurations (\mathbf{l} and \mathbf{m}), and geodesic curvature (\mathbf{g}_1 and \mathbf{g}_2) between two adjacent fibers.	136

6.3	The illustration of boundary conditions: fixed boundaries ∂B and lateral pressure P applied on the domain B	146
6.4	Coordinate expression in initial and current configurations: X_1, X_2, X_3 for initial configuration and χ_1, χ_2, χ_3 for current configuration (X_3 and χ_3 are normal to the $X_1 - X_2$ and $\chi_1 - \chi_2$ plane, respectively).147	
6.5	Deformations of the fiber-reinforced composite subjected to $\kappa = 1Mpa, E_i = 2Mpa, C_i = 3Mpa, T = 3Mpa, P = 1Mpa$: (a) out-of-plane deflection of the matrix material, (b) in-plane material displacement vector field, (c) top view of (a).	149
6.6	Size/shape effects on the in-plane deformation of the matrix material subjected to $\kappa = 1Mpa, E_i = 2Mpa, C_i = 3Mpa, T = 3Mpa, P = 3Mpa$: (a) 5×5 square, (b) 10×10 square, (c) 10×5 rectangular. . . .	150
6.7	The material displacements of the matrix subjected to increasing lateral pressures: (a) $P/C_i = 1/3$ (3D view), (b) $P/C_i = 1/3$, (c) $P/C_i = 1$, (d) $P/C_i = 5/3$, (e) $P/C_i = 7/3$, (f) $P/C_i = 3$	151
6.8	Green-Lagrange strain distribution of the matrix material over the domain ($\kappa = 1Mpa, E_i = 2Mpa, C_i = 3Mpa, T = 3Mpa, P = 1Mpa$): (a) ε_1 , (b) ε_2	153
6.9	The illustration of fiber unit deformation determines the overall fiber deformation: (a) The mechanism of the elongated \mathbf{L} determines the elongation of a single fiber; (b) The mechanism of the curved \mathbf{L} determines the overall flexure of a single fiber.	154
6.10	Distribution of deformed fiber unit over the domain ($\kappa = 1Mpa, E_i = 2Mpa, C_i = 3Mpa, T = 3Mpa, P = 12Mpa$): (a) Deformed \mathbf{L} ; (b) Deformed \mathbf{M}	154
6.11	Fiber extension under increasing lateral pressures: (a) The locations of the sampled fibers; (b) The comparison of fiber extension.	155
6.12	Distributions of unit fibers' geodesic curvature \mathbf{g}_1 and \mathbf{g}_2 ($\kappa = 1Mpa, E_i = 2Mpa, C_i = 3Mpa, T = 3Mpa, P = 3Mpa$): (a) \mathbf{g}_1 ; (b) \mathbf{g}_2 ; (c) \mathbf{g}_1 and \mathbf{g}_2 intersection; (d) The illustration of intersections between \mathbf{g}_1 and \mathbf{g}_2	156
6.13	Geometry comparison between the initial meshwork and deformed meshwork ($\kappa = 1Mpa, E_i = 2Mpa, C_i = 3Mpa, T = 3Mpa, P = 3Mpa$): (a) deformed meshwork, (b) initial meshwork, (c) top view of (a). . .	157

6.14	Comparison of the meshwork deformation between proposed model results and the out-of-plane deflection results in [57] (bidirectional reinforcements case): (a) profile of meshwork ($\kappa = 0.24Mpa$, $E_i = 9.64Mpa$, $C_i = 5Mpa$, $T = 1Mpa$, $P = 0.085Mpa$.), (b) peaking values of the out-of-plane deformation subjected to increasing lateral pressures ($\kappa = 0.24Mpa$, $E_i = 9.64Mpa$, $C_i = 5Mpa$, $T = 1Mpa$, $P = 0.035 - 0.085Mpa$).	158
6.15	Experimental configuration on testing and measuring the woven fabric deformation in [57]: (a) the sketch of the deformation tester (left) and real tester (right), where the fabric edges are clamped by the bolts, nuts and retaining plate. The plate has a hole of radius of 50mm to expose the fabric to the air inside the cylinder container. Then, the lateral pressure is induced by the vacuum pumper connected at the cylinder container bottom and a pressure gauge is utilized to monitor the lateral pressure. In addition, the O-type silicone seal is applied to maintain the pressure. (b) the ruler and positioner for measuring the fabric meshwork out-of-plane deformation, and more details can be found in [57].	160
6.16	Fiber-reinforced composite deformation ($\kappa = 1Mpa$, $E_i = 2Mpa$, $C_i = 3Mpa$, $T = 3Mpa$, $P = 1Mpa$): (a) side view of 3-dimensional deformation, (b) top view of (a).	161
6.17	Damage pattern of FRCM specimens fabricated using different modes of fabric application [58]: (a) DA_{0-90} , (b) SA_{0-90} , (c) DA_{45} where D means direct, S presents sandwich, A for anchored, the subscript number represents the angle of fiber orientation. The fabric is mounted on the matrix/infill material with mechanical anchors in the vicinity of the blue zone and fabric ruptures are marked by dash lines.	162
6.18	Experimental setting on testing the out-of-plane performance of FRCM [58]: The left image is the side view of the right graph, in which the motion of the shake table is used for inducing the out-of-plane loading, and the side supports provide lateral supports for the specimen. The FRCM specimens are further positioned and fixed with abutment restraint slips and pre-tension cables near the boundaries, which align with the proposed model's boundary conditions in a clamped manner.	163
6.19	Green-Lagrange strain and meshwork deformation of fiber-reinforced composite over the domain ($\kappa = 1Mpa$, $E_i = 2Mpa$, $C_i = 3Mpa$, $T = 3Mpa$, $P = 1Mpa$).	163

6.20 Experimental configuration on shaping bamboo fabric-PLA composites [61]: (a) the blank PLA composite is placed on the top surface of the hemispherical female die surface to be reshaped by the male die, (b) the male and female die are matching to form the dome-like bamboo fabric-PLA composites, (c) the obtained dome-like bamboo fabric-PLA composites with the enlarged grids in the hinterland and shrunk grids in the vicinity of boundaries. 164

Chapter 1

Introduction

Hyperelastic models have drawn considerable research interest due to their extensive applications in the aerospace industry [1], construction sector [2], as well as biological tissue [3, 4]. Because of the highly non-linear strain-stiffness behavior of hyperelastic materials (such as the well-known “J-shaped” stress-strain responses of biological tissues [5]), they are highly deformable and can experience large deformation, notably retaining their initial shape when external loadings are removed [1]. The continuum models of hyperelastic material have been developed to describe the mechanics of biological material and composite material, e.g. the typical continuum model of lipid membrane is the well-known Canham-Helfrich model [6], and current research focuses on establishing the variants of the Canham-Helfrich model [7–12] to understand the cell functioning processes by investigating the mechanical response of lipid membrane. Meanwhile, the hyperelasticity of polymeric materials, in general, is modeled by computing the strain energy potential in terms of its invariants of strain [13]. Nevertheless, understanding and investigating the continuum model of hyperelastic material can not be independent of studying the physical features of the hyperelastic material, therefore, it is indispensable to focus on the hyperelastic material properties before investigating the mechanics. Hence, the physical properties of the hyperelastic materials will be introduced first, and then the studies of hyperelastic models will be presented sequentially in the subsections.

1.1 Lipid Membrane

Every single cell is enclosed by the semipermeable lipid membranes which are mainly composed of transversely opposed lipids (typically, phosphatidylcholine (POPC), phosphatidylethanolamine (POPE), phosphatidylserine (POPS), sphingomyelin (PSM), and cholesterol (CHL) [14–16]), peripheral and integral proteins (see, Figure 1.1) to envelope a cell's cytoplasm and maintain the shape of cell.

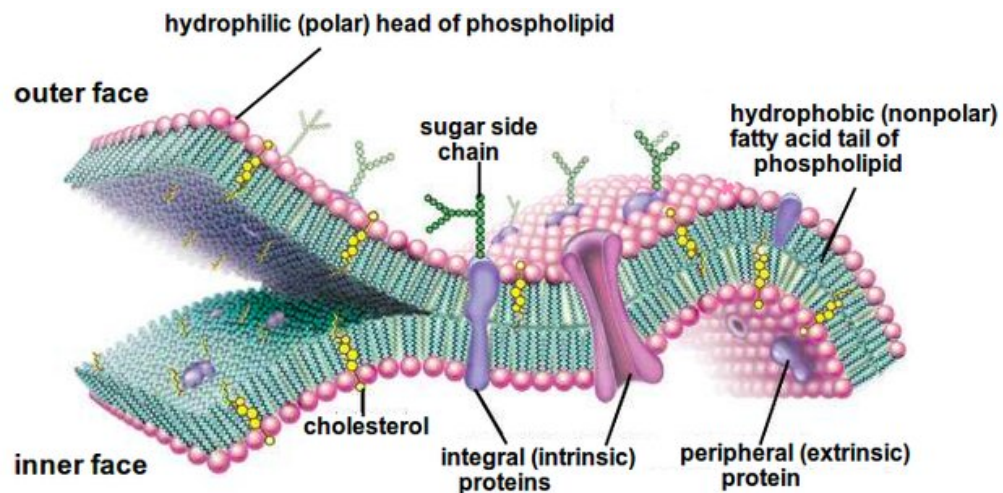


Figure 1.1: Schematic of cell membrane structure [17], where the use of the image was admitted by Encyclopaedia Britannica, Inc. ©2007.

Lipids are amphiphilic molecules that feature hydrophobic fatty acid tails and hydrophilic lipid headgroups (see Figure 1.1 and Figure 1.2). Under the hydrophobic effect, lipids assemble themselves into a lipid bilayer, arranging lipid molecules in a back-to-back configuration when they are in an aqueous solution (see Figure 1.1). Accordingly, the lipid membrane acts as a barrier, enclosing the cell cytoplasm and organelles inside the cell, such as the endoplasmic reticulum, Golgi apparatus, and mitochondria (for eukaryotic cell membranes) [18] and segregate internal cell constituents from the external environment. In addition to its role as a barrier, the lipid membrane is indispensable in assisting cell budding, tabulation, fission, and fusion. Furthermore, the lipid membrane plays a crucial role in the membrane-trafficking sys-

tem, supporting processes such as the export and uptake of extracellular substances, cellular interface remodeling, signaling, intracellular targeting, and the preservation of internal compartmentalization. More importantly, it is observed that cell remodeling and functional processes are intricately correlated. For instance, the biconcave disk shape of red blood cells (RBCs) is critical for cells to carry out their circulatory function [19]. Hence, to understand the cell functioning process, it is necessary to introduce the indicators that can impact the morphology of the lipid membrane.

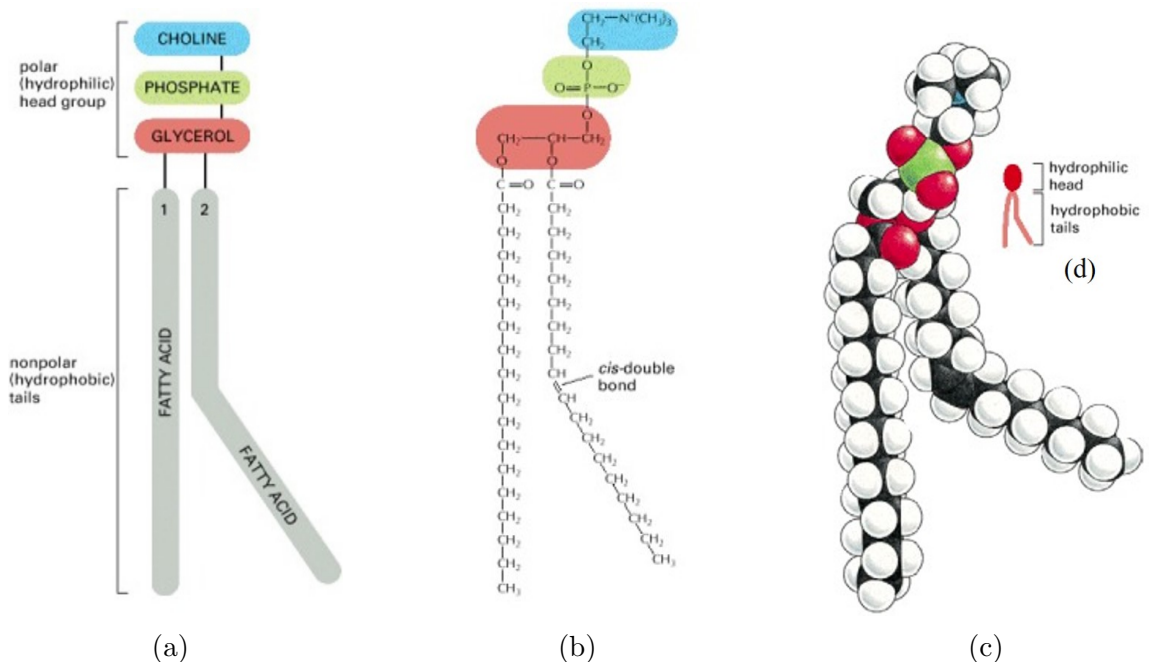


Figure 1.2: The structure of a lipid molecule (phosphatidylcholine), where (a) schematical structure, (b) formula structure, (c) space-filling model, and (d) symbol representation. The kink resulting from the *cis*-double bond is exaggerated for emphasis [20].

1.1.1 Lipid membrane curvature

The membrane curvature plays a crucial role in regulating cellular function. For instance, the highly folded membrane can significantly increase the capacity of the mitochondrion and boost the aerobic respiration rate of cells [21]. It is observed that the curvature of membranes not only affects the positioning of transmembrane

proteins [22] but also plays a critical role in recruiting numerous peripheral proteins to organelles [23]. In addition, the bent thylakoid membranes are indispensable in the formation of grana stacks in photosynthetic organisms [24]. To mediate various cell functions such as endo- and exocytosis or various types of fusion and fission, the associated reshaping and topology changes of membrane structures consistently result in strongly bent membranes [25]. Further, the increase in curvature leads to a softened membrane [26], significantly regulating their interaction with biological systems, particularly in processes of tumor penetration and endocytosis by cells [27–31]. In the pathogenesis view, neurodegeneration and aging-related diseases [32–34] are believed to be negatively impacted by accumulated high levels of oxidative stress, which are invoked due to the curvature alteration of the lipid membrane. In particular, the study [35] investigates the permeability of a probing molecule (D289 dye, positively charged) on the bilayers of DOPG lipid vesicle, showing the increase in curvature generation can reduce the bilayers’ permeability while a flatter bilayer owns a higher permeability. The mechanism of membrane curvature generation can be ascribed to various factors like the composition and asymmetry change of membrane, insertion of protein, protein crowding, and the partition of deformed transmembrane surface, etc [36].

1.1.2 Lipid membrane-protein interaction

Lipid membrane proteins are, in general, integrated into the lipid membrane and are indispensable for cellular function. Lipid membrane protein interacts with intricate networks that are integrated with other membrane-bound proteins and lipids, through which a variety of physiological processes are implemented. One protein-interaction form called membrane-bound form is believed to be induced by the peripheral membrane binding processes [37]. The peripheral-membrane binding proteins such as saposins can be involved in lipid degradation [38] while other saposin-like proteins are capable of dimerizing in the presence of micelles and liposomes [39], or even in-

ducing liposome fusion [40, 41]. Besides its cellular function, the binding proteins can be utilized to fabricate lipid nanoparticles for medical applications [42]. These applications might be derived from the mechanism that when viruses invade new host cells, viruses envelop themselves with lipid membranes which can facilitate their invasion, and the mechanism might be ascribed to the membrane-protein interaction can be selective in the assembly and budding of new virions [43]. From the aspect

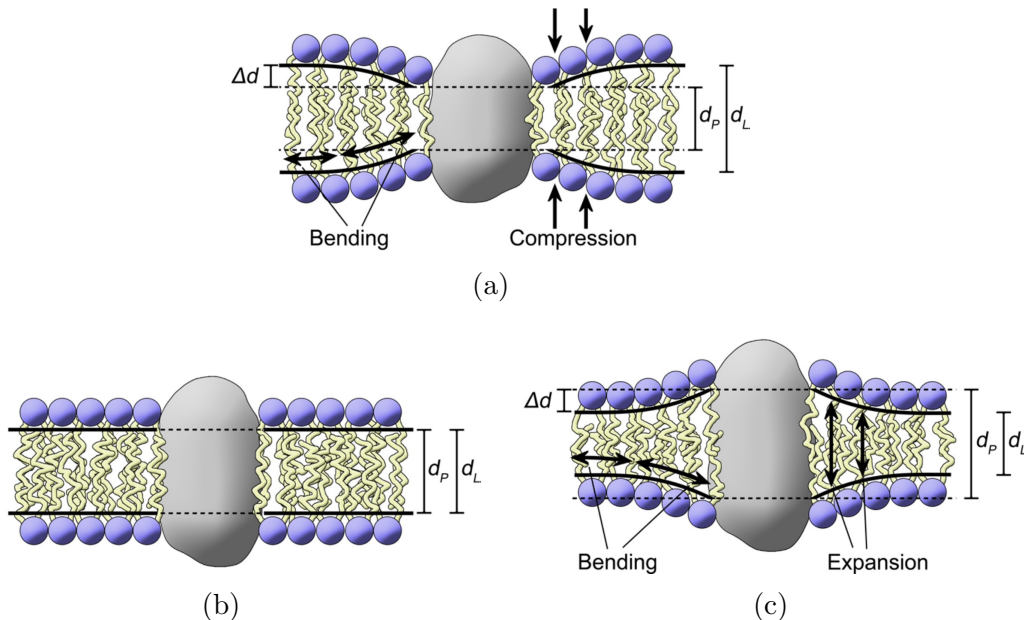


Figure 1.3: The illustration of the flexible surface model (FSM) in explaining the interaction between lipid membrane and protein [44]: (a) local bending and compression, (b) flat profile, and (c) alternative of local bending and compression in (a).

of mechanics, the study [44] has described the balance of curvature and hydrophobic forces in the membrane-protein interaction using an elastic surface model to demonstrate the relations between theory and experiment. It is found that both membrane-bound proteins and integral proteins can change cellular membrane shape by altering the membrane curvature when the membrane-protein interaction occurs (see, Figure 1.3). The mechanism indicates both membrane-bound protein and integral protein are sensitive to the membrane curvature [45], which is particularly evidenced in cases of mobile protein interaction [46]. Recent experiments have investigated the mechanical equilibrium of curvature-related conformation by monitoring membrane lateral

tension, showing the shape of protein can modify the bending constant of membrane and spontaneous curvature [22]. In there, the study interprets the interaction effects as a function of curvature while the factors behind can be physical based or/and chemical based [47].

1.1.3 Non-uniform morphology of lipid membrane and surface dilatation

The non-uniform morphology of the lipid membrane can be induced by the charge difference between the upper and downward layers of the lipid membrane. The factors affecting the non-uniform charge distribution include: electric potential externally applied across the membrane, the various ionic compositions of bathing solutions for lipid membranes, and changes in lipid membrane curvature [48]. In particular, the lipid membrane curvature can regulate intricate cell membrane morphologies and is considered an asymmetry-creating factor of the lipid membrane, because the alteration of lipid membrane curvature can significantly lead to the asymmetry in lipid distribution. It is even found that the favorable/unfavorable lipid–membrane–protein interactions can induce the non-uniformly distributed components of lipid membrane [49]. Additionally, the non-uniform and complex conformational transformations of the cell membrane are, in general, involved in the membrane exo- and endocytosis processes (e.g., invagination, vesicle fusion, and mitosis), which can be achieved by shrinking/enlarging the surface area of cells. During this process, the surface area can be compressed when lipid tubes are passively separated out of the membrane plane, while the membrane surface can dilate by merging the adhered lipid vesicles [50]. The adding and reducing of membrane surface can be considered as the passive results due to the fact that lipid membranes are fragile in the transverse dimension while maintaining their fluidity, consequently disabling cells from sustaining large strains transversely. In the mechanical view, membrane surface dilatation is the result of the membrane passively/actively adjusting the surface area by controlling the

membrane's surface tension within the complicated and coordinated work of various proteins and components of the lipid-protein matrix system [51, 52]. Hence, the non-uniform property and surface area regulation of the lipid membrane are critical characteristics of the cell membrane in understanding the cell remodeling and cell functioning processes.

1.1.4 Lipid membrane viscosity

It is believed that lipid membranes, at the molecular level, are two-dimensional fluid-like materials because the connection between the lipid bilayer is non-covalent bonded [53, 54]. Due to their fluidity and viscosity, the lipid membranes can spatially organize and transport lipids, lipid patches, and trans-proteins [55]. In particular, the fluidity and viscosity of lipid membranes allow cell membranes to perform reversible large and complex deformations: Krogh [56] found the cells of vertebrate animals undergo dramatic shape changes in the flow of cells within the microcirculation process. In this process, cells are passively transported into various channels, where the cell membranes are shrunk significantly when passing through apertures and large membrane deformations occur. Nevertheless, the cells can mostly recover to their initial size when the confined paths are eliminated. Regarding this, the lipid membrane undergoes a dynamic and non-equilibrium reshaping process due to the frequent changes of stress derived from viscous environments [57]. Hence, investigating the viscous effects on the lipid membrane is crucial in understanding the non-equilibrium shaping process of the lipid membrane.

1.1.5 Lipid membrane inflammation

Cell inflammation is critical in both the physiology and pathology of humankind, and can be invoked by cellular stress [58], pathogen [59], and microparticles from various cellular origins [60]. In particular, cell inflammation can alter the deformability of the cells by enhancing oxidative stress, resulting in abnormal RBC rheology [60]. It

is even found that inflammation occurs via diet, which accordingly triggers a modulation of plasma membrane domains [61]. Inflammation-associated diseases such as cardiovascular disease [62], type 2 diabetes [63], and cancers [64], in general, can be induced by chronic infection, obesity, intestinal disorders, psychological pressure, etc., which consequently alternate the heterogeneity and morphology of cells [65]. In particular, cells that have constant contact with blood (such as RBC, monocyte cells, and endothelial cells) suffer a high risk of encountering inflammation and performing abnormal morphology. For instance, erythroid-predominant hematopoiesis and sickled RBCs were found in humans who contracted fever, chills, and chest pain [66]. In addition, RBCs with distinct morphological features were observed from the blood samples of lung cancer patients [67]. Furthermore, dry eye disease (DED), induced by desiccating stress, can alter the morphology and kinetics of conventional dendritic cells (CDCs), i.e., CDCs become more spherical and more motile under DED [68]. In particular, the retinal ganglion cells' morphology is predominantly featured with a loss of thin spines during the suffering of Alzheimer's disease [69]. More importantly, understanding the morphology transition of cell membranes induced by the inflammation-related disease can assist in pathological diagnosis: to identify cancer cells with a high capability to metastasize, the research [70] extracted morphological features of cancer cells, which successfully predicts the cell migration and metastasis with a high accuracy which is critical in determining the people's death induced by cancers. For the purpose of evaluating the differentiation potential of neural stem cells in investigating neurological disorders, the study [71] proposes a computer-aided morphology-based prediction method to determine the cells' differentiation type and differentiation rate. It is even found that the differentiation stage of human bone marrow stromal cells can be predicted via cell morphology [72]. Hence, it can be concluded that the cell morphology is intricately coupled with inflammation and pathogens.

1.1.6 Lipid membrane thickness

Lipid membrane thickness is well recognized as the dimension between the two leaflets of the lipid bilayer, i.e., the distance spanning from the hydrophobic tails of the lipid molecules on each side of the bilayers. The lipid membrane thickness, if measured between the hydrophobic cores of the bilayer, is typically 3 to 5nm while the real bilayer thickness depends on the length of the lipid chain and composition of the lipid bilayer [73, 74]. The membrane thickness is critical in regulating permeability [75], protein-lipid interactions [76], and can mediate self-assembly via interactions of proteins [77]. It is even believed that cell spreading and proliferation can be enhanced by manipulating membrane thickness [78]. Membrane thickness is highly sensitive to changes in the environment including temperature, osmolarity, salinity, and pH levels. In particular, the existence of osmotic pressure between the inner and exterior membrane can induce thickness reduction of lipid membrane [79]. Additionally, temperature and phase transition can significantly alter the lipid bilayer thickness [80]. Further, the changes in membrane thickness, combined with membrane curvature transitions are considered important modulators of the membrane protein function [81–83]. To regulate of proteins of the lipid bilayer, the thickness differences are induced by the bilayer-protein interaction, specifically occurring in the vicinity of membrane-proteins [81, 84–86]. Notably, the changes in membrane thickness can mediate interactions of protein, and then regulate the membrane self-assembly [77].

1.2 Elastomeric Materials

Elastomeric materials are rubber/rubber-like materials, they are a specialized group of high polymers that are widely used in various mechanical fields such as aerospace, construction, soft robotics, and tissue engineering because they are highly deformable and can sustain heavy loadings [87]. The widespread use of elastomers necessitates the development of continuum models to study the mechanics of elastomeric materials,

e.g., the continuum model was developed to describe the mechanical performance of multinetwork elastomers (MNEs) due to its remarkable stiffness and fracture toughness [88]; Liquid crystal elastomer is studied in the continuum modeling approach by accounting for the interaction of polymer backbone and liquid crystal microstructure, where it is observed that the stress-deformation response and the director rotation are dependent on rate change, showing a good agreement to the results of the experimental approach [89]. In particular, the vast majority of research emphasizes establishing strain energy models to demonstrate the mechanics of elastomers, which are framed in work of hyperelasticity [90]. Most of these hyperelastic models are phenomenologically based, mathematically defined, and justified, where the associated experimental parameters are determined via experimental approaches [91]. The models, in general, present strain density potential in the form of the invariant of the Cauchy-Green deformation tensor or gradient of deformation. The typical hyperelastic models include Saint Venant–Kirchhoff type, Neo-Hookean, and Mooney-Rivlin models for the cases of incompressibility and their variants accounting for isotropy [92]. Though the strain energy potential model can describe the strain-stress behavior within a continuum context, the refinement work of the hyperelastic model continues to achieve a comprehensive description of elastomer mechanics [93]. This includes compensating discrepancies between theoretical results and experimental results when it comes to describing below-intermediate or high stretch levels of elastomers. For instance, the study [94] attributes this discrepancy to the lack of describing the swelling effects on elastomers and refining the strain energy model by introducing the Flory-Erman constrained on-chain model and the Arruda-Boyce non-Gaussian eight-chain model. Contemporary research focuses on investigating the elastomers reinforced with engineered filament materials to achieve high-performance fiber composite material [95].

1.3 Objectives and Overview of Dissertation

In this thesis, we demonstrate the mechanics of hyperelastic material by investigating the continuum models in describing lipid membrane and fiber-reinforced composite mechanics. This includes investigating the non-uniform morphology of lipid membranes subjected to interaction force and lateral pressures, elucidating the effects of viscous flow on the surface dilatation of lipid membranes undergoing lipid-membrane interaction force and lateral pressure, illustrating the mechanics of fiber-reinforced composite by proposing a three-dimensional continuum model, where both the in-plane and out-of-plane deformation, strain-loading relationship, fiber meshwork deformation are illustrated. To achieve accurate and reasonable mechanics descriptions of hyperelastic materials, emphasis is placed on deriving rigorous and general equilibrium shape equations to build the constitutive relations of mechanics while incorporating various factors such as non-uniformity, surface dilatation, viscosity, and fiber kinematics. For this aim, the primary approach is to furnish the established strain energy model by computing and introducing the non-uniform properties, viscous effects, surface dilatation, and microstructure kinematics into the strain energy and associated constitutive relations. It should be mentioned that we take the non-uniform/uniform morphology short for the non-uniformity/uniformity throughout the thesis, where the non-uniformity is in the sense of inhomogeneous properties, not the concept of material non-uniformity/uniformity defined in the continuum mechanics [96].

In this regard, the non-uniformity of the lipid membrane is discussed by considering the strain energy of the lipid membrane is non-uniformly distributed and an energy potential function based on surface coordinate is introduced into the Helfrich classic model; To investigate the effects of viscous flow on membrane deformation and surface dilation, the established strain energy potential is furnished by computing the gradient of surface distension and its product, and then the viscous stress on

the membrane surface is introduced into the corresponding equilibrium equations of the refined Helfrich classic model; As for the fiber-reinforced composite, the initial work is to compute the kinematics of embedded fiber (like extension, flexure, and twist), then, the emphasis is placed on configuring the corresponding strain energy contributions to the Neo-Hookean type hyperelastic strain energy model.

Aiming at establishing equilibrium equations, the variational approach is utilized to compute the variation of the refined strain energy potential, where the differential geometry is employed to present constitutive relations on the hyperelastic material surface. This involves computing the virtual displacement, surface metric, covariant derivative, and contravariant derivative of material position on the surface, through which the Euler-Lagrange equations are formulated and corresponding tangential and normal shape equations are achieved. To demonstrate the proposed model, first, we clarify the boundary conditions of the proposed model. Then, we implement the proposed model by projecting the equilibrium equations onto the Cartesian coordinate system where we obtain a system of partial differential equations (PDEs) with the associated boundary conditions presented explicitly. The PDEs are numerically solved via COMOSOL, MATLAB, or custom-built finite element method (FEM) procedures, and the obtained numerical results are compared with experimental results of current literature to validate the proposed model. In order to investigate the "small deformation" of hyperelastic material, we linearize the non-linear shape equations, furnishing a system of PDEs of Laplacian and Poisson's type from which the corresponding analytical solutions are obtained by employing the method of separating variables.

The theoretical results obtained from the proposed refined hyperelastic models remarkably advanced understandings of hyperelastic material behavior: The uniform morphology of lipid membrane subjected to substrate-interaction force and lateral pressure induced by protein-membrane interaction and cellular inflammation, respectively; The role of intra-surface viscous flow in affecting the lipid membrane surface dilatation; The deformation of fiber-reinforced composite and its embedded meshwork

deformation. In particular, the research regarding fiber-reinforced material unveiled how the microstructure of fiber determines the overall mechanical performance of fiber-reinforced material. The thesis provides insightful and reasonable evidence on the physical behavior of lipid bilayer and fiber-reinforced composites, especially valuable for predicting cell membrane function implementation related to cell morphology transition and designing high-performance fiber composite materials.

The thesis is organized as: Chapter 2 introduces mathematical preliminaries utilized in expressing and deriving constitutive relations. This includes index notation, surface configuration, differential geometry, the gradient of deformation on the hyperelastic material surface, and the targeted strain energy potentials in the following chapters. Emphasis is placed on explaining the physical parameters of the strain energy model aims to develop the refined energy potentials. Chapter 3 and Chapter 4 examine the non-uniform morphologies of lipid membranes subjected to trans-protein interaction and inflammation. In there, the substrate-interaction force is assumed to be induced by protein-membrane interaction, and lateral pressure is induced by local inflammation of the lipid membrane. The non-linear shape equations describing a non-uniform lipid membrane are obtained by discussing the lipid membrane strain energy that is non-uniformly distributed. For the purpose of describing the “small” deformation of the lipid membrane, we linearize the non-linear shape equation from which the corresponding analytical solutions are achieved. To demonstrate the validity of the proposed mode, we invoked the experimental results in the current literature for comparison with the numerical results and analytical results. The comparisons show a good agreement in explaining cell morphogenesis, and it shows that the non-linear solutions of substrate-interaction cases phenomenologically predict the off-centered biconcave morphology of lipid membranes and the multiple peak morphology of abnormal cell membranes (burr cells), which are commonly observed in uremia and chronic kidney disease. Evidently, the numerical and analytical results of inflammation assimilate the off-centered biconcave discoid structures of red blood

cells and the echinocyte formations of cell membranes induced by the incubation with lecithin.

Chapter 5 characterized the effects of viscous flow on the surface distension of the lipid membrane when the lipid membrane is undergoing substrate-interaction force/lateral pressures. In there, continuum modeling and molecular dynamics (MD) simulation are applied to reveal the surface distension of lipid membranes. Though continuum modeling and MD simulation are distinct approaches, the continuum modeling and MD simulation results prohibit a promising alignment in describing the performance of lipid membrane surface dilatation. The results show that the intra-surface viscous flow can locally induce surface compression and dilatation. Specifically, when the viscous flow is flowing toward the lipid membrane domain, the surface area is shrunk while the surface area of the lipid membrane is enlarged when the fluid is flowing out of the domain. It is noteworthy that the substrate-interaction force and bending effects of lateral pressure can both invoke the local area compression around the boundaries of the lipid membrane.

The highlight of Chapter 6 locates on invoking the spirit of lipid membrane theory (discussed in Chapters 3, 4, and 5) to investigate the mechanical performance of fiber-reinforced composite subjected to out-of-plane loadings. Unlike most of the established continuum models that focus on illustrating the in-plane deformations of fiber-reinforced composite, the proposed model addressed the concurrent three-dimensional deformation of the fiber-reinforced composite while maintaining the fiber kinematics are rigorously configured on the fiber composite surface. In particular, the proposed model reasonably and comprehensively explains the mechanism of the embedded fiber pieces to determine the overall mechanical performance of fiber composites.

References

- [1] M. Shahzad, A. Kamran, M. Z. Siddiqui, and M. Farhan, “Mechanical characterization and fe modelling of a hyperelastic material,” *Materials Research*, vol. 18, 5 2015, ISSN: 19805373. DOI: 10.1590/1516-1439.320414.
- [2] I. Major and M. Major, “Application of hyperelastic materials in a composite hollow brick for assessing the reduction of dynamic loads - numerical analysis,” vol. 585, 2019. DOI: 10.1088/1757-899X/585/1/012031.
- [3] G. Chagnon, M. Rebouah, and D. Favier, *Hyperelastic energy densities for soft biological tissues: A review*, 2015. DOI: 10.1007/s10659-014-9508-z.
- [4] A. A. Abbasi, M. T. Ahmadian, A. Alizadeh, and S. Tarighi, “Application of hyperelastic models in mechanical properties prediction of mouse oocyte and embryo cells at large deformations,” *Scientia Iranica*, vol. 25, 2B 2018, ISSN: 23453605. DOI: 10.24200/sci.2017.4321.
- [5] Y. Ma, X. Feng, J. A. Rogers, Y. Huang, and Y. Zhang, *Design and application of 'j-shaped' stress-strain behavior in stretchable electronics: A review*, 2017. DOI: 10.1039/c7lc00289k.
- [6] W. Helfrich, “Elastic properties of lipid bilayers: Theory and possible experiments,” *Zeitschrift fur Naturforschung - Section C Journal of Biosciences*, vol. 28, pp. 693–703, 11-12 Dec. 1973, ISSN: 18657125. DOI: 10.1515/znc-1973-11-1209.
- [7] Z. Liu and C. il Kim, “Deformation analysis of lipid membranes subjected to general forms of intra-membrane viscous flow and interactions with an elliptical-cross-section substrate,” *Scientific Reports*, vol. 10, 1 2020, ISSN: 20452322. DOI: 10.1038/s41598-019-57179-z.
- [8] W. Yao and C. I. Kim, “A lipid membrane morphology subjected to intra-membrane viscosity and membrane thickness dilation,” *Continuum Mechanics and Thermodynamics*, vol. 35, 2 2023, ISSN: 14320959. DOI: 10.1007/s00161-023-01204-0.
- [9] W. Yao and C. I. Kim, “Deformation analysis of nonuniform lipid membrane subjected to local inflammations,” *Mathematics and Mechanics of Complex Systems*, vol. 9, 2 2021, ISSN: 23253444. DOI: 10.2140/MEMOCS.2021.9.203.
- [10] M. Zeidi and C. I. Kim, “The effects of intra-membrane viscosity on lipid membrane morphology: Complete analytical solution,” *Scientific Reports*, vol. 8, 1 2018, ISSN: 20452322. DOI: 10.1038/s41598-018-31251-6.
- [11] T. Belay, K. C. Il, and P. Schiavone, “Mechanics of a lipid bilayer subjected to thickness distension and membrane budding,” *Mathematics and Mechanics of Solids*, vol. 23, 1 2018, ISSN: 17413028. DOI: 10.1177/1081286516666136.
- [12] W. Yao and C. I. Kim, *An analysis of lipid membrane morphology in the presence of coordinate-dependent non-uniformity*, 2021. DOI: 10.1177/1081286520939162.

- [13] S. K. Melly, L. Liu, Y. Liu, and J. Leng, *A review on material models for isotropic hyperelasticity*, 2021. DOI: 10.1002/msd2.12013.
- [14] S. L. Veatch and S. L. Keller, “Organization in lipid membranes containing cholesterol,” *Physical Review Letters*, vol. 89, 26 2002, ISSN: 10797114. DOI: 10.1103/PhysRevLett.89.268101.
- [15] B. B. Diaz-Rohrer, K. R. Levental, K. Simons, and I. Levental, “Membrane raft association is a determinant of plasma membrane localization,” *Proceedings of the National Academy of Sciences of the United States of America*, vol. 111, 23 2014, ISSN: 10916490. DOI: 10.1073/pnas.1404582111.
- [16] H. I. Ingólfsson *et al.*, “Lipid organization of the plasma membrane,” *Journal of the American Chemical Society*, vol. 136, 41 2014, ISSN: 15205126. DOI: 10.1021/ja507832e.
- [17] I. Ermilova, “Modeling of biomembranes: From computational toxicology to simulations of neurodegenerative diseases,” Ph.D. dissertation, Department of Materials and Environmental Chemistry, Stockholm University, 2019. DOI: 10.13140/RG.2.2.24409.57447.
- [18] A. M. Seddon, D. Casey, R. V. Law, A. Gee, R. H. Templer, and O. Ces, “Drug interactions with lipid membranes,” *Chemical Society Reviews*, vol. 38, 9 2009, ISSN: 14604744. DOI: 10.1039/b813853m.
- [19] H. Alimohamadi, A. S. Smith, R. B. Nowak, V. M. Fowler, and P. Rangamani, “Non-uniform distribution of myosin-mediated forces governs red blood cell membrane curvature through tension modulation,” *PLoS Computational Biology*, vol. 16, 5 2020, ISSN: 15537358. DOI: 10.1371/journal.pcbi.1007890.
- [20] B. Alberts, A. Johnson, J. Lewis, M. Raff, K. Roberts, and P. Walter, *Molecular Biology of the Cell*. W.W. Norton Company, Dec. 2007. DOI: 10.1201/9780203833445.
- [21] P. Paumard, “The atp synthase is involved in generating mitochondrial cristae morphology,” *EMBO Journal*, vol. 21, 3 2002, ISSN: 02614189. DOI: 10.1093/emboj/21.3.221.
- [22] S. Aimon, A. Callan-Jones, A. Berthaud, M. Pinot, G. E. Toombes, and P. Bassereau, “Membrane shape modulates transmembrane protein distribution,” *Developmental Cell*, vol. 28, 2 2014, ISSN: 15345807. DOI: 10.1016/j.devcel.2013.12.012.
- [23] S. Vanni, H. Hirose, H. Barelli, B. Antonny, and R. Gautier, *A sub-nanometre view of how membrane curvature and composition modulate lipid packing and protein recruitment*, 2014. DOI: 10.1038/ncomms5916.
- [24] M. Pribil *et al.*, “Fine-tuning of photosynthesis requires curvature thylakoid1-mediated thylakoid plasticity,” *Plant Physiology*, vol. 176, 3 2018, ISSN: 15322548. DOI: 10.1104/pp.17.00863.

- [25] K. V. Pinigin, P. I. Kuzmin, S. A. Akimov, and T. R. Galimzyanov, “Additional contributions to elastic energy of lipid membranes: Tilt-curvature coupling and curvature gradient,” *Physical Review E*, vol. 102, 4 2020, ISSN: 24700053. DOI: 10.1103/PhysRevE.102.042406.
- [26] C. P. Chng, Y. Sadosky, K. J. Hsia, and C. Huang, “Curvature-regulated lipid membrane softening of nano-vesicles,” *Extreme Mechanics Letters*, vol. 43, 2021, ISSN: 23524316. DOI: 10.1016/j.eml.2021.101174.
- [27] S. Zhang, J. Li, G. Lykotrafitis, G. Bao, and S. Suresh, “Size-dependent endocytosis of nanoparticles,” *Advanced Materials*, vol. 21, 4 2009, ISSN: 09359648. DOI: 10.1002/adma.200801393.
- [28] A. U. Andar, R. R. Hood, W. N. Vreeland, D. L. Devoe, and P. W. Swaan, “Microfluidic preparation of liposomes to determine particle size influence on cellular uptake mechanisms,” *Pharmaceutical Research*, vol. 31, 2 2014, ISSN: 07248741. DOI: 10.1007/s11095-013-1171-8.
- [29] Y. Takechi-Haraya, Y. Goda, and K. Sakai-Kato, “Control of liposomal penetration into three-dimensional multicellular tumor spheroids by modulating liposomal membrane rigidity,” *Molecular Pharmaceutics*, vol. 14, 6 2017, ISSN: 15438392. DOI: 10.1021/acs.molpharmaceut.7b00051.
- [30] X. Yi, X. Shi, and H. Gao, “Cellular uptake of elastic nanoparticles,” *Physical Review Letters*, vol. 107, 9 2011, ISSN: 10797114. DOI: 10.1103/PhysRevLett.107.098101.
- [31] Y. Hui *et al.*, *Role of nanoparticle mechanical properties in cancer drug delivery*, 2019. DOI: 10.1021/acsnano.9b03924.
- [32] I. Liguori *et al.*, *Oxidative stress, aging, and diseases*, 2018. DOI: 10.2147/CIA.S158513.
- [33] J. Emerit, M. Edeas, and F. Bricaire, *Neurodegenerative diseases and oxidative stress*, 2004. DOI: 10.1016/j.biopha.2003.11.004.
- [34] R. A. Floyd, R. A. Towner, T. He, K. Hensley, and K. R. Maples, “Translational research involving oxidative stress and diseases of aging,” *Free Radical Biology and Medicine*, vol. 51, 5 2011, ISSN: 08915849. DOI: 10.1016/j.freeradbiomed.2011.04.014.
- [35] B. Xu, S. L. Chen, Y. Zhang, B. Li, Q. Yuan, and W. Gan, “Evaluating the cross-membrane dynamics of a charged molecule on lipid films with different surface curvature,” *Journal of Colloid and Interface Science*, vol. 610, 2022, ISSN: 10957103. DOI: 10.1016/j.jcis.2021.12.015.
- [36] H. T. McMahon and E. Boucrot, “Membrane curvature at a glance,” *Journal of Cell Science*, vol. 128, 6 2015, ISSN: 14779137. DOI: 10.1242/jcs.114454.
- [37] E. D. Alba, S. Weiler, and N. Tjandra, “Solution structure of human saposin c: Ph-dependent interaction with phospholipid vesicles,” *Biochemistry*, vol. 42, 50 2003, ISSN: 00062960. DOI: 10.1021/bi0301338.

- [38] A. Darموise, P. Maschmeyer, and F. Winau, “The immunological functions of saposins,” in 2010, vol. 105. DOI: 10.1016/S0065-2776(10)05002-9.
- [39] C. A. Hawkins, E. D. Alba, and N. Tjandra, “Solution structure of human saposin c in a detergent environment,” *Journal of Molecular Biology*, vol. 346, 5 2005, ISSN: 00222836. DOI: 10.1016/j.jmb.2004.12.045.
- [40] A. Falco, R. M. Medina-Gali, J. A. Poveda, M. Bello-Perez, B. Novoa, and J. A. Encinar, “Antiviral activity of a turbot (*scophthalmus maximus*) nk-lysin peptide by inhibition of low-ph virus-induced membrane fusion,” *Marine Drugs*, vol. 17, 2 2019, ISSN: 16603397. DOI: 10.3390/md17020087.
- [41] S. I. Sandin, D. M. Gravano, C. J. Randolph, M. Sharma, and E. de Alba, “Engineering of saposin c protein chimeras for enhanced cytotoxicity and optimized liposome binding capability,” *Pharmaceutics*, vol. 13, 4 2021, ISSN: 19994923. DOI: 10.3390/pharmaceutics13040583.
- [42] A. Flayhan, H. D. Mertens, Y. Ural-Blimke, M. M. Molledo, D. I. Svergun, and C. Löw, “Saposin lipid nanoparticles: A highly versatile and modular tool for membrane protein research,” *Structure*, vol. 26, 2 2018, ISSN: 18784186. DOI: 10.1016/j.str.2018.01.007.
- [43] R. A. Villanueva, Y. Rouillé, and J. Dubuisson, *Interactions between virus proteins and host cell membranes during the viral life cycle*, 2005. DOI: 10.1016/S0074-7696(05)45006-8.
- [44] M. F. Brown, “Curvature forces in membrane lipid-protein interactions,” *Biochemistry*, vol. 51, 49 2012, ISSN: 00062960. DOI: 10.1021/bi301332v.
- [45] T. Baumgart, B. R. Capraro, C. Zhu, and S. L. Das, “Thermodynamics and mechanics of membrane curvature generation and sensing by proteins and lipids,” *Annual Review of Physical Chemistry*, vol. 62, 2011, ISSN: 0066426X. DOI: 10.1146/annurev.physchem.012809.103450.
- [46] R. Parthasarathy and J. T. Groves, *Curvature and spatial organization in biological membranes*, 2007. DOI: 10.1039/b608631d.
- [47] B. Božič, S. L. Das, and S. Svetina, “Sorting of integral membrane proteins mediated by curvature-dependent protein-lipid bilayer interaction,” *Soft Matter*, vol. 11, 12 2015, ISSN: 17446848. DOI: 10.1039/c4sm02289k.
- [48] B. G. Tenchov, “Nonuniform lipid distribution in membranes,” *Progress in Surface Science*, vol. 20, 4 1985, ISSN: 00796816. DOI: 10.1016/0079-6816(85)90014-0.
- [49] R. C. Capeta, J. A. Poveda, and L. M. Loura, “Non-uniform membrane probe distribution in resonance energy transfer: Application to protein-lipid selectivity,” vol. 16, 2006. DOI: 10.1007/s10895-005-0036-x.
- [50] M. Staykova, D. P. Holmes, C. Read, and H. A. Stone, “Mechanics of surface area regulation in cells examined with confined lipid membranes,” *Proceedings of the National Academy of Sciences of the United States of America*, vol. 108, 22 2011, ISSN: 00278424. DOI: 10.1073/pnas.1102358108.

- [51] H. Alimohamadi, A. S. Smith, R. B. Nowak, V. M. Fowler, and P. Rangamani, “Non-uniform distribution of myosin-mediated forces governs red blood cell membrane curvature through tension modulation,” *PLoS Computational Biology*, vol. 16, 5 2020, ISSN: 15537358. DOI: 10.1371/journal.pcbi.1007890.
- [52] H. Elliott *et al.*, “Myosin ii controls cellular branching morphogenesis and migration in three dimensions by minimizing cell-surface curvature,” *Nature Cell Biology*, vol. 17, 2 2015, ISSN: 14764679. DOI: 10.1038/ncb3092.
- [53] S. Singer and G. L. Nicolson, “The fluid mosaic model of the structure of cell membranes: Cell membranes are viewed as two-dimensional solutions of oriented globular proteins and lipids,” *Science*, vol. 175, 4023 1972.
- [54] H. A. Faizi, R. Dimova, and P. M. Vlahovska, “Viscosity of fluid membranes measured from vesicle deformation,” *bioRxiv*, 2021.
- [55] T. T. Hormel, S. Q. Kurihara, M. K. Brennan, M. C. Wozniak, and R. Parthasarathy, “Measuring lipid membrane viscosity using rotational and translational probe diffusion,” *Physical Review Letters*, vol. 112, 18 2014, ISSN: 10797114. DOI: 10.1103/PhysRevLett.112.188101.
- [56] E. A. Evans and R. M. Hochmuth, “Membrane viscoelasticity,” *Biophysical Journal*, vol. 16, 1 1976, ISSN: 00063495. DOI: 10.1016/S0006-3495(76)85658-5.
- [57] P. M. Vlahovska, “Nonequilibrium dynamics of lipid membranes: Deformation and stability in electric fields,” in 2010, vol. 12. DOI: 10.1016/B978-0-12-381266-7.00005-5.
- [58] M. E. Cerf, *Developmental programming and glucolipotoxicity: Insights on beta cell inflammation and diabetes*, 2020. DOI: 10.3390/metabo10110444.
- [59] R. Sanwlani and L. Gangoda, *Role of extracellular vesicles in cell death and inflammation*, 2021. DOI: 10.3390/cells10102663.
- [60] E. Nader, M. Romana, and P. Connes, *The red blood cell—inflammation vicious circle in sickle cell disease*, 2020. DOI: 10.3389/fimmu.2020.00454.
- [61] J. Schumann, “Does plasma membrane lipid composition impact the mirna-mediated regulation of vascular inflammation?” *Medical Hypotheses*, vol. 88, 2016, ISSN: 15322777. DOI: 10.1016/j.mehy.2016.01.012.
- [62] G. Battineni, G. G. Sagaro, N. Chintalapudi, F. Amenta, D. Tomassoni, and S. K. Tayebati, “Impact of obesity-induced inflammation on cardiovascular diseases (cvd),” *International Journal of Molecular Sciences*, vol. 22, 9 2021, ISSN: 14220067. DOI: 10.3390/ijms22094798.
- [63] T. V. Rohm, D. T. Meier, J. M. Olefsky, and M. Y. Donath, *Inflammation in obesity, diabetes, and related disorders*, 2022. DOI: 10.1016/j.immuni.2021.12.013.
- [64] N. Singh, D. Baby, J. Rajguru, P. Patil, S. Thakkannavar, and V. Pujari, “Inflammation and cancer,” *Annals of African Medicine*, vol. 18, 3 2019, ISSN: 09755764. DOI: 10.4103/aam.aam_56_18.

- [65] J. Ngo, C. Osto, F. Villalobos, and O. S. Shirihai, “Mitochondrial heterogeneity in metabolic diseases,” *Biology*, vol. 10, 9 Sep. 2021, ISSN: 20797737. DOI: 10.3390/biology10090927.
- [66] M. Parilla and S. Gurbuxani, *Red cell morphology in sickle cell disease*, 2020. DOI: 10.1182/BLOOD.2020007602.
- [67] Y. Wu, Y. Niu, F. Lv, W. Gao, and X. Shen, “Morphology classification of circulating tumor cells could be a predictor of recurrent disease in patients with non-small cell lung cancer after surgery.,” *Journal of Clinical Oncology*, vol. 38, 15_{suppl} 2020, ISSN: 0732-183X. DOI: 10.1200/jco.2020.38.15_suppl.e15530.
- [68] A. Jamali *et al.*, “Intravital multiphoton microscopy of the ocular surface: Alterations in conventional dendritic cell morphology and kinetics in dry eye disease,” *Frontiers in Immunology*, vol. 11, 2020, ISSN: 16643224. DOI: 10.3389/fimmu.2020.00742.
- [69] R. J. Bevan, T. R. Hughes, P. A. Williams, M. A. Good, B. P. Morgan, and J. E. Morgan, “Retinal ganglion cell degeneration correlates with hippocampal spine loss in experimental alzheimer’s disease,” *Acta Neuropathologica Communications*, vol. 8, 1 2020, ISSN: 20515960. DOI: 10.1186/s40478-020-01094-2.
- [70] Z. Zhang *et al.*, “Morphology-based prediction of cancer cell migration using an artificial neural network and a random decision forest,” *Integrative Biology (United Kingdom)*, vol. 10, 12 2018, ISSN: 17579708. DOI: 10.1039/c8ib00106e.
- [71] M. Fujitani *et al.*, “Morphology-based non-invasive quantitative prediction of the differentiation status of neural stem cells,” *Journal of Bioscience and Bioengineering*, vol. 124, 3 2017, ISSN: 13474421. DOI: 10.1016/j.jbiosc.2017.04.006.
- [72] D. Chen, J. P. Dunkers, W. Losert, and S. Sarkar, “Early time-point cell morphology classifiers successfully predict human bone marrow stromal cell differentiation modulated by fiber density in nanofiber scaffolds,” *Biomaterials*, vol. 274, 2021, ISSN: 18785905. DOI: 10.1016/j.biomaterials.2021.120812.
- [73] B. A. Lewis and D. M. Engelman, *Lipid bilayer thickness varies linearly with acyl chain length in fluid phosphatidylcholine vesicles*, 1983. DOI: 10.1016/S0022-2836(83)80007-2.
- [74] W. Rawicz, K. C. Olbrich, T. McIntosh, D. Needham, and E. A. Evans, “Effect of chain length and unsaturation on elasticity of lipid bilayers,” *Biophysical Journal*, vol. 79, 1 2000, ISSN: 00063495. DOI: 10.1016/S0006-3495(00)76295-3.
- [75] J. Frallicciardi, J. Melcr, P. Siginou, S. J. Marrink, and B. Poolman, “Membrane thickness, lipid phase and sterol type are determining factors in the permeability of membranes to small solutes,” *Nature Communications*, vol. 13, 1 2022, ISSN: 20411723. DOI: 10.1038/s41467-022-29272-x.

- [76] L. B. Li, I. Vorobyov, and T. W. Allen, “The role of membrane thickness in charged protein-lipid interactions,” *Biochimica et Biophysica Acta - Biomembranes*, vol. 1818, pp. 135–145, 2 Feb. 2012, ISSN: 00052736. DOI: 10.1016/j.bbamem.2011.10.026.
- [77] X. Liao and P. K. Purohit, “Kinetics of self-assembly of inclusions due to lipid membrane thickness interactions,” *Soft Matter*, vol. 17, 9 2021, ISSN: 17446848. DOI: 10.1039/d0sm01752c.
- [78] B. E. Uygun, T. Bou-Akl, M. Albanna, and H. W. Matthew, “Membrane thickness is an important variable in membrane scaffolds: Influence of chitosan membrane structure on the behavior of cells,” *Acta Biomaterialia*, vol. 6, 6 2010, ISSN: 17427061. DOI: 10.1016/j.actbio.2009.11.018.
- [79] A. Anishkin, S. H. Loukin, J. Teng, and C. Kung, *Feeling the hidden mechanical forces in lipid bilayer is an original sense*, 2014. DOI: 10.1073/pnas.1313364111.
- [80] H. Träuble and D. H. Haynes, “The volume change in lipid bilayer lamellae at the crystalline-liquid crystalline phase transition,” *Chemistry and Physics of Lipids*, vol. 7, 4 1971, ISSN: 00093084. DOI: 10.1016/0009-3084(71)90010-7.
- [81] O. S. Andersen and R. E. Koeppe, *Bilayer thickness and membrane protein function: An energetic perspective*, 2007. DOI: 10.1146/annurev.biophys.36.040306.132643.
- [82] J. A. Lundbæk, S. A. Collingwood, H. I. Ingólfsson, R. Kapoor, and O. S. Andersen, *Lipid bilayer regulation of membrane protein function: Gramicidin channels as molecular force probes*, 2010. DOI: 10.1098/rsif.2009.0443.
- [83] A. R. Battle, P. Ridone, N. Bavi, Y. Nakayama, Y. A. Nikolaev, and B. Martinac, *Lipid-protein interactions: Lessons learned from stress*, 2015. DOI: 10.1016/j.bbamem.2015.04.012.
- [84] H. W. Huang, “Deformation free energy of bilayer membrane and its effect on gramicidin channel lifetime,” *Biophysical Journal*, vol. 50, 6 1986, ISSN: 00063495. DOI: 10.1016/S0006-3495(86)83550-0.
- [85] N. Dan, P. Pincus, and S. A. Safran, *Membrane-induced interactions between inclusions*, 1993. DOI: 10.1021/la00035a005.
- [86] R. Phillips, T. Ursell, P. Wiggins, and P. Sens, *Emerging roles for lipids in shaping membrane-protein function*, 2009. DOI: 10.1038/nature08147.
- [87] I. M. Alarifi, *A comprehensive review on advancements of elastomers for engineering applications*, 2023. DOI: 10.1016/j.aiepr.2023.05.001.
- [88] S. R. Lavoie, P. Millereau, C. Creton, R. Long, and T. Tang, “A continuum model for progressive damage in tough multinetwork elastomers,” *Journal of the Mechanics and Physics of Solids*, vol. 125, 2019, ISSN: 00225096. DOI: 10.1016/j.jmps.2019.01.001.

- [89] Y. Zhang, C. Xuan, Y. Jiang, and Y. Huo, “Continuum mechanical modeling of liquid crystal elastomers as dissipative ordered solids,” *Journal of the Mechanics and Physics of Solids*, vol. 126, 2019, ISSN: 00225096. DOI: 10.1016/j.jmps.2019.02.018.
- [90] A. Ricker and P. Wriggers, *Systematic fitting and comparison of hyperelastic continuum models for elastomers*, 2023. DOI: 10.1007/s11831-022-09865-x.
- [91] H. Darijani and R. Naghdabadi, “Hyperelastic materials behavior modeling using consistent strain energy density functions,” *Acta Mechanica*, vol. 213, 3-4 2010, ISSN: 00015970. DOI: 10.1007/s00707-009-0239-3.
- [92] R Ogden, “Non-linear elastic deformations,” *Engineering Analysis with Boundary Elements*, vol. 1, 2 1984, ISSN: 09557997. DOI: 10.1016/0955-7997(84)90049-3.
- [93] A. Anssari-Benam and A. Bucchi, “A generalised neo-hookean strain energy function for application to the finite deformation of elastomers,” *International Journal of Non-Linear Mechanics*, vol. 128, 2021, ISSN: 00207462. DOI: 10.1016/j.ijnonlinmec.2020.103626.
- [94] M. C. Boyce and E. M. Arruda, “Swelling and mechanical stretching of elastomeric materials,” *Mathematics and Mechanics of Solids*, vol. 6, 6 2001, ISSN: 10812865. DOI: 10.1177/108128650100600605.
- [95] L. Bokobza and M. Kolodziej, “On the use of carbon nanotubes as reinforcing fillers for elastomeric materials,” *Polymer International*, vol. 55, 9 2006, ISSN: 09598103. DOI: 10.1002/pi.2064.
- [96] W. Noll, “Materially uniform simple bodies with inhomogeneities,” *Archive for Rational Mechanics and Analysis*, vol. 27, 1 1967, ISSN: 00039527. DOI: 10.1007/BF00276433.

Chapter 2

General Formulation and Preliminaries

2.1 Differential Geometry

To investigate the mechanics of hyperelastic material subjected to out-of-plane loadings, it is necessary to establish a surface coordinate system to express material positions in the referential and current configurations. The basic assumption is to treat the sheet of hyperelastic material as a continuous elastic surface (see, for instance, [1–3]). Within this postulation, we utilize the well-established relations from the differential geometry [4] for the model derivations. Let us suppose that Ω represents the referential configuration of the domain and ω for the evolving surface of the domain (Figure 2.1), where the material positions, before and after deformation, are respectively parameterized by the position vector \mathbf{X} and $\mathbf{r} \in \mathbb{R}^3$, where \mathbf{r} is defined by the mapping $\mathbf{r} = \mathbf{r}(\theta^\alpha)$.

Thus, the tangent vectors on the surface Ω and ω involve the material position \mathbf{X} and $\mathbf{r}(\theta^\alpha)$ can be correspondingly computed as

$$\mathbf{X}_\alpha = \frac{\partial \mathbf{X}}{\partial \theta^\alpha} \text{ and } \mathbf{a}_\alpha = \frac{\partial \mathbf{r}(\theta^\alpha)}{\partial \theta^\alpha}. \quad (2.1)$$

The normal field \mathbf{n} on the surface ω is the local orientation of the current configuration and is computed as $\mathbf{n}(\theta^1, \theta^2) = \frac{1}{2} \varepsilon^{\alpha\beta} \mathbf{a}_\alpha \times \mathbf{a}_\beta$, where $\varepsilon^{\alpha\beta} = e^{\alpha\beta} / \sqrt{a}$ refers to the permutation tensor density with $a = \det(a_{\alpha\beta})$, where $e^{11} = e^{22} = 0$ and $e^{12} = -e^{21} =$

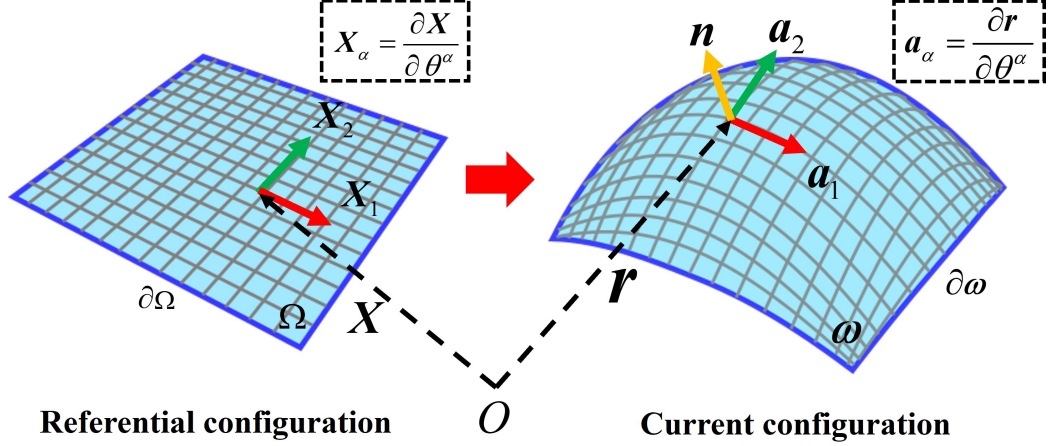


Figure 2.1: Schematic of surface configurations: surface vectors to the specific trajectories in referential (Ω) and current configurations (ω), respectively.

1, $a_{\alpha\beta}$ is the surface metric of the current configuration and is positive-definite in general (i.e. $a > 0$), given by

$$a_{\alpha\beta} = \mathbf{a}_\alpha \cdot \mathbf{a}_\beta. \quad (2.2)$$

The positive definiteness of a metric $a_{\alpha\beta}$ further suggests the existence of dual metric $a^{\alpha\beta}$ which is the inverse of the metric $a_{\alpha\beta}$ (i.e. $a^{11} = \frac{a_{22}}{a}$, $a^{22} = \frac{a_{11}}{a}$, $a^{21} = a^{12} = \frac{-a_{12}}{a}$). Hence, the dual basis of \mathbf{a}_β can be defined via the relation $\mathbf{a}^\alpha = a^{\alpha\beta} \mathbf{a}_\beta$. These relations furnish the well-known Gauss and Weingarten equations

$$\mathbf{a}_{\alpha;\beta} = \Gamma_{\alpha\beta}^\gamma \mathbf{a}_\gamma + b_{\alpha\beta} \mathbf{n}; \quad b_{\alpha\beta} = \mathbf{a}_{\alpha,\beta} \cdot \mathbf{n} \quad (\text{Gauss}) \quad \text{and} \quad (2.3)$$

$$b_{\alpha\beta} = -\mathbf{n}_{,\alpha} \cdot \mathbf{a}_\beta \quad (\text{Weingarten}), \quad (2.4)$$

with

$$\mathbf{a}_{\alpha;\beta} = b_{\alpha\beta} \mathbf{n} \quad \text{and} \quad \mathbf{n}_{,\alpha} = -b_{\alpha\beta} \mathbf{a}^\beta = -b_\alpha^\beta \mathbf{a}_\beta. \quad (2.5)$$

In the above, the semi-colon denotes the surface covariant differentiation in the sense of the Levi-Civita connection on a surface, the covariant derivative leads to

$$\mathbf{r}_{;ij} = (\mathbf{r}_{;i})_{,j} - \bar{\Gamma}_{ij}^\varepsilon \mathbf{r}_{,\varepsilon} \quad \text{and} \quad \mathbf{a}_{\alpha;\beta} = \mathbf{a}_{\alpha,\beta} - \Gamma_{\alpha\beta}^\lambda \mathbf{a}_\lambda, \quad (2.6)$$

where $\bar{\Gamma}_{ij}^k$ and $\Gamma_{\alpha\beta}^\lambda$ represent the Christoffel symbols in the reference and current configurations, respectively; the $b_{\alpha\beta}$ are the coefficients of the second fundamental

form and b_α^β are the mixed components of the curvature. Lastly, the covariant cofactor is defined by

$$\tilde{b}^{\alpha\beta} = \varepsilon^{\alpha\lambda}\varepsilon^{\beta\gamma}b_{\lambda\gamma}. \quad (2.7)$$

2.2 Canham–Helfrich Theory

The long history of developing the strain energy models of lipid bilayer dates back to 50 years ago when Canham was devising a model for explaining the biconcave profile of red blood cells [5]. The model is described as a bending-energy density in terms of the square of the mean curvature on the membrane surface. The proceeding work of Helfrich further clarified that the strain energy density of a lipid bilayer surface is dependent on the surface curvatures and their product [6]. These works jointly define the strain energy density of lipid bilayer as

$$W(H, K) = k(H - H_0)^2 + \bar{k}K, \quad (2.8)$$

where k and \bar{k} are bending rigidities, H_0 is spontaneous mean-curvature, H and K are respectively the mean and Gaussian curvatures (H and K , in fact, are scalar invariants that describe the shape of the lipid bilayer [7]). Using differential geometry and expression of tensor, H and K are given by [4]

$$H = \frac{1}{2}a^{\alpha\beta}b_{\alpha\beta} \quad \text{and} \quad K = \frac{1}{2}\varepsilon^{\alpha\beta}\varepsilon^{\lambda\mu}b_{\alpha\lambda}b_{\beta\mu}, \quad (2.9)$$

where $a_{\alpha\beta}$ is the surface metric and $a^{\alpha\beta}$ is the inverse of $a_{\alpha\beta}$. $\varepsilon^{\alpha\beta} = e^{\alpha\beta}/\sqrt{a}$ is the permutation tensor with $a = \det(a_{\alpha\beta})$, where $e^{12} = -e^{21} = 1$, $e^{11} = e^{22} = 0$. $b^{\alpha\beta}$ are the covariant components of the surface curvature tensor in the second fundamental form.

2.3 Neo-Hookean Hyperelastic Model

The Neo-Hookean model is the hyperelastic material model which is utilized to present the strain energy density of matrix material for fiber-reinforced composites in this dis-

sertation. This model is one of the most typical and widely used hyperelastic material models for predicting the strain-stress behavior of hyperelastic materials [8]. Similar to Hooke’s law, such type of material performs a linear stress-strain relationship when subjected to small deformations, while it shows a non-linear strain-stress trend for significant deformation conditions. The incompressible and compressible types of the Neo-Hookean model are respectively

$$W(I_1) = \mu(I_1 - 3) \quad (2.10)$$

and

$$W(I_1, J) = \mu(I_1 - 3 - 2\ln J) + \eta(J - 1)^2, \quad (2.11)$$

where μ and η are material constants, I_1 is the first principal invariant of the right Cauchy–Green tensor, i.e.,

$$I_1 = \text{tr}(\mathbf{F}^T \mathbf{F}), \quad (2.12)$$

in which, \mathbf{F} is the deformation gradient defined as

$$\mathbf{F} = \frac{\partial \mathbf{r}(\theta^\alpha)}{\partial \mathbf{X}} = \frac{\partial \mathbf{r}(\theta^\alpha)}{\partial \theta^\alpha} \otimes \frac{\partial \theta^\alpha}{\partial \mathbf{X}} = \mathbf{a}_\alpha \otimes \mathbf{X}^\alpha \quad (2.13)$$

on the deformed hyperelastic material surface (see, Figure 2.1), where \mathbf{X}^α are bases of the initial configuration. Using \mathbf{F} , the surface distension J of hyperelastic material is expressed with

$$J = \det(\mathbf{F}), \quad (2.14)$$

and the hyperelastic material is incompressible for $J = 1$.

2.4 Notation

Throughout the thesis, the transpose, inverse, cofactor, and trace of tensor \mathbf{A} are expressed using standard notations \mathbf{A}^T , \mathbf{A}^{-1} , \mathbf{A}^* and $\text{tr}(\mathbf{A})$, respectively. The calculation of tensor is implemented by utilizing symbol \otimes , and the inner product between tensors \mathbf{A} and \mathbf{B} is denoted as $\mathbf{A} \cdot \mathbf{B} = \text{tr}(\mathbf{A}\mathbf{B}^T)$. $|\mathbf{A}|$ is the determinant of tensor

A. For the index of tensor components, Latin symbols index $\{1, 2, 3\}$, Greek indices take the values in $\{1, 2\}$, and when they are repeated, they are summed over their ranges. Lastly, $(*)_{,\alpha}$ denotes the derivative of “*” with respect to a coordinate θ^α and W_K stands for the derivatives of a scalar-valued function $W(K)$ with respect to the parameter K . The same prescription is applied when taking the partial derivative of a scalar-valued function \mathcal{F} to tensor \mathbf{A} , which is presented using the subscript form $\mathcal{F}_A = \partial\mathcal{F}/\partial\mathbf{A}$. The explained differential geometry equations will be applied directly in the formulation process for the sake of brevity.

References

- [1] D. J. Steigmann, “Fluid films with curvature elasticity,” *Archive for Rational Mechanics and Analysis*, vol. 150, 2 1999, ISSN: 00039527. DOI: 10.1007/s002050050183.
- [2] D. J. Steigmann, “On the relationship between the cosserat and kirchhoff-love theories of elastic shells,” *Mathematics and Mechanics of Solids*, vol. 4, 3 1999, ISSN: 10812865. DOI: 10.1177/108128659900400301.
- [3] C. Goodbrake and D. J. Steigmann, “Mechanics of an elastic membrane infused with a liquid,” *International Journal of Mechanical Sciences*, vol. 149, 2018, ISSN: 00207403. DOI: 10.1016/j.ijmecsci.2017.07.062.
- [4] I. Sokolnikoff, *Tensor Analysis: Theory and Applications* (Applied mathematics series). Wiley, 1951. [Online]. Available: https://books.google.ca/books?id=q_pQAAAAMAAJ.
- [5] P. B. Canham, “The minimum energy of bending as a possible explanation of the biconcave shape of the human red blood cell,” *Journal of Theoretical Biology*, vol. 26, 1 1970, ISSN: 10958541. DOI: 10.1016/S0022-5193(70)80032-7.
- [6] W. Helfrich, “Elastic properties of lipid bilayers: Theory and possible experiments,” *Zeitschrift fur Naturforschung - Section C Journal of Biosciences*, vol. 28, 11-12 1973, ISSN: 18657125. DOI: 10.1515/znc-1973-11-1209.
- [7] B. Seguin and E. Fried, “Microphysical derivation of the canham-helfrich free-energy density,” *Journal of Mathematical Biology*, vol. 68, 3 2014, ISSN: 14321416. DOI: 10.1007/s00285-013-0647-9.
- [8] A. Kossa, M. T. Valentine, and R. M. McMeeking, “Analysis of the compressible, isotropic, neo-hookean hyperelastic model,” *Meccanica*, vol. 58, 1 2023, ISSN: 15729648. DOI: 10.1007/s11012-022-01633-2.

Chapter 3

An Analysis of Lipid Membrane Morphology in the Presence of Coordinate Dependent Non-uniformity

In this Chapter, a model for the mechanics of lipid membranes with non-uniform (coordinate-dependent) properties is discussed. The coordinate-dependent responses of the lipid membranes are investigated via the augmented non-uniform energy function, and the associated material parameters are dependent explicitly on the surface coordinates. To demonstrate the mechanics of lipid membranes, the normal and tangential Euler equilibrium equations are formulated, through which the coordinate-dependent responses of membranes are characterized. Additionally, the admissible boundary conditions are invoked from the existing literature describing the corresponding non-linear model, yet the boundary conditions are reformulated and adapted to the present framework. Within the prescription of superposed incremental deformations, a compatible linearized model is formulated where a complete analytical solution is obtained to describe the non-uniform responses of the membrane subjected to protein-membrane interactions.

3.1 Introduction

The study of the morphological responses of lipid membranes has been the subject of intense research that has significantly enhanced our understanding of a wide range of essential cellular functions such as fusion, budding and vesicular transport [1–3]. Since the lipid membranes are quite fragile and extremely thin (typically 3 to 5nm), the analyses of the various mechanical properties of lipid membranes are, most often, achieved via the use of an artificial “model”. This includes the development of continuum models describing the mechanics of the membranes which is also in a period of intense study (see, for example, [4–7]). Lipid bilayers are complex assemblies of lipid molecules (typically, phospholipids) that are characterized by hydrophilic head groups and hydrophobic tails. Driven by the hydrophobic effect, these molecules arrange themselves into a two-layer sheet (lipid bilayer) with reverse molecule orientations for each layer, providing a selective permeability barrier for single cells [6–9]. Therefore, a lipid bilayer can be regarded as a closed membrane, much like a thin film sandwich structure where a fluid-like substance is present between the two films. Within this context, the development of theoretical prediction models for the mechanics of lipid membranes are facilitated by the differential geometry of a surface and the bending energy of a lipid membrane can be expressed by the function of mean and Gaussian curvature on a membrane surface [10, 11]. Under the principle of free energy minima, the energy potential regarding the Helfrich type is proposed by accommodating the bilayer symmetry [12], from which a system of “membrane shape equation” is formulated. Such type of model has been successfully implemented in a wide range of membrane problems, including budding formations [13, 14], protein-membrane interactions [5, 15, 16], and spontaneous curvatures [17, 18].

Recent efforts highlighted refining the lipid membrane’s energy potential and the associated mathematical framework to obtain more comprehensive and accurate models for the descriptions of lipid membranes. The authors in [19] developed the general

non-linear model of membranes which incorporates the effects of intra-membrane viscosity on membrane surfaces [20, 21] and predicted the deformations of membranes subjected to uniformly distributed pressures. Within this prescription, a compatible linear model was formulated in [22] and solved within the prescription of superposed incremental deformations. In there, the authors obtained a complete analytical solution that describes the deformations of lipid membranes subjected to intra-membrane viscous flow and protein-membrane interactions. Furthermore, the tilt and distension of lipid membranes were discussed in [23] where the author established a constitutive framework that incorporates the tilt and distention-involved responses of membranes. The model is further adopted in the studies of variable tilt [24] and thickness distension (without tilt) [25] of the membranes. To this end, the author in [6] developed a series of comprehensive models (including the shape equations and admissible boundary conditions) for the mechanics of lipid membranes which accommodates tilt, distension, diffusion, and viscous flow from the theory of the three-dimensional liquid crystal [26–28].

Most of the aforementioned studies presume uniform properties throughout the membrane (i.e. coordinate independent) to obtain mathematically tractable systems and analyses. Nevertheless, in general, the responses of membranes are coordinate-dependent due to the complex nature of membrane systems and processes such as diffusion and non-uniform protein distributions [29]. For instance, the drug-induced protein diffusion may be considered as an energy dissipating process [30] and therefore may further induce non-uniformity in the membranes. In addition, phase separations and/or local enrichments of particular lipid species arising in membrane-protein interactions [31], may be considered as a source of non-uniformity. Furthermore, protein-induced deformations may give rise to the potential of non-uniformity. For example, BIN-amphiphysin-Rvs (BAR) proteins behave like scaffold-like structures, acting as a local tension field, which may be viewed as non-uniformity [32].

A class of problems pertaining to the non-uniform properties of lipid membranes

were discussed in [4] and [20] where the non-uniformity was accommodated via the coordinate-dependent energy function of membranes. Further, authors in [17] and [29] investigated the non-uniform properties of membranes induced by the surface diffusion and possible non-uniform protein distributions, where the non-uniform spontaneous curvature of the membranes was predicted. However, the deformation analysis of membranes accounting for explicit coordinate-dependent non-uniformity, particularly those arising in the membrane shape equation, remains lacking in the literature.

In the present work, we study the continuum model regarding the Helfrich type that describes the non-uniform properties of lipid membranes subjected to protein-membrane interactions and lateral pressures. The non-uniformity of the membrane is incorporated via the introduction of non-uniform energy distribution functions which are explicitly dependent on the surface coordinates. Then, the corresponding normal and tangential Euler equilibrium equations are derived through which the coordinate-dependent responses of membranes are characterized. To demonstrate the physical performance of lipid membranes, the admissible set of boundary conditions is invoked from the work of [5] and is reformulated in the present context to accommodate the continuum model of non-uniform membranes. Within the prescription of superposed incremental deformations [33, 34], the shape equations of linear type are developed and solved analytically for the purpose of describing the non-uniform responses of the membrane undergoing protein-membrane interactions. The formulation of the linear tangential and normal Euler equations shows that the terms associated with the material parameters (coordinate-dependent) vanish in case of small deformations. The analytical and numerical results suggest that the non-uniform responses of membranes are intrinsically limited to the augmented energy potential which is explicitly dependent on the surface coordinates. To demonstrate the model, both circumferentially and radially non-uniform energy distribution functions are considered to assimilate the potential non-uniformity of the lipid membrane, and the resulting deformation fields demonstrate clear signs of coordinate dependency. Furthermore, the solutions

obtained from the proposed linear model demonstrate reasonable agreement with those obtained from the non-linear analysis for the small deformation regime. In particular, we have shown that the principle of superposition from linear elasticity remains valid for the present application. It is noteworthy that the analytical results in the case of combined radially and circumferentially non-uniform membranes can be directly obtained via the summation of the analytical solutions obtained respectively from the circumferentially and radially non-uniform cases. The numerical solutions of non-linear cases are also obtained for comparisons with those from the linear analysis and demonstrations of the more general coordinate-dependent responses of membranes. Particularly, the non-linear solutions phenomenologically predict the off-centered biconcave morphology of lipid membranes [35, 36] and the multiple peak formations of abnormal cell membranes (burr cell), which are commonly observed in uremia and chronic kidney disease [37, 38]. Lastly, the presented solutions demonstrate the model's capability and generality of recovering to the uniform membranes as described in [5] and [22].

3.2 Non-uniform Membrane Shape Equation

The membrane shape equations are given by [5]

$$\Delta\left(\frac{1}{2}W_H\right) + (W_K)_{;\beta\alpha}\tilde{b}^{\beta\alpha} + W_H(2H^2 - K) + 2KHW_K - 2H(W + \lambda) = P \quad (3.1)$$

and

$$\lambda_{,\alpha} = -\frac{\partial W}{\partial \theta^\alpha} \quad \text{on } \omega, \quad (3.2)$$

where the Δ means the surface Laplacian, P presents lateral pressure, and λ is the Lagrange multiplier determining the intrinsic property of the lipid membrane. Eq. (3.2) indicates the derivative to λ is the negative of the partial derivative of strain energy density on the surface coordinate θ^α . If the membrane energy potential W does not depend explicitly on the coordinates (i.e., membranes with uniformly distributed

strain energy), the Eq. (3.2) yields [17]

$$\lambda = \text{constant}, \quad \because \lambda_{,\alpha} = 0, \quad (3.3)$$

and the values of λ may be configured via the intrinsic properties of lipid membrane (see, for example, [16]). In the case of a non-uniform membrane, it is found that [5]

$$\lambda_{,\alpha} = -\frac{\partial W}{\partial \theta^\alpha} \neq 0. \quad (3.4)$$

Eq. (3.4) presents the explicit coordinate dependence of the strain energy function W which arises from the possible non-uniformity of the membrane. Hence, to accommodate a particular state of non-uniformity, λ must be determined by solving the relevant Euler equations, i.e., two tangential equations in the respective direction of the coordinate (Eq.(3.4)) and the membrane normal shape equation (Eq. (3.1)). In the present study, we assimilate non-uniform responses of membranes by proposing the modified Helfrich energy potential

$$W(H, K; \theta^\alpha) = \phi(\theta^\alpha) + \alpha(\theta^\alpha)H^2 + \beta(\theta^\alpha)K. \quad (3.5)$$

It is noted that the uniform membrane case (i.e. $W = kH^2 + \bar{k}K$ [12]) can be retrieved from Eq. (3.5) by setting $\phi(\theta^\alpha) = 0$, $\alpha(\theta^\alpha) = k$ and $\beta(\theta^\alpha) = \bar{k}$. In view of Eq. (3.5), we evaluate

$$W_H = 2\alpha(\theta^\alpha)H, \quad W_K = \beta(\theta^\alpha), \quad (3.6)$$

therefore, the furnished normal shape equation is obtained from Eq. (3.1)

$$\Delta(\alpha(\theta^\alpha)H) + (\beta(\theta^\alpha))_{;\beta\alpha} \tilde{b}^{\beta\alpha} + 2\alpha(\theta^\alpha)H(H^2 - K) - 2H(\phi(\theta^\alpha) + \lambda) = P. \quad (3.7)$$

In the above, since $\beta(\theta^\alpha)$ is a scalar-valued function, $(\beta(\theta^\alpha))_{;\beta\alpha}$ can be evaluated as

$$\beta(\theta^\alpha)_{;\beta\alpha} = (\beta(\theta^\alpha))_{;\beta\alpha} = \beta(\theta^\alpha)_{,\beta\alpha} - \beta(\theta^\alpha)_{,\lambda} \Gamma_{\beta\alpha}^\lambda, \quad (3.8)$$

and $\tilde{b}^{\beta\alpha}$ is the contravariant cofactor defined in Chapter 2 (Eq. (2.7)). Further, from Eq. (3.5), we compute

$$\begin{aligned} W_{,\alpha} &= W_H H_{,\alpha} + W_K K_{,\alpha} + \frac{\partial W}{\partial \theta^\alpha} \Big|_{expl} \\ &= 2\alpha(\theta^\alpha) H H_{,\alpha} + \beta(\theta^\alpha) K_{,\alpha} + \frac{\partial W}{\partial \theta^\alpha} \Big|_{expl}, \end{aligned} \quad (3.9)$$

where $\partial W/\partial\theta^\alpha$ is the explicit coordinate derivatives of W computed as

$$\frac{\partial W}{\partial\theta^\alpha} = \frac{\partial\phi(\theta^\alpha)}{\partial\theta^\alpha} + \frac{\partial\alpha(\theta^\alpha)}{\partial\theta^\alpha}H^2 + \frac{\partial\beta(\theta^\alpha)}{\partial\theta^\alpha}K. \quad (3.10)$$

Thus, the associated Euler equilibrium equations are found to be

$$\lambda_{,r} = -\frac{\partial W}{\partial\theta^r} = -\left[\frac{\partial\phi(\theta^\alpha)}{\partial\theta^r} + \frac{\partial\alpha(\theta^\alpha)}{\partial\theta^r}H^2 + \frac{\partial\beta(\theta^\alpha)}{\partial\theta^r}K\right] \quad (3.11)$$

and

$$\lambda_{,\theta} = -\frac{\partial W}{\partial\theta^\theta} = -\left[\frac{\partial\phi(\theta^\alpha)}{\partial\theta^\theta} + \frac{\partial\alpha(\theta^\alpha)}{\partial\theta^\theta}H^2 + \frac{\partial\beta(\theta^\alpha)}{\partial\theta^\theta}K\right], \quad (3.12)$$

where $\phi(\theta^\alpha)$, $\beta(\theta^\alpha)$ and $\gamma(\theta^\alpha)$ can be chosen to achieve particular types of non-uniform distributions.

It is noteworthy that the proposed energy density function Eq. (3.5), can be directly used in conjunction with the existing results (Eqs. (3.1)-(3.2)) to yield the associated Euler equations (i.e. Eqs. (3.7), (3.11) and (3.12)) without further modifications (see, **Remark 1** below). The analogous cases regarding the refinement of the energy density function W results in non-standard forms of the shape equation have been discussed in [4], [17], and [29].

Remark 1. Since the coordinate derivatives of W appear only on the tangential variations, the introduction of the non-uniform energy function which depends on the surface coordinates θ^α (e.g $\phi(\theta^\alpha)$, $\alpha(\theta^\alpha)$, etc...), has no effects on the structure of the shape equation (Eq. (3.1)). To see this, we consider the virtual displacement of the equilibrium position field $\mathbf{r}(\theta^\alpha)$ evaluated at the particular configuration of the surface (for instance, $\epsilon = 0$) as

$$\mathbf{u}(\theta^\alpha) = \frac{\partial\mathbf{r}(\theta^\alpha; \epsilon)}{\partial\epsilon} \equiv \dot{\mathbf{r}}. \quad (3.13)$$

The decompositions of $\mathbf{u}(\theta^\alpha)$ onto the tangential and normal directions then yield

$$\mathbf{u}(\theta^\alpha) = u^\alpha \mathbf{a}_\alpha + w(\theta^\alpha) \mathbf{n}, \quad (3.14)$$

where $u^\alpha = \dot{\mathbf{r}} \cdot \mathbf{a}^\alpha$ and $w = \dot{\mathbf{r}} \cdot \mathbf{n}$ are respectively the tangential and normal components of displacement \mathbf{u} . Now, the variations of the energy function W are evaluated using

the chain rule

$$\dot{W} = \frac{\partial W}{\partial \epsilon} = \frac{dW}{d\theta^\alpha} \frac{\partial \theta^\alpha}{\partial \mathbf{r}} \cdot \frac{\partial \mathbf{r}}{\partial \epsilon} + \frac{dW}{dn(\theta^\alpha)} \frac{\partial n(\theta^\alpha)}{\partial \mathbf{r}} \cdot \frac{\partial \mathbf{r}}{\partial \epsilon} = W_{,\alpha} \mathbf{a}^\alpha \cdot \mathbf{u} + W_n \mathbf{n} \cdot \mathbf{u}. \quad (3.15)$$

Substituting Eq. (3.14) into Eq. (3.15) and using $\mathbf{a}^\alpha \cdot \mathbf{n} = \mathbf{a}_\alpha \cdot \mathbf{n} = \mathbf{0}$, we find

$$\dot{W} = W_{,\alpha} u^\alpha + W_n w, \quad (3.16)$$

where $W_{,\alpha}$ includes the explicit coordinate derivative $\partial W / \partial \theta^\alpha$ (see, Eq. (3.9) and Eq. (3.10)). Further, the associated Euler equations are given by (see, [5] and [25])

$$u^\alpha [W_H H_{,\alpha} + W_K K_{,\alpha} - (W_{,\alpha} + \lambda_{,\alpha})] = 0 \quad (3.17)$$

and

$$w [\Delta (\frac{1}{2} W_H) + (W_K)_{;\beta\alpha} \tilde{b}^{\beta\alpha} + W_H (2H^2 - K) + 2KH W_K - 2H(W + \lambda)] = wP, \quad (3.18)$$

where $W_{,\alpha}$ and $\lambda_{,\alpha}$ are expressed in Eqs. (3.9)-(3.11), and caution needs to be taken that $W_{,\alpha}$ should not be confused with $\partial W / \partial \theta^\alpha$ unlike other terms (e.g., $H_{,\alpha} = \partial H / \partial \theta^\alpha$, etc...), since, in general, W is explicitly dependent on the surface coordinate θ^α (i.e., $W_{,\alpha} \neq \partial W / \partial \theta^\alpha$). Lastly, by invoking Eq. (3.9), Eq. (3.17) is reduced to

$$\lambda_{,\alpha} = -\frac{\partial W}{\partial \theta^\alpha}. \quad (3.19)$$

Therefore, it is evident from Eqs. (3.18)-(3.19) that the resulting Euler equations remain intact despite the presence of the non-uniform distributions of $\phi(\theta^\alpha)$, $\alpha(\theta^\alpha)$ and $\beta(\theta^\alpha)$.

3.2.1 Formulations under Monge parametric representation

Using the Monge representation, the parametric position vector can be expressed as

$$\mathbf{r}(\theta^\alpha) = \theta(\theta^\alpha) + z(\theta^\alpha) \mathbf{k}, \quad (3.20)$$

where $\theta(\theta^\alpha)$ is the surface coordinates of a plane ω , and \mathbf{k} is the unit normal on ω . Hence, the out-of-plane deformation of the membrane is determined by the single

function $z(\theta^\alpha)$. In the axisymmetric Polar coordinates, Eq. (3.20) becomes

$$\mathbf{r} = r\mathbf{e}_r(\theta) + z(r, \theta)\mathbf{k}, \quad \mathbf{e}_r(\theta) = \cos\theta\mathbf{e}_1 + \sin\theta\mathbf{e}_2. \quad (3.21)$$

The substitution of Eq. (3.21) into surface tangent \mathbf{a}_α , surface metric $a_{\alpha\beta}$ and its determinant a yields

$$\mathbf{a}_1 = \mathbf{e}_r + z_{,r}\mathbf{k}, \quad \mathbf{a}_2 = r\mathbf{e}_\theta + z_{,\theta}\mathbf{k}, \quad (3.22)$$

$$a_{11} = \mathbf{a}_1 \cdot \mathbf{a}_1 = 1 + z_{,r}^2, \quad a_{22} = r^2 + z_{,\theta}^2, \quad a_{12} = z_{,r}z_{,\theta} = a_{21}, \quad (3.23)$$

and

$$a = \det(a_{\alpha\beta}) = r^2(1 + z_{,r}^2) + z_{,\theta}^2, \quad (3.24)$$

which are respectively, the surface tangents, the surface metric, and the determinant of surface metric. Similarly, the contravariant dual basis and corresponding metric components ($a^{11} = \frac{a_{22}}{a}$, $a^{22} = \frac{a_{11}}{a}$, $a^{21} = a^{12} = \frac{-a_{12}}{a}$) can be computed as

$$\begin{aligned} \mathbf{a}^1 &= a^{11}\mathbf{a}_1 + a^{12}\mathbf{a}_2 = \frac{1}{a}[(r^2 + z_{,\theta}^2)\mathbf{e}_r - rz_{,r}z_{,\theta}\mathbf{e}_\theta + r^2z_{,r}\mathbf{k}], \\ \mathbf{a}^2 &= \frac{1}{a}[-rz_{,r}z_{,\theta}\mathbf{e}_r + r(1 + z_{,r}^2)\mathbf{e}_\theta + z_{,\theta}\mathbf{k}], \quad \text{and} \end{aligned} \quad (3.25)$$

$$a^{11} = \frac{r^2 + z_{,\theta}^2}{a}, \quad a^{22} = \frac{1 + z_{,r}^2}{a}, \quad a^{12} = a^{21} = -\frac{z_{,r}z_{,\theta}}{a}. \quad (3.26)$$

Further, from Eqs. (3.22)-(3.26), the resulting surface normal and the curvature tensor are defined by

$$\mathbf{n} = \frac{\mathbf{a}^1 \times \mathbf{a}^2}{\sqrt{a}} = \frac{1}{\sqrt{a}}(-z_{,\theta}\mathbf{e}_\theta - rz_{,r}\mathbf{e}_r + r\mathbf{k}), \quad \mathbf{b} = b_{\alpha\beta}\mathbf{a}^\alpha \otimes \mathbf{a}^\beta; \quad b_{\alpha\beta} = \mathbf{a}_{\beta,\alpha} \cdot \mathbf{n}. \quad (3.27)$$

Thus, the complete expression of \mathbf{b} , under the axisymmetric Polar coordinate is obtained as

$$\begin{aligned} \mathbf{b} &= \frac{rz_{,rr}}{a^2\sqrt{a}}[(r^2 + z_{,\theta}^2)\mathbf{e}_r - rz_{,r}z_{,\theta}\mathbf{e}_\theta + r^2z_{,r}^2\mathbf{k}] \otimes [(r^2 + z_{,\theta}^2)\mathbf{e}_r - rz_{,r}z_{,\theta}\mathbf{e}_\theta + r^2z_{,r}^2\mathbf{k}] + \\ &\quad \frac{rz_{,r\theta} - z_{,\theta}}{a^2\sqrt{a}}[(r^2 + z_{,\theta}^2)\mathbf{e}_r - rz_{,r}z_{,\theta}\mathbf{e}_\theta + r^2z_{,r}^2\mathbf{k}] \otimes [-rz_{,r}z_{,\theta}\mathbf{e}_r + r(1 + z_{,r}^2)\mathbf{e}_\theta + z_{,\theta}\mathbf{k}] + \\ &\quad \frac{rz_{,r\theta} - z_{,\theta}}{a^2\sqrt{a}}[-rz_{,r}z_{,\theta}\mathbf{e}_r + r(1 + z_{,r}^2)\mathbf{e}_\theta + z_{,\theta}\mathbf{k}] \otimes [(r^2 + z_{,\theta}^2)\mathbf{e}_r - rz_{,r}z_{,\theta}\mathbf{e}_\theta + r^2z_{,r}^2\mathbf{k}] + \\ &\quad \frac{r^2z_{,r} - rz_{,\theta\theta}}{a^2\sqrt{a}}[-rz_{,r}z_{,\theta}\mathbf{e}_r + r(1 + z_{,r}^2)\mathbf{e}_\theta + z_{,\theta}\mathbf{k}] \otimes \\ &\quad [-rz_{,r}z_{,\theta}\mathbf{e}_r + r(1 + z_{,r}^2)\mathbf{e}_\theta + z_{,\theta}\mathbf{k}], \end{aligned} \quad (3.28)$$

where the coefficients of the second fundamental form $b_{\alpha\beta}$ can be formulated using Eqs. (3.22), (3.25), (3.27) and (3.26), for example,

$$b_{11} = \mathbf{n} \cdot \mathbf{a}_{1,1} = \frac{1}{\sqrt{a}} r z_{,rr}; \quad \mathbf{a}_{1,1} = \frac{\partial(\mathbf{e}_r(\theta) + z_{,r}(r, \theta)\mathbf{k})}{\partial r} = z_{,rr}\mathbf{k}, \quad (3.29)$$

and the computations are likewise for b_{22} , b_{12} and b_{21} .

Lastly, from Eqs. (2.9) (in Chapter 2) and (3.26)-(3.28), we find the following expressions for the mean and Gaussian curvature

$$H = \frac{1}{2a^{3/2}} [r^3 z_{,rr} + r^2 z_{,r} + r^2 z_{,r}^3 + r z_{,rr} z_{,\theta}^2 - 2r z_{,r\theta} z_{,r} z_{,\theta} + r z_{,\theta\theta} + r z_{,\theta\theta} z_{,r}^2 + 2z_{,r} z_{,\theta}^2] \quad (3.30)$$

and

$$K = \frac{1}{a^2} [r^3 z_{,r} z_{,rr} + r^2 z_{,rr} z_{,\theta\theta} - r^2 z_{,r\theta}^2 + 2r z_{,r\theta} - z_{,\theta}^2]. \quad (3.31)$$

In the implementation of the Monge parameterization, Eq. (3.7) can be reformulated by using the results in Eqs. (3.22)-(3.31). The corresponding formulations are relatively straightforward and hence omitted for the sake of simplicity.

Our intention is to assimilate the protein-membrane interactions within the presence of non-uniform energy distributions. For this purpose, the following interaction boundary conditions are adopted from the work of [5]

$$F_v \cos \gamma + F_n \sin \gamma - M \mathbf{n} \cdot (\nabla_{\Gamma} \gamma - \mathbf{B} \mathbf{n}) = \sigma, \quad F_{\tau} - M \boldsymbol{\tau} \cdot (\nabla_{\Gamma} \gamma - \mathbf{B} \mathbf{n}) = \mathbf{0}, \quad (3.32)$$

$$F_v = W + \lambda - \kappa_v M, \quad F_{\tau} = -\tau M, \quad F_n = (\tau W_K)' - \left(\frac{1}{2} W_H\right)_{,v} - (W_K)_{,\beta} \tilde{b}^{\alpha\beta} v_{\alpha}, \quad (3.33)$$

where F_i , M are respectively the forces in i directions and bending moment on the boundary. Also, \mathbf{B} , $\boldsymbol{\tau} \cdot \mathbf{v} \cdot \mathbf{n}$ and γ are, respectively, the curvature tensor of the interacting boundary, the associated normal-tangential coordinates and the interaction angle. In the present case, the protein-membrane interaction can be considered as the non-uniform membrane interacting with the cylinder owning radius R , we find

$$\mathbf{B} = -R^{-1} \mathbf{e}_{\theta} \otimes \mathbf{e}_{\theta} \text{ and } \gamma = \pi/2. \quad (3.34)$$

Accordingly, Eq. (3.32) reduces to

$$F_n = \sigma \text{ and } F_{\tau} = 0 \quad (\because \cos \gamma = 0, \nabla_{\Gamma} \gamma = 0, \text{ and } \mathbf{n} \cdot \mathbf{e}_{\theta} = 0) \quad (3.35)$$

on the interacting boundary Γ . Further, in view of Eqs. (3.6) and (3.32)₁, Eq. (3.33)₃ yields

$$F_n = [\tau(s)\beta(\theta^\alpha)]' - [\alpha(\theta^\alpha)H]_{,v} - [\beta(\theta^\alpha)]_{,\beta}\tilde{b}^{\alpha\beta}v_\alpha = \sigma, \quad (3.36)$$

where $[\tau(s)\beta(\theta^\alpha)]'$ is the arc-length derivative of $\tau(s)\beta(\theta^\alpha)$ which can be evaluated as

$$\begin{aligned} \tau(s)' &= \frac{\partial\tau}{\partial s} = \frac{\partial\tau}{\partial\theta^\beta} \frac{\partial\theta^\beta}{\partial s} = (\tau)_{,\beta}\tau^\beta \\ &= (b^{\alpha\beta}\tau_\alpha v_\beta)_{,\gamma}\tau^\gamma = (b^{\alpha\beta}\tau^\beta a_{\alpha\beta}v^\alpha a_{\alpha\beta})_{,\gamma}\tau^\gamma \end{aligned} \quad (3.37)$$

and

$$\beta(\theta^\alpha)' = [\beta(\theta^\alpha)]_{,\beta}\tau^\beta. \quad (3.38)$$

The above expressions are then rewritten using the Monge representation for further analysis. For example, we have

$$(b^{\alpha\beta}\tau^\beta a_{\alpha\beta}v^\alpha a_{\alpha\beta})_{,\gamma}\tau^\gamma = \left[\frac{1}{\sqrt{r^2[1+(z_{,r})^2] + (z_{,\theta})^2}} (rz_{,r\theta} - z_{,\theta})(z_{,r}z_{,\theta})^2 \right]_{,\theta}, \quad (3.39)$$

and similar treatments for other implicit terms.

Detailed derivations and phenomenological implications of these boundary forces are available in [5] and [6]. The interaction boundary conditions (i.e. Eqs. (3.35)-(3.36)), together with Eqs. (3.7), (3.12) solve the deformation of the non-uniform membrane subjected to protein-membrane interactions. In the model implementation, we employed commercial packages (e.g., Matlab, Comsol, etc...) to solve the obtained partial differential equations (PDEs), and the corresponding results are presented in the later sections.

3.2.2 Linear model for non-uniform membranes

The formulation of the non-uniform equilibrium equations (i.e., Eqs. (3.7), (3.12)) in terms of Eqs. (3.25)-(3.31) yields a highly nonlinear PDE system which often requires considerable computational resources. Alternatively, the ‘‘admissible linearization’’ may be considered through which one could obtain mathematically tractable systems

and, more importantly, analytical expressions of solutions with minimal loss of generality. The concept has been widely and successfully implemented in the relevant subject of studies (see, for example, [5], [7] and [15]). Within this setting, the derivative of $z(\theta^\alpha)$ of all orders are considered to be “small” (i.e., $z_{,\alpha} \ll 1$) and thus, their products can be neglected. Accordingly, using the notation “ \simeq ” to identify equations to the leading order approximation of $z(\theta^\alpha)$, we find

$$\begin{aligned}
a_{11} &\simeq 1, \quad a_{22} \simeq r^2, \quad a_{12} = a_{21} \simeq 0, \quad a = \det |a_{\alpha\beta}| \simeq r^2, \\
a^{11} &\simeq 1, \quad a^{22} \simeq \frac{1}{r^2}, \quad a^{12} = a^{21} \simeq 0, \quad \Gamma_{12}^1 = \Gamma_{21}^1 = \Gamma_{11}^2 = \Gamma_{11}^1 = \Gamma_{22}^2 = 0, \\
\Gamma_{12}^2 &= \Gamma_{21}^2 = \frac{1}{r}, \quad \Gamma_{22}^1 = -r, \quad \mathbf{n} \simeq \mathbf{k} - \nabla_p z, \quad \mathbf{a}^1 \simeq \mathbf{e}_r + z_{,r} \mathbf{k}, \quad \mathbf{a}^2 \simeq \frac{1}{r} \mathbf{e}_\theta + \frac{1}{r^2} \mathbf{k}, \text{ and} \\
\mathbf{b} &\simeq z_{,rr} (\mathbf{e}_r \otimes \mathbf{e}_r) + \frac{r z_{,r\theta} - z_{,\theta}}{r^2} [(\mathbf{e}_r \otimes \mathbf{e}_\theta) + (\mathbf{e}_\theta \otimes \mathbf{e}_r)] + \frac{r z_{,r} + z_{,\theta\theta}}{r^2} (\mathbf{e}_\theta \otimes \mathbf{e}_\theta) \\
&= \nabla_p^2 z,
\end{aligned} \tag{3.40}$$

where the subscript $(*)_p$ denotes the projected counterparts of $(*)$ on the coordinate plane ω_p , $\nabla_p^2 z$ is the second-order gradient of z and $\Delta_p z = \text{tr}(\nabla_p^2 z)$ is the corresponding Laplacian, respectively.

Thus, applying the results in Eq. (3.40), the mean and Gaussian curvatures (Eqs. (3.30), (3.31)) can be approximated as

$$H \simeq \frac{1}{2} [z_{,rr} + \frac{1}{r} z_{,r} + \frac{1}{r^2} z_{,\theta\theta}] = \frac{1}{2} \Delta_p z \text{ and } K \simeq 0. \tag{3.41}$$

In addition, from Eq. (3.41), we reduce Eqs. (3.11)-(3.12) to

$$\lambda_{,r} = \left(-\frac{\partial W}{\partial r}\right)(r, \theta) = -[\phi(\theta^\alpha)]_{,r} \tag{3.42}$$

and

$$\lambda_{,\theta} = \left(-\frac{\partial W}{\partial \theta}\right)(r, \theta) = -[\phi(\theta^\alpha)]_{,\theta}, \tag{3.43}$$

which serve as the linearized Euler equilibrium equations in the tangential directions of the coordinate system.

Remark 2. It is evident from Eqs. (3.11), (3.12), (3.42) and (3.43) that the terms associated with $\alpha(\theta^\alpha)$ and $\beta(\theta^\alpha)$ identically vanish after admissible linearization

regardless of the types of the distribution function $\alpha(\theta^\alpha)$ and $\beta(\theta^\alpha)$. For instance,

$$\frac{\partial\alpha(\theta^\alpha)}{\partial\theta^r}H^2 \simeq 0 \text{ and } \frac{\partial\beta(\theta^\alpha)}{\partial\theta^r}K \simeq 0, \quad \because H^2 \simeq 0 \text{ and } K \simeq 0. \quad (3.44)$$

This alternatively means the non-uniform potentials of $\alpha(\theta^\alpha)$ and $\beta(\theta^\alpha)$ do not necessarily result in non-uniform responses of membranes via tangential equilibrium equations (see, Eqs. (3.42)-(3.43)). This further implies that, within the setting of superposed incremental deformations, the descriptions of non-uniform membranes are intrinsically determined by introducing a non-uniform distribution function $\phi(\theta^\alpha)$, while maintaining $\alpha(\theta^\alpha)$ and $\beta(\theta^\alpha)$ as constants (i.e., $\alpha(\theta^\alpha) = k$ and $\beta(\theta^\alpha) = \bar{k}$).

Based on the **Remark 2**, the following compact form of the membrane energy potential may be proposed to accommodate the non-uniform responses of membranes, yielding

$$W(H, K; \theta^\alpha) = kH^2 + \bar{k}K + \phi(\theta^\alpha), \quad (3.45)$$

where $\phi(\theta^\alpha)$ characterizes the particular states of non-uniformity. Therefore, Eqs. (3.7) can be approximated in accordance with Eq. (3.45) as

$$k\Delta H - 2H[\phi(\theta^\alpha) + \lambda] = P, \quad (3.46)$$

which may serve as the compatible form of the shape equation for non-uniform membranes within the linear description.

3.2.3 Example 1: Circumferentially non-uniform membranes

We consider the following form of the non-uniformity function

$$\phi(\theta) + \lambda(\theta) = \alpha[\tilde{\theta}(\cos(n\theta))]^2; \quad n = 1, 2, 3, \dots, \quad (3.47)$$

where α defines the rigidity of the membrane and n controls the degrees of non-uniformity in the circumferential direction of θ . Thereby, Eq. (3.47) yields

$$\lambda_{,\theta} = -\phi_{,\theta} + 2\alpha\frac{\partial\tilde{\theta}}{\partial\theta} \text{ and } \lambda_{,r} = \phi_{,r} = 0 \text{ for the tangential equations,} \quad (3.48)$$

so that the membrane is radially uniform ($\lambda_{,r} = 0$) but circumferentially non-uniform ($\lambda_{,\theta} \neq 0$). Now, combining Eqs. (3.46)-(3.47), we find

$$H_{,rr} + \frac{1}{r}H_{,r} + \frac{1}{r^2}H_{,\theta\theta} - \frac{2\alpha\tilde{\theta}^2}{k}H = 0, \quad (3.49)$$

where we set $P = 0$ from the bilayer symmetry (see, [5]). The solution of Eq. (3.49) may take the following form

$$H(r, \theta) = \sum_{m=0}^{\infty} R(r, \theta)(C_m \sin(m\theta) + D_m \cos(m\theta)). \quad (3.50)$$

In the above, the expression of $R(r, \theta)$ can be obtained via the standard separation of variables (i.e. $\bar{\theta}(\theta)_{,\theta\theta}/\bar{\theta}(\theta) = -m^2$) as

$$R(r, \theta) = A_m I_m(\sqrt{\frac{2\alpha}{k}}r\tilde{\theta}) + B_m K_m(\sqrt{\frac{2\alpha}{k}}r\tilde{\theta}), \quad (3.51)$$

where I_m and K_m are, respectively, the first and second kind of modified Bessel functions. Since the surface evolution of membranes diminishes as it approaches the boundary, Eqs (3.50)-(3.51) may be further reduced to

$$H(r, \theta) = \sum_{m=0}^{\infty} K_m(\sqrt{\frac{2\alpha}{k}}r\tilde{\theta})(A_m \sin(m\theta) + B_m \cos(m\theta)). \quad (3.52)$$

By combining Eqs. (3.41) and (3.52), and we obtain

$$\sum_{m=0}^{\infty} K_m(\sqrt{\frac{2\alpha}{k}}r\tilde{\theta})[A_m \cos(m\theta) + B_m \sin(m\theta)] = \frac{1}{2}(z_{,rr} + \frac{1}{r}z_{,r} + \frac{1}{r^2}z_{,\theta\theta}). \quad (3.53)$$

The solution of the above PDEs can be sought in a similar form to that in Eq. (3.50)

$$z(r, \theta) = \sum_{m=0}^{\infty} S(r, \theta)(C_m \sin(m\theta) + D_m \cos(m\theta)). \quad (3.54)$$

Further, the substitution of Eq. (3.54) into Eq. (3.53) yields

$$\sum_{m=0,1,2,\dots}^{\infty} 2K_m(\sqrt{\frac{2\alpha}{k}}r\tilde{\theta}) \frac{A_m \cos(m\theta) + B_m \sin(m\theta)}{C_m \cos(m\theta) + D_m \sin(m\theta)} = S(r, \theta)_{,rr} + \frac{1}{r}S(r, \theta)_{,r} - \frac{m^2}{r^2}S(r, \theta), \quad (3.55)$$

where m is the separation variable. Thus, we obtain the following expression

$$\begin{aligned}
z(r, \theta) = & \sum_{m=1,3,5\dots}^{\infty} [-A_m \cosh(0.35 \log r) \int_a^r \frac{\sinh(0.35 \log \xi_1) \xi_1 K_{\frac{m}{4}}(\sqrt{\frac{2\alpha}{k}} \xi_1 \tilde{\theta})}{\frac{m}{4}} d\xi_1 + \\
& B_m \sinh(0.35 \log r) \int_a^r \frac{\cosh(0.35 \log \xi_2) \xi_2 K_{\frac{m}{4}}(\sqrt{\frac{2\alpha}{k}} \xi_2 \tilde{\theta})}{\frac{m}{4}} d\xi_2] * \\
& [C_m \sin(\frac{m}{4}\theta) + D_m \cos(\frac{m}{4}\theta)],
\end{aligned} \tag{3.56}$$

where a is the radius of the interaction boundary. The unknown coefficients (i.e., A_m , B_m , C_m , and D_m) can be completely determined by imposing the admissible boundary conditions (see, [5]):

$$\nabla z(a) = 0 \text{ and } H_{,r}(a) = \sigma/k. \tag{3.57}$$

To accommodate the superimposed form of solution (Eq. (3.56)), we expand the applied interaction force in terms of Fourier series as

$$\frac{\sigma}{k} = \sum_{m=1,3,5\dots}^{\infty} \frac{10}{m\pi} \sin(\frac{m\pi}{4}) + \sum_{m=1,3,5\dots}^{\infty} (-1)^{(\frac{m-1}{2})} \frac{10}{m\pi} \cos(\frac{m\pi}{4}). \tag{3.58}$$

Therefore, the unknowns A_m and B_m , can be determined from Eqs. (3.52), (3.57) and (3.58) that

$$A_m = \frac{10}{m\pi K_{\frac{m}{4}}(\sqrt{\frac{2\alpha}{k}} a\theta)_{,r}} \text{ and } B_m = (-1)^{(\frac{m-1}{4})} \frac{10}{m\pi K_{\frac{m}{2}}(\sqrt{\frac{2\alpha}{k}} a\theta)_{,r}}. \tag{3.59}$$

In the assimilation, we adopt the flexural modulus of the membrane as $k = 82pN \cdot nm$ based on the results in [39] and [40]. The value of λ is dependent on the settings of the membrane systems and does not have a definite range of values. The commonly used value is $\lambda \propto 10^{-4}pN/nm$ (see, for example, [13], [22] and [25]). Also, the corresponding data are obtained under the normalized setting. The dimensionless parameters used in the simulations are adopted from the works of [5], [19], and [24] as

$$\begin{aligned}
\mu &= \sqrt{2\lambda/k}: \text{ inverse of natural length scale,} \\
\sigma/\lambda &: \text{ force scale (e.g. } f_n = \sigma/\lambda: \text{ interaction force).}
\end{aligned} \tag{3.60}$$

Figure 3.1 illustrates the deflections of a non-uniform membrane predicted by the proposed model at a particular configuration of θ (e.g. $\theta = \pi/2, \pi$ etc...). It is evident that the transverse deflection of the membrane increases as the intensity of the membrane's energy distributions (α) decreases. This is due to the fact that less energy is required to induce the membranes' deformation for small α values. Further, when the intensity factor α is set as $\alpha = 1$, the energy potential of the non-uniform membrane at the particular configuration of $\theta = 1rad$ becomes equivalent to that of the uniform membrane so that the obtained solution recovers the results in [5] (see, Figure 3.1). Figure 3.2 indicates that the disparity between the linear and non-linear solutions becomes considerable with increasing interaction forces. Lastly, the non-

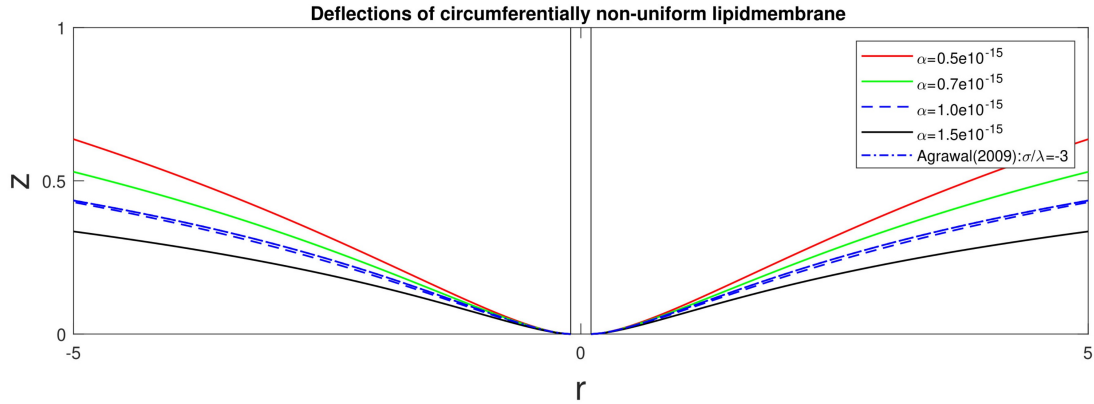


Figure 3.1: Transverse deflections of lipid membrane subjected to different α when: $\lambda + \phi = \alpha\theta^2$.

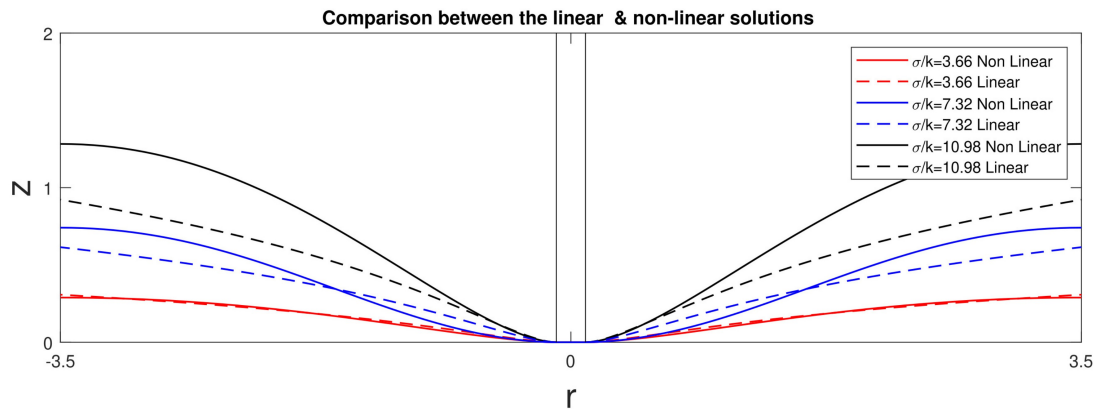


Figure 3.2: Transverse deflections of circumferentially non-uniform membranes: linear vs non-linear solutions.

uniform responses of drug-treated diseased cell membrane [41] may be assimilated by using the proposed model. For this purpose, we adopt the following form of the periodic energy density distribution:

$$\phi + \lambda = \alpha(\cos(n\theta) + A), \quad (3.61)$$

where n characterizes circumferentially non-uniform energy distributions, α is the particular rigidity of the membrane, and A is an arbitrary positive constant. Figure 3.3 illustrates that the obtained solution assimilates the echinocyte formations of the cell membrane, which is one of the common abnormalities observed in diseased cells (see, for example, [41], [42], and [43]). The exact mechanisms for the phenomenon have yet to be understood or predicted by the proposed model. However, the obtained solution may provide phenomenologically compatible non-uniform energy distributions of lipid membranes leading to such morphological formations. The non-uniform responses of red blood cell membranes, which results in their distinct (off-centered) biconcave discoid structure [35] may also be simulated using the proposed energy potential (Eq. (3.61)). It is shown in Figure 3.4 that the proposed model reproduces the off-centered non-uniform morphology of the abnormal cell membranes.

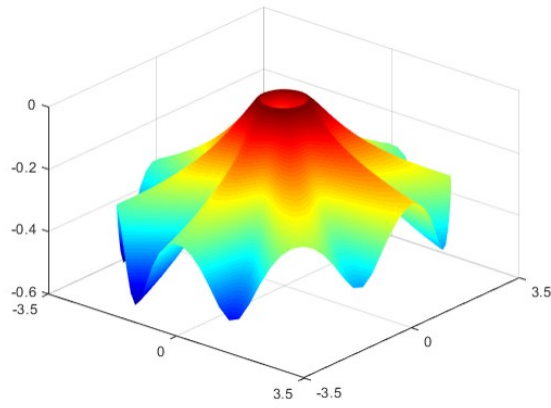
3.2.4 Example 2: Radially non-uniform membranes

The radial distribution function for strain energy is characterized by

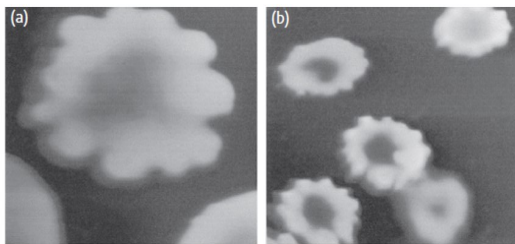
$$\phi(r) + \lambda(r) = \alpha r^n, \quad (3.62)$$

and we demonstrated the $n = 1/2$ case in the proceeding analysis. Similar to the previous section, the solutions of arbitrary n cases can be accommodated using the same procedures discussed in this section. For $n = 1/2$, Eq. (3.62) furnishes

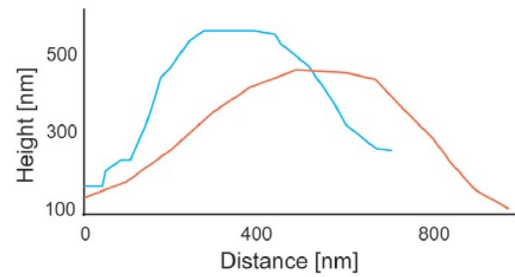
$$\lambda_{,r} = -\phi_{,r} + \frac{\alpha}{2}r^{-1/2}, \text{ and } \lambda_{,\theta} = \phi_{,\theta} = 0, \quad (3.63)$$



(a)

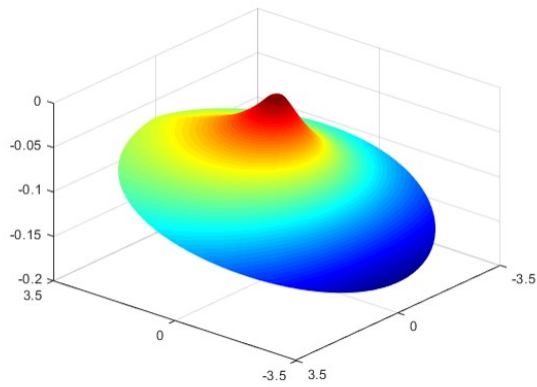


(b)

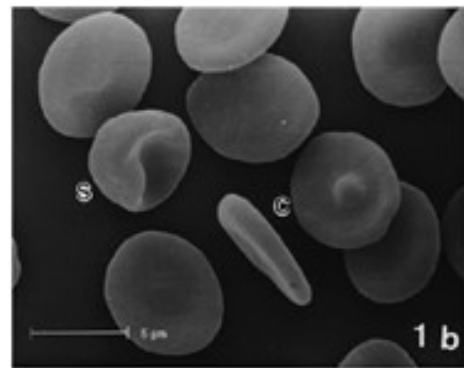


(c)

Figure 3.3: (a) The assimilation of the echinocyte formation: when $\phi + \lambda = \alpha[\cos(8\theta) + \pi]$, (b, c) the echinocyte formation of the cell membrane [41].



(a)



(b)

Figure 3.4: The assimilation of the off-centered non-uniform morphology: (a) when $\phi + \lambda = \alpha(\cos(\theta) + \pi)$, (b) the off-centered non-uniform morphology of red blood cell [35].

from which the radially non-uniform membrane ($\lambda_r \neq 0$) may be assimilated. Then, we substitute Eq. (3.62) into Eq. (3.46) and obtain

$$H_{,rr} + \frac{1}{r}H_{,r} + \frac{1}{r^2}H_{,\theta\theta} - \frac{2\alpha\sqrt{r}}{k}H = 0. \quad (3.64)$$

Hence, combining Eqs. (3.41)₁ and (3.64) furnishes

$$\begin{aligned} 0 = & z_{,rrrr} + \frac{2}{r^2}z_{,rr\theta\theta} + \frac{1}{r^4}z_{,\theta\theta\theta\theta} + \frac{2}{r}z_{,rrr} - \frac{2}{r^3}z_{,r\theta\theta} - \frac{1}{r^2}z_{,rr} + \frac{4}{r^4}z_{,\theta\theta} + \frac{1}{r^3}z_{,r} - \\ & \frac{2\alpha\sqrt{r}}{k}[z_{,rr} + \frac{1}{r}z_{,r} + \frac{1}{r^2}z_{,\theta\theta}]. \end{aligned} \quad (3.65)$$

In the case of axisymmetric energy density distributions (i.e. circumferentially uniform and radially non-uniform), Eq. (3.65) may be further reduced to

$$z_{,rrrr} + \frac{2}{r}z_{,rrr} - \frac{1}{r^2}z_{,rr} + \frac{1}{r^3}z_{,r} - \frac{2\alpha\sqrt{r}}{k}[z_{,rr} + \frac{1}{r}z_{,r}] = 0. \quad (3.66)$$

The solution of Eq. (3.66) can be found as

$$\begin{aligned} z = & A_1 r^2 {}_2\mathbf{F}_3\left(\left[\frac{4}{5}, \frac{4}{5}\right]; \left[1, \frac{9}{5}, \frac{9}{5}\right]; \frac{4}{25} \frac{2\alpha}{k} r^{\frac{5}{2}}\right) + A_1 r \mathbf{G}_{2,4}^{2,2}\left(\frac{4}{25} \frac{2\alpha}{k} r^{\frac{5}{2}} \mid \begin{matrix} \frac{3}{5}, \frac{3}{5} \\ \frac{4}{5}, \frac{4}{5}, -\frac{4}{5}, -\frac{4}{5} \end{matrix}\right) + \\ & A_2 \ln(r) + A_3. \end{aligned} \quad (3.67)$$

In the above, $\mathbf{G}_{p,q}^{m,n}$ is the Merjer \mathbf{G} function [40] where m, n, p , and q are integers corresponding to the number of matrix group $[\frac{3}{5}, \frac{3}{5}, \frac{4}{5}, \frac{4}{5}, -\frac{4}{5}, -\frac{4}{5}]$ and ${}_2\mathbf{F}_3$ is the Hypergeometric function [44] such that the subscripts 2 and 3 refer to the length of $n \times 1$ matrices (i.e. $[\frac{4}{5}, \frac{4}{5}] = 2 \times 1$ and $[1, \frac{9}{5}, \frac{9}{5}] = 3 \times 1$). We seek a bounded solution within a reasonably finite domain of $a \leq r \leq r_{Finite}$ ($r_{Finite} \propto a$, a : radius of a substrate) and therefore find from Eq. (3.67) that,

$$z(r) = A_1 r \mathbf{G}_{2,4}^{2,2}\left(\frac{4}{25} \frac{2\alpha}{k} r^{\frac{5}{2}} \mid \begin{matrix} \frac{3}{5}, \frac{3}{5} \\ \frac{4}{5}, \frac{4}{5}, -\frac{4}{5}, -\frac{4}{5} \end{matrix}\right) + A_2 \ln(r) + A_3, \quad (3.68)$$

where, the unknown constants A_1, A_2 and A_3 can be uniquely determined by imposing the admissible boundary conditions (see, also, [5]):

$$z(a) = 0, \quad z_{,r}(a) = 0 \quad \text{and} \quad z_{,rrr}(a) + \frac{1}{r}z_{,rr}(a) - \frac{1}{r^2}z_{,r}(a) = \frac{2\sigma}{k}. \quad (3.69)$$

Thus, we find

$$\begin{aligned}
A_1 &= -\frac{16r^2\sigma}{125k\mathbf{G}_{0,2}^{2,0}\left[\frac{4}{25}\frac{2\alpha}{k}a^{\frac{5}{2}} \mid \begin{matrix} - \\ \frac{2}{5}, \frac{7}{5} \end{matrix}\right]}, & A_2 &= \frac{8r^3\sigma\mathbf{G}_{1,3}^{2,1}\left[\frac{4}{25}\frac{2\alpha}{k}a^{\frac{5}{2}} \mid \begin{matrix} \frac{3}{5} \\ \frac{2}{5}, \frac{2}{5}, -\frac{2}{5} \end{matrix}\right]}{25k\mathbf{G}_{0,2}^{2,0}\left[\frac{4}{25}\frac{2\alpha}{k}a^{\frac{5}{2}} \mid \begin{matrix} - \\ \frac{2}{5}, \frac{7}{5} \end{matrix}\right]}, \text{ and} \\
A_3 &= -\frac{8r^3\sigma[5\log(r) * \mathbf{G}_{1,3}^{2,1}\left[\frac{4}{25}\frac{2\alpha}{k}a^{\frac{5}{2}} \mid \begin{matrix} \frac{3}{5} \\ \frac{2}{5}, \frac{2}{5}, -\frac{2}{5} \end{matrix}\right] - 2\mathbf{G}_{2,4}^{2,2}\left[\frac{4}{25}\frac{2\alpha}{k}a^{\frac{5}{2}} \mid \begin{matrix} \frac{3}{5}, \frac{3}{5} \\ \frac{2}{5}, \frac{2}{5}, -\frac{2}{5}, -\frac{2}{5} \end{matrix}\right]}{125k\mathbf{G}_{0,2}^{2,0}\left[\frac{4}{25}\frac{2\alpha}{k}a^{\frac{5}{2}} \mid \begin{matrix} - \\ \frac{2}{5}, \frac{7}{5} \end{matrix}\right]}.
\end{aligned} \tag{3.70}$$

The assimilation of the obtained solution is performed within the same normalized setting, as depicted in Eq. (3.60). Similar to the circumferentially non-uniform cases, the transverse deflection of membranes increases as the intensity of the membrane's energy distribution (coefficient α) decreases (see, Figure 3.5). As the intensity factor approaches unity ($\alpha = 1$), the radially non-uniform energy potential becomes essentially equivalent to those deflections from the Helfrich potential [12] within the domain of interest and thus accommodates the results in [5]. Figure 3.6 illustrates that the

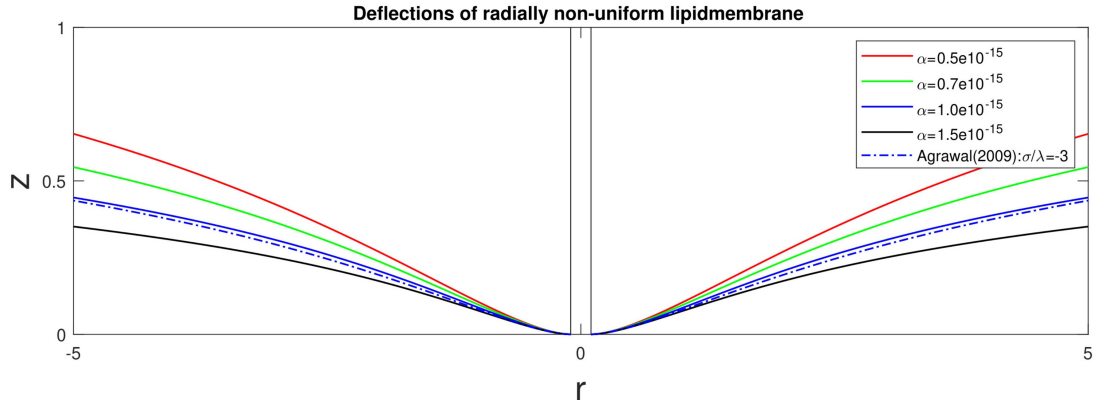


Figure 3.5: Transverse deflections of lipid membrane subjected to different α : when $\phi + \lambda = \alpha\sqrt{r}$.

obtained linear solutions produce reasonably close predictions when compared with those from the non-linear analysis for the relatively “small” deformation regime. The

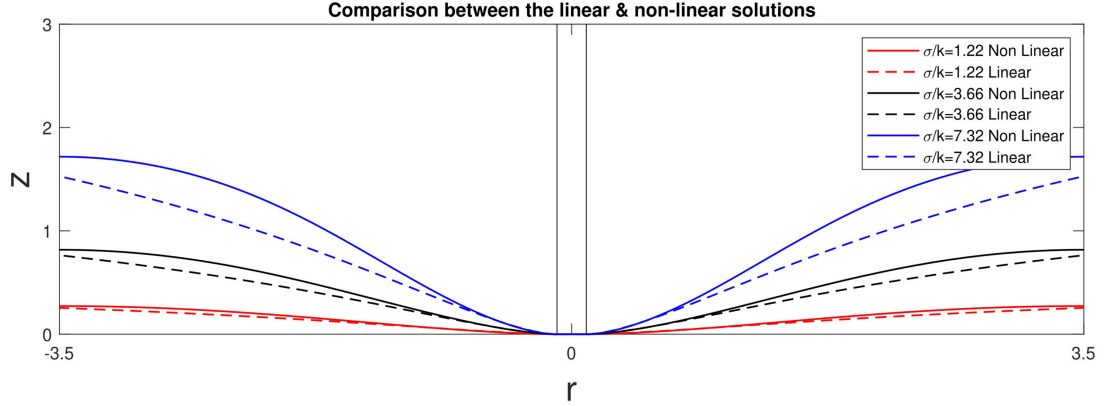


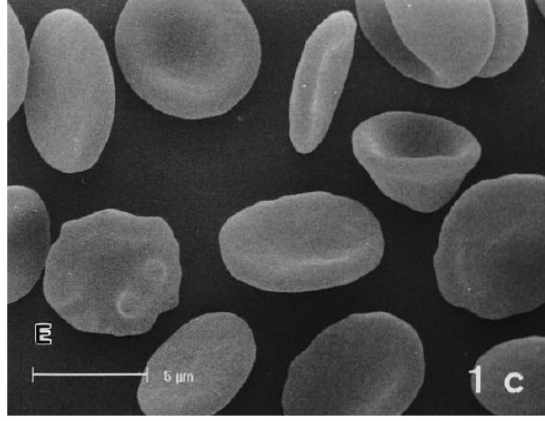
Figure 3.6: Transverse deflections of radially non-uniform membrane: Linear VS Non-linear solutions.

disparity between the linear and non-linear solutions becomes considerable in the cases of membranes subjected to “large” transverse deformation.

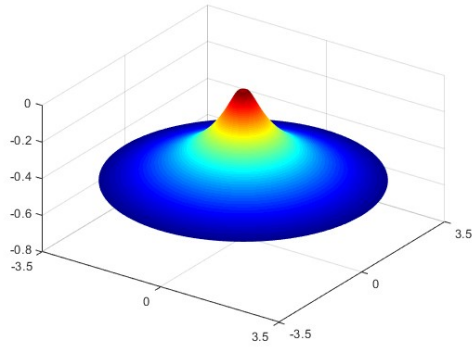
The sequences of discocyte-stomatocyte morphology in cell membranes [45] may be mapped using the proposed energy density function (Eq. (3.62)) via α and n (see, Figure 3.7). The obtained results could have phenomenological implications by estimating the desired elastic energy to form such morphological configurations and, therefore may further promote relevant studies (see, for example, [46, 47]).

It is also noted that the principles of superposition from the linear elasticity remain valid in the present case so that the solution of the combined non-uniform energy distribution case (e.g. $\phi + \lambda = \alpha(\cos(\theta) + \pi) + \alpha\sqrt{r}$) can be directly obtained via the summation of the solutions from the respective circumferentially and radially non-uniform cases. Within this prescription, the results in Figure 3.3(a) and Figure 3.7(b) or Figure 3.7(c) can be added to yield the deformation in Figure 3.8.

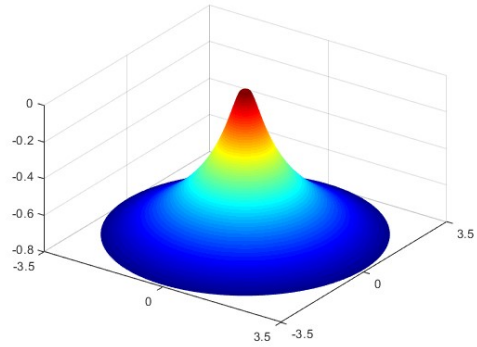
Lastly, we remark that more general membrane configurations may be characterized by combining the proposed non-uniform energy density functions. For example, the deformation contour predicted by the obtained non-linear model demonstrates close similarity to the highly off-centered protrusion of red blood cell membranes which are treated under 14 days of storage in a liquid medium [36] (see, Figure 3.9). Also, Figure 3.10 illustrates that the non-linear solution predicts the multiple peak formations



(a)



(b)



(c)

Figure 3.7: (a) The image of discocyte-stomatocyte morphology in sequential stages [45]; (b, c) The sequence of deformation mapping when $\phi + \lambda = \alpha r^n$ where α and n are adjusted to achieve the transitioning membrane morphology.

of abnormal cell membranes (burr cells) commonly observed in uremia and chronic kidney disease [37, 38]. In the cases of assimilation into experimental results, the intensity of membrane deflection is controlled by the intensity parameters (α and β) in the proposed energy potential (see, Figure 3.10), and the number of peaks can be characterized by the multiplied periodic functions (e.g. $\cos(\theta - \beta\pi)$).

We also note here the non-uniform energy density distributions considered in the present study may have equivalent effects on the resulting deformations of the membranes compared to those included by prescribed non-uniform tension fields. In fact, authors in [48] have shown that both the surface tension and surface energy of

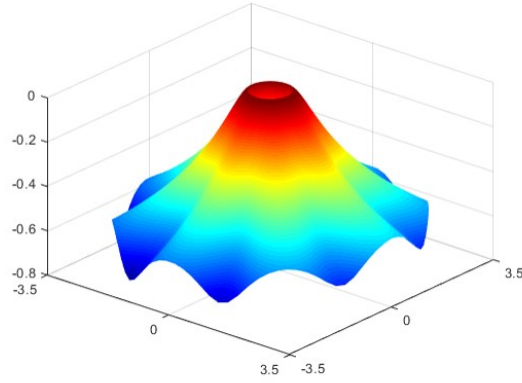


Figure 3.8: Deformation of combined radially and circumferentially non-uniform membrane when $\phi + \lambda = \alpha(\cos(\theta) + \pi) + \alpha\sqrt{r}$.

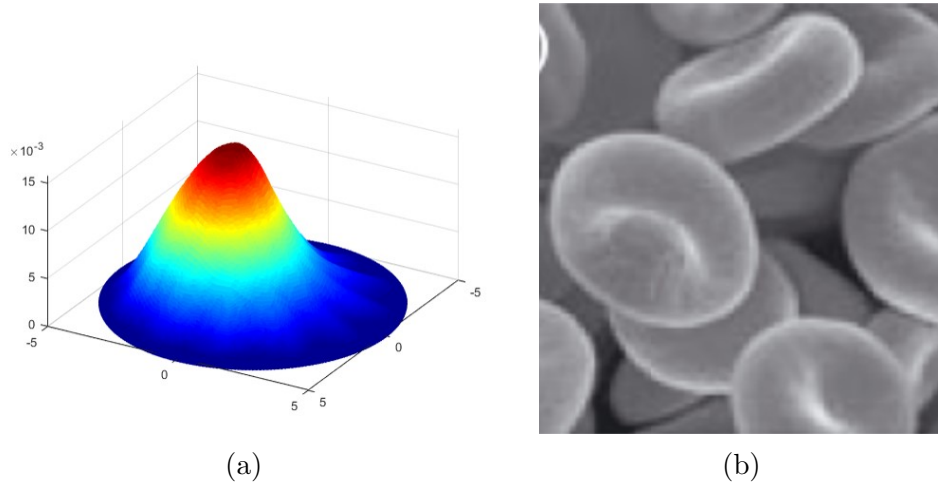
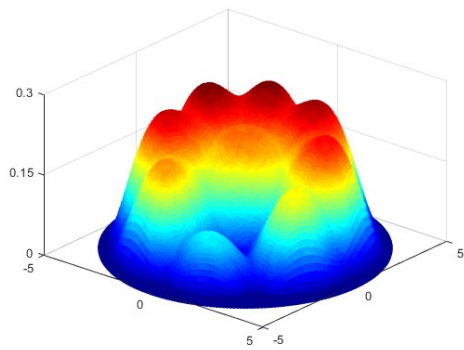
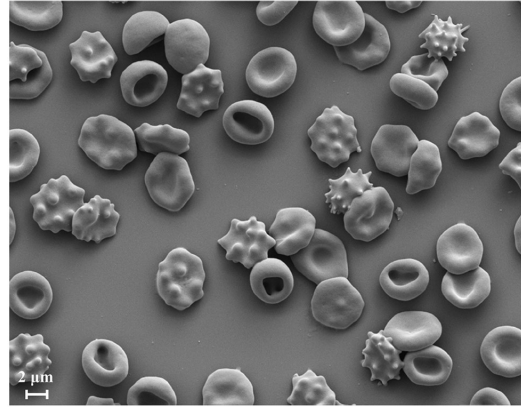


Figure 3.9: (a) The off-centered deformation of lipid membrane characterized by the potential of $\phi(\theta, r) = \alpha|\cos(r - 1)\theta|$, in which r is treated as non-dimensional coordinate with r/R_{ext} , in which $R_{ext} = 1$ with the same spacial configuration of r ; (b) The scanning electron images of long-stored RBCs [36].

Lennard-Jones fluids can be computed via the proposed radial distribution function. Given the fact that the thickness effect has been neglected, the induced variation for the free energy of the membrane mainly appears in the form of curvature changes of the surface through which both the surface tension and surface energy function can be altered, and vice versa [49]. Therefore, the prescription of a non-uniform energy density function can lead to non-uniformity in both the surface curvature (membrane's deformation) and the surface tension field.



(a)



(b)

Figure 3.10: (a) The multiple peak deformation of lipid membrane characterized by the function $\phi(\theta, r) = -\alpha \cos(r) \cos(\theta) \cos(r-1) \cos(\theta - \beta\pi)$, where the r is treated as non-dimensional coordinate with r/R_{ext} , where $R_{ext} = 1$ with the same spacial configuration of r ; (b) The scanning electron microscope (SEM) image of cell membranes with different morphological configurations of stomatocytosis and echinocytosis [37].

As mentioned in earlier sections, the proposed model may not be sufficient for immediate uses in the phenomenological and/or clinical research of cell membrane morphology. However, it could still provide quantitative information pertaining to such membrane formation via the estimations of required elastic energy and the corresponding non-uniform energy distributions over the domain of interest.

References

- [1] L. V. Chernomordik and M. M. Kozlov, *Mechanics of membrane fusion*, Jul. 2008. DOI: 10.1038/nsmb.1455.
- [2] M. Lenz, S. Morlot, and A. Roux, *Mechanical requirements for membrane fission: Common facts from various examples*, 2009. DOI: 10.1016/j.febslet.2009.11.012.
- [3] J. E. Rothman, “The machinery and principles of vesicle transport in the cell,” *Nature medicine*, vol. 8, no. 10, pp. 1059–1062, 2002. DOI: <https://doi.org/10.1038/nm770>.
- [4] A. Agrawal and D. J. Steigmann, “Coexistent fluid-phase equilibria in biomembranes with bending elasticity,” *Journal of Elasticity*, vol. 93, 1 2008, ISSN: 03743535. DOI: 10.1007/s10659-008-9165-1.
- [5] A. Agrawal and D. J. Steigmann, “Boundary-value problems in the theory of lipid membranes,” *Continuum Mechanics and Thermodynamics*, vol. 21, pp. 57–82, 1 Jun. 2009, ISSN: 09351175. DOI: 10.1007/s00161-009-0102-8.
- [6] D. J. Steigmann, “Mechanics and physics of lipid bilayers,” *The role of mechanics in the study of lipid bilayers*, pp. 1–61, 2018. [Online]. Available: https://link.springer.com/chapter/10.1007/978-3-319-56348-0_1.
- [7] T. Belay, C. I. Kim, and P. Schiavone, “Analytical solution of lipid membrane morphology subjected to boundary forces on the edges of rectangular membranes,” *Continuum Mechanics and Thermodynamics*, vol. 28, 1-2 2016, ISSN: 09351175. DOI: 10.1007/s00161-015-0426-5.
- [8] E. Gorter and F. Grendel, “On bimolecular layers of lipoids on the chromocytes of the blood,” *Journal of Experimental Medicine*, vol. 41, 4 1925, ISSN: 15409538. DOI: 10.1084/jem.41.4.439.
- [9] J. D. Robertson, “The ultrastructure of cell membranes and their derivatives,” *Biochemical Society symposium*, vol. 16, pp. 3–43, 1959. [Online]. Available: <https://api.semanticscholar.org/CorpusID:7814193>.
- [10] P. M. Naghdi, “On a variational theorem in elasticity and its application to shell theory,” *Journal of Applied Mechanics, Transactions ASME*, vol. 31, 4 1964, ISSN: 15289036. DOI: 10.1115/1.3629726.
- [11] M. E. Gurtin, “The linear theory of elasticity,” in *Linear Theories of Elasticity and Thermoelasticity: Linear and Nonlinear Theories of Rods, Plates, and Shells*, C. Truesdell, Ed. Berlin, Heidelberg: Springer Berlin Heidelberg, 1973, pp. 1–295, ISBN: 978-3-662-39776-3. DOI: 10.1007/978-3-662-39776-3_1. [Online]. Available: https://doi.org/10.1007/978-3-662-39776-3_1.
- [12] W. Helfrich, “Elastic properties of lipid bilayers: Theory and possible experiments,” *Zeitschrift fur Naturforschung - Section C Journal of Biosciences*, vol. 28, 11-12 1973, ISSN: 18657125. DOI: 10.1515/znc-1973-11-1209.

- [13] T. Belay, K. C. Il, and P. Schiavone, “Mechanics of a lipid bilayer subjected to thickness distension and membrane budding,” *Mathematics and Mechanics of Solids*, vol. 23, 1 2018, ISSN: 17413028. DOI: 10.1177/1081286516666136.
- [14] T. Belay, C. I. Kim, and P. Schiavone, “Bud formation of lipid membranes in response to the surface diffusion of transmembrane proteins and line tension,” *Mathematics and Mechanics of Solids*, vol. 22, 11 2017, ISSN: 17413028. DOI: 10.1177/1081286516657684.
- [15] M. Zeidi and C. I. Kim, “Notes on superposed incremental deformations in the mechanics of lipid membranes,” *Mathematics and Mechanics of Solids*, vol. 24, 1 2019, ISSN: 17413028. DOI: 10.1177/1081286517734608.
- [16] C. I. Kim, “A discussion on the mechanics of lipid membranes: Lagrange multipliers and a singular substrate,” *Zeitschrift für Angewandte Mathematik und Physik*, vol. 68, 4 2017, ISSN: 00442275. DOI: 10.1007/s00033-017-0825-5.
- [17] A. Agrawal and D. J. Steigmann, “Modeling protein-mediated morphology in biomembranes,” *Biomechanics and Modeling in Mechanobiology*, vol. 8, 5 2009, ISSN: 16177959. DOI: 10.1007/s10237-008-0143-0.
- [18] N. Walani, J. Torres, and A. Agrawal, “Anisotropic spontaneous curvatures in lipid membranes,” *Physical Review E - Statistical, Nonlinear, and Soft Matter Physics*, vol. 89, 6 2014, ISSN: 15502376. DOI: 10.1103/PhysRevE.89.062715.
- [19] P. Rangamani, A. Agrawal, K. K. Mandadapu, G. Oster, and D. J. Steigmann, “Interaction between surface shape and intra-surface viscous flow on lipid membranes,” *Biomechanics and Modeling in Mechanobiology*, vol. 12, 4 2013, ISSN: 16177959. DOI: 10.1007/s10237-012-0447-y.
- [20] D. J. Steigmann, “Fluid films with curvature elasticity,” *Archive for Rational Mechanics and Analysis*, vol. 150, 2 1999, ISSN: 00039527. DOI: 10.1007/s002050050183.
- [21] D. J. Steigmann, “On the relationship between the cosserat and kirchhoff-love theories of elastic shells,” *Mathematics and Mechanics of Solids*, vol. 4, 3 1999, ISSN: 10812865. DOI: 10.1177/108128659900400301.
- [22] M. Zeidi and C. I. Kim, “The effects of intra-membrane viscosity on lipid membrane morphology: Complete analytical solution,” *Scientific Reports*, vol. 8, 1 2018, ISSN: 20452322. DOI: 10.1038/s41598-018-31251-6.
- [23] D. J. Steigmann, “A model for lipid membranes with tilt and distension based on three-dimensional liquid crystal theory,” *International Journal of Non-Linear Mechanics*, vol. 56, 2013, ISSN: 00207462. DOI: 10.1016/j.ijnonlinmec.2013.02.006.
- [24] P. Rangamani and D. J. Steigmann, “Variable tilt on lipid membranes,” *Proceedings of the Royal Society A: Mathematical, Physical and Engineering Sciences*, vol. 470, 2172 2014, ISSN: 14712946. DOI: 10.1098/rspa.2014.0463.

- [25] C. I. Kim and D. J. Steigmann, “Distension-induced gradient capillarity in lipid membranes,” *Continuum Mechanics and Thermodynamics*, vol. 27, 4-5 2015, ISSN: 09351175. DOI: 10.1007/s00161-014-0333-1.
- [26] J. L. Ericksen, “Conservation laws for liquid crystals,” *Transactions of the Society of Rheology*, vol. 5, 1 1961, ISSN: 0038-0032. DOI: 10.1122/1.548883.
- [27] J. L. Ericksen, “Hydrostatic theory of liquid crystals,” *Archive for Rational Mechanics and Analysis*, vol. 9, 1 1962, ISSN: 00039527. DOI: 10.1007/BF00253358.
- [28] J. Ericksen, “Equilibrium theory of liquid crystals,” in 1976. DOI: 10.1016/b978-0-12-025002-8.50012-9.
- [29] A. Agrawal and D. J. Steigmann, “A model for surface diffusion of transmembrane proteins on lipid bilayers,” *Zeitschrift fur Angewandte Mathematik und Physik*, vol. 62, 3 2011, ISSN: 00442275. DOI: 10.1007/s00033-011-0132-5.
- [30] A. Mahapatra, D. Saintillan, and P. Rangamani, “Transport phenomena in fluid films with curvature elasticity,” *Journal of Fluid Mechanics*, 2020, ISSN: 14697645. DOI: 10.1017/jfm.2020.711.
- [31] R. C. Capeta, J. A. Poveda, and L. M. Loura, “Non-uniform membrane probe distribution in resonance energy transfer: Application to protein-lipid selectivity,” vol. 16, 2006. DOI: 10.1007/s10895-005-0036-x.
- [32] D. Kabaso *et al.*, “Attachment of rod-like (bar) proteins and membrane shape,” *Mini Reviews in Medicinal Chemistry*, vol. 11, 4 2011, ISSN: 13895575. DOI: 10.2174/138955711795305353.
- [33] R Ogden, “Non-linear elastic deformations,” *Engineering Analysis with Boundary Elements*, vol. 1, 2 1984, ISSN: 09557997. DOI: 10.1016/0955-7997(84)90049-3.
- [34] D. J. Steigmann, *Finite elasticity theory*. 2017. DOI: 10.1093/oso/9780198567783.001.0001.
- [35] K. I. Tsubota, S. Wada, and H. Liu, “Elastic behavior of a red blood cell with the membrane’s nonuniform natural state: Equilibrium shape, motion transition under shear flow, and elongation during tank-treading motion,” *Biomechanics and Modeling in Mechanobiology*, vol. 13, 4 2014, ISSN: 16177940. DOI: 10.1007/s10237-013-0530-z.
- [36] B. Blasi, A. D’Alessandro, N. Ramundo, and L. Zolla, “Red blood cell storage and cell morphology,” *Transfusion Medicine*, vol. 22, 2 2012, ISSN: 09587578. DOI: 10.1111/j.1365-3148.2012.01139.x.
- [37] N. M. Geekiyanage *et al.*, “A coarse-grained red blood cell membrane model to study stomatocyte-discocyteechinocyte morphologies,” *PLoS ONE*, vol. 14, 4 Apr. 2019, ISSN: 19326203. DOI: 10.1371/journal.pone.0215447.
- [38] C. Spier, “Wintrobe’s atlas of clinical hematology,” *American Journal of Surgical Pathology*, vol. 32, 9 2008, ISSN: 0147-5185. DOI: 10.1097/pas.0b013e31816955c5.

- [39] R. M. Hochmuth and R. E. Waugh, “Erythrocyte membrane elasticity and viscosity,” *Annual Review of Physiology*, vol. Vol. 49, 1987, ISSN: 00664278. DOI: 10.1146/annurev.ph.49.030187.001233.
- [40] I. Derényi, F. Jülicher, and J. Prost, “Erratum: Formation and interaction of membrane tubes [phys. rev. lett.prltao0031-9007 88, 238101 (2002)],” *Phys. Rev. Lett.*, vol. 89, p. 209901, 20 2002. DOI: 10.1103/PhysRevLett.89.209901. [Online]. Available: <https://link.aps.org/doi/10.1103/PhysRevLett.89.209901>.
- [41] K. J. V. Vliet and P. Hinterdorfer, “Probing drug-cell interactions,” *Nano Today*, vol. 1, 3 2006, ISSN: 17480132. DOI: 10.1016/S1748-0132(06)70076-7.
- [42] P. G. Gallagher, *Red cells red cell membrane disorders*, 2005. [Online]. Available: <http://ashpublications.org/hematology/article-pdf/2005/1/13/645048/013.pdf>.
- [43] L. Blanc and L. C. Wolfe, “Chapter 7 - general considerations of hemolytic diseases, red cell membrane, and enzyme defects,” in *Lanzkowsky’s Manual of Pediatric Hematology and Oncology (Seventh Edition)*, J. D. Fish, J. M. Lipton, and P. Lanzkowsky, Eds., Seventh Edition, Academic Press, 2022, pp. 125–149, ISBN: 978-0-12-821671-2. DOI: <https://doi.org/10.1016/B978-0-12-821671-2.00030-1>. [Online]. Available: <https://www.sciencedirect.com/science/article/pii/B9780128216712000301>.
- [44] J. B. Seaborn, *Hypergeometric functions and their applications*. Springer Science & Business Media, 2013, vol. 8. DOI: <https://doi.org/10.1007/978-1-4757-5443-8>.
- [45] A. Escudero *et al.*, “Effect of dietary (n-9), (n-6) and (n-3) fatty acids on membrane lipid composition and morphology of rat erythrocytes,” *Biochimica et Biophysica Acta - Lipids and Lipid Metabolism*, vol. 1394, 1 1998, ISSN: 00052760. DOI: 10.1016/S0005-2760(98)00095-2.
- [46] H. W. Lim, M. Wortis, and R. Mukhopadhyay, “Stomatocyte-discocyte-echinocyte sequence of the human red blood cell: Evidence for the bilayer-couple hypothesis from membrane mechanics,” *Proceedings of the National Academy of Sciences of the United States of America*, vol. 99, 26 2002, ISSN: 00278424. DOI: 10.1073/pnas.202617299.
- [47] S. Muñoz, J. L. Sebastián, M. Sancho, and G. Álvarez, “Elastic energy of the discocyte-stomatocyte transformation,” *Biochimica et Biophysica Acta - Biomembranes*, vol. 1838, 3 2014, ISSN: 00052736. DOI: 10.1016/j.bbmem.2013.10.020.
- [48] C. A. Galán, A. Mulero, and F. Cuadros, “Calculation of the surface tension and the surface energy of lennard-jones fluids from the radial distribution function in the liquid phase,” *Molecular Physics*, vol. 103, 4 2005, ISSN: 00268976. DOI: 10.1080/00268970512331317372.
- [49] T. D. Gurkov and P. A. Kralchevsky, “Surface tension and surface energy of curved interfaces and membranes,” *Colloids and Surfaces*, vol. 47, C 1990, ISSN: 01666622. DOI: 10.1016/0166-6622(90)80061-8.

Chapter 4

Deformation Analysis of Non-uniform Lipid Membrane Subjected to Local Inflammations

Within this Chapter, we present complete analytical solutions describing the deformations of both rectangular and circular-shaped lipid membranes subjected to local inflammations and coordinate-dependent (non-uniform) property distributions. The membrane energy potential of the Helfrich type is refined to accommodate the coordinate-dependent responses of the membranes. Within the description of the superposed incremental deformations and Monge parameterization, a linearized version of the shape equation describing coordinate-dependent membrane morphology is obtained. The local inflammation of a lipid membrane is accommodated by the prescribed uniform internal pressure and/or lateral pressure. This furnishes a partial differential equation of Poisson's type from which a complete analytical solution is obtained by employing the variation of parameters method. The obtained solutions qualitatively predict the smooth and coordinate-dependent morphological transitions over the domain of interest and are reduced to those from the classical uniform membrane shape equation when the equivalent energy potential is applied. In particular, the obtained model accurately demonstrated the effects of inflammation-induced lateral pressure on lipid membranes where only quantitatively equivalent analyses were reported via the impositions of equivalent edge moments.

4.1 Introduction

The mechanics of lipid membrane has consistently been the subject of intense study [1–5] that has significantly advanced our understanding of various cellular functions and enriches continuum mechanics in general. Historically, it was believed that a thin oil-like barrier surrounds cells, yet the structure of this membrane was not well known. In 1925, Evert Gorter and F. Grendel [6] found that a lipid bilayer is a constituent of cell membranes and, later, David Robertson [7] revealed that the bilayer structures are, in fact, characteristics of all biological membranes (biomembranes). When dispersed into aqueous solutions, lipid molecules form a unique bilayer structure (a lipid bilayer) with opposing orientations under the hydrophobic effects, enabling the lipid bilayers to maintain symmetry about a mid-surface. Lipid membranes are quite fragile and exceedingly thin (typically 3-5 nm), the analyses of various aspects of lipid membranes are often assisted by theoretical models to overcome the formidable difficulties arising in experimental studies. Contemporary modeling approaches are based on the idealization of the membrane as a thin elastic film, through which the responses of the membrane can be characterized by the mean and Gaussian curvatures of a surface. Within this prescription, the development of a continuum-based model describing the responses of lipid membranes is facilitated by the differential geometry on membrane surfaces and the theory of elasticity on surface [8, 9]. In particular, the energy potential of lipid membrane (proposed by Helfrich [1]) has been successfully implemented in various membrane problems such as budding formations [10, 11] and membrane-protein interactions [12, 13] for its capability of characterizing the symmetry behavior of lipid membranes with ensuing energy minima [14, 15].

Recent research interests are devoted to the identifications of various conformational states of the membranes such as budding formations [11], off-centered biconcave discoid structures [16, 17], and echinocyte formations [18] in efforts to understand the mechanisms of essential cellular activities and the characterizations of the

associated mechanical forces. Since the induced morphologies are closely related to the mechanical responses of lipid membranes, the studies of the various morphological formations of the membranes are, most often, achieved via the assimilations of “idealized compatible deformations” through which the associated regulating forces such as bending moments, substrate interaction forces and intra-membrane viscous forces may be characterized [19, 20]. In this respect, authors in [21] proposed the non-linear model by investigating the deformations of membranes subjected to intra-membrane viscosity. Evans [19] investigated chemically-induced bending moments as a possible source of regulating forces for the shaping of red blood cells. Linear models of the lipid membrane have been devised in [22, 23] where authors presented complete analytical solutions describing substrate-membrane interactions in the presence of intra-membrane viscose flows. To this end, authors in [24] proposed the refined membrane energy potential to simulate the coordinate-dependent responses of the membranes when interacting with cylindrical substrates. Most of the above-mentioned studies, however, are limited to the deformation analyses of membranes induced by either the membrane-protein interactions or the resultant moments applied on the boundaries of membranes. The solution describing inflammations of the membrane is absent from the literature due to the mathematical complexities arising in the corresponding formulations and analyses. As a result, the inflammation analyses are often practiced by assimilating the equivalent deformations of the membrane via the impositions of interaction forces for circular membranes (see, for example, [25, 26]) and/or resultant bending moments in cases of rectangular membranes [27]. However, the membrane inflammation-induced deformations should be distinguished from those induced by membrane-protein interactions and bending effects on membranes, because the membrane inflammation-induced deformation can be induced by internal pressures of cells [28, 29], yet the deformations invoked by membrane-protein interaction can be derived from the prescribed forces on membrane boundaries [22–24]. Within this context, the lateral pressure variation can be attributed to various

“internal sources”. For instance, the enhanced trans-bilayer mobility alters the distribution of phospholipids and thus compromises the membrane-skeleton connection across the bilayer [30]. This reduced membrane stability potentially results in pressure variations during inflammation [28, 29]. Lateral diffusion induced by the hydrodynamic process of the Brownian motion may also induce pressure variations within the membrane system [31, 32]. Since the abovementioned processes occur throughout the membranes, the bending and/or membrane-protein interaction models which account for “external sources” from the boundaries of membranes may not be “ideal” for the membrane inflammation analysis. Further, considering the membrane-skeleton connections and lateral diffusion may vary within the membrane, the development of the coordinate-dependent inflammation model may be of more practical interest to describe more general types of membrane morphologies such as biconcave discoid structures and echinocyte formations [16–18].

In the present study, we seek to develop a complete analytical platform for the deformation analysis of the lipid membrane subjected to local inflammations. The membrane energy potential of the Helfrich type is refined to achieve more accurate descriptions of the coordinate-dependent inflammations. The expressions of admissible boundary conditions are adopted from the existing nonlinear theory [12] but they are reformulated and implemented into the present context. Emphasis is placed on the assimilation of the complex nature of membrane morphology regulated by internal pressures acting on the surface of the lipid membrane, at the same time, maintaining sufficient rigour and generality in the formulation of the membrane shape equation. The membrane inflammation is incorporated by considering the uniform internal pressure acting on the surface of the membranes. In the present context, this would mean the retainment of the constitutively indeterminate scalar field arising in the volume-constrained energy variations of the membrane-bulk liquid system. Using the Monge representation and the method of variation of parameters [33, 34], an exact analytical solution is obtained for the incremental deformations superposed on large. The

obtained solution showcases smooth transitions of deformation fields over the domain of interest and reduces to the results in [27] when the equivalent internal pressure is applied. In particular, the proposed inflammation model successfully illustrates the off-centered biconcave discoid structures of red blood cell [35] and the echinocyte formations of cell membranes induced by the incubation with lecithin [36]. Further, we have shown that the principle of superposition from the theory of linear elasticity remains valid for the cases of inflammation problems with coordinate-dependent membrane properties. That is the solution of the combined mode inflammation can be directly obtained by adding solutions from the respective circumferential and radial coordinate-dependent inflammations.

4.2 Membrane Shape Equation

The Canham-Helfrich model has been further refined to accommodate spontaneous curvatures [12], distension [37] and budding formations [11]. In the present study, we proposed the following strain energy potential to achieve a more comprehensive description of lipid membranes subjected to prescribed pressure and non-uniform membrane properties, given by

$$W(H, K; \theta^\alpha) = \phi(\theta^\alpha) + \alpha(\theta^\alpha)H^2 + \beta(\theta^\alpha)K, \quad (4.1)$$

where the explicit coordinate-dependent potentials of $\phi(\theta^\alpha)$, $\alpha(\theta^\alpha)$ and $\beta(\theta^\alpha)$ jointly regulate particular states of non-uniformities in membranes. We also note that the above membrane potential accommodates the uniform membrane case (i.e. $W(H, K; \theta^\alpha) = kH^2 + \bar{k}K$) in the limit of

$$\phi(\theta^\alpha) = 0, \quad \alpha(\theta^\alpha) = k \text{ and } \beta(\theta^\alpha) = \bar{k}. \quad (4.2)$$

Meanwhile, the membrane shape equations are given by [12]

$$\Delta\left(\frac{1}{2}W_H\right) + (W_K)_{;\beta\alpha}\tilde{b}^{\beta\alpha} + W_H(2H^2 - K) + 2KHW_K - 2H(W + \lambda) = P \quad \text{on } \omega \quad (4.3)$$

and

$$\lambda_{,\alpha} = -\frac{\partial W}{\partial \theta^\alpha}. \quad (4.4)$$

For uniform membranes, the latter yields [14]

$$\lambda = \text{constant}, \quad \because \lambda_{,\alpha} = 0, \quad (4.5)$$

where the constant may be determined via the membrane shape equation describing particular deformed states [26]. In cases of non-uniform membranes where the energy potential W depends explicitly on the surface coordinates θ^α , it is found that

$$\lambda_{,\alpha} = -\frac{\partial W}{\partial \theta^\alpha} \neq 0. \quad (4.6)$$

Eq. (4.6) arises from possible non-uniformity in the membrane properties where the unknown, λ can be determined by solving two Euler equilibrium equations projected on the surface coordinates (θ^α).

Hence, the complete Euler equation describing non-uniform responses of membranes can be formulated. More precisely, from Eq. (4.1), we find

$$W_H = 2\alpha(\theta^\alpha)H, \quad W_K = \beta(\theta^\alpha) \quad (4.7)$$

and

$$\begin{aligned} W_{,\alpha} &= W_H H_{,\alpha} + W_K K_{,\alpha} + \frac{\partial W}{\partial \theta^\alpha} \\ &= 2\alpha(\theta^\alpha)H H_{,\alpha} + \beta(\theta^\alpha)K_{,\alpha} + \left[\frac{\partial \phi(\theta^\alpha)}{\partial \theta^\alpha} + \frac{\partial \alpha(\theta^\alpha)}{\partial \theta^\alpha} H^2 + \frac{\partial \beta(\theta^\alpha)}{\partial \theta^\alpha} K \right]. \end{aligned} \quad (4.8)$$

The substitution of Eq. (4.7) into Eq. (4.3) then yields

$$\Delta(\alpha(\theta^\alpha)H) + (\beta(\theta^\alpha))_{;\beta\alpha} \tilde{b}^{\beta\alpha} + 2\alpha(\theta^\alpha)H(H^2 - K) - 2H(\phi(\theta^\alpha) + \lambda) = P, \quad (4.9)$$

where the covariant derivative of the scalar-valued function, $(\beta(\theta^\alpha))_{;\beta\alpha}$, can be evaluated as

$$\beta(\theta^\alpha)_{;\beta\alpha} = (\beta(\theta^\alpha))_{,\beta\alpha} = \beta(\theta^\alpha)_{,\beta\alpha} - \beta(\theta^\alpha)_{,\lambda} \Gamma_{\beta\alpha}^\lambda. \quad (4.10)$$

Lastly, from Eqs. (4.1) and (4.6)), we obtain

$$\lambda_{,\beta} = -\frac{\partial W}{\partial \theta^\beta} = -\left[\frac{\partial \phi(\theta^\alpha)}{\partial \theta^\beta} + \frac{\partial \alpha(\theta^\alpha)}{\partial \theta^\beta} H^2 + \frac{\partial \beta(\theta^\alpha)}{\partial \theta^\beta} K\right], \quad (4.11)$$

which serves as the associated tangential Euler equations. It is also noted here that $\partial W/\partial \theta^\alpha$ denotes the explicit coordinate derivative of W and thus, not to be confused with $W_{,\alpha}$ (see, also, [12], [14] and [15]).

In practice, the right side of Eq. (4.9) is often set to be zero (i.e. $P = 0$) to obtain mathematically tractable formulations and analyses. For example, authors in [27] applied alternative edge moments, instead of prescribing pressure P on the membrane surface, to describe the local inflammation-induced deformations of a membrane via the bending moment applied on membrane boundaries. Nevertheless, such simplification poses apparent limitations in the predictions of membranes' morphologies, especially those induced by internal pressure such as local inflammations and buddings, where the influences of P are not negligible. In the following sections, we present a comprehensive analysis for the mechanics of non-uniform membranes subjected to prescribed pressure P .

4.2.1 Monge parametric representation

The Monge parameterization and admissible linearization are widely adopted techniques for lipid membrane analyses (see, for example, [10], [12], and [25]). Here, we reformulate the results in the present context for the sake of completeness. Using the Monge parameterization, material points on the membrane surface, Ω , can be mapped as

$$\mathbf{r}(\theta^\alpha) = \theta(\theta^\alpha) + z(\theta^\alpha)\mathbf{k}, \quad (4.12)$$

where $\theta(\theta^\alpha)$ is position on a plane p with unit normal \mathbf{k} . Hence, the problem of determining the membranes' morphology is reduced to solving a single function $z(\theta)$.

For instance, in the axisymmetric polar coordinates, we find

$$\theta(\theta^\alpha) = \theta^\alpha \mathbf{e}_\alpha = r \mathbf{e}_r(\theta), \quad \mathbf{e}_r(\theta) = \cos \theta \mathbf{e}_1 + \sin \theta \mathbf{e}_2. \quad (4.13)$$

Accordingly, we compute

$$\begin{aligned}
\mathbf{a}_1 &= \mathbf{e}_r + z_{,r}\mathbf{k}, \quad \mathbf{a}_2 = r\mathbf{e}_r + z_{,\theta}\mathbf{k}, \quad a = \det(a_{\alpha\beta}) = r^2(1 + z_{,r}^2) + z_{,\theta}^2, \\
a_{11} &= 1 + z_{,r}^2, \quad a_{22} = r^2 + z_{,\theta}^2, \quad a_{12} = z_{,r}z_{,\theta} = a_{21}, \\
H &= \frac{1}{2a^{3/2}}[r^3z_{,rr} + r^2z_{,r} + r^2z_{,r}^3 + rz_{,rr}z_{,\theta}^2 - 2rz_{,r\theta}z_{,r}z_{,\theta} + rz_{,\theta\theta} + rz_{,\theta\theta}z_{,r}^2 + 2z_{,r}z_{,\theta}^2], \\
K &= \frac{1}{a^2}[r^3z_{,r}z_{,rr} + r^2z_{,rr}z_{,\theta\theta} - r^2z_{,r\theta}^2 + 2rz_{,r\theta} - z_{,\theta}^2], \\
\mathbf{n} &= \frac{1}{\sqrt{a}}(-z_{,\theta}\mathbf{e}_\theta - rz_{,r}\mathbf{e}_r + r\mathbf{k}), \quad \text{and } \mathbf{b} = b_{\alpha\beta}\mathbf{a}^\alpha \otimes \mathbf{a}^\beta \text{ with } b_{\alpha\beta} = \mathbf{a}_{\beta,\alpha} \cdot \mathbf{n}. \quad (4.14)
\end{aligned}$$

In the above, \mathbf{b} is the curvature tensor and the expressions of the dual basis can be obtained as

$$\begin{aligned}
\mathbf{a}^1 &= a^{11}\mathbf{a}_1 + a^{12}\mathbf{a}_2 = \frac{1}{a}[(r^2 + z_{,\theta}^2)\mathbf{e}_r - rz_{,r}z_{,\theta}\mathbf{e}_\theta + r^2z_{,r}\mathbf{k}], \\
\mathbf{a}^2 &= \frac{1}{a}[-rz_{,r}z_{,\theta}\mathbf{e}_r + r(1 + z_{,r}^2)\mathbf{e}_\theta + z_{,\theta}\mathbf{k}], \quad \text{and} \\
a^{11} &= \frac{r^2 + z_{,\theta}^2}{a}, \quad a^{22} = \frac{1 + z_{,r}^2}{a}, \quad a^{12} = a^{21} = -\frac{z_{,r}z_{,\theta}}{a}. \quad (4.15)
\end{aligned}$$

Lastly, the coefficients of the second fundamental form $b_{\alpha\beta}$, may be formulated as

$$b_{11} = \mathbf{n} \cdot \mathbf{a}_{1,1} = \frac{1}{\sqrt{a}}rz_{,rr} \text{ with } a_{1,1} = \frac{\partial(\mathbf{e}_r(\theta) + z_{,r}(r, \theta)\mathbf{k})}{\partial r} = z_{,rr}\mathbf{k}, \quad (4.16)$$

and similarly for b_{12} , b_{21} and b_{22} . The above equations can also be reformulated in the orthonormal Cartesian basis as

$$\theta = \theta^\alpha \mathbf{e}_\alpha = x\mathbf{e}_1 + y\mathbf{e}_2, \quad (4.17)$$

where the superscripts of the surface coordinates are dropped and replaced by x and y for convenience. Hence, we find

$$\begin{aligned}
\mathbf{a}_\alpha &= \mathbf{e}_\alpha + z_{,\alpha}\mathbf{k}, \quad a = 1 + z_{,x}^2 + z_{,y}^2, \quad \mathbf{n} = \frac{\mathbf{k} - (z_{,x}\mathbf{e}_1 + z_{,y}\mathbf{e}_2)}{\sqrt{a}}, \\
H &= \frac{(1 + z_{,y}^2)z_{,xx} - 2z_{,x}z_{,y}z_{,xy} + (1 + z_{,x}^2)z_{,yy}}{2a^{3/2}}, \\
K &= \frac{z_{,xx}z_{,yy} - z_{,xy}^2}{a^2}, \quad \mathbf{b} = \frac{z_{,\alpha\beta}\mathbf{a}^\alpha \otimes \mathbf{a}^\beta}{\sqrt{a}}, \quad (4.18)
\end{aligned}$$

which leads

$$\begin{aligned}
\mathbf{a}^1 &= \frac{1}{a}[(1 + z_{,y}^2)(\mathbf{e}_1 + z_{,x}\mathbf{k}) - z_{,x}z_{,y}(\mathbf{e}_2 + z_{,y}\mathbf{k})], \\
\mathbf{a}^2 &= \frac{1}{a}[(1 + z_{,x}^2)(\mathbf{e}_2 + z_{,y}\mathbf{k}) - z_{,x}z_{,y}(\mathbf{e}_1 + z_{,x}\mathbf{k})], \text{ and} \\
a_{\alpha\beta} &= \delta_{\alpha\beta} + z_{,\alpha}z_{,\beta}, (\delta_{\alpha\beta}: \text{Kronecker delta}).
\end{aligned} \tag{4.19}$$

Now, the admissible boundary conditions (i.e. boundary forces \mathbf{f} and moments \mathbf{M} on ∂w) are given by [15], [38] and [39], shown as

$$\begin{aligned}
\mathbf{f} &= F_\nu\nu + F_\tau\tau + F_n\mathbf{n}, \\
\mathbf{M} &= \frac{1}{2}W_H + \kappa_\tau W_K.
\end{aligned} \tag{4.20}$$

In the above, ν and $\tau = \mathbf{n} \times \nu$ are the unit normal and tangent to the boundary ∂w and

$$F_\nu = W + \lambda - \kappa_\nu M, F_\tau = -\tau M, F_n = (\tau W_K)' - \left(\frac{1}{2}W_H\right)_{,v} - (W_K)_{,\beta}\tilde{b}^{\alpha\beta}v_\alpha \tag{4.21}$$

are, respectively, the components of distributed forces per unit length applied on ∂w . Further, the expressions of τ , κ_ν and κ_τ can be obtained by

$$\tau = b^{\alpha\beta}\tau_\alpha\nu_\beta, \kappa_\nu = b^{\alpha\beta}\nu_\alpha\nu_\beta \text{ and } \kappa_\tau = b^{\alpha\beta}\tau_\alpha\tau_\beta, \tag{4.22}$$

which are the twist and normal curvatures of w in the directions of ν and τ , respectively. Thus, for example, we formulate from Eqs. (4.7), (4.21)₃ that

$$F_n = (\tau(s)\beta(\theta^\alpha))' - (\alpha(\theta^\alpha)H)_{,v} - (\beta(\theta^\alpha))_{,\beta}\tilde{b}^{\alpha\beta}v_\alpha, \tag{4.23}$$

where $(\tau(s)\beta(\theta^\alpha))'$ is the arc-length derivative of $\tau(s)\beta(\theta^\alpha)$ which can be evaluated as

$$\begin{aligned}
\tau(s)' &= \frac{\partial\tau}{\partial s} = \frac{\partial\tau}{\partial\theta^\beta} \frac{\partial\theta^\beta}{\partial s} = (\tau)_{,\beta}\tau^\beta = (b^{\alpha\beta}\tau_\alpha\nu_\beta)_{,\gamma}\tau^\gamma \\
&= (b^{\alpha\beta}\tau^\beta a_{\alpha\beta}v^\alpha a_{\alpha\beta})_{,\gamma}\tau^\gamma, \text{ and } \beta(\theta^\alpha)' = (\beta(\theta^\alpha))_{,\beta}\tau^\beta.
\end{aligned} \tag{4.24}$$

The above expressions can then be reformulated using the Monge representation for further analyses. In the case of general non-axisymmetric Polar coordinates, the above becomes

$$(b^{\alpha\beta}\tau^\beta a_{\alpha\beta}v^\alpha a_{\alpha\beta})_{,\gamma}\tau^\gamma = \left[\frac{1}{\sqrt{r^2[1+(z_{,r})^2] + (z_{,\theta})^2}}(rz_{,r\theta} - z_{,\theta})(z_{,r}z_{,\theta})^2 \right]_{,\theta}, \quad (4.25)$$

and similar treatments for the related terms.

4.2.2 Superposed incremental deformations

The evaluation of the resulting Euler equations and the associated boundary conditions in terms of Eqs. (4.14-4.19) furnishes a highly nonlinear PDE system, which in general requires heavy computational resources. Instead, a means of “admissible linearization” can be employed to make the system mathematically tractable with minimum loss of generality. The concept has been widely and successfully implemented in the relevant subject of studies (see, for example, [12], [25] and [27]). Within this prescription, the derivative of $z(\theta^\alpha)$ of all orders are considered to be “small” (e.g. $z_{,\alpha} \ll 1$) and thus, their products can be neglected. Accordingly, using the notation “ \simeq ” to identify equations to the leading order approximation of $z(\theta^\alpha)$, we obtain

$$\begin{aligned} a_{11} &\simeq r^2, \quad a_{22} \simeq 1, \quad a_{12} = a_{21} \simeq 0, \quad \det |a_{\alpha\beta}| = a \simeq r^2, \\ a^{11} &\simeq 1, \quad a^{22} \simeq \frac{1}{r^2}, \quad a^{12} = a^{21} \simeq 0, \\ \mathbf{n} &\simeq \mathbf{k} - \nabla_p z, \quad \mathbf{a}^1 \simeq \mathbf{e}_r + z_{,r}\mathbf{k}, \quad \mathbf{a}^2 \simeq \frac{1}{r}\mathbf{e}_\theta + \frac{1}{r^2}\mathbf{k}, \\ \mathbf{b} &\simeq z_{,rr}(\mathbf{e}_r \otimes \mathbf{e}_r) + \frac{rz_{,r\theta} - z_{,\theta}}{r^2}[(\mathbf{e}_r \otimes \mathbf{e}_\theta) + (\mathbf{e}_\theta \otimes \mathbf{e}_r)] + \frac{rz_{,r} + z_{,\theta\theta}}{r^2}(\mathbf{e}_\theta \otimes \mathbf{e}_\theta) \\ &= \nabla_p^2 z, \\ H &\simeq \frac{1}{2}[z_{,rr} + \frac{1}{r}z_{,r} + \frac{1}{r^2}z_{,\theta\theta}] = \frac{1}{2}\Delta_p z \text{ and } K \simeq 0, \end{aligned} \quad (4.26)$$

where the subscript $(*)_p$ denotes the projected counterparts of $(*)$ on the coordinate plane ω_p , $\nabla_p^2 z$ is the second gradient and $\Delta_p z = \text{tr}(\nabla_p^2 z)$ is the associated Laplacian.

In particular, using the results in Eq. (4.26), Eq. (4.11) reduces to

$$\lambda_{,r} = -\frac{\partial W}{\partial \theta^r} = -\frac{\partial \phi(\theta^\alpha)}{\partial \theta^r}, \quad \text{and} \quad \lambda_{,\theta} = -\frac{\partial W}{\partial \theta^\theta} = -\frac{\partial \phi(\theta^\alpha)}{\partial \theta^\theta}, \quad (4.27)$$

since

$$\frac{\partial\alpha(\theta^\alpha)}{\partial\theta^r}H^2 \simeq 0 \text{ and } \frac{\partial\beta(\theta^\alpha)}{\partial\theta^r}K \simeq 0. \quad (4.28)$$

Eq. (4.28) implies that the non-uniform potentials of $\alpha(\theta^\alpha)$ and $\beta(\theta^\alpha)$ in Eq. (4.1) do not necessarily result in non-uniform responses of membranes within the description of superposed incremental deformations. Hence, we deduce the linearized non-uniform energy density function as

$$W(H, K; \theta^\alpha) = \phi(\theta^\alpha) + kH^2 + \bar{k}(\theta^\alpha)K, \quad (4.29)$$

where the non-uniform properties of membranes may be characterized via the potential function $\phi(\theta^\alpha)$. In addition, using Eq. (4.29), we reduce Eq. (4.9) to

$$k\Delta H - 2H(\phi(\theta^\alpha) + \lambda) = P, \quad (4.30)$$

which may serve as the linearized shape equation for non-uniform membranes. The admissible linearization can also be implemented in the orthogonal Cartesian coordinates, where we find from Eqs. (4.18), (4.19) that

$$\begin{aligned} a &\cong 1, \mathbf{a}_\alpha = \mathbf{e}_\alpha + z_{,\alpha}\mathbf{k} \cong \mathbf{a}^\alpha, \mathbf{n} = \frac{\mathbf{k} - (z_{,x}\mathbf{e}_1 + z_{,y}\mathbf{e}_2)}{\sqrt{a}}, \\ H &\cong \frac{z_{,xx} + z_{,yy}}{2}, K \cong 0, \mathbf{b} = \frac{z_{,\alpha\beta}\mathbf{a}^\alpha \otimes \mathbf{a}^\beta}{\sqrt{a}}. \end{aligned} \quad (4.31)$$

Lastly, from Eqs. (4.11), (4.29), the associated tangential Euler equations can be obtained as

$$\lambda_{,x} = -\frac{\partial W}{\partial\theta^x} = -\frac{\partial\phi(\theta^\alpha)}{\partial\theta^x}, \text{ and } \lambda_{,y} = -\frac{\partial W}{\partial\theta^y} = -\frac{\partial\phi(\theta^\alpha)}{\partial\theta^y}. \quad (4.32)$$

4.3 Explanation on Inflammation from the Non-uniform Lipid Membrane morphology

In this section, we present analytical solutions for the previously obtained system of equations that describes the responses of lipid membranes subjected to local inflammations. The inflammations can be observed in membrane systems as a result of the

lateral pressure variation which may be induced by the weakened membrane-skeleton connection and/or the lateral diffusion induced by the hydrodynamic process of the Brownian motion (see, for example, [28–32]). In the assimilation of non-uniformity into the lipid membrane model, we adopt the flexural modulus of the membrane $k = 82pN \cdot nm$ from the work of [40] and [41]. The value of λ is dependent on the membrane systems under consideration and does not have a definite range of values (see, for example, [10, 22, 37]). In the present study, several different types of potential functions of λ are chosen to accommodate particular states of membranes' non-uniformity. The data are obtained under the normalized setting, unless otherwise specified, where the corresponding dimensional parameters are adopted from the works of [12], [42, 43] as

$$\begin{aligned} \mu &= \sqrt{2\lambda/k}: \text{inverse of natural length scale (e.g. } \mu a: \text{ radius of a circular membrane),} \\ \sigma/\lambda &: \text{force scale (e.g. } f_n = \sigma/\lambda: \text{ interaction force).} \end{aligned} \quad (4.33)$$

4.3.1 A rectangular membrane patch subjected to lateral pressures

In this section, we consider the deformations of a rectangular lipid membrane in the presence of lateral pressures and non-uniform distributions of strain energy. Emphasis is placed on the cases where the membrane is subjected to local inflammations where only quantitatively equivalent solutions were available via the impositions of the equivalent edge moments [27]. To proceed, we consider the following non-uniform energy distribution as

$$\lambda(\theta^\alpha) + \phi(\theta^\alpha) = \alpha \cos(nx), \quad (4.34)$$

and thereby it is obtained from Eq. (4.30) that

$$\frac{\partial^2 H(x, y)}{\partial x^2} + \frac{\partial^2 H(x, y)}{\partial y^2} - \frac{2\alpha \cos(nx)}{k} H(x, y) = \frac{P}{k}. \quad (4.35)$$

Utilizing the standard form of $H(x, y) = H(x)[A_m \sin(my) + B_m \cos(my)]$, the above becomes

$$\frac{\partial^2 H(x)}{\partial x^2} - m^2 H(x) - \frac{2\alpha \cos(nx)}{k} H(x) = \frac{P}{k[A_m \sin(my) + B_m \cos(my)]}. \quad (4.36)$$

The homogeneous solution of Eq. (4.36) is given by in the form of the modified Mathieu function as

$$H(x)_c = A_m \mathbf{Ce}\left(-\frac{4m^2}{n^2}, \frac{4\alpha}{n^2 k}, \frac{n}{2}x\right) + B_m \mathbf{Se}\left(-\frac{4m^2}{n^2}, \frac{4\alpha}{n^2 k}, \frac{n}{2}x\right), \quad (4.37)$$

where \mathbf{Ce} and \mathbf{Se} are respectively, the even and odd modified Mathieu function of the first kind. Now the Wronskian of the above solution yields

$$\begin{aligned} \mathbf{W}_1 = & \mathbf{Ce}\left(-\frac{4m^2}{n^2}, \frac{4\alpha}{n^2 k}, \frac{n}{2}x\right) [\mathbf{Se}\left(-\frac{4m^2}{n^2}, \frac{4\alpha}{n^2 k}, \frac{n}{2}x\right)]' - \\ & [\mathbf{Ce}\left(-\frac{4m^2}{n^2}, \frac{4\alpha}{n^2 k}, \frac{n}{2}x\right)]' \mathbf{Se}\left(-\frac{4m^2}{n^2}, \frac{4\alpha}{n^2 k}, \frac{n}{2}x\right). \end{aligned} \quad (4.38)$$

In view of Eq. (4.38), the particular solution is then given by

$$\begin{aligned} H(x, y)_p = & -\mathbf{Ce}\left(-\frac{4m^2}{n^2}, \frac{4\alpha}{n^2 k}, \frac{n}{2}x\right) \int_0^x \frac{\mathbf{Se}\left(-\frac{4m^2}{n^2}, \frac{4\alpha}{n^2 k}, \frac{n}{2}x\right) P}{\mathbf{W}_1} \frac{P}{k} dx + \\ & \mathbf{Se}\left(-\frac{4m^2}{n^2}, \frac{4\alpha}{n^2 k}, \frac{n}{2}x\right) \int_0^x \frac{\mathbf{Ce}\left(-\frac{4m^2}{n^2}, \frac{4\alpha}{n^2 k}, \frac{n}{2}x\right) P}{\mathbf{W}_1} \frac{P}{k} dx. \end{aligned} \quad (4.39)$$

Hence, the general solution of Eq. (4.35) can be found as

$$\begin{aligned} H(x, y) = & -\mathbf{Ce}\left(-\frac{4m^2}{n^2}, \frac{4\alpha}{n^2 k}, \frac{n}{2}x\right) \int_0^x \frac{\mathbf{Se}\left(-\frac{4m^2}{n^2}, \frac{4\alpha}{n^2 k}, \frac{n}{2}x\right) P}{\mathbf{W}_1} \frac{P}{k} dx + \\ & \mathbf{Se}\left(-\frac{4m^2}{n^2}, \frac{4\alpha}{n^2 k}, \frac{n}{2}x\right) \int_0^x \frac{\mathbf{Ce}\left(-\frac{4m^2}{n^2}, \frac{4\alpha}{n^2 k}, \frac{n}{2}x\right) P}{\mathbf{W}_1} \frac{P}{k} dx + \\ & A_m \mathbf{Ce}\left(-\frac{4m^2}{n^2}, \frac{4\alpha}{n^2 k}, \frac{n}{2}x\right) \cos(my), \end{aligned} \quad (4.40)$$

where the odd part of the modified Mathieu function is removed for the required membrane symmetry (i.e. $H(-x, y) = H(x, y)$). Also, from Eq. (4.31)₄ we find

$$2H(x, y) = \frac{\partial^2 z(x, y)}{\partial x^2} + \frac{\partial^2 z(x, y)}{\partial y^2}. \quad (4.41)$$

The above can be rewritten as

$$\frac{2H(x, y)}{[C_m \sin(my) + D_m \cos(my)]} = \frac{\partial^2 z(x)}{\partial x^2} - m^2 z(x), \quad (4.42)$$

where $z(x)$ is assumed to have the following form

$$z(x, y) = z(x)[C_m \sin(my) + D_m \cos(my)]. \quad (4.43)$$

The homogeneous solution of Eq. (4.42) and the associate Wronskian are then obtained by

$$\begin{aligned} z(x) &= E_m \sinh(mx) + F_m \cosh(mx), \\ \mathbf{W}_2 &= \sinh(mx)[\cosh(mx)]' - [\sinh(mx)]' \cosh(mx) = -m. \end{aligned} \quad (4.44)$$

Thus, the particular solution of $z(x, y)$ can be found as

$$z(x, y)_{p1} = 2 \sinh(x) \int_0^x \frac{\cosh(mx)}{m} H(x, y)_p dx - 2 \cosh(x) \int_0^x \frac{\sinh(mx)}{m} H(x, y)_p dx. \quad (4.45)$$

But, from Eq. (4.41), the complementary part of $H(x, y)$ also requires

$$\frac{\partial^2 z(x, y)}{\partial x^2} + \frac{\partial^2 z(x, y)}{\partial y^2} = 2H(x, y)_c, \quad (4.46)$$

where

$$H(x, y)_c = A_m \mathbf{Ce}\left(-\frac{4m^2}{n^2}, \frac{4\alpha}{n^2 k}, \frac{n}{2}x\right) \cos(my). \quad (4.47)$$

Therefore, we find the following complementary solution of $z(x, y)$:

$$\begin{aligned} z(x, y)_{c1} &= -A_m \frac{\cosh(\alpha_m x) \cos(\alpha_m y)}{\alpha_m} \int_0^x \sinh(\alpha_m x) \mathbf{Ce}\left(-\frac{4m^2}{n^2}, \frac{4\alpha}{n^2 k}, \frac{n}{2}x\right) dx \\ &+ A_m \frac{\sinh(\alpha_m x) \cos(\alpha_m y)}{\alpha_m} \int_0^x \cosh(\alpha_m x) \mathbf{Ce}\left(-\frac{4m^2}{n^2}, \frac{4\alpha}{n^2 k}, \frac{n}{2}x\right) dx \\ &+ C_m \cosh(\alpha_m x) \cos(\alpha_m y). \end{aligned} \quad (4.48)$$

The complete solution also requires the similar procedures with respect to y . This can be done by writing $H(x, y)$ as

$$H(x, y) = R(y)[H_m \sin(mx) + I_m \cos(mx)], \quad (4.49)$$

and thereby yields from Eq. (4.35) that

$$\frac{\partial^2 R(y)}{\partial y^2} - m^2 R(y) - \frac{2\alpha \cos(nx)}{k} R(y) = \frac{P}{k[H_m \sin(mx) + I_m \cos(mx)]}. \quad (4.50)$$

The complementary solution and the associated Wronskian of the above equation can then be respectively obtained as

$$R_c(y) = J_m \cosh\left(\sqrt{m^2 + \frac{2\alpha \cos(nx)}{k}} y\right) + K_m \sinh\left(\sqrt{m^2 + \frac{2\alpha \cos(nx)}{k}} y\right), \quad (4.51)$$

and

$$\mathbf{W} = \sqrt{m^2 + \frac{2\alpha \cos(nx)}{k}}. \quad (4.52)$$

Therefore, applying the same methodology as in Eqs. (4.36)-(4.48), we find the following particular and homogeneous solutions.

$$\begin{aligned} z(x, y)_{p2} = & \frac{-\cosh(my)P}{2km(m^2 + \frac{2\alpha \cos(nx)}{k})} \left[\frac{\cosh(my - \sqrt{m^2 + \frac{2\alpha \cos(nx)}{k}} y)}{m - \sqrt{m^2 + \frac{2\alpha \cos(nx)}{k}}} + \right. \\ & \left. \frac{\cosh(my + \sqrt{m^2 + \frac{2\alpha \cos(nx)}{k}} y)}{m + \sqrt{m^2 + \frac{2\alpha \cos(nx)}{k}}} + \frac{mk}{\alpha \cos(nx)} \right] + \\ & \frac{\sinh(my)P}{2mk(m^2 + \frac{2\alpha \cos(nx)}{k})} \left[\frac{\sinh(my - \sqrt{m^2 + \frac{2\alpha \cos(nx)}{k}} y)}{m - \sqrt{m^2 + \frac{2\alpha \cos(nx)}{k}}} + \right. \\ & \left. \frac{\sinh(my + \sqrt{m^2 + \frac{2\alpha \cos(nx)}{k}} y)}{m + \sqrt{m^2 + \frac{2\alpha \cos(nx)}{k}}} \right] + \\ & \frac{P}{km^2(m^2 + \frac{2\alpha \cos(nx)}{k})} [1 - \cosh(my)], \end{aligned} \quad (4.53)$$

and

$$\begin{aligned}
z(x, y)_{c2} = & -H_m \frac{\cosh(\beta_m y)}{\beta_m} \left[\frac{\cosh(\beta_m y - \sqrt{\beta_m^2 + \frac{2\alpha \cos(nx)}{k}} y)}{\beta_m - \sqrt{\beta_m^2 + \frac{2\alpha \cos(nx)}{k}}} + \right. \\
& \left. \frac{\cosh(\beta_m y + \sqrt{\beta_m^2 + \frac{2\alpha \cos(nx)}{k}} y)}{\beta_m + \sqrt{\beta_m^2 + \frac{2\alpha \cos(nx)}{k}}} + \frac{\beta_m k}{\alpha \cos(nx)} \right] \cos(\beta_m x) + \\
& \frac{H_m \sinh(\beta_m y)}{\beta_m} \left[\frac{\sinh(\beta_m y - \sqrt{\beta_m^2 + \frac{2\alpha \cos(nx)}{k}} y)}{\beta_m - \sqrt{\beta_m^2 + \frac{2\alpha \cos(nx)}{k}}} + \right. \\
& \left. \frac{\sinh(\beta_m y + \sqrt{\beta_m^2 + \frac{2\alpha \cos(nx)}{k}} y)}{\beta_m + \sqrt{\beta_m^2 + \frac{2\alpha \cos(nx)}{k}}} \right] \cos(\beta_m x) + \\
& J_m \cosh(\beta_m y) \cos(\beta_m x). \tag{4.54}
\end{aligned}$$

Finally, the complete solution of $z(x, y)$ can be obtained as

$$z(x, y) = \sum_{m=2,4,6}^{\infty} z(x, y)_{p1} + z(x, y)_{c1} + z(x, y)_{p2} + z(x, y)_{c2}, \tag{4.55}$$

where the expressions of $z(x, y)_{p1}$, $z(x, y)_{c1}$, $z(x, y)_{p2}$ and $z(x, y)_{c2}$ are respectively defined in Eqs. (4.45), (4.48), (4.53), and (4.54). The unknown constants α_m , β_m , A_m , C_m , H_m , and J_m can be completely determined by imposing the admissible sets of boundary conditions. For example, if the rectangular-shaped membrane is characterized by the width a and length b and subjected to the following boundary conditions

$$z\left(\frac{a}{2}, y\right) = z\left(-\frac{a}{2}, y\right) = 0 \text{ and } z\left(x, \frac{b}{2}\right) = z\left(x, -\frac{b}{2}\right) = 0, \tag{4.56}$$

thereby, the unknowns can be determined as

$$\begin{aligned}
a_m &= \frac{\pi}{b}, \beta_m = \frac{\pi}{a}, A_m = H_m = 1, \\
C_m &= \frac{-z(\frac{a}{2}, y)_{p1} - z(\frac{a}{2}, y)_{p2}}{\cosh(\alpha_m \frac{a}{2}) \cos(\alpha_m y)} + \frac{1}{\alpha_m} \int_0^{\frac{a}{2}} \sinh(\alpha_m x) \mathbf{Ce}(-\frac{4m^2}{n^2}, \frac{4\alpha}{n^2 k}, \frac{n}{2} x) dx \\
&\quad - \frac{\sinh(\alpha_m \frac{a}{2})}{\cosh(\alpha_m \frac{a}{2}) \alpha_m} \int_0^{\frac{a}{2}} \cosh(\alpha_m x) \mathbf{Ce}(-\frac{4m^2}{n^2}, \frac{4\alpha}{n^2 k}, \frac{n}{2} x) dx \\
J_m &= \frac{-z(x, \frac{b}{2})_{p1} - z(x, \frac{b}{2})_{p3}}{\cosh(\beta_m \frac{b}{2}) \cos(\beta_m x)} + \frac{1}{\beta_m} \left[\frac{\cosh(\beta_m \frac{b}{2} - \sqrt{\beta_m^2 + \frac{2\alpha \cos(nx)}{k}} \frac{b}{2})}{\beta_m - \sqrt{\beta_m^2 + \frac{2\alpha \cos(nx)}{k}}} + \right. \\
&\quad \left. \frac{\cosh(\beta_m \frac{b}{2} + \sqrt{\beta_m^2 + \frac{2\alpha \cos(nx)}{k}} \frac{b}{2})}{\beta_m + \sqrt{\beta_m^2 + \frac{2\alpha \cos(nx)}{k}}} + \frac{\beta_m k}{\alpha \cos(nx)} \right] - \\
&\quad \frac{\sinh(\beta_m \frac{b}{2})}{\cosh(\beta_m \frac{b}{2}) \beta_m} \left[\frac{\sinh(\beta_m \frac{b}{2} - \sqrt{\beta_m^2 + \frac{2\alpha \cos(nx)}{k}} \frac{b}{2})}{\beta_m - \sqrt{\beta_m^2 + \frac{2\alpha \cos(nx)}{k}}} + \right. \\
&\quad \left. \frac{\sinh(\beta_m \frac{b}{2} + \sqrt{\beta_m^2 + \frac{2\alpha \cos(nx)}{k}} \frac{b}{2})}{\beta_m + \sqrt{\beta_m^2 + \frac{2\alpha \cos(nx)}{k}}} \right]. \tag{4.57}
\end{aligned}$$

With the determined solution, Figure 4.1 illustrates the deformation contour of the lipid membrane with different types of non-uniform energy distributions. Depending

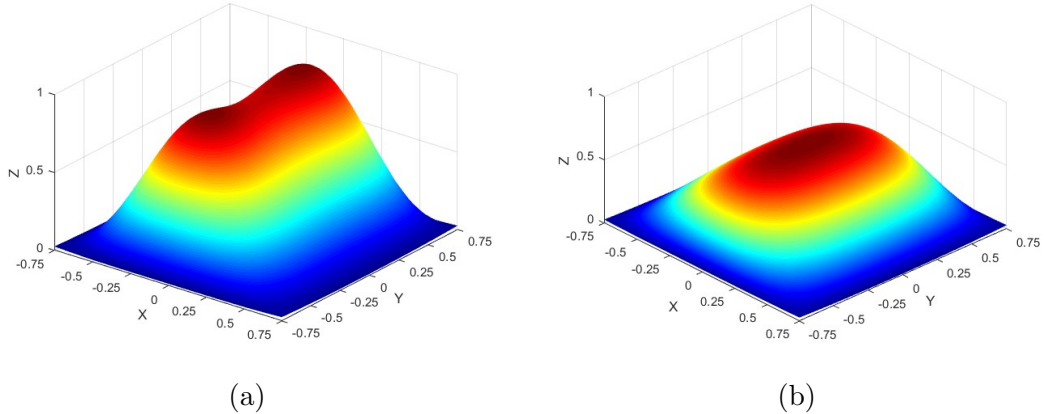


Figure 4.1: Deformation contour of non-uniform lipid membrane subjected to uniform pressure $P = 1$: (a) double-peak morphology, (b) single-peak morphology.

on the choice of a particular non-uniformity, the proposed model illustrates the double peak formations (Figure 4.1 left) and single peak but non-uniform morphology (Fig-

ure 4.1 right) of lipid membranes. The transverse deflections of lipid membranes (at $y=0$) with respect to the intensity of non-uniform energy distributions are presented in Figure 4.2. It is shown that the non-uniformity is gradually diminished with vanishing non-uniform energy distribution and the corresponding deformed configuration tends to resemble those obtained from the uniform membrane cases [27] (see, Figure 4.2). Finally, the solution of uniform membrane cases can also be obtained from the

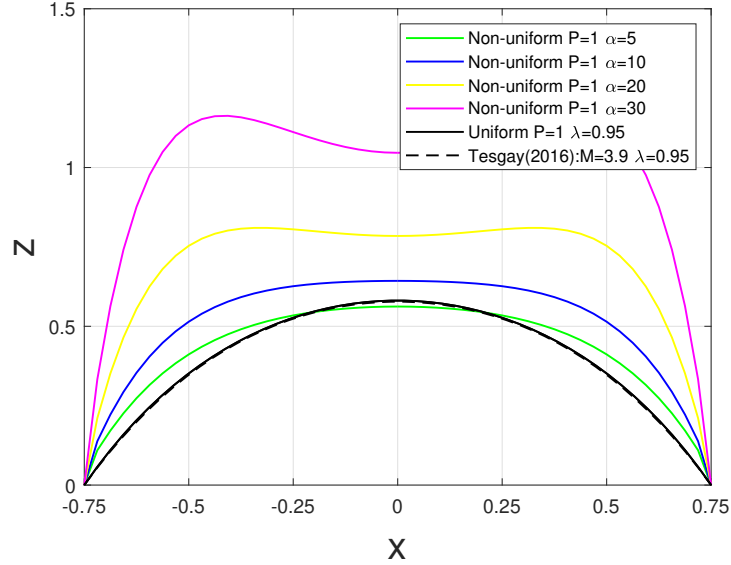


Figure 4.2: Transverse deflections of the lipid membrane with respect to different α when $P = 1$.

proposed non-uniform model. To see this, we replace $\alpha \cos(nx)$ in Eq. (4.55) by λ and thereby obtain

$$\begin{aligned}
 & z(x, y) \\
 = & P \left[\left(\sum_{m=1}^{\infty} (A_m \cosh(\beta_m y) + \cosh(\alpha_m y)) \cos(\alpha_m x) + \frac{2}{k \alpha_m'^2 (\alpha_m'^2 + \mu^2)} + \right. \right. \\
 & \left. \left. (B_m \cosh(\gamma_m x) + \cosh(\theta_m x)) \cos(\theta_m y) \right) - C_m \right], \tag{4.58}
 \end{aligned}$$

where

$$\begin{aligned}
A_m &= -\frac{\cosh(0.5b\alpha_m)}{\cosh(0.5b\beta_m)}, \beta_m = -\frac{\cosh(0.5a\theta_m)}{\cosh(0.5a\gamma_m)}, \\
C_m &= \sum_{m=1}^{\infty} [(A_m \cosh(\beta_m y) + \cosh(\alpha_m y)) \cos(\alpha_m x) + \frac{2}{k\alpha_m'(\alpha_m'^2 + \mu^2)} + \\
&\quad (B_m \cosh(\gamma_m x) + \cosh(\theta_m x)) \cos(\theta_m y)], \\
\alpha_m' &= \frac{m\pi}{a}, \alpha_m = \frac{\pi}{a}, \beta_m^2 = \alpha_m^2 + \mu^2, \theta_m = \frac{\pi}{b}, \text{ and } \gamma_m^2 = \theta_m^2 + \mu^2. \quad (4.59)
\end{aligned}$$

The above expression may be used as an alternative form of the non-uniform membrane solution and, perhaps, is of practical interest due to its relative simplicity in the associated analyses. It is shown in Figure 4.3 that the obtained uniform membrane

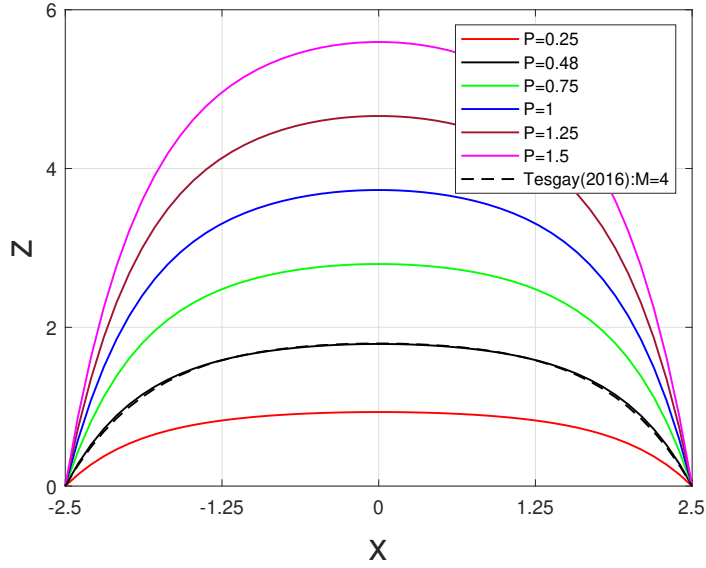


Figure 4.3: Transverse deflections of uniform lipid membrane under increasing lateral pressure P .

solution adequately predicts the deformations of the membrane when subjected to uniform internal pressure (i.e. the transverse deformation increases as the internal pressure intensifies). In particular, the presented solution accommodates the results in [27] when the equivalent internal pressure is applied (see, Figure 4.3).

4.3.2 Inflammations of circumferentially non-uniform membranes

To describe the inflammation-induced deformations of membranes with circumferentially non-uniform responses, we consider the following non-uniform potential

$$\lambda(\theta^\alpha) + \phi(\theta^\alpha) = \alpha\tilde{\theta}(\theta), \quad (4.60)$$

where α defines the rigidity of the membrane and $\tilde{\theta}(\theta)$ describes the states of non-uniformity in circumferential direction. For the purpose of demonstration, we consider the periodic non-uniform distributions of the form

$$\tilde{\theta}(\theta) = \cos(n\theta) + \pi, \quad (4.61)$$

where n controls particular states of periodic distributions. Hence we find

$$[\lambda(\theta^\alpha) + \phi(\theta^\alpha)]_{,r} = 0, \text{ and } [\lambda(\theta^\alpha) + \phi(\theta^\alpha)]_{,\theta} = -n\alpha \sin(n\theta), \quad (4.62)$$

so that the membrane is radially uniform (i.e. $[\lambda(\theta^\alpha) + \phi(\theta^\alpha)]_{,r} = 0$) but circumferentially non-uniform (i.e. $[\lambda(\theta^\alpha) + \phi(\theta^\alpha)]_{,\theta} \neq 0$). The substitution of Eqs. (4.60)-(4.61) into Eq. (4.30) then yields

$$H_{,rr} + \frac{1}{r}H_{,r} + \frac{1}{r^2}H_{,\theta\theta} - \frac{2\alpha[\cos(n\theta) + \pi]}{k}H = \frac{P}{k}. \quad (4.63)$$

The general solution to the above can be solved as

$$H(r, \theta) = R(r, \theta)[F_m \sin(m\theta) + G_m \cos(m\theta)]. \quad (4.64)$$

Accordingly, combining Eqs. (4.63)-(4.64), we obtain that

$$R_{,rr} + \frac{1}{r}R_{,r} - \frac{m^2}{r^2}R - \frac{2\alpha[\cos(n\theta) + \pi]}{k}R = \frac{P}{k[F_m \sin(m\theta) + G_m \cos(m\theta)]}. \quad (4.65)$$

The complementary solution for the above differential equation is given by

$$R(r, \theta) = C_m I_m\left(\sqrt{\frac{2\alpha[\cos(n\theta) + \pi]}{k}}r\right) + D_m K_m\left(\sqrt{\frac{2\alpha[\cos(n\theta) + \pi]}{k}}r\right). \quad (4.66)$$

In view of Eq. (4.66), the particular solution of Eq. (4.65) can be obtained via the method of variation of parameters [33, 34], shown as

$$\begin{aligned}
& H(r, \theta) \\
= & I_m \left(\sqrt{\frac{2\alpha\tilde{\theta}(\theta)}{k}} r \right) [F_m \sin(m\theta) + G_m \cos(m\theta)] + \\
& \frac{P}{k} \left[I_m \left(\sqrt{\frac{2\alpha\tilde{\theta}(\theta)}{k}} r \right) \int_0^r \left(\frac{K_m \left(\sqrt{\frac{2\alpha\tilde{\theta}(\theta)}{k}} \xi_1 \right)}{\left[\begin{array}{l} \sqrt{\frac{2\alpha\tilde{\theta}(\theta)}{k}} I_{m+1} \left(\sqrt{\frac{2\alpha\tilde{\theta}(\theta)}{k}} \xi_1 \right) K_m \left(\sqrt{\frac{2\alpha\tilde{\theta}(\theta)}{k}} \xi_1 \right) + \\ \sqrt{\frac{2\alpha\tilde{\theta}(\theta)}{k}} I_m \left(\sqrt{\frac{2\alpha\tilde{\theta}(\theta)}{k}} \xi_1 \right) K_{m+1} \left(\sqrt{\frac{2\alpha\tilde{\theta}(\theta)}{k}} \xi_1 \right) \end{array} \right]} \right) d\xi_1 - \\
& K_m \left(\sqrt{\frac{2\alpha\tilde{\theta}(\theta)}{k}} r \right) \int_0^r \left(\frac{I_m \left(\sqrt{\frac{2\alpha\tilde{\theta}(\theta)}{k}} \xi_1 \right)}{\left[\begin{array}{l} \sqrt{\frac{2\alpha\tilde{\theta}(\theta)}{k}} I_{m+1} \left(\sqrt{\frac{2\alpha\tilde{\theta}(\theta)}{k}} \xi_1 \right) K_m \left(\sqrt{\frac{2\alpha\tilde{\theta}(\theta)}{k}} \xi_1 \right) + \\ \sqrt{\frac{2\alpha\tilde{\theta}(\theta)}{k}} I_m \left(\sqrt{\frac{2\alpha\tilde{\theta}(\theta)}{k}} \xi_1 \right) K_{m+1} \left(\sqrt{\frac{2\alpha\tilde{\theta}(\theta)}{k}} \xi_1 \right) \end{array} \right]} \right) d\xi_1 \right].
\end{aligned} \tag{4.67}$$

Now, from Eq. (4.26)₅(the expression of H), $H(r, \theta)$ satisfies

$$2H = Z_{,rr} + \frac{1}{r}Z_{,r} + \frac{1}{r^2}Z_{,\theta\theta}. \tag{4.68}$$

Using the general form of solution $Z(r, \theta) = S(r)[A_m \sin(m\theta) + B_m \cos(m\theta)]$, the above may be recast as

$$S_{,rr} + \frac{1}{r}S_{,r} - \frac{m^2}{r^2}S = \frac{2H}{A_m \sin(m\theta) + B_m \cos(m\theta)}, \tag{4.69}$$

where the solution of $S(r)$ is obtained as

$$S(r) = C_m r^{-m} + D_m r^m, \tag{4.70}$$

which serves as the homogeneous solution of the PDE. Then, with the given Eq. (4.7), we utilize the method of variation of parameters [33, 34] and find that

$$\begin{aligned}
Z(r, \theta) = & \sum_{m=1,2,3..}^{\infty} \frac{r^m P}{k} \left\{ \int_0^r \frac{1}{m\xi^{m-1}} [I_m(\sqrt{\frac{2\alpha\tilde{\theta}(\theta)}{k}}\xi) \int_0^{\xi} \frac{K_m(\sqrt{\frac{2\alpha\tilde{\theta}(\theta)}{k}}\xi_1)d\xi_1 -}{K_m(\sqrt{\frac{2\alpha\tilde{\theta}(\theta)}{k}}\xi) \int_0^{\xi} (\sqrt{\frac{2\alpha\tilde{\theta}(\theta)}{k}}\xi_1)d\xi_1] d\xi \right\} - \\
& \frac{P}{kmr^m} \left\{ \int_0^r \xi^{m+1} [I_m(\sqrt{\frac{2\alpha\tilde{\theta}(\theta)}{k}}\xi) \int_0^{\xi} \frac{K_m(\sqrt{\frac{2\alpha\tilde{\theta}(\theta)}{k}}\xi_1)d\xi_1 -}{K_m(\sqrt{\frac{2\alpha\tilde{\theta}(\theta)}{k}}\xi) \int_0^{\xi} \frac{I_m(\sqrt{\frac{2\alpha\tilde{\theta}(\theta)}{k}}\xi_1)d\xi_1}{L_m}(\sqrt{\frac{2\alpha\tilde{\theta}(\theta)}{k}}\xi_1)] d\xi \right\} + \\
& [\sin(m\theta) + A_m \cos(m\theta)] \left[\begin{array}{l} r^m \int_0^r \frac{I_m(\sqrt{\frac{2\alpha\tilde{\theta}(\theta)}{k}}\xi)}{m\xi^{m-1}} d\xi - \\ r^{-m} \int_0^r \frac{\xi^{m+1} I_m(\sqrt{\frac{2\alpha\tilde{\theta}(\theta)}{k}}\xi)}{m} d\xi \end{array} \right], \quad (4.71)
\end{aligned}$$

where

$$\begin{aligned}
L_m = & \sqrt{\frac{2\alpha\tilde{\theta}(\theta)}{k}} I_{m+1}(\sqrt{\frac{2\alpha\tilde{\theta}(\theta)}{k}}\xi_1) K_m(\sqrt{\frac{2\alpha\tilde{\theta}(\theta)}{k}}\xi_1) + \\
& \sqrt{\frac{2\alpha\tilde{\theta}(\theta)}{k}} I_m(\sqrt{\frac{2\alpha\tilde{\theta}(\theta)}{k}}\xi_1) K_{m+1}(\sqrt{\frac{2\alpha\tilde{\theta}(\theta)}{k}}\xi_1). \quad (4.72)
\end{aligned}$$

The unknown coefficients A_m in Eq. (4.71) can be completely determined by imposing the boundary condition

$$Z(r, \theta)_{,r} = 0 \text{ at } r = a, \quad (4.73)$$

from which we find

$$A_m = \frac{\left\{ \frac{r^m P}{k} \int_0^r \left(\frac{1}{m\xi^{m-1}} M_m - N_m \right) d\xi - \frac{P}{kmr^m} \int_0^r (\xi^{m+1} M_m - N_m) d\xi \right\}_{,r}}{\cos(m\theta) \left[r^m \int_0^r \frac{I_m(\sqrt{\frac{2\alpha\tilde{\theta}(\theta)}{k}}\xi)}{m\xi^{m-1}} d\xi - r^{-m} \int_0^r \frac{\xi^{m+1} I_m(\sqrt{\frac{2\alpha\tilde{\theta}(\theta)}{k}}\xi)}{m} d\xi \right]_{,r}} - \tan(m\theta), \quad (4.74)$$

where

$$\begin{aligned}
M_m = & I_m(\sqrt{\frac{2\alpha\tilde{\theta}(\theta)}{k}}\xi) \int_0^{\xi} \frac{K_m(\sqrt{\frac{2\alpha\tilde{\theta}(\theta)}{k}}\xi_1)}{L_m} d\xi_1 \text{ and} \\
N_m = & K_m(\sqrt{\frac{2\alpha\tilde{\theta}(\theta)}{k}}\xi) \int_0^{\xi} \frac{I_m(\sqrt{\frac{2\alpha\tilde{\theta}(\theta)}{k}}\xi_1)}{L_m} d\xi_1. \quad (4.75)
\end{aligned}$$

Figure 4.4 illustrates the transverse deformations of circumferentially non-uniform membrane subjected to lateral pressure P and the coefficient of energy distribution

α , respectively. It is shown that the obtained solution demonstrates sufficient sensitivity to simulate the membrane's morphology when subjected to increasing lateral pressures (Figure 4.4(a)). In particular, the proposed model demonstrates membrane deformations with respect to the membranes' energy density characterized by the periodic function of strain energy (Eq. (4.61)). For instance, the transverse deflections of the membrane gradually decrease with increasing energy density distribution coefficient α , since more energy is required for non-uniformity (see, Figure 4.4(b)). Further, the non-uniform membrane solution reduces to those obtained from uniform membrane when equivalent energy density distribution is applied (i.e. $\alpha = 1$, see, black lines in Figure 4.4(b)). Lastly, the non-uniform responses of artificially treated

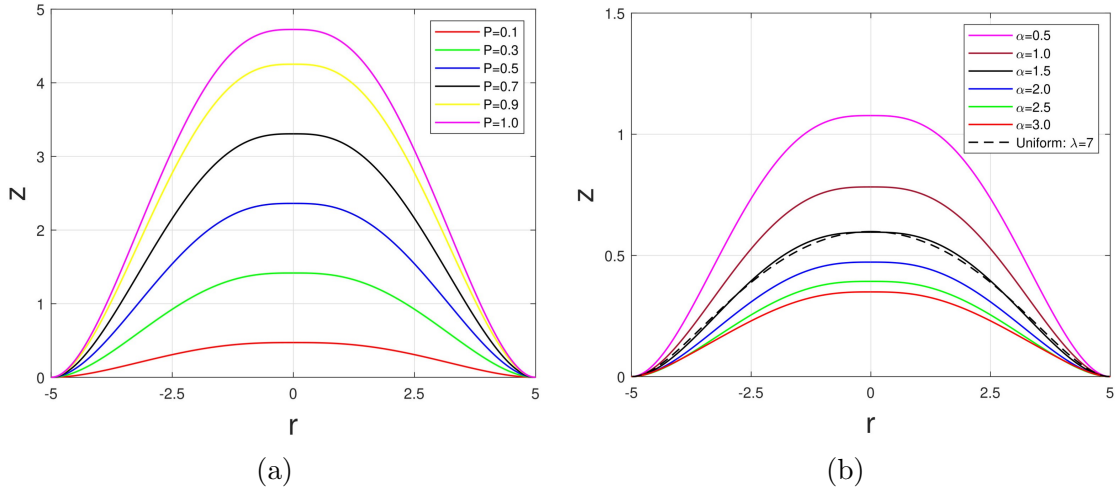


Figure 4.4: (a) The transverse deflection of circumferentially non-uniform lipid membrane with respect to increasing lateral pressure P ; (b) The transverse deflection of circumferentially non-uniform lipid membrane with respect to increasing α .

cell membranes [36] may be simulated by using the proposed model. Figure 4.5 illustrates that the obtained solution might demonstrate the echinocyte formation of the cell membrane induced by the incubation with lecithin [36]. The type of analysis was not accommodated by the existing membrane-substrate interaction models due to their limited predictions near and/or in the vicinity of the center of membranes (i.e. $r = 0$, see, for example, [22–24]). The off-centered biconcave discoid structures of non-uniform red blood cells [35] may also be simulated using the proposed en-

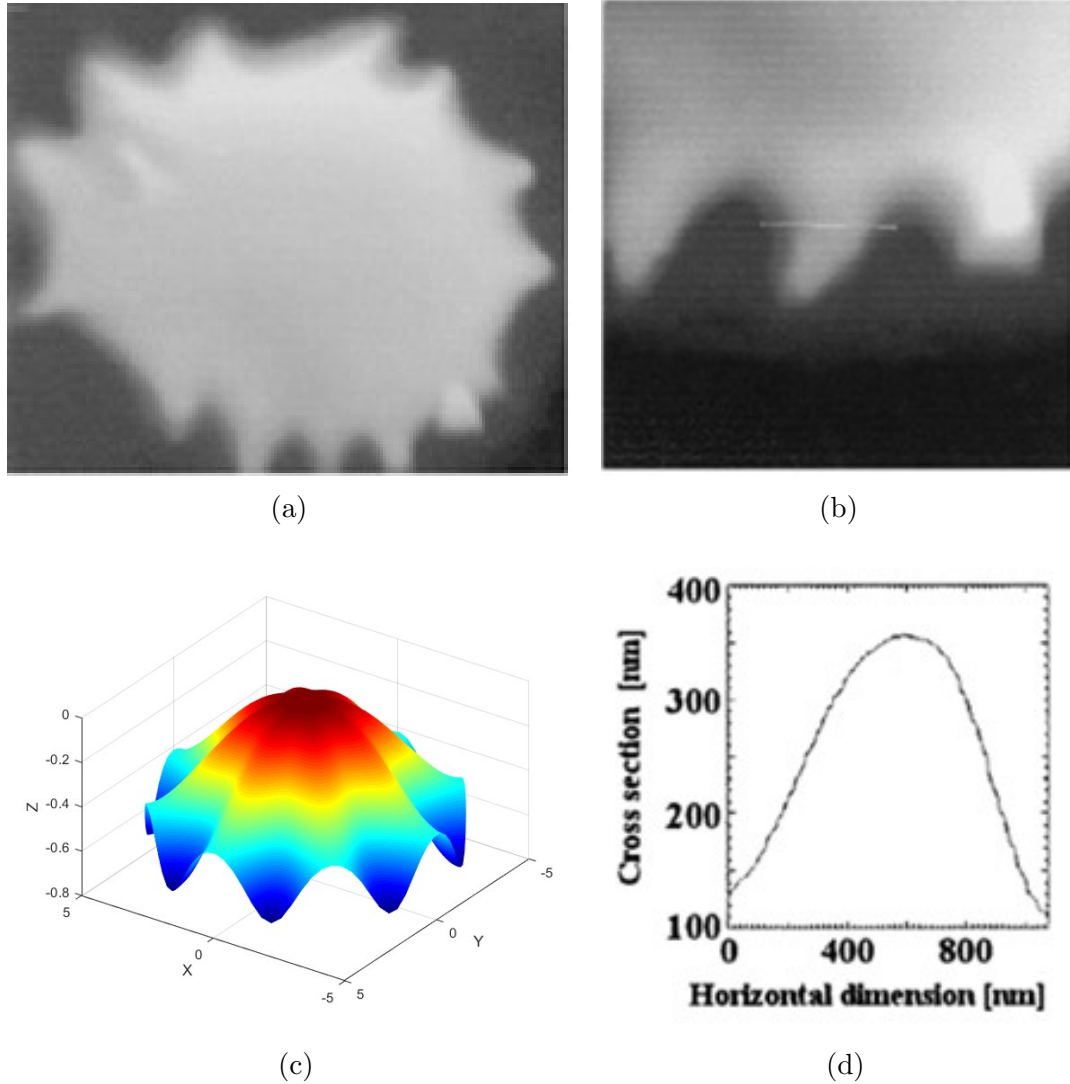


Figure 4.5: (a, b, d): The morphologies and cross-section image of the lecithin-treated cell [36]; (c): The deformation of circumferentially non-uniform membrane when $\tilde{\theta}(\theta) = \cos(8\theta) + \pi$.

ergy potential (Figure 4.6). The mechanisms for the above-mentioned membranes' morphologies have yet to be fully understood. The obtained results could provide phenomenologically meaningful implications by estimating the required energy density distributions leading to such morphological formations of membranes.

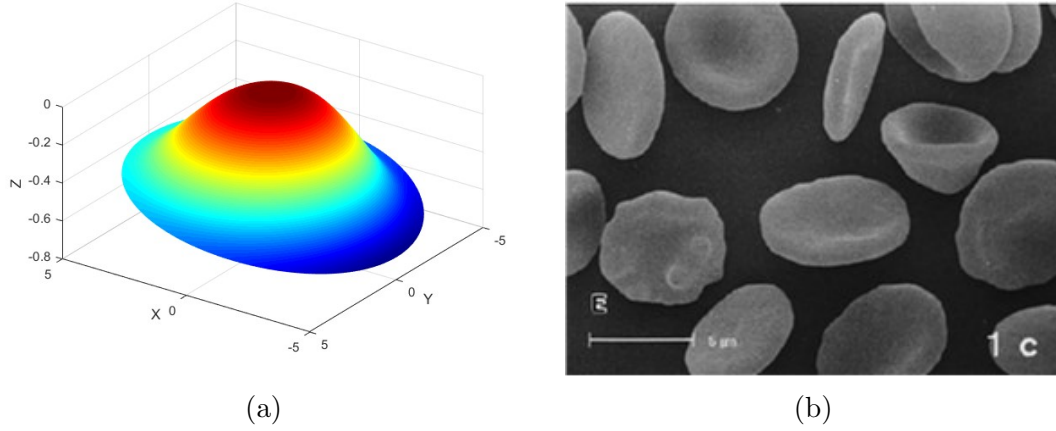


Figure 4.6: (a) The simulation result of the off-centered non-uniform morphology when $\phi + \lambda = \cos(\theta) + \pi$; (b) The off-centered biconcave discoid morphology of red blood cell [35].

4.3.3 Inflammations of radially non-uniform membranes

The inflammations of radially non-uniform membranes can also be examined using the energy distribution potentials of the form:

$$\lambda(\theta^\alpha) + \phi(\theta^\alpha) = \alpha r^n, \quad (4.76)$$

where α and n characterize the states of non-uniformities. In the forgoing analysis, we demonstrate the cases when $n = -2$ for the sake of simplicity. It is noted that the solutions of arbitrary n cases can be accommodated using the same procedures, as illustrated in this section. For $n = -2$, we evaluate from Eq. (4.76) that

$$[\lambda(\theta^\alpha) + \phi(\theta^\alpha)]_{,r} = -\frac{2\alpha}{r^3} \text{ and } [\lambda(\theta^\alpha) + \phi(\theta^\alpha)]_{,\theta} = 0, \quad (4.77)$$

so that the properties of radially non-uniform membrane ($\lambda_{,r} \neq 0$) maybe accommodated. Thus, the substitution of Eq. (4.76) into Eq. (4.30) yields

$$H_{,rr} + \frac{1}{r}H_{,r} + \frac{1}{r^2}H_{,\theta\theta} - \frac{2\alpha}{kr^2}H = \frac{P}{k} \quad (4.78)$$

Now, in view of Eq. (4.26)₅ (the expression of H), the above becomes

$$\begin{aligned} \frac{2P}{k} = & Z_{,rrrr} + \frac{2}{r^2}Z_{,rr\theta\theta} + \frac{1}{r^4}Z_{,\theta\theta\theta\theta} + \frac{2}{r}Z_{,rrr} - \frac{2}{r^3}Z_{,r\theta\theta} - \\ & \frac{1}{r^2}Z_{,rr} + \frac{4}{r^4}Z_{,\theta\theta} + \frac{1}{r^3}Z_{,r} - \frac{2\alpha}{kr^2}[Z_{,rr} + \frac{1}{r}Z_{,r} + \frac{1}{r^2}Z_{,\theta\theta}]. \end{aligned} \quad (4.79)$$

Since the response of radially non-uniform membrane is axisymmetric, Eq. (4.79) may be further reduced to

$$Z_{,rrrr} + \frac{2}{r}Z_{,rrr} - \frac{1}{r^2}Z_{,rr} + \frac{1}{r^3}Z_{,r} - \frac{2\alpha}{kr^2}[Z_{,rr} + \frac{1}{r}Z_{,r}] = \frac{2P}{k}. \quad (4.80)$$

The solution of Eq. (4.80) is then found as

$$Z(r) = \frac{P}{k} \frac{r^4}{32 - \frac{16\alpha}{k}} + C \frac{1}{\sqrt{\frac{2\alpha}{k} + 2}} r^{\sqrt{\frac{2\alpha}{k} + 2}} + D, \quad (4.81)$$

where, the unknown constants C and D can be uniquely determined by imposing the admissible boundary conditions

$$Z(r, \theta)_{,r} = 0, \quad Z(r, \theta) = 0, \quad r = a. \quad (4.82)$$

Therefore, we obtain

$$C = -\frac{Pa^3}{4a\sqrt{\frac{2\alpha}{k} + 1}(2k - \alpha)} \quad \text{and} \quad D = -\frac{Pa^3(\sqrt{\frac{2\alpha}{k} - 2})a\sqrt{\frac{2\alpha}{k} + 2}}{16(\sqrt{\frac{2\alpha}{k} + 2})(2k - \alpha)\sqrt{\frac{2\alpha}{k} + 1}}. \quad (4.83)$$

The transverse deformations of radially non-uniform membranes at a particular configuration of cross-section (i.e. $\theta = \pi/2$) are illustrated in Figure 4.7. Similarly, as in the previous cases, the obtained solution successfully demonstrates the deformations of radially non-uniform membranes subjected to increasing lateral pressures and the coefficient of non-uniformity α . Figure 4.7 illustrates that the magnitude of the transverse deflection increases under larger lateral pressure (Figure 4.7(a)) while the out-of-plane deflection decreases with increasing α (Figure 4.7(b)). The reduction in membrane deflection results from the larger α allows the membrane strain energy distributed to the membrane non-uniformity. It is noteworthy that the solution of the non-uniform membrane coincides with the result of the uniform membrane case when the equivalent non-uniformity coefficient is prescribed ($\alpha = \lambda = 1.8$, see, black line in Figure 4.7 (b)). Lastly, the discocyte-stomatocyte morphology of cell membranes [44] may be explained using the proposed non-uniformity function (Eq. (4.76)) (see,

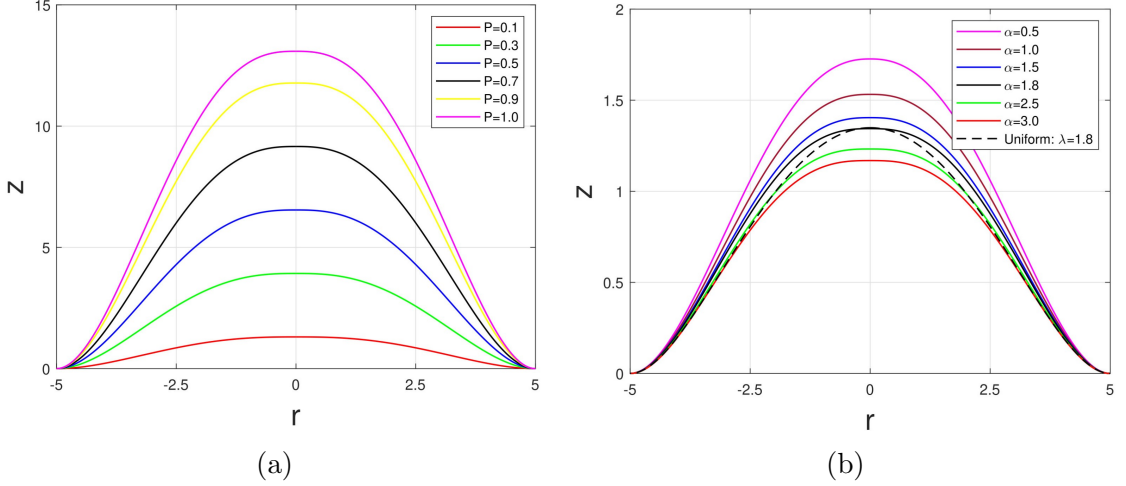
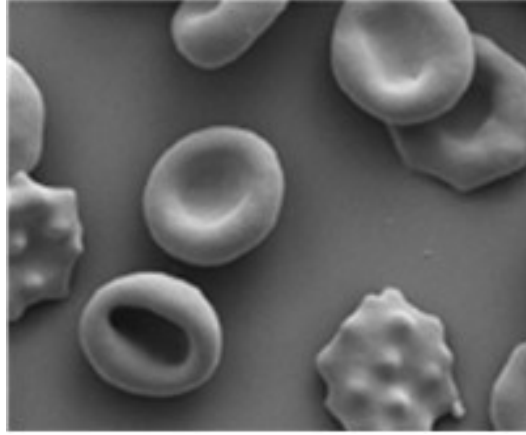


Figure 4.7: (a) The transverse deflection of radially non-uniform lipid membrane subjected to increasing lateral pressure P ; (b) The transverse deflection of radially non-uniform lipid membrane with respect to different α .

Figure 4.8). Despite the exact mechanisms causing these morphological formations may not be explained by the proposed model, the obtained solution may still serve as a useful analytical tool to simulate the possible states of energy distributions of membranes resulting in non-uniform morphologies and, particularly, may further facilitate relevant studies (see, for example, [45, 46]). It is also noted that the principle of superposition from the linear elasticity remains valid in the present case. More precisely, the solution of the combined mode ($\lambda + \phi = \alpha(\cos(n\theta) + \pi) + \alpha/r^n$) can be directly obtained via the superposition of the solutions from the respective circumferentially ($\lambda + \phi = \alpha(\cos(n\theta) + \pi)$) and radially ($\lambda + \phi = \alpha r^{-n}$) non-uniform cases. For example, the analytical results in Figure 4.5. and Figure 4.8 may be superimposed to produce the deformation field in Figure 4.9.



(a)

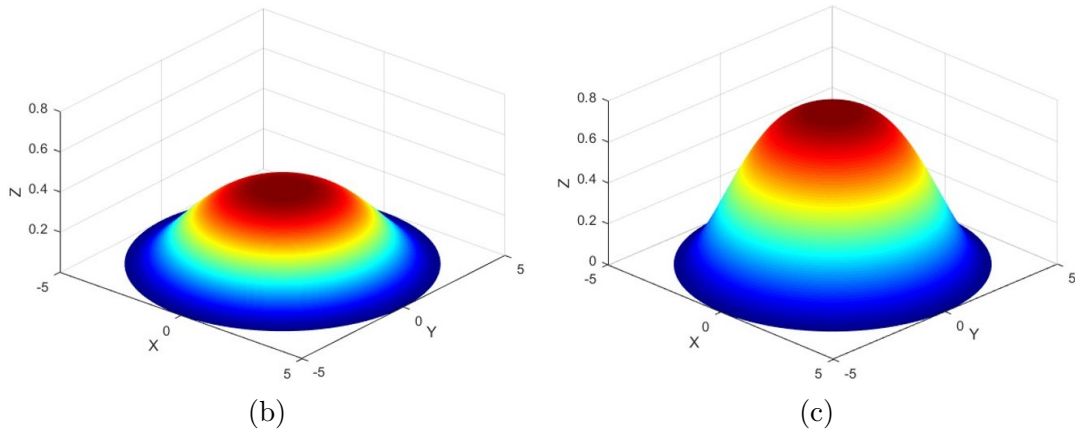


Figure 4.8: (a) The discocyte-stomatocyte morphology of red blood cell [44]; (b, c) The deformation contour mappings with $\lambda(\theta^\alpha) + \phi(\theta^\alpha) = \alpha r^{-2}$, where the α is adjusted to obtain the transitioning morphology from (b) to (c).

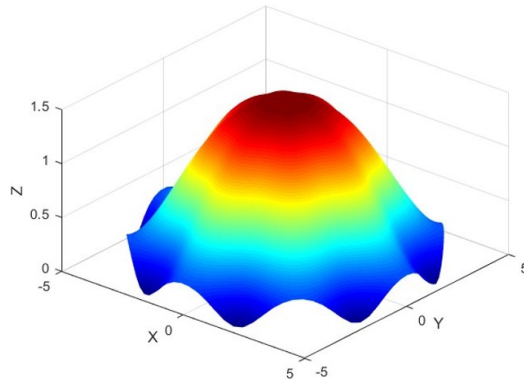


Figure 4.9: The deformation contour achieved by superimposing the radial and circumferential non-uniform distribution potential when $\lambda(\theta^\alpha) + \phi(\theta^\alpha) = \alpha(\cos(8\theta) + \pi) + \alpha r^{-2}$.

4.4 Conclusion

This study presents a complete analytical solution describing the mechanical responses of lipid membranes subjected to local inflammations and coordinate-dependent non-uniformity. Emphasis is placed on the assimilation of the complex nature of membrane morphology regulated by lateral pressure applied on the surface of the lipid membrane while maintaining rigorous and sufficient generality in the derivation of the corresponding linear theory. As such, more general forms of the energy potential of the Helfrich type are proposed, where the strain energy of the lipid membrane depends explicitly on the surface coordinates. To be precise, the inflammation of a non-uniform lipid membrane is discussed via the non-uniform (coordinate-dependent) energy potential and the lateral pressure prescribed on the surface of the membranes. Within the prescription of superposed incremental deformations and the Monge parameterization, a linear model is formulated and used to obtain complete analytical solutions. The admissible set of boundary conditions from the existing non-linear model is reformulated in the present context to determine the solution analytically. To validate the proposed model, a wealth of examples demonstrating the evolutions of the membrane in response to lateral pressures have been demonstrated in the cases of circular and rectangular membrane patches. Particularly, the proposed inflammation model predicts smooth morphological transitions of the membrane and accommodates the reported results of the membrane's bending deformations when the equivalent lateral pressure is applied. More importantly, the obtained solution phenomenologically illustrates the sequences of discocyte-stomatocyte morphology in cell membranes and the off-centered biconcave discoid formation of the red blood cells. Potential application of the proposed model may be expected in the conformation analyses of membranes associated with the compromised membrane-skeleton connections and/or lateral diffusions by providing coordinate-dependent deformation of membranes during inflammations. It is also found that the principle of superposition remains valid

even in the cases of coordinate-dependent inflammations of the membrane, suggesting that a more general class of membrane formations may be characterized by the superposition of the obtained solutions, which may accommodate a correspondingly wide set of phenomenologically relevant problems.

References

- [1] W. Helfrich, “Elastic properties of lipid bilayers: Theory and possible experiments,” *Zeitschrift für Naturforschung c*, vol. 28, no. 11-12, pp. 693–703, 1973. DOI: 10.1515/znc-1973-11-1209.
- [2] E. A. Evans and R. Skalak, *Mechanics and thermodynamics of biomembranes*. 2018. DOI: 10.1201/9781351074339.
- [3] T. W. Secomb and R. Skalak, “Surface flow of viscoelastic membranes in viscous fluids,” *Quarterly Journal of Mechanics and Applied Mathematics*, vol. 35, 2 1982, ISSN: 00335614. DOI: 10.1093/qjmam/35.2.233.
- [4] U. Seifert, “Configurations of fluid membranes and vesicles,” *Advances in Physics*, vol. 46, 1 1997, ISSN: 14606976. DOI: 10.1080/00018739700101488.
- [5] M. Jarić, U. Seifert, W. Wintz, and M. Wortis, “Vesicular instabilities: The prolate-to-oblate transition and other shape instabilities of fluid bilayer membranes,” *Physical Review E*, vol. 52, no. 6, p. 6623, 1995. DOI: 10.1103/physreve.52.6623.
- [6] E. Gorter and F. Grendel, “On bimolecular layers of lipoids on the chromocytes of the blood,” *Journal of Experimental Medicine*, vol. 41, 4 1925, ISSN: 15409538. DOI: 10.1084/jem.41.4.439.
- [7] J. D. Robertson, “The ultrastructure of cell membranes and their derivatives.,” *Biochemical Society symposium*, vol. 16, pp. 3–43, 1959. [Online]. Available: <https://api.semanticscholar.org/CorpusID:7814193>.
- [8] P. M. Naghdi, “On a variational theorem in elasticity and its application to shell theory,” *Journal of Applied Mechanics, Transactions ASME*, vol. 31, 4 1964, ISSN: 15289036. DOI: 10.1115/1.3629726.
- [9] P. M. Naghdi, “The theory of shells and plates,” in 1973. DOI: 10.1007/978-3-662-39776-3_5.
- [10] T. Belay, C. I. Kim, and P. Schiavone, “Mechanics of a lipid bilayer subjected to thickness distension and membrane budding,” *Mathematics and Mechanics of Solids*, vol. 23, 1 2018, ISSN: 17413028. DOI: 10.1177/1081286516666136.
- [11] T. Belay, C. I. Kim, and P. Schiavone, “Bud formation of lipid membranes in response to the surface diffusion of transmembrane proteins and line tension,” *Mathematics and Mechanics of Solids*, vol. 22, 11 2017, ISSN: 17413028. DOI: 10.1177/1081286516657684.
- [12] A. Agrawal and D. J. Steigmann, “Boundary-value problems in the theory of lipid membranes,” *Continuum Mechanics and Thermodynamics*, vol. 21, 1 2009, ISSN: 09351175. DOI: 10.1007/s00161-009-0102-8.
- [13] T. Belay, C. I. Kim, and P. Schiavone, “Interaction-induced morphological transitions of lipid membranes in contact with an elliptical cross section of a rigid substrate,” *Journal of Applied Mechanics, Transactions ASME*, vol. 83, 1 2016, ISSN: 15289036. DOI: 10.1115/1.4031485.

- [14] A. Agrawal and D. J. Steigmann, “Coexistent fluid-phase equilibria in biomembranes with bending elasticity,” *Journal of Elasticity*, vol. 93, 1 2008, ISSN: 03743535. DOI: 10.1007/s10659-008-9165-1.
- [15] A. Agrawal and D. J. Steigmann, “Modeling protein-mediated morphology in biomembranes,” *Biomechanics and Modeling in Mechanobiology*, vol. 8, 5 2009, ISSN: 16177959. DOI: 10.1007/s10237-008-0143-0.
- [16] K. I. Tsubota, S. Wada, and H. Liu, “Elastic behavior of a red blood cell with the membrane’s nonuniform natural state: Equilibrium shape, motion transition under shear flow, and elongation during tank-treading motion,” *Biomechanics and Modeling in Mechanobiology*, vol. 13, pp. 735–746, 4 2014, ISSN: 16177940. DOI: 10.1007/s10237-013-0530-z.
- [17] B. Blasi, A. D’Alessandro, N. Ramundo, and L. Zolla, “Red blood cell storage and cell morphology,” *Transfusion Medicine*, vol. 22, 2 2012, ISSN: 09587578. DOI: 10.1111/j.1365-3148.2012.01139.x.
- [18] K. J. V. Vliet and P. Hinterdorfer, “Probing drug-cell interactions,” *Nano Today*, vol. 1, 3 2006, ISSN: 17480132. DOI: 10.1016/S1748-0132(06)70076-7.
- [19] E. A. Evans, “Bending resistance and chemically induced moments in membrane bilayers,” *Biophysical Journal*, vol. 14, 12 1974, ISSN: 00063495. DOI: 10.1016/S0006-3495(74)85959-X.
- [20] P. B. Canham, “The minimum energy of bending as a possible explanation of the biconcave shape of the human red blood cell,” *Journal of Theoretical Biology*, vol. 26, 1 1970, ISSN: 10958541. DOI: 10.1016/S0022-5193(70)80032-7.
- [21] P. Rangamani, A. Agrawal, K. K. Mandadapu, G. Oster, and D. J. Steigmann, “Interaction between surface shape and intra-surface viscous flow on lipid membranes,” *Biomechanics and Modeling in Mechanobiology*, vol. 12, pp. 833–845, 4 Aug. 2013, ISSN: 16177959. DOI: 10.1007/s10237-012-0447-y.
- [22] M. Zeidi and C. I. Kim, “The effects of intra-membrane viscosity on lipid membrane morphology: Complete analytical solution,” *Scientific Reports*, vol. 8, 1 2018, ISSN: 20452322. DOI: 10.1038/s41598-018-31251-6.
- [23] Z. Liu and C. il Kim, “Deformation analysis of lipid membranes subjected to general forms of intra-membrane viscous flow and interactions with an elliptical-cross-section substrate,” *Scientific Reports*, vol. 10, 1 2020, ISSN: 20452322. DOI: 10.1038/s41598-019-57179-z.
- [24] W. Yao and C. I. Kim, “An analysis of lipid membrane morphology in the presence of coordinate-dependent non-uniformity,” *Mathematics and Mechanics of Solids*, vol. 26, no. 1, pp. 45–61, 2021. DOI: 10.1177/1081286520939162.
- [25] M. Zeidi and C. I. Kim, “Notes on superposed incremental deformations in the mechanics of lipid membranes,” *Mathematics and Mechanics of Solids*, vol. 24, 1 2019, ISSN: 17413028. DOI: 10.1177/1081286517734608.

- [26] C. I. Kim, "A discussion on the mechanics of lipid membranes: Lagrange multipliers and a singular substrate," *Zeitschrift fur Angewandte Mathematik und Physik*, vol. 68, 4 2017, ISSN: 00442275. DOI: 10.1007/s00033-017-0825-5.
- [27] T. Belay, C. I. Kim, and P. Schiavone, "Analytical solution of lipid membrane morphology subjected to boundary forces on the edges of rectangular membranes," *Continuum Mechanics and Thermodynamics*, vol. 28, 1-2 2016, ISSN: 09351175. DOI: 10.1007/s00161-015-0426-5.
- [28] W. C. Hwang and R. E. Waugh, "Energy of dissociation of lipid bilayer from the membrane skeleton of red blood cells," *Biophysical Journal*, vol. 72, 6 1997, ISSN: 00063495. DOI: 10.1016/S0006-3495(97)78910-0.
- [29] D. Allan and P. Raval, "Some morphological consequences of uncoupling the lipid bilayer from the plasma membrane skeleton in intact erythrocytes," *Biomedica Biochimica Acta*, vol. 42, 11-12 1983, ISSN: 0232766X.
- [30] P. F. Franck *et al.*, "Uncoupling of the membrane skeleton from the lipid bilayer. the cause of accelerated phospholipid flip-flop leading to an enhanced procoagulant activity of sickled cells," *Journal of Clinical Investigation*, vol. 75, 1 1985, ISSN: 00219738. DOI: 10.1172/JCI111672.
- [31] H. J. Müller and H. J. Galla, "Pressure variation of the lateral diffusion in lipid bilayer membranes," *BBA - Biomembranes*, vol. 733, 2 1983, ISSN: 00052736. DOI: 10.1016/0005-2736(83)90535-7.
- [32] P. G. Saffman and M. Delbrueck, "Brownian motion in biological membranes," *Proceedings of the National Academy of Sciences of the United States of America*, vol. 72, 8 1975, ISSN: 00278424. DOI: 10.1073/pnas.72.8.3111.
- [33] S. T. Mohyud-Din, M. A. Noor, and K. I. Noor, "Modified variation of parameters method for second-order integro-differential equations and coupled systems," *World Applied Sciences Journal*, vol. 6, pp. 1139–1146, 8 2009, ISSN: 1818-4952.
- [34] M. A. Noor, S. T. Mohyud-Din, and A. Waheed, "Variation of parameters method for solving fifth-order boundary value problems," *Applied Mathematics and Information Sciences*, vol. 2, 2 2008, ISSN: 19350090.
- [35] A. Escudero *et al.*, "Effect of dietary (n-9), (n-6) and (n-3) fatty acids on membrane lipid composition and morphology of rat erythrocytes," *Biochimica et Biophysica Acta - Lipids and Lipid Metabolism*, vol. 1394, 1 1998, ISSN: 00052760. DOI: 10.1016/S0005-2760(98)00095-2.
- [36] M. Girasole, A. Cricenti, R. Generosi, A. Congiu-Castellano, G. Boumis, and G. Amiconi, "Artificially induced unusual shape of erythrocytes: Anatomic force microscopy study," *Journal of Microscopy*, vol. 204, 1 2001, ISSN: 00222720. DOI: 10.1046/j.1365-2818.2001.00937.x.
- [37] C. I. Kim and D. J. Steigmann, "Distension-induced gradient capillarity in lipid membranes," *Continuum Mechanics and Thermodynamics*, vol. 27, 4-5 2015, ISSN: 09351175. DOI: 10.1007/s00161-014-0333-1.

- [38] D. J. Steigmann, “On the relationship between the cosserat and kirchhoff-love theories of elastic shells,” *Mathematics and Mechanics of Solids*, vol. 4, 3 1999, ISSN: 10812865. DOI: 10.1177/108128659900400301.
- [39] D. J. Steigmann, “Fluid films with curvature elasticity,” *Archive for Rational Mechanics and Analysis*, vol. 150, 2 1999, ISSN: 00039527. DOI: 10.1007/s002050050183.
- [40] R. M. Hochmuth and R. E. Waugh, “Erythrocyte membrane elasticity and viscosity,” *Annual Review of Physiology*, vol. Vol. 49, 1987, ISSN: 00664278. DOI: 10.1146/annurev.ph.49.030187.001233.
- [41] I. Derényi, F. Jülicher, and J. Prost, “Formation and interaction of membrane tubes,” *Physical Review Letters*, vol. 88, 23 2002, ISSN: 10797114. DOI: 10.1103/PhysRevLett.88.238101.
- [42] “Interaction between surface shape and intra-surface viscous flow on lipid membranes,” *Biomechanics and Modeling in Mechanobiology*, vol. 12, pp. 833–845, 4 Aug. 2013, ISSN: 16177959. DOI: 10.1007/s10237-012-0447-y.
- [43] P. Rangamani and D. J. Steigmann, “Variable tilt on lipid membranes,” *Proceedings of the Royal Society A: Mathematical, Physical and Engineering Sciences*, vol. 470, 2172 2014, ISSN: 14712946. DOI: 10.1098/rspa.2014.0463.
- [44] N. M. Geekiyanage *et al.*, “A coarse-grained red blood cell membrane model to study stomatocyte-discocyteechinocyte morphologies,” *PLoS ONE*, vol. 14, 4 2019, ISSN: 19326203. DOI: 10.1371/journal.pone.0215447.
- [45] G. Lim, M. Wortis, and R. Mukhopadhyay, *Stomatocyte-discocyte-echinocyte sequence of the human red blood cell: Evidence for the bilayer-couple hypothesis from membrane mechanics*, 2002. [Online]. Available: www.pnas.org/cgi/doi/10.1073/pnas.202617299.
- [46] S. Muñoz, J. L. Sebastián, M. Sancho, and G. Álvarez, “Elastic energy of the discocyte-stomatocyte transformation,” *Biochimica et Biophysica Acta - Biomembranes*, vol. 1838, 3 2014, ISSN: 00052736. DOI: 10.1016/j.bbamem.2013.10.020.

Chapter 5

A Lipid Membrane Morphology Subjected to Intra-membrane Viscosity and Membrane Thickness Dilation

Through this Chapter, we study the morphological transitions of lipid membrane under the presence of the intra-surface viscous flow and membrane thickness dilation using the continuum model of Helfrich type. The effects of intra-membrane viscosity and membrane distension are simultaneously formulated into the continuum model based on the dimension reduction procedure applied to the three-dimensional liquid crystal theory. The admissible set of boundary conditions is taken from the existing model yet reformulated into the present context for the sake of completeness. Among other interesting features, the proposed model phenomenologically predicts the off-centered protrusion of the lipid membrane when it is subjected to both local inflammation and intra-surface viscous flow. In addition, the substrate-interaction force may invoke local bending effects on the membrane, resulting in thickness reduction in the vicinity of the substrate. Lastly, the obtained results are cross-examined with coarse-grained molecular dynamics (CGMD) simulations which demonstrate reasonable consistency in the predictions of membrane morphology and thickness dilation.

5.1 Introduction

The morphological transition of lipid membranes has consistently aroused intense research interest due to its association with essential cellular functions. Indeed, exocytosis and/or endo-cytosis are important processes for cells to transport inbound and outbound cargo across a membrane barrier through which lipid membrane can develop small buds, finger-like protrusions, and pseudopods [1]. Further, the lipid membrane houses a significant set of proteins, ligands, and other various macromolecules. Particularly, morphological transitions such as cell fission, signaling, and replication processes constantly involve the intracellular trafficking of these sophisticated organisms and organelles [2].

The understanding of the morphological transitions of lipid bilayer membranes may be achieved by theoretical models that involve molecular dynamics (MD) simulations (the lipid membrane is mainly composed of phospholipid molecules with opposing orientations) and the development of continuum models describing the mechanical responses of lipid membranes. MD simulation, despite its relatively high computational demands, has shown its priority in understanding and describing the structural details of lipid bilayers because phospholipid molecules (lipid molecules) can be analyzed as a group or individual molecules [3]. Further, the coarse-grained (CG) MD simulation has shown its advantages in describing the mechanics of membrane systems with relatively low computational resources, and a series of studies regarding the membranes' morphological transitions have been conducted in [3–5]. On the other hand, the continuum-based lipid membrane models have been significantly advanced by differential geometry and the theory of elastic surface. In particular, the energy potential of Helfrich type [6] based on the mean and Gaussian curvature of surfaces has been widely and successfully adopted in various membrane problems [7–10].

The majority of recent studies focus on the implementation and refinement of the Helfrich energy potential and have successfully demonstrated a wide range of

membrane problems such as substrate-protein interactions [7], budding formation [9], membrane intra-surface viscous flow [10, 11] and membrane thickness distension [12]. By assuming that the budding process is driven by diffusion of transmembrane protein and line tensions, the membrane budding processes have been demonstrated in [9]. To explain the morphological transition of diseased cells, the work [8] has developed a coordinate-dependent model of lipid membrane through which the substrate interaction and membrane inflammation problem of non-uniform lipid membranes have been investigated. The work [10] has proposed a series of non-linear membrane shape equations predicting the deformations of membranes subjected to lateral pressure and intra-membrane viscosity. Further, the linearized shape equation has been investigated through which a complete analytical solution is obtained, demonstrating the wrinkle morphology of lipid membrane when subjected to intra-membrane viscous flow [11].

A significant amount of research has been devoted to the analysis of membrane thickness because it plays a critical role in regulating membrane permeability [13], self-assembly [14], and protein distribution [15]. In particular, the membrane thickness fluctuation has been utilized to estimate membrane viscosity which is essential for measuring membrane fluidity [16–19] and functioning biomolecule mobility [20–22]. Meanwhile, the continuum model approach has emphasized the effects of viscosity on membrane morphology, showing that the influences of intra-membrane viscosity are of particular importance in explaining various membrane morphologies and associated essential cellular functions [7, 10, 12, 23–27]. However, in recent work investigating membrane thickness distension (see, for example, [12, 28]), the targeted membrane thickness is indirectly formulated in the refined shape equations by relaxing the constraint of bulk incompressibility via a Lagrange multiplier, resulting in the contemporary Helfrich type models are intrinsically limited in providing comprehensive descriptions of lipid distension and associated membrane morphology. Further, though the viscous effects on the morphology of membranes have been investigated

by introducing viscous stress into the equilibrium equations [10, 11], the analysis of viscous effects on membrane thickness distension, including the development of the corresponding mathematical framework, are largely absent from the literature.

In the present study, we refine classical Helfrich theory that is cast in the framework of two-dimensional liquid crystal theory to accommodate the simultaneous effects of intra-membrane viscosity and thickness dilation on the morphological transitions of the lipid bilayer. Utilizing variational methods and Monge representation, we obtain the tangential and normal shape equations of membrane distension. The viscous stress is formulated into the equilibrium equations to study the effects of intra-surface viscosity on membrane morphology and thickness. The cases of membrane-protein interaction and local inflammation are considered for demonstrating the refined model. In particular, we cross-examine the results obtained from the proposed continuum model using CGMD simulation. It is found that the results of CGMD simulation show reasonable consistency when compared with the results obtained from the proposed continuum model in predicting both the membrane morphology and thickness distension. In addition, the acting viscous flow can shear the membrane surface to form off-centered morphology in the case of the membrane's local inflammation. At the same time, the viscous flow can compress and pull the lipid membrane out-of-plane direction resulting in thickness reduction in the vicinity of the substrate. The obtained results may explain the morphological transitions of lipid membranes induced by the pH level, storage time, and nanoparticle interaction.

5.2 Energy Potential of Lipid Membrane

The lipid membrane theory accounts for the effects of thickness distension has been presented in [12]. In this paper, we reformulate the results directly from the membrane free-energy density $W = W(H, K, J, G; \theta^\alpha)$ for the sake of consistency and completeness.

The model demonstrated in this study is based on the liquid crystal theory where

the lipid tilt and membrane distension are discussed [29]. Therein, lipid tilt is suppressed because the areal density of lipids on the membrane can be sufficiently high. In this sense, the treatment for suppressing tilt is to align the liquid crystal material vector to the lipid molecule direction. Due to the molecule vector gradient scale being significantly larger than the molecule dimension, the underlying energy density based on liquid crystal is homogeneous-quadratic in the vector gradient. Thus, the areal density of the lipid membrane is invoked as [29]

$$W(H, K, J, G; \theta^\alpha) = F(J; \theta^\alpha) + \beta(J; \theta^\alpha)H^2 + \gamma(J; \theta^\alpha)K + \sigma(J; \theta^\alpha)G^2, \quad (5.1)$$

where F presents energy potential from experiments, the energy minimizer principle defines the coefficients β and σ are non-negative, H is mean curvature and K is the Gaussian curvature defined by

$$H = \frac{1}{2}a^{\alpha\beta}b_{\alpha\beta}, \quad K = \frac{1}{2}\varepsilon^{\alpha\beta}\varepsilon^{\lambda\mu}b_{\alpha\lambda}b_{\beta\mu}, \quad (5.2)$$

in which $a_{\alpha\beta}$ is the surface metric and $a^{\alpha\beta}$ is the inverse of $a_{\alpha\beta}$. $\varepsilon^{\alpha\beta} = e^{\alpha\beta}/\sqrt{a}$ is the permutation tensor with $a = \det(a_{\alpha\beta})$, where $e^{12} = -e^{21} = 1$, $e^{11} = e^{22} = 0$. $b^{\alpha\beta}$ are the covariant components of the surface curvature tensor in the second fundamental form which satisfy

$$b^{\alpha\beta} = 2Ha^{\alpha\beta} - \tilde{b}^{\alpha\beta}. \quad (5.3)$$

In the above, the contravariant cofactor of the curvature $\tilde{b}^{\alpha\beta}$ are introduced by

$$\tilde{b}^{\alpha\beta} = \varepsilon^{\alpha\lambda}\varepsilon^{\beta\gamma}b_{\lambda\gamma}. \quad (5.4)$$

Also, contravariant cofactor $\tilde{b}^{\alpha\beta}$ are related to the mixed components of the curvature b_μ^β pertaining to

$$b_\mu^\beta \tilde{b}^{\mu\alpha} = Ka^{\beta\alpha}. \quad (5.5)$$

Further, $G = |\nabla J|$ is the gradient of surface dilatation (J) of lipid membrane used for describing the thickness distension of lipid membrane due to ∇J is theoretically

linear in thickness distension [29], which is formulated by

$$\nabla J = J_{,\alpha} \mathbf{a}^\alpha, \text{ and } G^2 = J_{,\alpha} \mathbf{a}^\alpha \cdot J_{,\beta} \mathbf{a}^\beta = a^{\alpha\beta} J_{,\alpha} J_{,\beta}, \quad (5.6)$$

in which \mathbf{a}^α are the dual basis of \mathbf{a}_β following the relation $\mathbf{a}^\alpha = a^{\alpha\beta} \mathbf{a}_\beta$, where \mathbf{a}_β are the tangential plane vectors. To compute surface deformation, the surface covariant differentiation is computed as

$$\mathbf{a}_{\alpha;\beta} = \mathbf{a}_{\alpha,\beta} - \Gamma_{\alpha\beta}^\lambda \mathbf{a}_\lambda, \quad (5.7)$$

where $\Gamma_{\alpha\beta}^\lambda$ are the Christoffel symbols on membrane domain ω . We obtain membrane surface vector $\mathbf{a}_\alpha = \mathbf{r}_{,\alpha}$, where \mathbf{r} represents the position of the membrane's surface point in three-dimensional space. \mathbf{a}_α are related to the surface metric by $a_{\alpha\beta} = \mathbf{a}_\alpha \cdot \mathbf{a}_\beta$, and the local surface orientation for the unit-vector field is $\mathbf{n} = \frac{1}{2} \varepsilon^{\alpha\beta} \mathbf{a}_\alpha \times \mathbf{a}_\beta$. These relations contribute to the Gauss and Weingarten equations

$$\mathbf{a}_{\alpha,\beta} = b_{\alpha\beta} \mathbf{n} \text{ and } \mathbf{n}_{,\alpha} = -b_\alpha^\beta \mathbf{a}_\beta. \quad (5.8)$$

At last, under the render of stationary configurations, the energy potential over the membrane domain ω is defined by

$$E = \int_\omega W(H, K, J, G; \theta^\alpha) dA. \quad (5.9)$$

5.3 Distension Induced Lipid Membrane Equilibria

To establish equilibrium equations of the membrane, it is customary to compute variational derivatives of the energy potential W . Hence, we develop a variational framework by taking the derivative of W with respect to the surface configuration parameter ϵ , which is denoted with a superposed dot, and the variable bearing a superposed dot owns the same meaning. Thus, the variational work of surface position vector \mathbf{r} is expressed by $\dot{\mathbf{r}} = \partial \mathbf{r}(\theta^\alpha) / \partial \epsilon \mid \epsilon = \mathbf{0}$, where $\dot{\mathbf{r}} = \mathbf{u}(\theta^\alpha)$ and \mathbf{u} is called virtual

displacement. For a deformed membrane domain denoted by ω , the variation work of energy potential yields

$$\dot{E} = \int_{\omega} (\dot{W} + W\dot{J}/J) da, \quad (5.10)$$

immediately,

$$\dot{W} = W_J\dot{J} + W_H\dot{H} + W_K\dot{K} + W_G\dot{G}, \quad (5.11)$$

where

$$W_H = 2\beta(J; \theta^\alpha)H, \quad W_K = \gamma(J; \theta^\alpha), \quad W_G = 2\sigma(J; \theta^\alpha)G. \quad (5.12)$$

The variational derivatives of J , H , K are recalled from [30], which are

$$\dot{J}/J = \mathbf{a}^\alpha \cdot \dot{\mathbf{a}}_\alpha, \quad 2\dot{H} = a^{\alpha\beta} \mathbf{n} \cdot \mathbf{u}_{;\alpha\beta} - 2b^{\alpha\beta} \mathbf{a}_\beta \cdot \mathbf{u}_{;\alpha} \quad \text{and} \quad \dot{K} = \tilde{b}^{\alpha\beta} \mathbf{n} \cdot \mathbf{u}_{;\alpha\beta} - 2K \mathbf{a}^\alpha \cdot \mathbf{u}_{;\alpha}. \quad (5.13)$$

To compute \dot{G} , we begin with

$$G^2 = \nabla J^2, \quad (5.14)$$

and the variational work on both sides of Eq. (5.14) gives rise to

$$\dot{G} = G^{-1} \nabla J \cdot (\nabla J)^\cdot, \quad (5.15)$$

where

$$(\nabla J)^\cdot = \dot{J}_{;\alpha} \mathbf{a}^\alpha + J_{;\alpha} (\mathbf{a}^\alpha)^\cdot, \quad (5.16)$$

in which [15]

$$(\mathbf{a}^\alpha)^\cdot = [\mathbf{n} \cdot (a^{\alpha\mu} \dot{\mathbf{a}}_\mu)] \mathbf{n} - a^\mu (a^\alpha \dot{\mathbf{a}}_\mu), \quad J_{;\alpha} = JS_{\lambda\alpha}^\lambda \quad \text{and} \quad \dot{J}_{;\alpha} = \dot{J}S_{\lambda\alpha}^\lambda + J\dot{S}_{\lambda\alpha}^\lambda, \quad (5.17)$$

where $\dot{S}_{\lambda\alpha}^\lambda = \mathbf{a}^\beta \cdot \mathbf{u}_{;\alpha\beta} + b_\alpha^\beta \mathbf{n} \cdot \mathbf{u}_{;\beta}$ [29], and $S_{\alpha\beta}^\lambda = \Gamma_{\alpha\beta}^\lambda - \bar{\Gamma}_{\alpha\beta}^\lambda$, $\bar{\Gamma}_{\alpha\beta}^\lambda$ are Christoffel symbols which are derived from the reference surface coordinate. Accordingly, Eqs. (5.15-5.17) contribute to

$$\dot{G} = JG^{-1} J_{;\lambda} a^{\alpha\lambda} \mathbf{a}^\beta \cdot \mathbf{u}_{;\alpha\beta} + [G \mathbf{a}^\alpha - JG^{-1} J_{;\lambda} a^{\alpha\lambda} \nabla J + JG^{-1} J_{;\lambda} b^{\lambda\alpha} \mathbf{n}] \cdot \mathbf{u}_{;\alpha}. \quad (5.18)$$

To cast the introduced variational work in the framework of two-dimensional elastic theory, it is expected to seek tensor fields \mathbf{N}^α and $\mathbf{M}^{\alpha\beta}$ satisfying

$$\dot{E} = \int_{\omega} (\dot{W} + W\dot{J}/J) da = \int_{\omega} (\mathbf{N}^\alpha \cdot \mathbf{u}_{;\alpha} + \mathbf{M}^{\alpha\beta} \cdot \mathbf{u}_{;\alpha\beta}) da, \quad (5.19)$$

where $\mathbf{u}_{;\alpha\beta} = \mathbf{u}_{,\alpha\beta} - \Gamma_{\alpha\beta}^{\lambda} \mathbf{u}_{,\lambda}$ are the second covariant derivative of the virtual displacement \mathbf{u} , in which $\Gamma_{\alpha\beta}^{\lambda}$ are the Christoffel symbols on membrane surface ω . To proceed, we rewrite

$$\dot{W} + W\dot{J}/J = \varphi_{;\alpha}^{\alpha} - \mathbf{u} \cdot \mathbf{T}_{;\alpha}^{\alpha}, \quad (5.20)$$

where

$$\varphi^{\alpha} = \mathbf{T}^{\alpha} \cdot \mathbf{u} + \mathbf{M}^{\alpha\beta} \cdot \mathbf{u}_{,\beta}, \quad (5.21)$$

in which

$$\mathbf{T}^{\alpha} = \mathbf{N}^{\alpha} - \mathbf{M}_{;\beta}^{\alpha\beta}, \quad (5.22)$$

where the \mathbf{T}^{α} are components of stress tensor with directions on the membrane surface. For equilibrium state of a purely elastic surface subject to lateral pressure P in describing membrane inflammation is given by [29–31],

$$\mathbf{T}_{;\alpha}^{\alpha} + P\mathbf{n} = 0. \quad (5.23)$$

To formulate tangential and normal equilibrium equations, we decompose \mathbf{N}^{α} and $\mathbf{M}^{\alpha\beta}$ into tangential and normal components, which are respectively

$$\mathbf{N}^{\alpha} = N^{\beta\alpha} \mathbf{a}_{\beta} + N^{\alpha} \mathbf{n} \text{ and } \mathbf{M}^{\alpha\beta} = M^{\lambda\alpha\beta} \mathbf{a}_{\lambda} + M^{\alpha\beta} \mathbf{n}. \quad (5.24)$$

Substituting Eqs. (5.22, 5.24) into Eq. (5.23) and invoking Gauss and Weingarten equations (Eq. (5.8)) yields

$$\begin{aligned} & [(N^{\mu\alpha} + M^{\beta\alpha} b_{\beta}^{\mu} - M_{;\beta}^{\mu\beta\alpha})_{;\alpha} + (M_{;\beta}^{\beta\alpha} + M^{\lambda\beta\mu} b_{\lambda\beta} - N^{\alpha}) b_{\alpha}^{\mu}] \mathbf{a}_{\lambda} + \\ & [(N^{\alpha} - M_{;\beta}^{\beta\alpha} - M^{\lambda\beta\alpha} b_{\lambda\beta})_{;\alpha} + (N^{\beta\alpha} + M^{\lambda\alpha} b_{\lambda}^{\beta} - M_{;\mu}^{\mu\beta\alpha}) b_{\beta\alpha} + P] \mathbf{n} = 0. \end{aligned} \quad (5.25)$$

Projecting Eq. (5.25) onto normal direction \mathbf{n} and tangential direction \mathbf{a}_{λ} , the equilibrium equations in normal and tangential direction are respectively

$$(N^{\alpha} - M_{;\beta}^{\beta\alpha} - M^{\lambda\beta\alpha} b_{\lambda\beta})_{;\alpha} + (N^{\beta\alpha} + M^{\lambda\alpha} b_{\lambda}^{\beta} - M_{;\mu}^{\mu\beta\alpha}) b_{\beta\alpha} + P = 0 \quad (5.26)$$

and

$$(N^{\mu\alpha} + M^{\beta\alpha} b_{\beta}^{\mu} - M_{;\beta}^{\mu\beta\alpha})_{;\alpha} + (M_{;\beta}^{\beta\alpha} + M^{\lambda\beta\mu} b_{\lambda\beta} - N^{\alpha}) b_{\alpha}^{\mu} = 0, \quad (5.27)$$

in which

$$M_{;\beta}^{\lambda\beta\alpha} = M_{,\beta}^{\lambda\beta\alpha} + M^{\lambda\beta\alpha}\Gamma_{\mu\beta}^{\mu} + M^{\lambda\beta\mu}\Gamma_{\mu\beta}^{\alpha} + M^{\mu\beta\alpha}\Gamma_{\mu\beta}^{\lambda}. \quad (5.28)$$

To provide explicit expressions of Eqs. (5.26, 5.27), we compare Eq. (5.11) with Eq. (5.20) and invoke the Cayley-Hamilton theorem $\tilde{b}^{\alpha\beta} = 2Ha^{\alpha\beta} - b^{\alpha\beta}$, the tensor field $\mathbf{M}^{\alpha\beta}$, \mathbf{N}^{α} are achieved by

$$\mathbf{M}^{\alpha\beta} = \frac{1}{2}JG^{-1}W_G J_{,\mu}(a^{\alpha\mu}\mathbf{a}^{\beta} + a^{\beta\mu}\mathbf{a}^{\alpha}) + \left(\frac{1}{2}W_H a^{\alpha\beta} + W_K \tilde{b}^{\alpha\beta}\right)\mathbf{n} \quad (5.29)$$

and

$$\begin{aligned} \mathbf{N}^{\alpha} = & \left\{ [W + JW_J - 2(HW_H + KW_K)]a^{\alpha\beta} + W_H \tilde{b}^{\alpha\beta} \right\} \mathbf{a}_{\beta} + \\ & W_G [G\mathbf{a}^{\alpha} - JG^{-1}J_{,\lambda}a^{\alpha\lambda}\nabla J + JG^{-1}J_{,\lambda}b^{\lambda\alpha}\mathbf{n}]. \end{aligned} \quad (5.30)$$

Combining Eqs. (5.29, 5.30) and Eq. (5.24), which gives rise to the tangential and normal component of each tensor field $\mathbf{M}^{\alpha\beta}$ and \mathbf{N}^{α} , which are

$$\begin{aligned} M^{\lambda\alpha\beta} &= JG^{-1}W_G J_{,\mu}a^{\alpha\mu}a^{\beta\lambda} \\ &= \frac{1}{2}JG^{-1}W_G J_{,\mu}(a^{\alpha\mu}a^{\beta\lambda} + a^{\beta\mu}a^{\alpha\lambda}) \\ &= JG^{-1}W_G J_{,\mu}a^{\beta\mu}a^{\alpha\lambda}, \\ M^{\alpha\beta} &= \frac{1}{2}W_H a^{\alpha\beta} + W_K \tilde{b}^{\alpha\beta} \end{aligned} \quad (5.31)$$

and

$$\begin{aligned} N^{\alpha\beta} &= [W + JW_J - 2(HW_H + KW_K) + GW_G]a^{\alpha\beta} - \\ & \quad G^{-1}W_G J_{,\lambda}J_{,\mu}a^{\alpha\lambda}a^{\beta\mu} + W_H \tilde{b}^{\alpha\beta}, \\ N^{\alpha} &= JG^{-1}W_G J_{,\lambda}b^{\lambda\alpha} = JG^{-1}W_G J_{,\lambda}(2Ha^{\lambda\alpha} - \tilde{b}^{\lambda\alpha}). \end{aligned} \quad (5.32)$$

By substituting Eqs. (5.31, 5.32) into the Eqs. (5.26, 5.27), and invoking Eqs. (5.2, 5.5) and relations $b_{\beta\alpha} = b_{\alpha}^{\mu}a_{\mu\beta}$, $a^{\alpha\lambda}a^{\beta\mu}b_{\beta\alpha} = b^{\mu\lambda}$, the normal and tangential shape equations are respectively

$$\begin{aligned} \frac{1}{2}\Delta W_H + (W_K)_{;\beta\alpha}\tilde{b}^{\beta\alpha} + W_H(2H^2 - K) + 2HW_K K - 2H(W + JW_J) + \\ [JG^{-1}W_G(J_{,\alpha})_{;\beta} + G^{-1}W_G J_{,\alpha}J_{,\beta}]b^{\alpha\beta} = P \end{aligned} \quad (5.33)$$

and

$$[2J_{,\alpha}W_J + J(W_J)_{;\alpha} + W_G G_{,\alpha}]a^{\lambda\alpha} - G^{-1}W_G(J_{,\varepsilon})_{;\alpha}J_{,\mu}a^{\lambda\varepsilon}a^{\alpha\mu} - G^{-1}W_G J_{,\varepsilon}(J_{,\mu})_{;\alpha}a^{\lambda\varepsilon}a^{\alpha\mu} - [J_{,\alpha}G^{-1}W_G(J_{,\mu})_{;\beta} + JG^{-1}W_G(J_{,\mu})_{;\beta\alpha}]a^{\beta\mu}a^{\alpha\lambda} = 0. \quad (5.34)$$

5.4 Intra-membrane Viscosity

Since the membrane subjected to viscous stress is a typical biology environment [5], we consider the time derivative of the evolving the surface metric can accommodate the corresponding strain effects and give rise to viscous stress [32]

$$\sigma^{\alpha\beta} = -\gamma a^{\alpha\beta} + \pi^{\alpha\beta}, \quad (5.35)$$

where γ is scalar parameter and

$$\pi^{\alpha\beta} = \nu a^{\alpha\lambda}a^{\beta\mu}\dot{a}_{\lambda\mu}, \quad (5.36)$$

in which ν is the intra-membrane shear viscosity, it should be noted the superposed dot presents the time derivative and the Newtonian viscous stress $\pi^{\alpha\beta}$, in general, is frame-dependent as indicated by the evolution of the velocity gradient over the time in Eq. (5.39). To proceed, we find

$$\dot{a}_{\lambda\mu} = (\mathbf{a}_\lambda \cdot \mathbf{a}_\mu)^\cdot = \dot{\mathbf{a}}_\lambda \cdot \mathbf{a}_\mu + \mathbf{a}_\lambda \cdot \dot{\mathbf{a}}_\mu, \quad (5.37)$$

where

$$\begin{aligned} \dot{\mathbf{a}}_\lambda &= \mathbf{u}_{,\lambda} = (v^\alpha \mathbf{a}_\alpha + w \mathbf{n})_{,\lambda} \\ &= v_{,\lambda}^\alpha \mathbf{a}_\alpha + v^\alpha \mathbf{a}_{\alpha,\lambda} + w_{,\lambda} \mathbf{n} + w \mathbf{n}_{,\lambda} = (v_{\alpha;\lambda} - w b_{\alpha\lambda}) \mathbf{a}^\alpha + (v^\alpha b_{\alpha\lambda} + w_{,\lambda}) \mathbf{n}, \end{aligned} \quad (5.38)$$

in which $\mathbf{u} = \dot{\mathbf{r}}$ is the velocity of a material point on the initial surface pertaining to $\partial \mathbf{u} / \partial \theta^\lambda = \mathbf{u}_{,\lambda} = \dot{\mathbf{a}}_\lambda$ and $\mathbf{u} = v^\alpha \mathbf{a}_\alpha + w \mathbf{n}$, v^α and w are tangential component and normal component of velocity \mathbf{u} , respectively. The Eq. (5.38) advances the Eq. (5.35) and Eq. (5.37) to be

$$\sigma^{\alpha\beta} = -\gamma a^{\alpha\beta} + \nu [a^{\alpha\lambda} b^{\beta\mu} (\mathbf{v}_{\lambda;\mu} + \mathbf{v}_{\mu;\lambda} - 2w b_{\mu\lambda})] \text{ and } \dot{a}_{\lambda\mu} = v_{\mu;\lambda} + v_{\lambda;\mu} - 2w b_{\lambda\mu}, \quad (5.39)$$

respectively. In the sense that the viscous stress $\sigma^{\alpha\beta}$ aligns to the stress \mathbf{T}^α (Eq. (5.23)) in the tangential plane, the viscous stress is incorporated into the Eqs. (5.26, 5.27), yielding

$$(N^\alpha - M_{;\beta}^{\beta\alpha} - M^{\lambda\beta\alpha}b_{\lambda\beta})_{;\alpha} + (N^{\beta\alpha} + M^{\lambda\alpha}b_\lambda^\beta - M_{;\mu}^{\mu\beta\alpha} + \sigma^{\alpha\beta})b_{\beta\alpha} + P = 0 \quad (5.40)$$

and

$$(N^{\mu\alpha} + M^{\beta\alpha}b_\beta^\mu - M_{;\beta}^{\mu\beta\alpha} + \sigma^{\alpha\beta})_{;\alpha} + (M_{;\beta}^{\beta\alpha} + M^{\lambda\beta\mu}b_{\lambda\beta} - N^\alpha)b_\alpha^\mu = 0. \quad (5.41)$$

The added terms in Eqs. (5.40, 5.41) compare to Eqs. (5.26, 5.27) are respectively

$$\begin{aligned} \pi^{\alpha\beta}b_{\beta\alpha} &= \nu[a^{\alpha\lambda}b^{\beta\mu}(\mathbf{v}_{\lambda;\mu} + \mathbf{v}_{\mu;\lambda} - 2wb_{\mu\lambda})]b_{\alpha\beta} \\ &= 2\nu\left[\frac{1}{2}(\mathbf{v}_{\alpha;\beta} + \mathbf{v}_{\beta;\alpha})b^{\alpha\beta} - 2w(2H^2 - K)\right] \text{ and} \\ \pi^{\alpha\beta}_{;\alpha} &= \nu[a^{\beta\lambda}b^{\alpha\mu}(\mathbf{v}_{\lambda;\mu} + \mathbf{v}_{\mu;\lambda} - 2wb_{\mu\lambda})]_{;\alpha} \\ &= \nu a^{\beta\alpha}[a^{\lambda\mu}(\mathbf{v}_{\alpha;\mu} + \mathbf{v}_{\mu;\alpha})_{;\lambda} - 2w_{,\lambda}b_\alpha^\lambda - 4wH_{,\alpha}]. \end{aligned} \quad (5.42)$$

Therefore, the shape equations describing the mechanics of lipid membrane in the presence of intra-membrane viscous flow are obtained from Eqs. (5.33, 5.34, 5.42)

$$\begin{aligned} \frac{1}{2}\Delta W_H + (W_K)_{;\beta\alpha}\tilde{b}^{\beta\alpha} + W_H(2H^2 - K) + 2HW_KK - 2H(W + JW_J) + \\ [JG^{-1}W_G(J_{,\alpha})_{;\beta} + G^{-1}W_GJ_{,\alpha}J_{,\beta}]b^{\alpha\beta} - \pi^{\alpha\beta}b_{\alpha\beta} = P \text{ and} \end{aligned} \quad (5.43)$$

$$\begin{aligned} [2J_{,\alpha}W_J + J(W_J)_{;\alpha} + W_GG_{,\alpha}]a^{\lambda\alpha} - G^{-1}W_G(J_{,\varepsilon})_{;\alpha}J_{,\mu}a^{\lambda\varepsilon}a^{\alpha\mu} - G^{-1}W_GJ_{,\varepsilon}(J_{,\mu})_{;\alpha}a^{\lambda\varepsilon}a^{\alpha\mu} \\ - [J_{,\alpha}G^{-1}W_G(J_{,\mu})_{;\beta} + JG^{-1}W_G(J_{,\mu})_{;\beta\alpha}]a^{\beta\mu}a^{\alpha\lambda} + \pi_{;\alpha}^{\beta\alpha} = 0. \end{aligned}$$

Given that the viscous flow is induced by incompressible fluid over the membrane, the incompressible condition $\dot{J}/J = \frac{1}{2}a^{\alpha\beta}\dot{a}_{\alpha\beta} = 0$ [10] together with Eqs. (5.37, 5.38) formulate

$$v_{;\alpha}^\alpha - 2wH = 0. \quad (5.44)$$

Since the proposed model is based on the conventional Helfrich theory while is cast in the framework of two-dimensional elastic theory accounting for two-dimensional liquid crystal theory, it is necessary to trace the refined model to the classic Helfrich

theory. To see this, we cancel the thickness distension and viscous flow contributions to the model (remove the relevant thickness distension and viscous flow terms of Eq. (5.43), yielding normal shape equation

$$\frac{1}{2}\Delta W_H + (W_K)_{;\beta\alpha}\tilde{b}^{\beta\alpha} + W_H(2H^2 - K) + 2HW_KK - 2HW = P, \quad (5.45)$$

and tangential equation automatically meets the form “0 = 0”, where the normal shape equation Eq. (5.45) almost recovers to the normal shape equation of classic Helfrich type [7]

$$\frac{1}{2}\Delta W_H + (W_K)_{;\beta\alpha}\tilde{b}^{\beta\alpha} + W_H(2H^2 - K) + 2HW_KK - 2H(W + \lambda) = P \text{ on } \omega, \quad (5.46)$$

the difference between Eq. (5.45) and Eq. (5.46) is located at the $\lambda(\theta^\alpha)$ which is Lagrange-multiplier field determining the membrane’s intrinsic property while it is not involved in our model because we demonstrate the problem in the framework of two-dimensional elastic theory. For an uniform membrane, $\lambda(\theta^\alpha)$ is constant and the tangential shape equation of classic Helfrich type automatically meets [7]

$$\lambda_{,\alpha} = -\partial W/\partial\theta^\alpha = 0, \quad (5.47)$$

showing the proposed tangential shape equation (Eq. (5.43)) can completely restore to the tangential shape equation of the classic Helfrich type. Further, it is necessary to compare the refined model with the precedent model describing membrane thickness distension formulated from the classic Helfrich type (Eq. (5.49) below). Accordingly, on one hand, the elimination of viscous flow effects in Eq. (5.43) yields the shape equations accommodating thickness distension, which are

$$\begin{aligned} \frac{1}{2}\Delta W_H + (W_K)_{;\beta\alpha}\tilde{b}^{\beta\alpha} + W_H(2H^2 - K) + 2HW_KK - 2H(W + JW_J) + \\ [JG^{-1}W_G(J,\alpha)_{;\beta} + G^{-1}W_GJ_{,\alpha}J_{,\beta}]b^{\alpha\beta} = P \text{ and} \quad (5.48) \\ [2J_{,\alpha}W_J + J(W_J)_{;\alpha} + W_GG_{,\alpha}]a^{\lambda\alpha} - G^{-1}W_G(J,\varepsilon)_{;\alpha}J_{,\mu}a^{\lambda\varepsilon}a^{\alpha\mu} - G^{-1}W_GJ_{,\varepsilon}(J_{,\mu})_{;\alpha}a^{\lambda\varepsilon}a^{\alpha\mu} \\ - [J_{,\alpha}G^{-1}W_G(J_{,\mu})_{;\beta} + JG^{-1}W_G(J_{,\mu})_{;\beta\alpha}]a^{\beta\mu}a^{\alpha\lambda} = 0. \end{aligned}$$

On the other hand, the precedent study [12] has investigated the thickness distension and formulated the corresponding shape equations which are invoked as

$$\begin{aligned} \frac{1}{2}\Delta W_H + (W_K)_{;\beta\alpha}\tilde{b}^{\beta\alpha} + W_H(2H^2 - K) + 2HW_KK - \\ 2H(W + q\varphi) + G^{-1}W_G b^{\alpha\beta}\varphi_{,\alpha}\varphi_{,\beta} = P \text{ and} \\ q_{,\alpha}\varphi = \partial W/\partial\theta^\alpha. \end{aligned} \quad (5.49)$$

The differences between Eq. (5.48) and Eq. (5.49) lie in the thickness distension-related terms because we couple membrane thickness distension with membrane deformation by invoking relation $S_{\alpha\beta}^\lambda = \Gamma_{\alpha\beta}^\lambda - \bar{\Gamma}_{\alpha\beta}^\lambda$ in this work, while in the previous work on membrane thickness distension [12], the thickness does not play an explicit role by treating $\lambda = q\varphi$.

5.5 Boundary Conditions

The Eq. (5.20) yields the the variation of energy potential (Eq. (5.1)) which is

$$\dot{E} = \int_{\omega} (\varphi_{;\alpha}^\alpha - \mathbf{u} \cdot \mathbf{T}_{;\alpha}^\alpha) da. \quad (5.50)$$

In sense of the Stokes' theorem, we figure out

$$\int_{\omega} \varphi_{;\alpha}^\alpha da = \int_{\partial\omega} (\mathbf{T}^\alpha \cdot \mathbf{u} + \mathbf{M}^{\alpha\beta} \cdot \mathbf{u}_{,\beta}) v_\alpha ds, \quad (5.51)$$

where

$$\mathbf{u}_{,\beta} = \frac{\partial \mathbf{u}}{\partial \theta^\beta} = \frac{\partial \mathbf{u}}{\partial \tau} \frac{\partial \tau}{\partial \theta^\beta} + \frac{\partial \mathbf{u}}{\partial v} \frac{\partial v}{\partial \theta^\beta} = \mathbf{u}' \tau_\beta + \mathbf{u}_v v_\beta, \quad (5.52)$$

in which τ is the unit tangent to $\partial\omega$, and $v = v_\alpha \mathbf{a}^\alpha = \tau \times \mathbf{k}$ for a flat boundary on which $\mathbf{n} = \mathbf{k}$. Accordingly, Eq. (5.51) becomes

$$\begin{aligned} & \int_{\partial\omega} (\mathbf{T}^\alpha \cdot \mathbf{u} + \mathbf{M}^{\alpha\beta} \cdot \mathbf{u}_{,\beta}) v_\alpha ds \\ = & \int_{\partial\omega} \mathbf{T}^\alpha \cdot \mathbf{u} v_\alpha ds + \int \mathbf{M}^{\alpha\beta} \cdot (\mathbf{u}' \tau_\beta + \mathbf{u}_{,v} v_\beta) v_\alpha ds \\ = & \int_{\partial\omega} \mathbf{T}^\alpha \cdot \mathbf{u} v_\alpha ds + \int_{\partial\omega} \mathbf{M}^{\alpha\beta} \cdot \mathbf{u}' \tau_\beta v_\alpha ds + \int_{\partial\omega} \mathbf{M}^{\alpha\beta} \cdot \mathbf{u}_{,v} v_\beta v_\alpha ds, \end{aligned} \quad (5.53)$$

where we treat

$$\mathbf{M}^{\alpha\beta} \cdot \mathbf{u}' \tau_\beta v_\alpha = (\mathbf{M}^{\alpha\beta} \cdot \mathbf{u} \tau_\beta v_\alpha)' - (\mathbf{M}^{\alpha\beta} \tau_\beta v_\alpha)' \cdot \mathbf{u}. \quad (5.54)$$

As such, the Eq. (5.53) proceeds to be

$$\begin{aligned} & \int_{\partial\omega} (\mathbf{T}^\alpha \cdot \mathbf{u} + \mathbf{M}^{\alpha\beta} \cdot \mathbf{u}_{,\beta}) v_\alpha ds \\ = & \int_{\partial\omega} \mathbf{T}^\alpha \cdot \mathbf{u} v_\alpha ds - \int_{\partial\omega} (\mathbf{M}^{\alpha\beta} v_\alpha \tau_\beta)' \cdot \mathbf{u} ds + \int_{\partial\omega} \mathbf{M}^{\alpha\beta} \cdot \mathbf{u}_{,\nu} v_\beta v_\alpha ds + \\ & \int_{\partial\omega} (\mathbf{M}^{\alpha\beta} \cdot \mathbf{u} \tau_\beta v_\alpha)' ds. \end{aligned} \quad (5.55)$$

Immediately, Eq. (5.55) follows the form

$$\int_{\partial\omega} (\mathbf{f} \cdot \mathbf{u} + \mathbf{c} \cdot \mathbf{u}_\nu) ds. \quad (5.56)$$

Hence, the membrane boundary conditions are

$$\mathbf{T}^\alpha v_\alpha - (\mathbf{M}^{\alpha\beta} v_\alpha \tau_\beta)' = \mathbf{f} \text{ and } \mathbf{M}^{\alpha\beta} v_\alpha \tau_\beta = c \text{ on } \partial\omega, \quad (5.57)$$

which involves substrate-interaction forces \mathbf{f} and bending moment c on membrane boundaries.

5.6 Monge Parametrization

To formulate membrane shape equations in the form of partial differential equations (PDEs), we project the equilibrium equations onto Cartesian coordinate using the Monge representation. To begin with, we represent material points with space vector $\mathbf{r}(\theta^\alpha, t)$ on the membrane surface ω , which are given by

$$\mathbf{r}(\theta^\alpha, t) = \theta(\theta^\alpha) + z(\theta, t) \mathbf{k}, \quad (5.58)$$

where $\theta(\theta^\alpha)$ represents point position on membrane plane, \mathbf{k} is unit normal, and $z(\theta)$ is deflection function that determines the membrane shape. Since the Monge representation is an approximation of out-of-plane deformations in which no folds of

the membrane are allowed, i.e., $z(\theta, t)$ is restricted to a single-valued function. The membrane surface can be represented by orthonormal Cartesian basis $\theta = \theta^\alpha \mathbf{e}_\alpha$. With these settings, we compute

$$\mathbf{a}_\alpha = \mathbf{e}_\alpha + z_{,\alpha} \mathbf{k}, \quad a = \det(a_{\alpha\beta}) = 1 + (z_{,\alpha})^2, \quad \text{and} \quad a^{\alpha\beta} = \delta_{\alpha\beta} + z_{,\alpha} z_{,\beta}, \quad (5.59)$$

in which the $\delta_{\alpha\beta}$ is Kronecker delta. To represent surface curvature, we evaluate

$$\mathbf{n} = \frac{\mathbf{k} - \nabla z}{\sqrt{a}} \quad \text{and} \quad \mathbf{b} = \frac{z_{,\alpha\beta}}{\sqrt{a}} (\mathbf{a}^\alpha \otimes \mathbf{a}^\beta), \quad (5.60)$$

where $\nabla z = z_{,\alpha} \mathbf{e}_\alpha$ is the gradient evaluated on membrane surface, and \mathbf{b} is curvature tensor with components $b_{\alpha\beta} = \frac{z_{,\alpha\beta}}{\sqrt{a}}$. After some algebra, we find

$$\begin{aligned} \mathbf{a}^1 &= \frac{1}{a} [(1 + z_{,2}^2)(\mathbf{e}_1 + z_{,1} \mathbf{k}) - z_{,1} z_{,2} (\mathbf{e}_2 + z_{,2} \mathbf{k})] \quad \text{and} \\ \mathbf{a}^2 &= \frac{1}{a} [(1 + z_{,1}^2)(\mathbf{e}_2 + z_{,2} \mathbf{k}) - z_{,1} z_{,2} (\mathbf{e}_1 + z_{,1} \mathbf{k})]. \end{aligned} \quad (5.61)$$

Using these expressions, we can represent the mean and Gaussian curvature (Eq. (5.2)) by

$$H = \frac{[1 + (z_{,2})^2]z_{,11} + [1 + (z_{,1})^2]z_{,22} - 2z_{,1}z_{,2}z_{,12}}{2a^{3/2}} \quad (5.62)$$

and

$$K = \frac{z_{,11}z_{,22} - z_{,12}^2}{a^2}. \quad (5.63)$$

Utilizing these relations and algebra operations, we obtain a system of PDEs regarding shape equations Eq. (5.43), boundary conditions Eq. (5.57), and incompressible flow conditions Eq. (5.44). The algebra procedures are refrained for the sake of brevity.

5.7 Numerical Analysis and Discussion

The solution of the PDEs system (Eqs. (5.43, 5.44)) can be obtained using the commercial software COMSOL. Emphasis is placed on demonstrating the membrane thickness distension by the simulation results of J . It should be noted that the J is the surface dilatation of lipid membrane while is interpreted as the direct indicator

of membrane thickness because ∇J is linear in thickness distension as discussed in the previous section.

Since the lipid membrane inflammation and substrate-interaction cases have been successfully utilized in investigating lipid membrane morphology transition such as membrane-protein interactions [7], abnormal cell membranes formation [8] and long-stored red blood cell morphology [33], we demonstrate the proposed model by applying lateral pressure P , substrate-interaction force f_n (in direction $\mathbf{n} = \mathbf{k}$), respectively. For the substrate-interaction problem, the interaction force f_n is applied on the membrane inner boundary (Figure 5.1(a), circular boundary $r = a = 0.2$) while the membrane's outer boundaries (membrane's four edges) are fixed ($z = 0$). Considering the morphological transition happens at $pN \cdot nm$ scale (the bending modulus of the membrane is invoked with $82 pN \cdot nm$ [10]), we implement a non-dimensional treatment for solving the PDEs system for eliminating dimensional effects, thereby, the continuum model results might be comparable to the MD simulation results obtained under the scale of nanosecond and nanometer. To reduce computational resources, we solve the PDEs system by applying a non-dimensional 2×2 square domain to simulate the non-dimensional deformation and thickness distension of lipid membrane. Meanwhile, the boundary condition of water flux is introduced by applying boundary conditions of Neumann type from the left and bottom boundaries to investigate the viscous effects on membrane deformation.

5.7.1 Coarse-grained MD simulation

Since the MARTINI CG force field has been successfully utilized to validate the physical properties of lipids membrane [3], the MARTINI 2.3 [34] force field is applied in the designated simulation. Using this force field, we build a $40nm \times 40nm$ membrane patch (Figure 5.1(a)) which is immersed in polarized water (Figure 5.1(b)). The membrane-water system is constituted of 5408 dipalmitoyl phosphatidylcholine (DPPC) molecules and 500000 water molecules. Each lipid molecule contains 12 CG

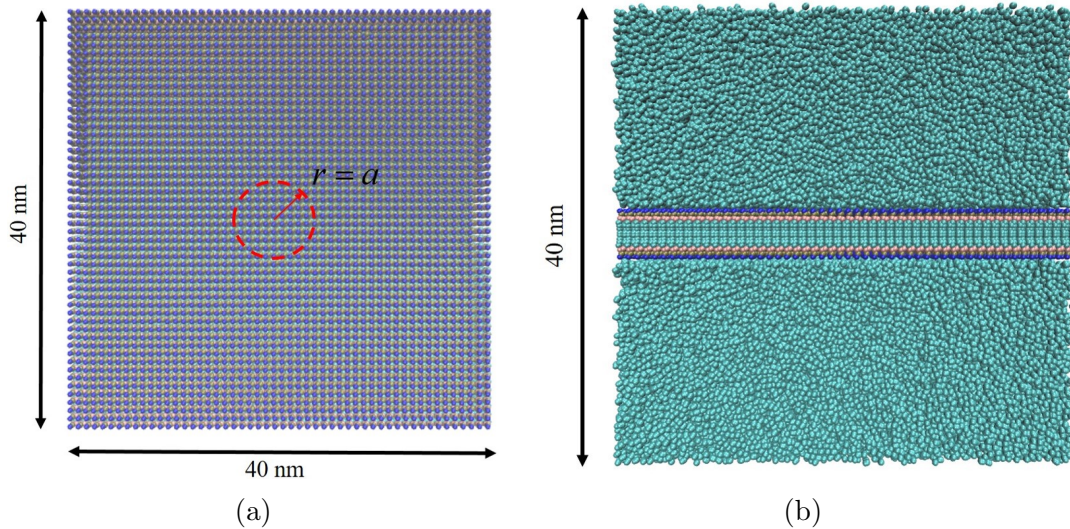


Figure 5.1: Schematic view of the computational model: (a) $40\text{nm} \times 40\text{nm}$ lipid membrane, (b) illustration of membrane-water system.

particles, and per water molecule owns 3 particles. The details of DPPC and water molecule parameters can be found in [3, 5]. To validate the formulated continuum model, we use the GRoningen MACHine for Chemical Simulations (GROMACS) 4.6 version package to simulate the local inflammation and substrate-interaction problem. The membrane edges are fixed using the “freezegrps” code to align with the continuum model edge condition $z = 0$. To introduce viscous flow, the water molecules are pulled using the center of mass (COM) “pulling” code [35] so that the water can flow in the designated direction (diagonally from bottom left to top right), and periodic boundary conditions are applied to maintain a continuous flow. For the lateral pressure problem, water molecules are grouped and accelerated using “acc-grps” code and it induces a 5.6 Mpa lateral pressure toward the membrane patch surface. Precede the simulation, the initial structure’s energy is minimized shortly. Then, the simulation is implemented using a 20 ns canonical NVT ensemble [36], including constant temperature $T = 323\text{K}$ and the integration time step of 20 fs. The thermostat used in the simulations is V-rescale, and we use the reaction-field technique for the long-range electrostatic interactions. As for the substrate-interaction problem, the interaction force is applied to the membrane’s central area which is aligned to the membrane’s

normal direction k . The central area, which is a circular area with a radius of $a = 4$ nm (Figure 5.1(a)), is selected and grouped for interaction purposes. The interaction force applied on the central area is applied by imposing an acceleration on the molecule using “acc-grps” code with acceleration 6×10^{-2} nm/ps². The rest of the MD simulation procedures in substrate-interaction problems (like energy minimum, production, etc.) obey the analogous procedures in simulating local inflammation problems. To demonstrate the effects of viscous flow and boundary conditions on the membrane thickness, we calculate membrane thickness using the tool FATSLiM [37].

5.7.2 Local inflammation of a rectangular membrane patch

The results of the continuum model and MD simulation regarding membrane morphology are compared between Figure 5.2 and Figure 5.3 while the thickness distension results are compared between Figure 5.5 and Figure 5.6, showing a reasonable consistency.

As shown in Figure 5.2 (continuum model approach) and Figure 5.3 (MD simulation approach), the simulation presents transverse deflections of membrane and off-centered membrane morphology when the membrane is subjected to diagonal water flow. At the early stage of $t = 3.4$ s (Figure 5.2(a)) and $t = 2.95$ ns in Figure 5.3(a), the membrane deformation peaks at the center of the membrane because the deformation is mainly dominated by the lateral pressure P when the water starts flowing into the membrane surface. The progressive flow of water eventually leads to the off-centered membrane morphology at $t = 4.0$ s in Figure 5.2(d) and $t = 3.10$ ns in Figure 5.3(d).

To validate the simulation results, the cross-section results of the continuum model and MD simulation are compared in Figure 5.4, illustrating the diagonal water flow of the continuum model and MD simulation can give rise to analogous off-centered deformation because the flow of water pushes the peak of membrane deformation diagonally. Furthermore, the adopted Monge parameterization simplifies the responses

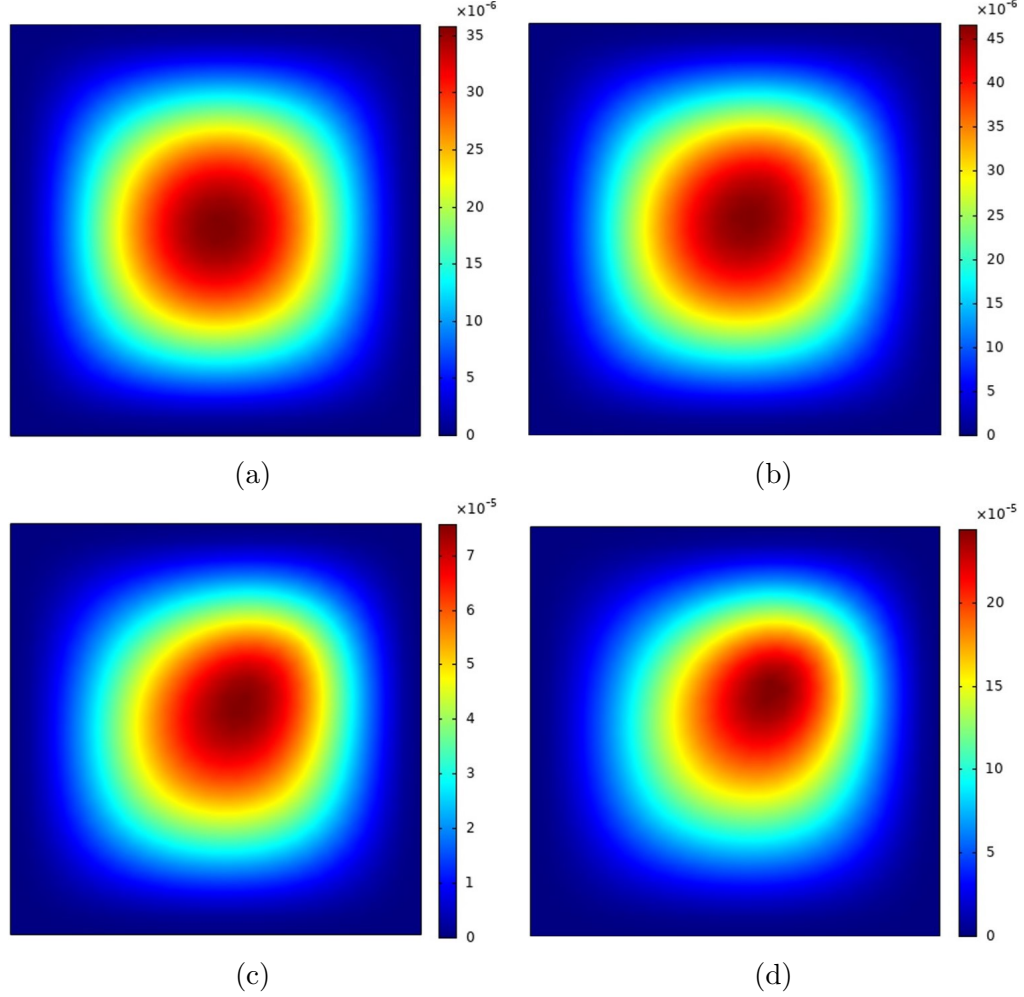


Figure 5.2: Formation of membrane morphology subjected to lateral pressure and viscous flow: (a) continuum model results at $t = 3.4s$, (b) at $t = 3.6s$, (c) at $t = 3.8s$, and (d) at $t = 4.0s$.

of the lipid membrane in the out-of-plane direction z , which may not be ideal for large deformation analyses such as budding and vesicle formations. The refinement of the proposed model to address the abovementioned deficiencies may be possible via the considerations of the Green-Lagrange strain measure [38] and the generalized parameterization [9, 28] which are certainly of more interest, yet it is beyond the scope of the present study.

As shown in Figure 5.5 and Figure 5.6, when the membrane is subjected to a diagonal viscous flow, the membrane thickness fluctuates through the domain for both continuum model and MD simulation approaches. Initially (Figure 5.5(a), at $t = 0s$),

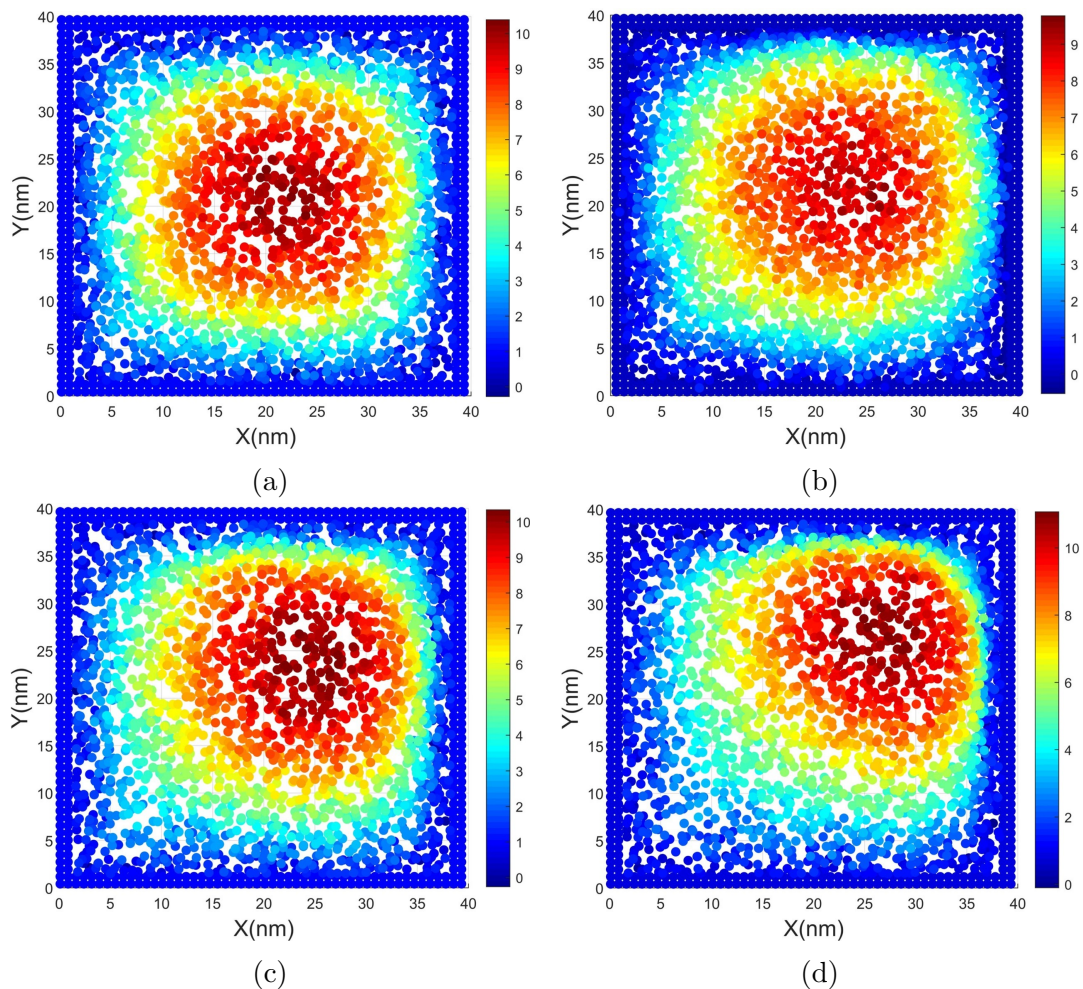


Figure 5.3: Formation of membrane morphology subjected to lateral pressure and viscous flow: (a) MD simulation results at $t = 2.95\text{ns}$, (b) $t = 3.00\text{ns}$, (c) $t = 3.05\text{ns}$, and (d) $t = 3.10\text{ns}$.

the thickness is uniform across the membrane due to the zero flux of water on the membrane surface. Meanwhile, we observe unregulated perturbations of thickness at $t = 3.00\text{ns}$ for MD simulation (Figure 5.6(a)) which can be invoked by the thermodynamics effects. The water flux progresses and eventually leads to the thickness fluctuation on the membrane. It is shown in Figure 5.5(b-d) and Figure 5.6(b-d) that the membrane thickness in the bottom left area is reduced while the thickness in the opposite area is increased. This is because when the water flows onto the membrane the flow direction is acute to the membrane surface (water is flowing towards the membrane), where the membrane is compressed before the water flows over the peak

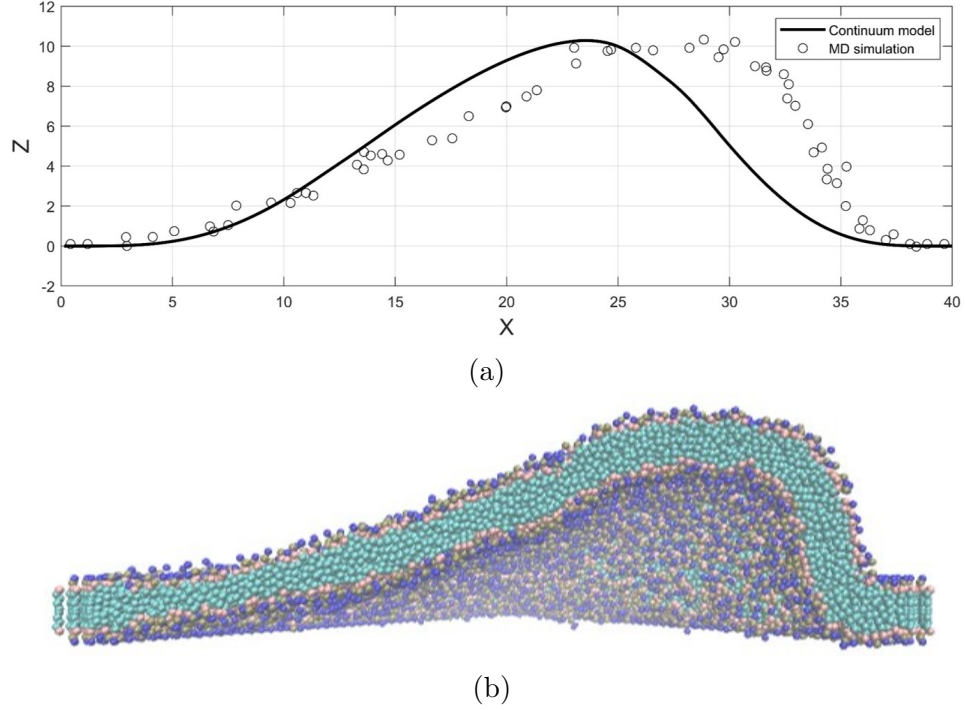


Figure 5.4: Membrane deformation subjected to lateral pressure and viscous flow: (a) comparison between continuum model result at $t = 4.0s$ and MD simulation result at $t = 2ns$, (b) cross-section of MD simulation result at $t = 2ns$.

of the membrane deformation. After water flows past the peak of deformation, the top right area of the membrane is subjected to a stretch by the water flow because the hydrophilic beads are attracted when the water is flowing away from the membrane. Hence, the compress and stretch force contribute to the thickness reduction and increase, respectively. In the results of the continuum model (Figure 5.5(b-d)), we should notice that the thickness of the membrane in the central area persists uniform before the flow expands all over the domain while there is no such appearance for MD simulation results (Figure 5.6). This difference can be explained that it takes time for the water to expand all the domains when it starts flowing into the boundaries (continuum model approach), while for MD simulation, the membrane is immersed into the water initially.

By fixing the flux magnitude of water, the effects of viscosity on membrane morphology and thickness are demonstrated in Figure 5.7 and Figure 5.8, respectively. As

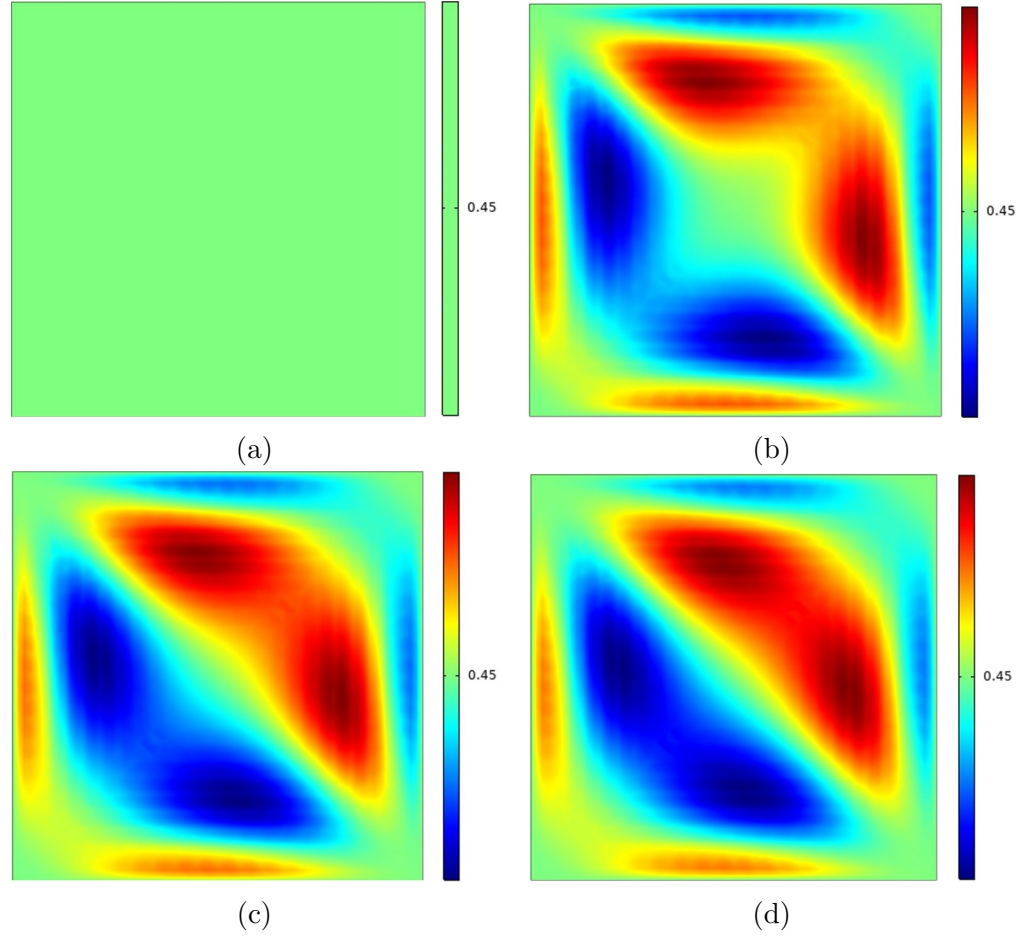


Figure 5.5: Membrane thickness distension subjected to lateral pressure and viscous flow: (a) continuum model results ($\nu = 40$) at $t = 0$ s, (b) at $t = 0.16$ s, (c) at $t = 0.32$ s, and (d) at $t = 0.48$ s.

shown in Figure 5.7, larger viscosity exacerbates the off-centered membrane morphology because the viscous stress increases subject to a larger viscosity, which can result in the morphology deflecting in the diagonal direction. Figure 5.8 demonstrates that viscosity can further alter membrane thickness distribution across the membrane by fixing flux magnitude. The thickness difference between the top right area and the bottom left area is weak at the viscosity of $\nu = 20$ (membrane thickness $J = 0.45$), while the thickness difference between the two areas is enlarged subject to larger viscosity as shown in Figure 5.8(b-d) where the thickness J ranges from 0.42 to 0.5. This can be explained that larger viscosity raises larger viscous stress, which accordingly enhances the compression on the bottom left area and stretches on the top right area

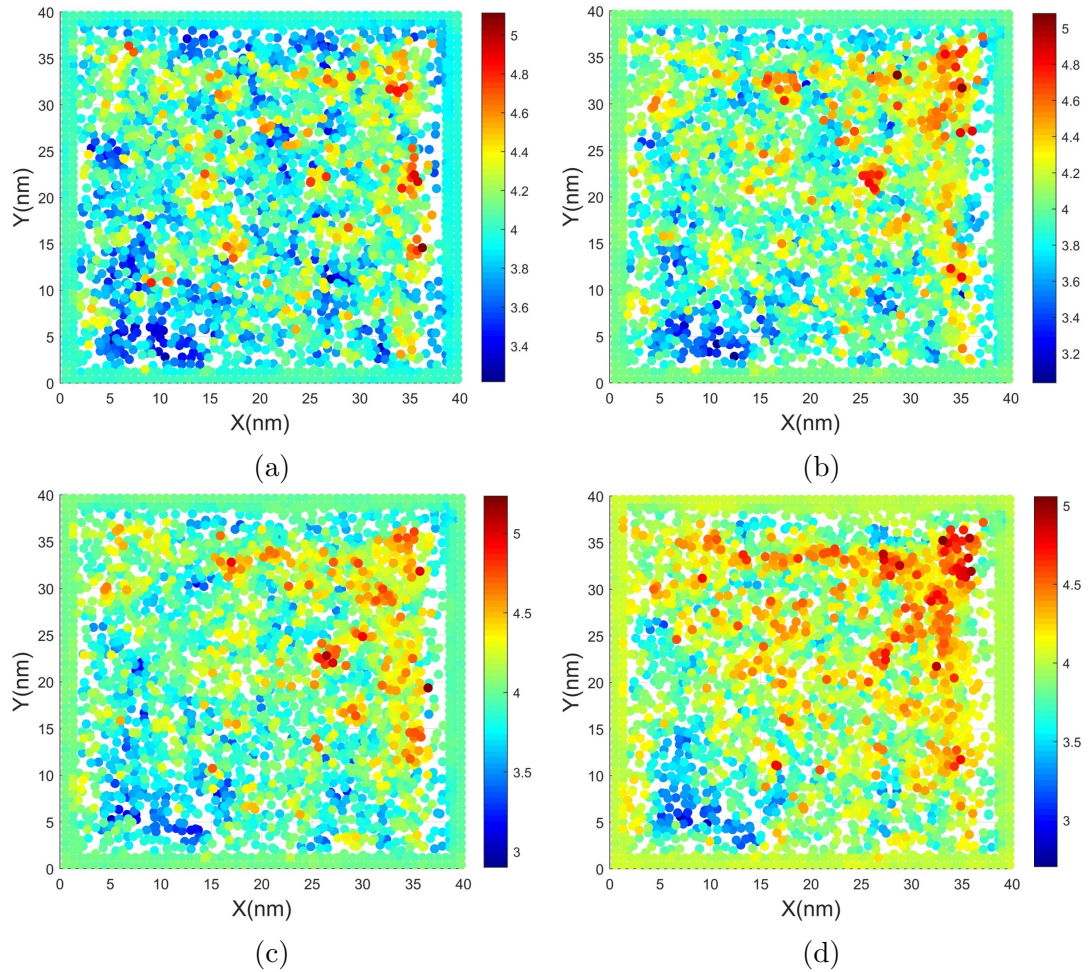


Figure 5.6: Membrane thickness distension subjected to lateral pressure and viscous flow: (a) MD simulation results at $t = 3.00\text{ns}$, (b) at $t = 3.02\text{ns}$, (c) at $t = 3.04\text{ns}$, and (d) at $t = 3.06\text{ns}$.

of the membrane, resulting in a larger thickness difference.

5.7.3 Membrane-protein interactions

The continuum model and MD simulation results of the membrane subjected to interaction force are compared in this section, and the interaction force is applied to the inner circle boundary, i.e., the “hole” inside the lipid membrane domain. As shown in Figure 5.9(a) and Figure 5.10(a), the membrane’s initial deformation peaks on the membrane inner boundary ($r = 0.2$ for continuum simulation $t = 0.002\text{s}$, $r = 4\text{ nm}$ for MD simulation at $t = 1.75\text{ns}$) which are dominated by interaction force on the inner

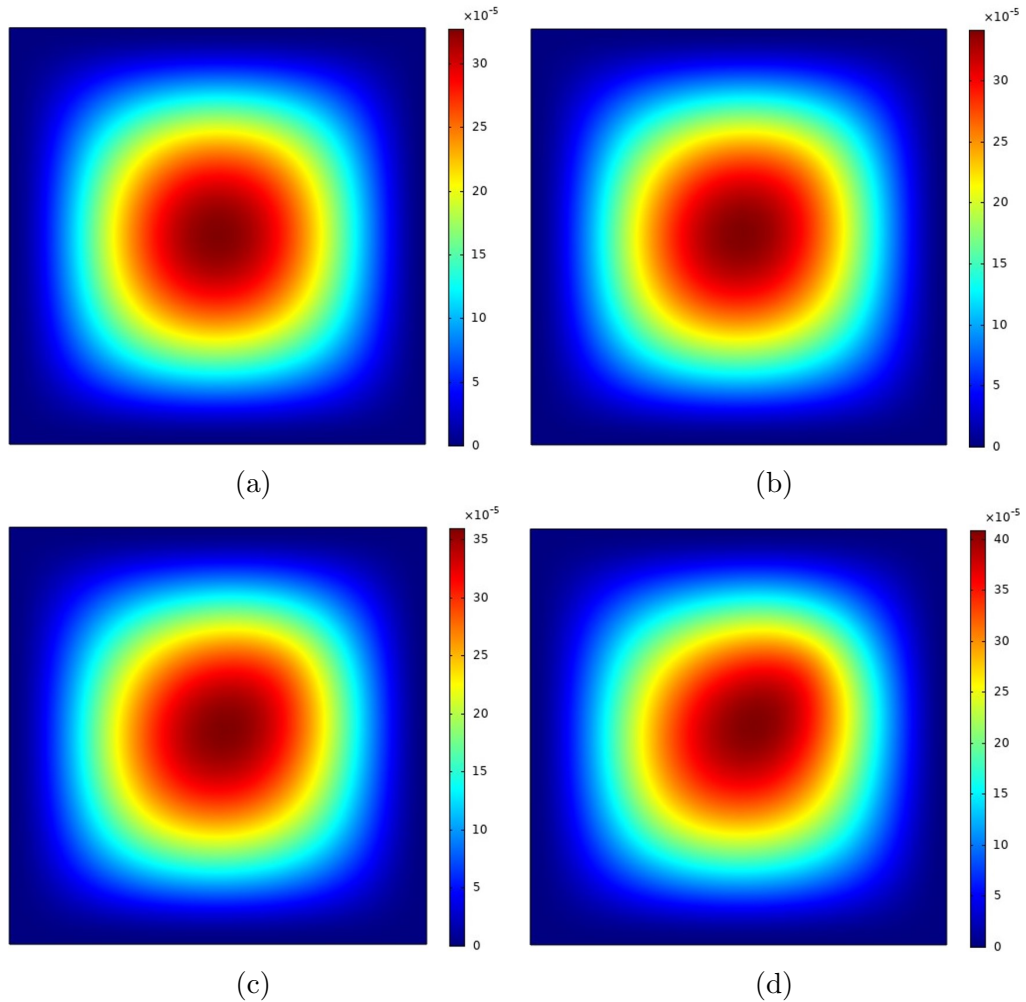


Figure 5.7: Formation of membrane morphology subjected to lateral pressure and various viscosity at $t = 4s$: (a) $\nu = 20$, (b) $\nu = 80$, (c) $\nu = 140$, (d) $\nu = 200$.

boundary. Progressively, the membrane's inner boundary performs a deflection which can be seen in Figure 5.11(right part of the inner boundary is higher than the other), and the deformation tends to peak in the diagonal direction on membrane (Figure 5.9(b-d) and Figure 5.10(b-d)). Such deformation is induced because the bottom left of the inner boundary is both horizontally and vertically compressed when water is flowing over the inner boundary. The top right part of the inner boundary is elevated because the water flow can stretch the membrane since the membrane's hydrophilic beads are attracted when the water is flowing past the inner boundary (Fig.10 (b-d)). Both the continuum model and MD simulation results demonstrate that the viscous

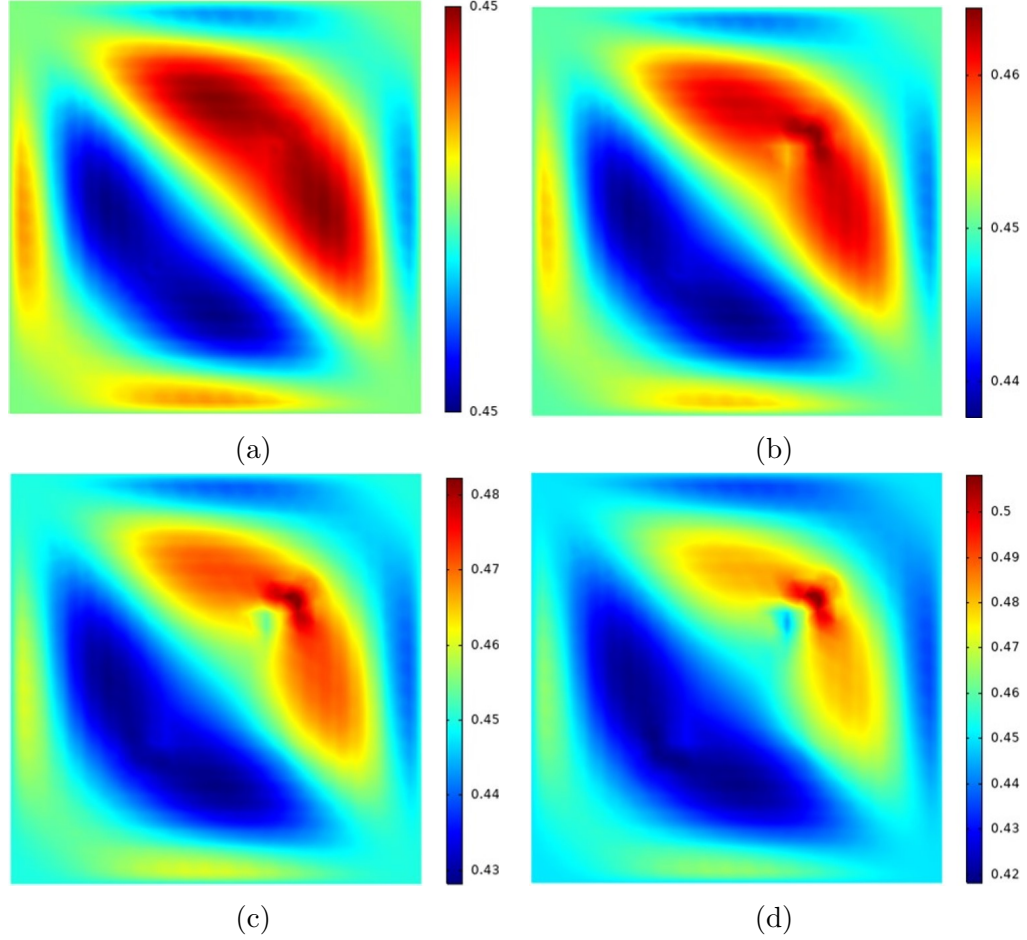


Figure 5.8: Thickness distension of lipid membrane subjected to lateral pressure and different viscosity at $t = 4s$: (a) $\nu = 20$, (b) $\nu = 80$, (c) $\nu = 140$, (d) $\nu = 200$.

flow in diagonal direction can reduce the inner boundary deformation of the bottom left part while it raises the deformation on the top right part of the inner boundary.

The continuum model and MD simulation results are compared between Figure 5.12 and Figure 5.13, showing the membrane thickness fluctuates when the membrane is subjected to interaction force and viscous flow. Initially, the thickness result of the continuum model remains uniform because of no water flux (Figure 5.12(a)). As for the MD simulation result (Figure 5.13(a)) at $t = 0.2ns$, thickness is reduced around the bottom and left boundary because the thickness of other areas remains affected while the water just starts flowing into the domain. Such flux proceeds and results in the membrane thickness fluctuation across the domain, namely, the mem-

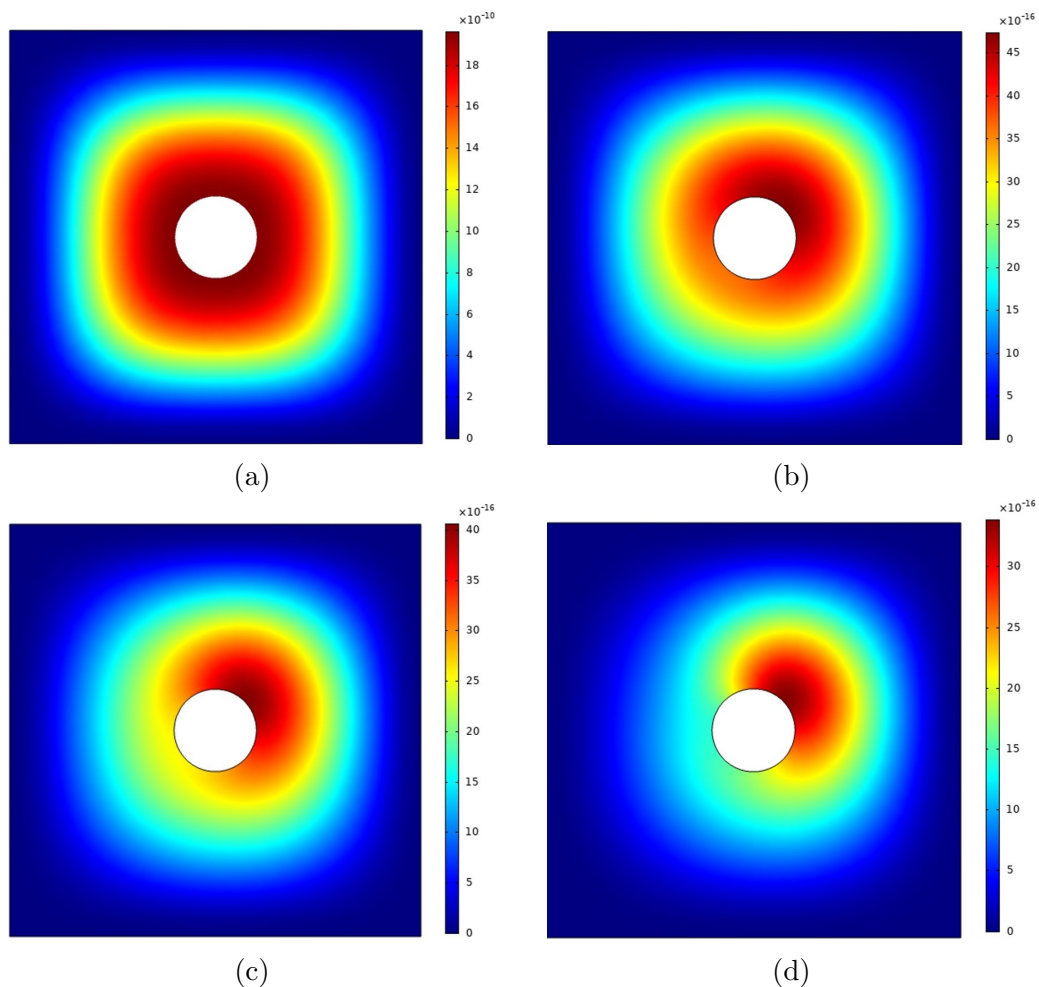


Figure 5.9: Formation of membrane morphology subjected to interaction force and viscous flow: (a) continuum model results at $t = 0.002\text{s}$, (b) $t = 0.003\text{s}$, (c) $t = 0.004\text{s}$, (d) $t = 0.005\text{s}$.

brane thickness of the bottom left part is reduced while the top right part of the membrane behaves larger thickness (Figure 5.12(b) and Figure 5.13(b)). This phenomenon occurs because when the membrane is subjected to viscous flow, the bottom left part of the membrane is compressed while the top right part of the membrane is stretched when the water begins flowing past the interaction area. The stretch can be induced by the opposite and transverse hydrophilic force because though both the lipid beads of the top layer and bottom layer are hydrophilic, they are subjected to transverse hydrophilic force from each side's water. It should be noticed that compared to the MD simulation results in Figure 5.13(b) the thickness of the partial inner

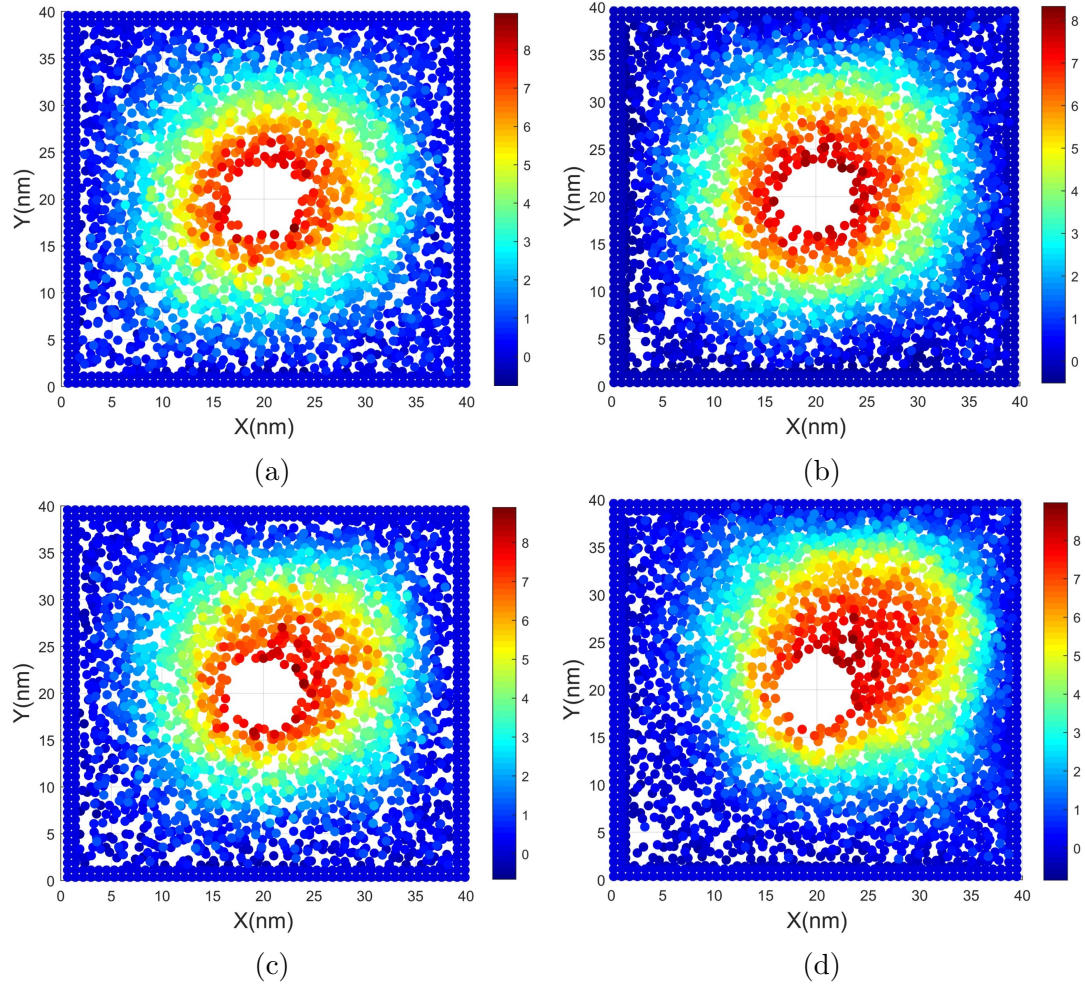
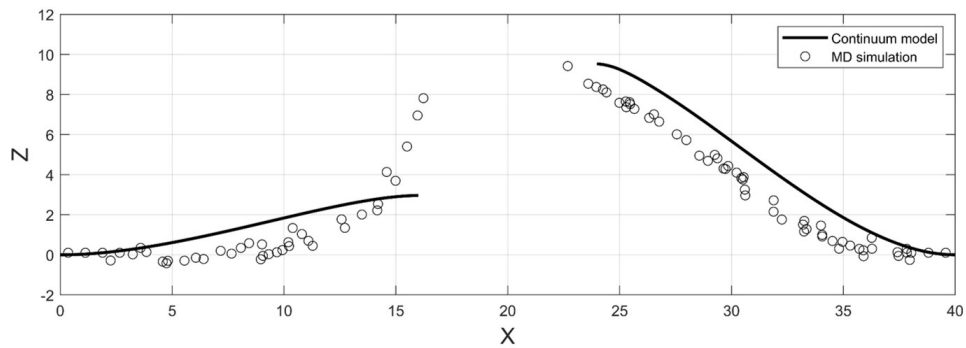
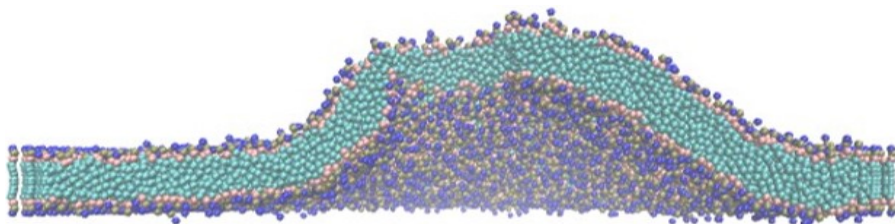


Figure 5.10: Formation of membrane morphology subjected to interaction force and viscous flow: (a) MD simulation results at $t = 1.75\text{ns}$, (b) at $t = 1.85\text{ns}$, (c) at $t = 1.95\text{ns}$, (d) at $t = 2.05\text{ns}$.

boundary is reduced or enhanced, while the thickness of the inner boundary remains uniform for continuum model results. This can be explained that there is no water flowing through the inner boundary for the continuum model while for MD simulation the water flows over the whole membrane area and induces thickness fluctuation across the whole membrane.

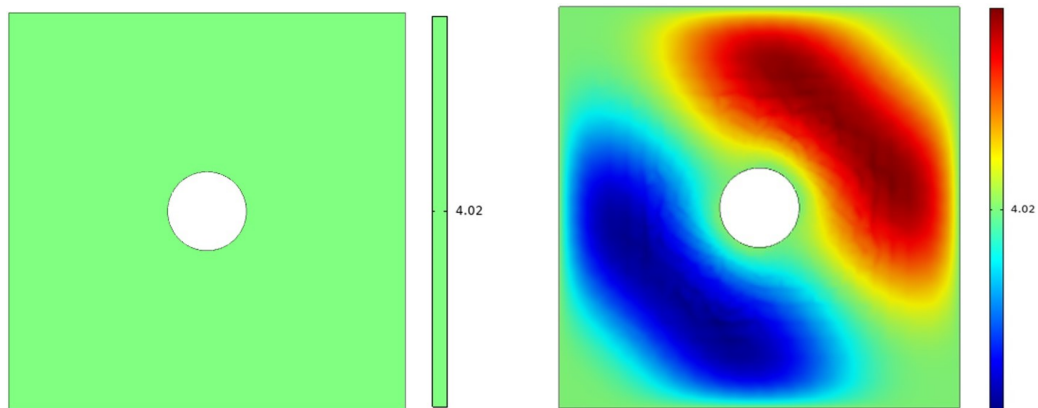


(a)



(b)

Figure 5.11: Membrane morphological transition (diagonal cross-section) subjected to lateral pressure and viscous flow: (a) comparison between continuum model result at $t=0.004s$ and MD simulation result at $t = 2ns$, (b) cross-section of MD simulation result.



(a)

(b)

Figure 5.12: Membrane thickness distension subjected to interaction force and viscous flow: (a) results of continuum model at $t = 0s$ and (b) at $t = 0.001s$.

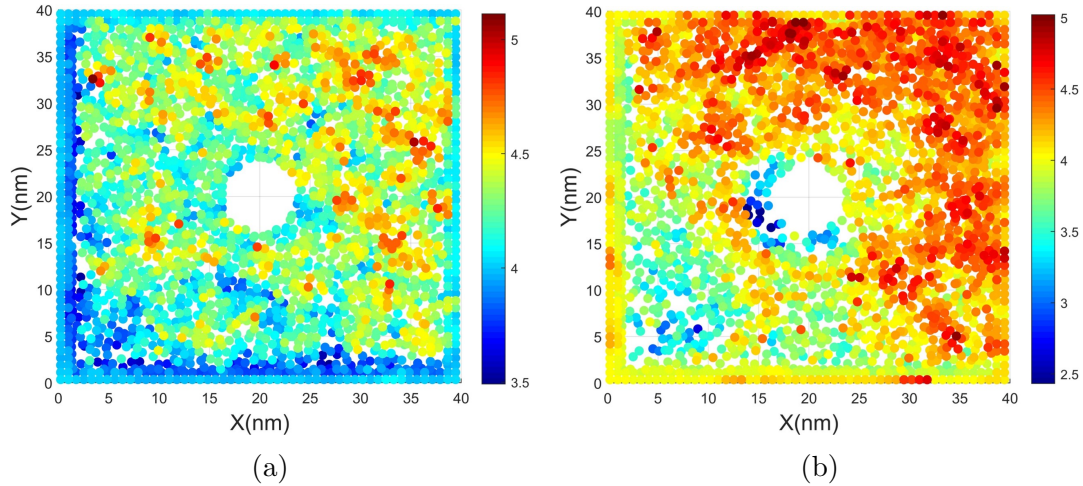


Figure 5.13: Membrane thickness distension subjected to interaction force and viscous flow: (a) MD simulation results at $t = 0.2\text{ns}$, (b) at $t = 2.05\text{ns}$.

5.7.4 Effects of intra-membrane viscous flow and interaction forces on lipid membrane

The precedent validations have demonstrated the effects of viscous flow on the membrane. In this section, we proceed to investigate the effects of interaction force on the membrane because the interaction area is, in general, subjected to both viscous flow and interaction force. As shown in Figure 5.14(a, b), the thickness distension surges on the inner boundary and reduces in the vicinity of the inner boundary. The thickness hikes on the inner boundary because of the resultant force differences between the top and the bottom layer of the membrane on the inner boundary: when the interaction force is applied on the inner boundary, the upper layer is subjected to interaction force and hydrophilic force in the same direction; while for bottom layer, the interaction force and hydrophilic force are opposite, per se, assuming the magnitude of interaction force and hydrophilic force acting on membrane are respectively f_n , f_h , the upper layer of membrane is subjected to $f_n + f_h$, while for the bottom layer the resultant is $f_n - f_h$. The thickness reduction around the inner boundary is shown in Figure 5.14 can be explained that the interaction force can induce bending effects around the inner boundary; the upper layer and bottom layer are locally bent,

resulting in the curvature difference between the upper layer and bottom layer which can lead to the reduction in membrane thickness. In addition, we notice the viscous

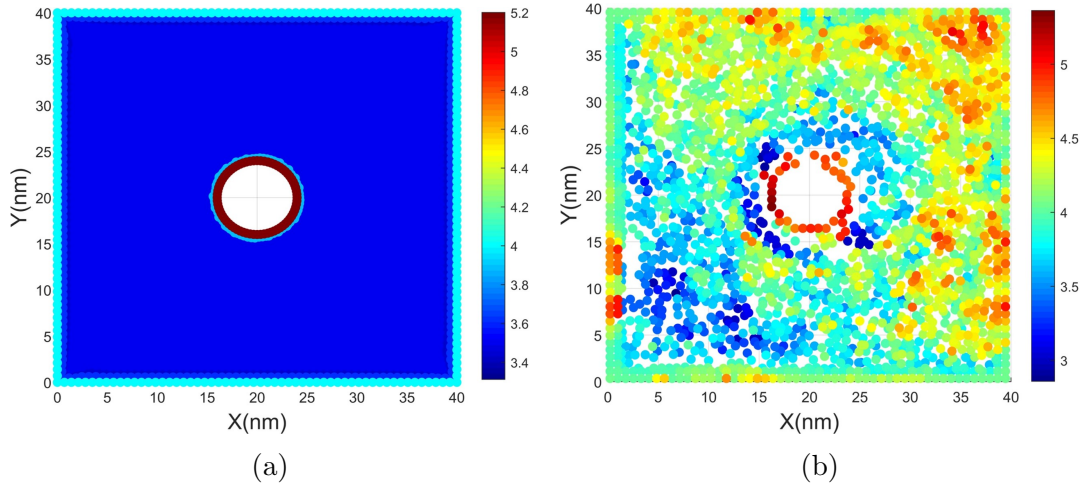


Figure 5.14: Membrane thickness distribution subjected to interaction force and viscous flow: (a) continuum model result at $t = 4s$, (b) MD simulation result at $t = 1.1ns$.

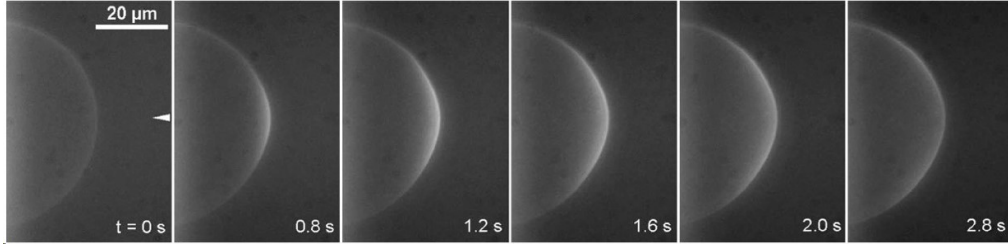
flow can further reduce the thickness of the membrane located at the bottom left inner boundary (Figure 5.14(b)), while the thickness of the top right inner boundary is slightly higher than that of the bottom left inner boundary. The explanations have been illustrated in precedent sections associated with viscous flow effects on membrane thickness induced by compression and stretch.

5.7.5 Experimental comparison

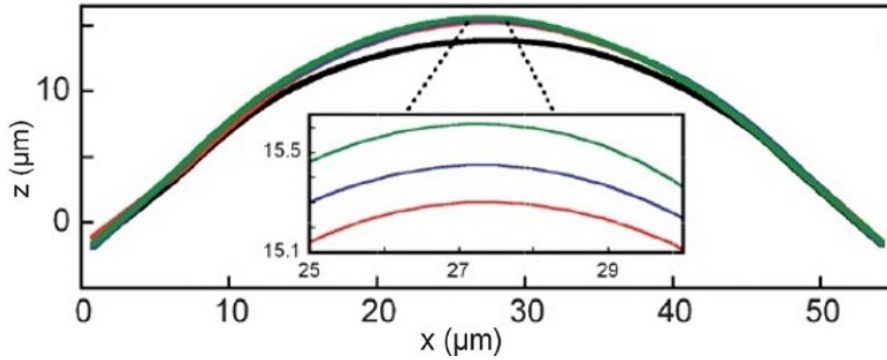
The illustrated simulation results may improve our understanding of cellular phenomena such as the pH level, storage time, and nanoparticle interaction effects on membrane morphology.

As shown in Figure 5.15 [39], the pH level can invoke a morphological transition of the membrane which is analogous to the simulated membrane inflammation problem in Figure 5.16. Experimentally, the membrane morphology evolves, and the membrane deformation increases when subjected to pH level which can be assimilated by continuum model results (see, Figure 5.16, where the membrane deflection increases

gradually with respect to time t), showing the membrane morphology transforms due to the viscous flow.



(a)



(b)

Figure 5.15: Experimental results of lipid membrane morphology transition: (a) fluorescence microscopy images of the membrane subjected to the increasing pH values, (b) quantitative results of membrane deformation in (a); black, $t = 0$ s; red, $t = 0.8$ s; blue, $t = 1.2$ s; green, $t = 2.8$ s [39].

Furthermore, the continuum model result in Figure 5.17(a) aligns with the off-centered morphology (Figure 5.17(b) [33]) as a result of a long storage time, showing the off-centered morphology might be induced by viscous flow and membrane inflammation. It is shown in Figure 5.18 that the simulation result (Figure 5.18(a)) might demonstrate the interaction effect of nuclear pore complexes (NPCs) on the membrane (Figure 5.18(b) [40]). Figure 5.18(a) demonstrates the interaction effects on the inner boundary of the lipid membrane, leading to the out-of-plane deflection of the lipid membrane, and high curvatures are observed near the inner boundary. Likewise, when the NPCs are inserted into the nuclear envelope, it induces a highly curved pore membrane and dome-shaped evagination of the INM due to the substrate-interaction

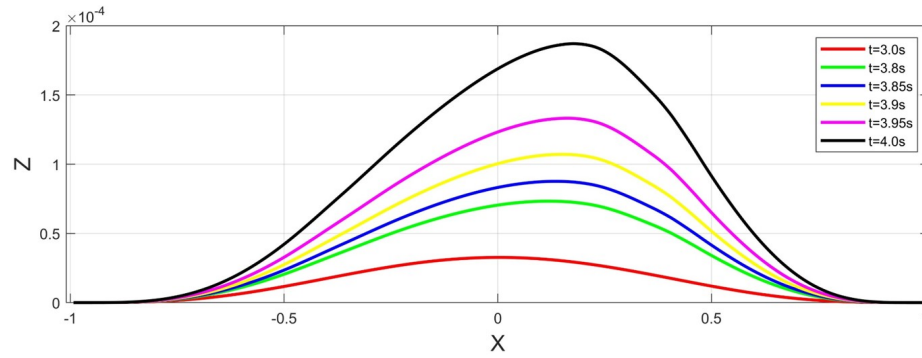


Figure 5.16: Continuum modeling results of membrane inflammation at different time steps.

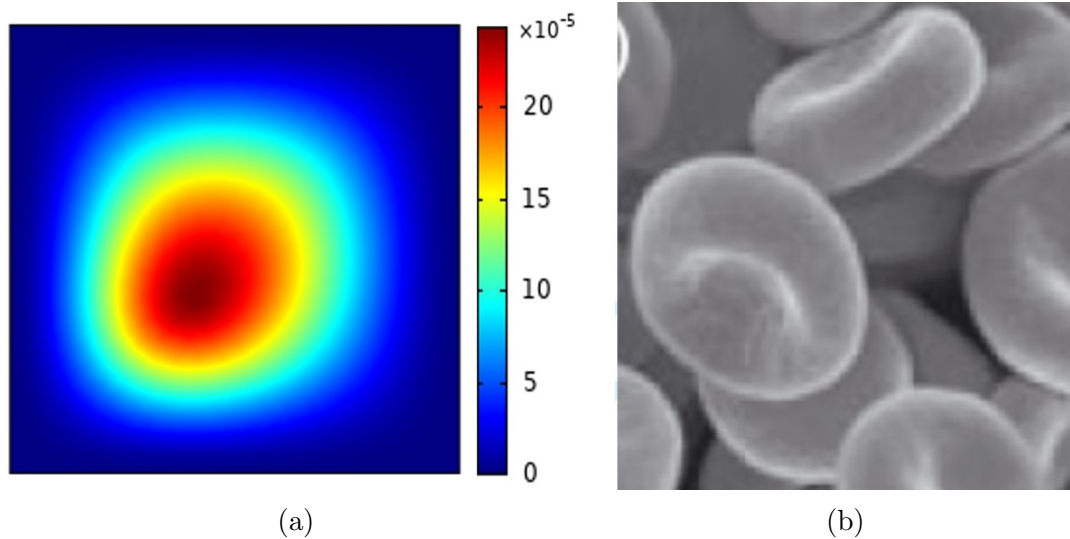


Figure 5.17: Comparison between simulation result and experimental result: (a) continuum modeling result of membrane inflammation subject to viscous flow at $t = 4s$, (b) scanning electron microscope (SEM) images of long-stored red blood cells [33].

effects. In particular, the distance between INM and ONM is reduced, showing the interaction force might decrease the membrane thickness (for instance, the reduction of membrane thickness on the inner boundary in Figure 5.14). It is noteworthy that the substrate-interaction effects can be induced by bilayer-protein interaction, resulting in the differences in membrane thickness in the vicinity of membrane proteins [41–45].

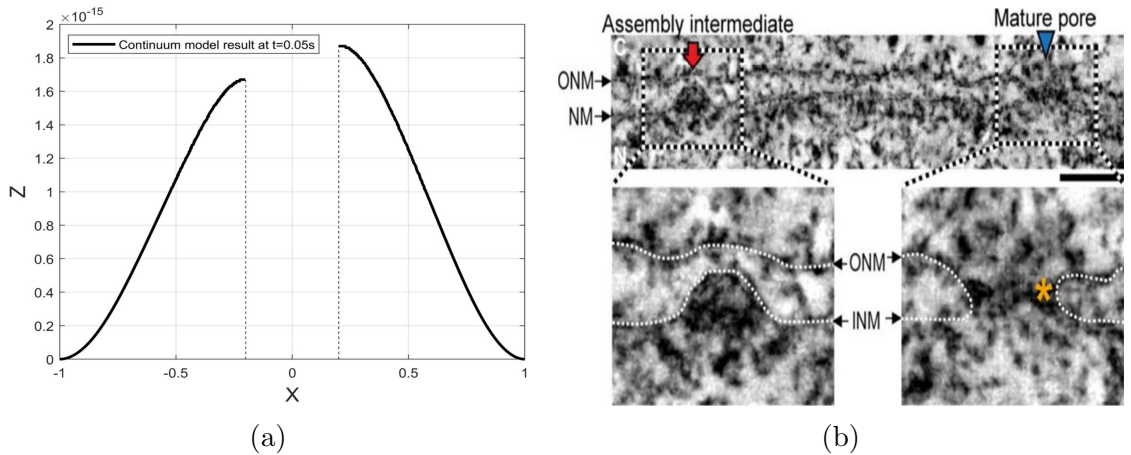


Figure 5.18: Comparison between simulation result and experimental result: (a) simulation result of substrate interaction subjected to viscous flow at $t = 0.005s$, (b) electron-tomographic slice of Hela cells, in which the highly curved pore-membrane deformation is induced as the NPCs are inserted into the nuclear envelope. ONM, outer nuclear membrane; INM, inner nuclear membrane [40].

5.8 Conclusion

We study the thickness distension and morphological transitions of lipid bilayer membranes through the continuum-based model and CGMD simulation. To accommodate the simultaneous effects of intra-membrane viscosity and thickness distension, the classic Helfrich-type model is reformulated into the framework of a crystal thin-film which is deduced from the three-dimensional liquid crystal theory. Utilizing variational framework and Monge representations, tangential and normal shape equations of the lipid membranes have been formulated in the presence of viscous stress, and the resulting system of PDEs is solved numerically. The problems of membrane inflammation and substrate interaction are considered for model demonstration. In addition, MD simulations are implemented to further investigate the results obtained from the proposed continuum model. It is found that viscous flow may result in the off-centered membrane morphology and, at the same time, may increase/reduce the membrane thickness by compressing and stretching the membrane in the out-of-surface direction. In the case of membrane-substrate interactions, the acting interaction force gives rise to local bending effects in the neighborhood of the inner boundary and,

hence, reduces the membrane thickness. Further, a set of existing experimental results have been revisited in light of the proposed work to advance our understanding of lipid membranes' local inflammation and substrate interaction effects. For example, the proposed continuum model may provide quantitative descriptions for the highly curved morphology and the associated thickness reduction of the membrane when NPCs interact with the nuclear envelope. Lastly, the results from the obtained continuum model and MD simulations are compared to examine the performance of the proposed continuum model. Although the MD simulation and the continuum model are two distinct approaches (with different constitutive backgrounds) in the lipid membrane studies, they show close similarity in predicting both the membranes' deformation and thickness dilation except in some particular neighborhoods of the interacting boundary where the MD results experience high fluctuations. The difference between the results obtained from the proposed continuum model and MD simulation may be due to the fact that the MD simulation can identify the intermediate structures with tilted lipid molecules whereas the proposed continuum model describes the membranes' substructure as essentially non-tilted lipids. Further research in this respect is certainly of more practical interest yet is beyond the scope of the study.

References

- [1] U. Seifert and R. Lipowsky, “Chapter 8 - morphology of vesicles,” in *Structure and Dynamics of Membranes*, ser. Handbook of Biological Physics, R. Lipowsky and E. Sackmann, Eds., vol. 1, North-Holland, 1995, pp. 403–463. DOI: [https://doi.org/10.1016/S1383-8121\(06\)80025-4](https://doi.org/10.1016/S1383-8121(06)80025-4). [Online]. Available: <https://www.sciencedirect.com/science/article/pii/S1383812106800254>.
- [2] G. Cevc and H. Richardsen, “Lipid vesicles and membrane fusion,” *Advanced Drug Delivery Reviews*, vol. 38, 3 1999, ISSN: 0169409X. DOI: 10.1016/S0169-409X(99)00030-7.
- [3] J. Yoo, M. B. Jackson, and Q. Cui, “A comparison of coarse-grained and continuum models for membrane bending in lipid bilayer fusion pores,” *Biophysical Journal*, vol. 104, 4 2013, ISSN: 00063495. DOI: 10.1016/j.bpj.2012.12.043.
- [4] S. P. Fu, Z. Peng, H. Yuan, R. Kfoury, and Y. N. Young, “Lennard-jones type pair-potential method for coarse-grained lipid bilayer membrane simulations in lammmps,” *Computer Physics Communications*, vol. 210, 2017, ISSN: 00104655. DOI: 10.1016/j.cpc.2016.09.018.
- [5] I. Hanasaki, J. H. Walther, S. Kawano, and P. Koumoutsakos, “Coarse-grained molecular dynamics simulations of shear-induced instabilities of lipid bilayer membranes in water,” *Physical Review E - Statistical, Nonlinear, and Soft Matter Physics*, vol. 82, 5 Nov. 2010, ISSN: 15393755. DOI: 10.1103/PhysRevE.82.051602.
- [6] W. Helfrich, “Elastic properties of lipid bilayers: Theory and possible experiments,” *Zeitschrift fur Naturforschung - Section C Journal of Biosciences*, vol. 28, 11-12 1973, ISSN: 18657125. DOI: 10.1515/znc-1973-11-1209.
- [7] A. Agrawal and D. J. Steigmann, “Boundary-value problems in the theory of lipid membranes,” *Continuum Mechanics and Thermodynamics*, vol. 21, 1 2009, ISSN: 09351175. DOI: 10.1007/s00161-009-0102-8.
- [8] W. Yao and C. I. Kim, *An analysis of lipid membrane morphology in the presence of coordinate-dependent non-uniformity*, 2021. DOI: 10.1177/1081286520939162.
- [9] T. Belay, C. I. Kim, and P. Schiavone, “Bud formation of lipid membranes in response to the surface diffusion of transmembrane proteins and line tension,” *Mathematics and Mechanics of Solids*, vol. 22, 11 2017, ISSN: 17413028. DOI: 10.1177/1081286516657684.
- [10] P. Rangamani, A. Agrawal, K. K. Mandadapu, G. Oster, and D. J. Steigmann, “Interaction between surface shape and intra-surface viscous flow on lipid membranes,” *Biomechanics and Modeling in Mechanobiology*, vol. 12, pp. 833–845, 4 Aug. 2013, ISSN: 16177959. DOI: 10.1007/s10237-012-0447-y.
- [11] M. Zeidi and C. I. Kim, “The effects of intra-membrane viscosity on lipid membrane morphology: Complete analytical solution,” *Scientific Reports*, vol. 8, 1 2018, ISSN: 20452322. DOI: 10.1038/s41598-018-31251-6.

- [12] C. I. Kim and D. J. Steigmann, “Distension-induced gradient capillarity in lipid membranes,” *Continuum Mechanics and Thermodynamics*, vol. 27, 4-5 2015, ISSN: 09351175. DOI: 10.1007/s00161-014-0333-1.
- [13] J. Frallicciardi, J. Melcr, P. Siginou, S. J. Marrink, and B. Poolman, “Membrane thickness, lipid phase and sterol type are determining factors in the permeability of membranes to small solutes,” *Nature Communications*, vol. 13, 1 2022, ISSN: 20411723. DOI: 10.1038/s41467-022-29272-x.
- [14] X. Liao and P. K. Purohit, “Kinetics of self-assembly of inclusions due to lipid membrane thickness interactions,” *Soft Matter*, vol. 17, 9 2021, ISSN: 17446848. DOI: 10.1039/d0sm01752c.
- [15] A. Shrestha, O. Kahraman, and C. A. Haselwandter, “Regulation of membrane proteins through local heterogeneity in lipid bilayer thickness,” *Physical Review E*, vol. 102, 6 2020, ISSN: 24700053. DOI: 10.1103/PhysRevE.102.060401.
- [16] B. A. Camley, C. Esposito, T. Baumgart, and F. L. Brown, “Lipid bilayer domain fluctuations as a probe of membrane viscosity,” *Biophysical Journal*, vol. 99, 6 2010, ISSN: 15420086. DOI: 10.1016/j.bpj.2010.07.007.
- [17] M. Nagao, E. G. Kelley, R. Ashkar, R. Bradbury, and P. D. Butler, “Probing elastic and viscous properties of phospholipid bilayers using neutron spin echo spectroscopy,” *Journal of Physical Chemistry Letters*, vol. 8, 19 2017, ISSN: 19487185. DOI: 10.1021/acs.jpcclett.7b01830.
- [18] E. G. Kelley, P. D. Butler, R. Ashkar, R. Bradbury, and M. Nagao, “Scaling relationships for the elastic moduli and viscosity of mixed lipid membranes,” *Proceedings of the National Academy of Sciences of the United States of America*, vol. 117, 38 2020, ISSN: 10916490. DOI: 10.1073/pnas.2008789117.
- [19] M. Nagao *et al.*, “Relationship between viscosity and acyl tail dynamics in lipid bilayers,” *Physical Review Letters*, vol. 127, 7 2021, ISSN: 10797114. DOI: 10.1103/PhysRevLett.127.078102.
- [20] A. E. Cohen and Z. Shi, “Do cell membranes flow like honey or jiggle like jello?” *BioEssays*, vol. 42, 1 2020, ISSN: 15211878. DOI: 10.1002/bies.201900142.
- [21] A. L. L. Roux, X. Quiroga, N. Walani, M. Arroyo, and P. Roca-Cusachs, *The plasma membrane as a mechanochemical transducer*, 2019. DOI: 10.1098/rstb.2018.0221.
- [22] R. Illukkumbura, T. Bland, and N. W. Goehring, *Patterning and polarization of cells by intracellular flows*, 2020. DOI: 10.1016/j.ceb.2019.10.005.
- [23] A. Agrawal and D. J. Steigmann, “Modeling protein-mediated morphology in biomembranes,” *Biomechanics and Modeling in Mechanobiology*, vol. 8, pp. 371–379, 5 Oct. 2009, ISSN: 16177959. DOI: 10.1007/s10237-008-0143-0.
- [24] A. Agrawal and D. J. Steigmann, “A model for surface diffusion of transmembrane proteins on lipid bilayers,” *Zeitschrift für Angewandte Mathematik und Physik*, vol. 62, 3 2011, ISSN: 00442275. DOI: 10.1007/s00033-011-0132-5.

- [25] D. J. Steigmann and A. Agrawal, “Electromechanics of polarized lipid bilayers,” *Mathematics and Mechanics of Complex Systems*, vol. 4, pp. 31–54, 1 2016, ISSN: 23253444. DOI: 10.2140/memocs.2016.4.31.
- [26] R. A. Sauer and R. A. Sauer, *The role of mechanics in the study of lipid bilayers*, D. J. Steigmann, Ed. Springer, 2018, vol. 577, ISBN: 9783319563473.
- [27] P. Rangamani, A. Benjamini, A. Agrawal, B. Smit, D. J. Steigmann, and G. Oster, “Small scale membrane mechanics,” *Biomechanics and Modeling in Mechanobiology*, vol. 13, 4 2014, ISSN: 16177940. DOI: 10.1007/s10237-013-0528-6.
- [28] T. Belay, C. I. Kim, and P. Schiavone, “Mechanics of a lipid bilayer subjected to thickness distension and membrane budding,” *Mathematics and Mechanics of Solids*, vol. 23, pp. 67–84, 1 Jan. 2018, ISSN: 17413028. DOI: 10.1177/1081286516666136.
- [29] D. J. Steigmann, “A model for lipid membranes with tilt and distension based on three-dimensional liquid crystal theory,” *International Journal of Non-Linear Mechanics*, vol. 56, 2013, ISSN: 00207462. DOI: 10.1016/j.ijnonlinmec.2013.02.006.
- [30] D. Steigmann, E. Baesu, R. E. Rudd, J. Belak, and M. McElfresh, “On the variational theory of cell-membrane equilibria,” *Interfaces and Free Boundaries*, vol. 5, 4 2003, ISSN: 14639963. DOI: 10.4171/IFB/83.
- [31] W. Yao and C. I. Kim, “Deformation analysis of nonuniform lipid membrane subjected to local inflammations,” *Mathematics and Mechanics of Complex Systems*, vol. 9, 2 2021, ISSN: 23253444. DOI: 10.2140/MEMOCS.2021.9.203.
- [32] R. Aris, *Vectors, tensors, and the basic equations of fluid mechanics*, 1989.
- [33] B. Blasi, A. D’Alessandro, N. Ramundo, and L. Zolla, “Red blood cell storage and cell morphology,” *Transfusion Medicine*, vol. 22, 2 2012, ISSN: 09587578. DOI: 10.1111/j.1365-3148.2012.01139.x.
- [34] S. J. Marrink, H. J. Risselada, S. Yefimov, D. P. Tieleman, and A. H. D. Vries, “The martini force field: Coarse grained model for biomolecular simulations,” *Journal of Physical Chemistry B*, vol. 111, 27 2007, ISSN: 15206106. DOI: 10.1021/jp071097f.
- [35] A. M. Herrera-Rodríguez, V. Miletić, C. Aponte-Santamaría, and F. Gräter, “Molecular dynamics simulations of molecules in uniform flow,” *Biophysical Journal*, vol. 116, 9 2019, ISSN: 15420086. DOI: 10.1016/j.bpj.2018.12.025.
- [36] A. Kadoura, A. Salama, and S. Sun, “Switching between the nvt and npt ensembles using the reweighting and reconstruction scheme,” vol. 51, 2015. DOI: 10.1016/j.procs.2015.05.309.
- [37] S. Buchoux, “Fatslim: A fast and robust software to analyze md simulations of membranes,” *Bioinformatics*, vol. 33, 1 2017, ISSN: 14602059. DOI: 10.1093/bioinformatics/btw563.

- [38] R. Höller, F. Libisch, and C. Hellmich, “A membrane theory for circular graphene sheets, based on a hyperelastic material model for large deformations,” *Mechanics of Advanced Materials and Structures*, pp. 1–11, 2020, ISSN: 15376532. DOI: 10.1080/15376494.2020.1785598.
- [39] A. F. Bitbol, N. Puff, Y. Sakuma, M. Imai, J. B. Fournier, and M. I. Angelova, “Lipid membrane deformation in response to a local pH modification: Theory and experiments,” *Soft Matter*, vol. 8, 22 2012, ISSN: 1744683X. DOI: 10.1039/c2sm25519g.
- [40] H. W. Huang, “Deformation free energy of bilayer membrane and its effect on gramicidin channel lifetime,” *Biophysical Journal*, vol. 50, 6 1986, ISSN: 00063495. DOI: 10.1016/S0006-3495(86)83550-0.
- [41] N. Dan, P. Pincus, and S. A. Safran, *Membrane-induced interactions between inclusions*, 1993. DOI: 10.1021/la00035a005.
- [42] O. S. Andersen and R. E. Koeppe, *Bilayer thickness and membrane protein function: An energetic perspective*, 2007. DOI: 10.1146/annurev.biophys.36.040306.132643.
- [43] R. Phillips, T. Ursell, P. Wiggins, and P. Sens, *Emerging roles for lipids in shaping membrane-protein function*, 2009. DOI: 10.1038/nature08147.
- [44] A. Shrestha, O. Kahraman, and C. A. Haselwandter, “Mechanochemical coupling of lipid organization and protein function through membrane thickness deformations,” *Physical Review E*, vol. 105, 5 2022, ISSN: 24700053. DOI: 10.1103/PhysRevE.105.054410.
- [45] B. W. Peeters, A. C. Piët, and M. Fornerod, “Generating membrane curvature at the nuclear pore: A lipid point of view,” *Cells*, vol. 11, 3 2022, ISSN: 20734409. DOI: 10.3390/cells11030469.

Chapter 6

The Mechanics of Elastomeric Sheet Reinforced with Bi-directional Fiber Mesh under Lateral Pressure

In this Chapter, we investigate the concurrent three-dimensional deformations of fiber-reinforced composite sheets undergoing lateral pressure via a three-dimensional continuum model. Our approaches involve the utilization of the Neo-Hookean strain energy model for the matrix material while incorporating the strain energy of bidirectional fibers (orthogonally cross-linked) into the hyperelastic material model. The strain energy contribution of bidirectional fibers is modeled by accounting for the stretching, bending, and twisting responses of the fibers. In addition, we derive the Euler equation and loading conditions describing the mechanics of the fiber-matrix composite system. The presented results encompass various kinematical aspects of the fiber-matrix systems such as out-of-plane and in-plane deformation, bending, twisting, and stretching of fibers within the matrix material, as well as the deformation of the fiber network. The simulation results provide phenomenologically meaningful insights into the damage patterns of the fiber-reinforced building material, the hemispherical dome shaping results of bamboo poly (lactic) acid (PLA) composites, and the out-of-plane deformation of woven fabric.

6.1 Introduction

Fiber-reinforced composite (FRC) materials, characterized by their reinforcements and matrix materials, have been the subject of extensive research in the field of material science and engineering due to their unique properties like high durability, stiffness, flexural strength, etc [1–3]. Notably, FRC, particularly for biological tissues, owns a distinctive J-shaped stress-strain response that plays a crucial role in preventing material damage caused by excessive strain while enabling high deformability [4–6]. Via the optimization of the interpenetrating network within the matrix material of the FRC, the J-shaped stress-strain performance can be significantly improved [6]. Thereby, the significant enhancements in the unique properties enable the FRCs to be highly promising candidates for a wide range of engineering applications, such as robotics engineering, building construction, and biological tissue manufacturing [7–10].

The optimization of FRC performance necessitates the development of predictive models that delve into the internal microstructure of the material to enhance its mechanical properties. A fundamental assumption in this regard is to treat fibers as densely and continuously distributed microstructures embedded within the matrix material. This consideration facilitates continuum modeling descriptions that are particularly well-suited for investigating isotropic matrix-fiber composites while accounting for the mechanical deformation of the composite material stemming from the response of the embedded fiber polymers [11]. Within this context, early studies have primarily focused on computing the first-order gradient of deformation to analyze the deformation of FRC. These investigations involve examining fiber elongation through the consideration of unidirectional fiber reinforcement while treating the FRC as transversely isotropic [12]. Alternatively, the FRC materials have been treated as incompressible, and it is assumed the embedded fibers are inextensible [13]. However, both approaches have their limitations in describing the mechanics of FRC,

as FRC generally possesses a dense network of fibers within the isotropic matrix material, by which the composite can be isotropic in the orthogonal and bidirectional dimensions. In addition, the embedded fibers are extensible due to the deformations of the embedded fiber kinematically depending on the overall deformation of the FRC [11].

Considerable efforts have been dedicated to developing the continuum theories framed in the higher-order gradient of deformation, aiming to provide accurate and comprehensive descriptions of the mechanics of fiber-reinforced composites. This involves the calculation of the first and second-order gradient of deformations, facilitating the continuum model's capability to elucidate the fibers' resistance to both flexure and stretch, especially in its applicability to describe the mechanics of transversely isotropic materials [14, 15]. Within this prescription, it has been feasible to simulate and test network structures under plane bias extension and coupled bending conditions, enabling the examination of shear strain distributions within the mesh structure [16–18]. In this regard, the authors in [11] propose the gradient elasticity theory (which might serve as an alternative Cosserat theory of non-linear elasticity), in which the kinematics of the embedded fibers are assimilated into the hyperelastic strain energy model by computing the first and second-order gradients of fiber deformation. This model provides accurate descriptions of the smooth transitions of the shear strain fields of FRC, addressing the significant discontinuity observed in the first gradient theory. In addition, the anisotropic type of this model successfully predicts the J-shaped stress-strain response of elastomeric composites, the shear strain distributions, and the deformation profiles [19]. To capture the moderate strain-stiffening and rapid strain-stiffening responses of bidirectionally reinforced fibers, the gradient-based continuum model has been refined by incorporating the bending and twisting kinematics of fibers into the well-known Mooney-Rivlin hyperelastic strain energy potential [20] and invoking strain energy of higher order polynomials and exponential form, in which the J-shaped strain-stiffening characteristics and in-plane deforma-

tion behaviors of FRC are accurately predicted, showcasing a reasonable alignment between theoretical outcomes and empirical observations. Recent advancements in characterizing fiber kinematics have even extended to the third-order gradient of deformation to capture and understand phenomena related to network localization [21]. These works can be framed within the strain-gradient theory [14].

Nevertheless, though the strain-gradient-based models have successfully proven their capability in capturing the two-dimensional mechanical performance of FRC, they overlook any out-of-plane components, resulting in deformation fields such as displacement and strain-stiffness responses solely independent of the out-of-plane coordinate. In addition, the current models fall short of addressing the critical role of the embedded fiber units in determining the overall mechanical performance of fiber meshwork. These unexplored aspects might hedge against comprehending the mechanics of FRC and, hence, impede the development of a continuum model that can provide a comprehensive understanding of the concurrent three-dimensional deformation of FRC materials, which encompasses key aspects such as loading-response behavior, strain distribution, meshwork deformation, and the effects of microstructure on the overall deformation of FRC.

In this study, we investigate the mechanics of bidirectionally fiber-reinforced (orthogonally cross-linked fibers) elastomeric sheets undergoing lateral pressure by demonstrating a three-dimensional continuum model. The derivation process involves the utilization of the Neo-Hookean strain energy model for the matrix material and the incorporation of bidirectional fibers' strain energy into the hyperelastic material model by accounting for the stretching, bending and twisting of the fibers. The strain energy of the fiber reinforcement is formulated via the computation of the first-order gradient of deformation in terms of configuring fiber extension, and then formulating fiber bending and twisting contributions to the strain energy through the second-order gradient of deformation. To establish the constitutive equations for the FRC, we derive the Euler-Lagrange equations in the variational approach and configure the

surface of the FRC via differential geometry on the FRC surface, which involves calculating the surface metric, covariant derivative, and contravariant derivative, as well as the first and second-order gradient of deformation on FRC surface. The formulation leads to a system of coupled Partial Differential Equations (PDEs), which are numerically solved via a custom-built Finite Element Analysis (FEA) procedure. The numerical results emphasize elucidating the concurrent three-dimensional response of FRC and revealing the mechanism that the embedded fiber unit deformation governs the overall mechanical response of the fiber meshwork. The simulation results comprehensively demonstrate the proposed model's capability to predict the concurrent three-dimensional deformation of FRC subjected to lateral pressure, encompassing the three-dimensional deformation of matrix material and the embedded fiber network, as well as the bending, twisting, and stretching of fiber units. It is observed that FRC exhibits concurrent three-dimensional deformations when subjected to lateral pressures, and the matrix material is more deformable in plane than out-of-plane, resulting in the diagonal direction of the FRC showcasing the maximum deformation. In addition, the in-plane deformation exhibits considerable dependency on the size and shape of the FRC. Notably, the simulation results of unit fiber kinematics (extension, flexure, and twist) reasonably explain the formation of the overall mechanical performance of the FRC meshwork. Further, the network of fibers experiences compression in the vicinity of the FRC edges, while the meshwork located in the hinterland of the material undergoes intense stretch, corresponding to the observed large compressing strain in the vicinity of FRC boundaries and the stretching strain inside the domain, respectively. More importantly, the theoretical kinematics differences between the matrix material and reinforcements reasonably explain the damage patterns in the fabric material used for strengthening construction material, the hemispherical dome shaping of bamboo Poly (lactic) acid (PLA) composites, and the out-of-plane deflection of woven fabric.

Throughout the manuscript, the derivation process involves computing the trans-

pose, inverse, cofactor, and trace of tensor \mathbf{A} which are presented using standard notations \mathbf{A}^T , \mathbf{A}^{-1} , \mathbf{A}^* and $\text{tr}(\mathbf{A})$, respectively. We utilize the symbol \otimes for tensor expression and calculation, and the inner product of between tensors \mathbf{A} and \mathbf{B} is denoted as $\mathbf{A} \cdot \mathbf{B} = \text{tr}(\mathbf{A}\mathbf{B}^T)$. The determinant of tensor \mathbf{A} is expressed as $|\mathbf{A}|$. For tensor components, Latin symbols index $\{1, 2, 3\}$ and they are summed up when repeated. The partial derivative of a scalar-valued function \mathcal{F} to tensor \mathbf{A} is presented using subscript form $\mathcal{F}_A = \partial\mathcal{F}/\partial\mathbf{A}$. Similarly, the subscript i of $(*)_{,i}$ (i.e., $\partial(*)/\partial\theta^i$) denotes the differentiation of surface coordinate θ^i .

6.2 Kinematics

In this section, we present the kinematics of fibers on the FRC surface configured by the general curvilinear coordinate, aiming at achieving the constitutive equilibrium equations of a hyperelastic matrix reinforced with elastic extensible and flexible fibers. Emphasis is placed on deriving concise kinematic descriptions for a bidirectional fiber family via the computation of the first and second-order gradient of continuum deformations.

Let θ^α present coordinate parameterizing material position in three-dimensional space. Then, continuum mechanics introduces the concept of the reference and current material positions, denoted as $\mathbf{X}(\theta^\alpha)$ and $\mathbf{r}(\theta^\alpha)$, respectively. Corresponding to these two configurations are their respective natural bases (as illustrated in Figure 6.1)

$$\mathbf{X}_\alpha = \frac{\partial\mathbf{X}(\theta^\alpha)}{\partial\theta^\alpha} \text{ and } \mathbf{a}_\alpha = \frac{\partial\mathbf{r}(\theta^\alpha)}{\partial\theta^\alpha}, \quad (6.1)$$

Therefore, the surface metric in reference and the current configurations are respectively computed as $A_{\alpha\beta} = \mathbf{X}_\alpha \cdot \mathbf{X}_\beta$ and $a_{\alpha\beta} = \mathbf{a}_\alpha \cdot \mathbf{a}_\beta$. The determinant of surface metric yields $A = \det(A_{\alpha\beta})$ and $a = \det(a_{\alpha\beta})$, and the positive-definite surface metric renders their inverse, i.e. $a^{11} = \frac{a_{22}}{a}$, $a^{22} = \frac{a_{11}}{a}$, $a^{21} = a^{12} = \frac{-a_{12}}{a}$, and the same for $A^{\alpha\beta}$, based on which we compute dual basis $\mathbf{X}^\alpha = A^{\alpha\beta}\mathbf{X}_\beta$, $\mathbf{a}^\alpha = a^{\alpha\beta}\mathbf{a}_\beta$. The connections between the referential and current bases are established via the first-order gradient

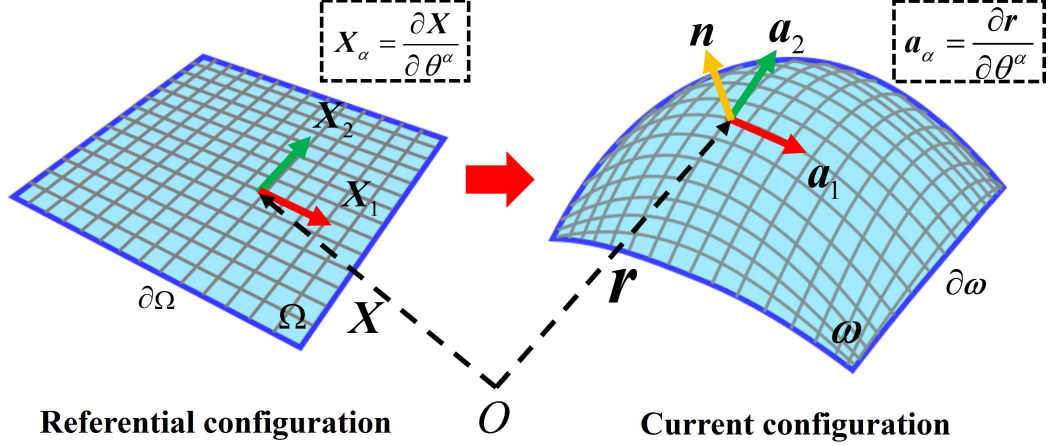


Figure 6.1: Schematic of surface configurations: surface vectors to the specific trajectories in referential (Ω) and current configurations (ω), respectively.

of deformation [22], i.e.,

$$\mathbf{F} = \frac{\partial \mathbf{r}(\theta^\alpha)}{\partial \mathbf{X}} = \frac{\partial \mathbf{r}(\theta^\alpha)}{\partial \theta^\alpha} \otimes \frac{\partial \theta^\alpha}{\partial \mathbf{X}} = \mathbf{a}_\alpha \otimes \mathbf{X}^\alpha, \quad (6.2)$$

and to compute the stretch and flexure of fibers, we express the fiber units (unit tangents to the trajectories of the fibers) in the reference configuration as [23]

$$\mathbf{L} = \frac{d\mathbf{X}(S, U)}{dS} \quad \text{and} \quad \mathbf{M} = \frac{d\mathbf{X}(S, U)}{dU}, \quad (6.3)$$

where S and U are respectively the arclength parameters in the increasing directions of \mathbf{L} and \mathbf{M} (see, Figure 6.2). In the case of initial state, the uniformly and orthogonally oriented fibers obey $\mathbf{L} \cdot \mathbf{M} = 0$, while $\mathbf{L} \cdot \mathbf{M} \neq 0$ for initially non-orthogonal fibers [24–26]. To make the work concise and clarified, we adopt uniform and orthogonal fibers. Then, the deformed \mathbf{L} and \mathbf{M} (regarding \mathbf{l} and \mathbf{m} , see Figure 6.2) can be computed via the first-order gradient of deformation as [23, 26–28]

$$\lambda \mathbf{l} = \mathbf{F} \mathbf{L} \quad \text{and} \quad \mu \mathbf{m} = \mathbf{F} \mathbf{M}, \quad (6.4)$$

in which λ and μ are stretch that are expressed with

$$\lambda = \frac{ds}{dS}, \quad \mu = \frac{du}{dU}, \quad (6.5)$$

where s and u are deformed fiber arclength parameters corresponding to \mathbf{L} and \mathbf{M} directions, and Eq. (6.4) alternatively furnishes the first-order gradient of deformation as

$$\mathbf{F} = \lambda \mathbf{l} \otimes \mathbf{L} + \mu \mathbf{m} \otimes \mathbf{M}. \quad (6.6)$$

Besides the stretch that fibers are subjected to, potential deformations of fiber may include bending, which necessitates the second derivative of position \mathbf{r} in three-dimensional space to compute the fiber piece curvature (see, Figure 6.2)

$$\begin{aligned} \mathbf{g}_1 &= \frac{d^2 \mathbf{r}(S)}{dS^2} = \frac{d\left(\frac{d\mathbf{r}(S)}{dS}\right)}{dS} = \frac{d(\mathbf{F}\mathbf{L})}{dS} = \frac{d(\mathbf{F}\mathbf{L})}{d\mathbf{X}} \frac{d\mathbf{X}}{dS} = \nabla(\mathbf{F}\mathbf{L})\mathbf{L} \text{ and} \\ \mathbf{g}_2 &= \frac{d^2 \mathbf{r}(U)}{dU^2} = \frac{d\left(\frac{d\mathbf{r}(U)}{dU}\right)}{dU} = \frac{d(\mathbf{F}\mathbf{M})}{dU} = \frac{d(\mathbf{F}\mathbf{M})}{d\mathbf{X}} \frac{d\mathbf{X}}{dU} = \nabla(\mathbf{F}\mathbf{M})\mathbf{M}. \end{aligned} \quad (6.7)$$

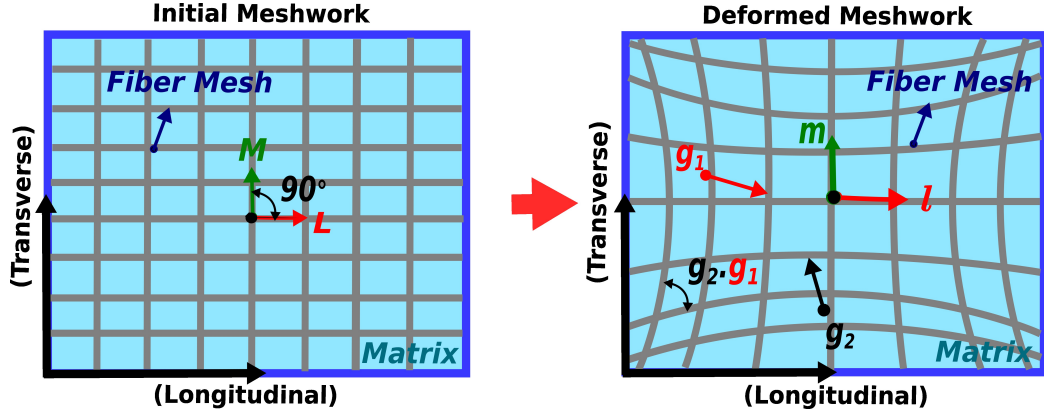


Figure 6.2: Schematic of fiber kinematics: unit tangents to the trajectories of the fibers in reference (\mathbf{L} and \mathbf{M}) and current configurations (\mathbf{l} and \mathbf{m}), and geodesic curvature (\mathbf{g}_1 and \mathbf{g}_2) between two adjacent fibers.

Here, we assume fibers are initially undeformed because fibers, in general, are aligned straightly before being deformed, so we idealize fibers as “locally straight” even if they might be slightly and locally curved. Under these assumptions, we write

$$\mathbf{g}_1 = \nabla \mathbf{F}(\mathbf{L} \otimes \mathbf{L}) \text{ and } \mathbf{g}_2 = \nabla \mathbf{F}(\mathbf{M} \otimes \mathbf{M}) \quad (6.8)$$

due to $\nabla \mathbf{L} = \nabla \mathbf{M} = \mathbf{0}$, where $\nabla \mathbf{F}$ is the second gradient of deformation. To compute the second-order gradient of deformation on the FRC surface, it is not trivial to

introduce Gauss and Weingarten equations

$$\mathbf{a}_{\alpha;\beta} = b_{\alpha\beta}\mathbf{n} \text{ and } \mathbf{n}_{,\alpha} = -b_{\alpha\beta}\mathbf{a}^\beta = -b_{\alpha}^\beta\mathbf{a}_\beta, \quad (6.9)$$

where semi-colon represents covariant differentiation, $b_{\alpha\beta}$ are coefficients of the second fundamental form, b_{α}^β are curvature components in mixed form, unit surface normal $\mathbf{n} = \frac{1}{2}\varepsilon^{\alpha\beta}\mathbf{a}_\alpha \times \mathbf{a}_\beta$, in which $\varepsilon^{\alpha\beta} = \frac{e^{\alpha\beta}}{\sqrt{a}}$ is the permutation tensor density. These relations denote surface covariant differentiation, for instance [22, 24, 27],

$$\mathbf{r}_{;ij} = (\mathbf{r}_{;i})_{,j} - \bar{\Gamma}_{ij}^\varepsilon \mathbf{r}_{,\varepsilon} \text{ and } \mathbf{a}_{\alpha;\beta} = \mathbf{a}_{\alpha,\beta} - \Gamma_{\alpha\beta}^\lambda \mathbf{a}_\lambda, \quad (6.10)$$

where $\bar{\Gamma}_{ij}^k$ and $\Gamma_{\alpha\beta}^\lambda$ represent the Christoffel symbols in the reference and current configurations, respectively. With the assistance of Eqs. (6.9, 6.10), we find (see, also [22, 24–27])

$$\nabla \mathbf{F} = (\mathbf{a}_{\alpha,\beta} - \bar{\Gamma}_{\alpha\beta}^\gamma \mathbf{a}_\gamma) \otimes \mathbf{X}^\alpha \otimes \mathbf{X}^\beta. \quad (6.11)$$

The introduced fiber kinematics encourages us to propose a mathematical a model describing the mechanical deformation of FRC material. Hence, the strain energy potential of matrix-fiber systems might be demonstrated as

$$W(\mathbf{F}, \varepsilon_i, \mathbf{g}_i) = W_{matrix}(\mathbf{F}) + W_{fiber\ extension}(\varepsilon_1, \varepsilon_2) + W_{fiber\ bending/twist}(\mathbf{g}_1, \mathbf{g}_2), \quad (6.12)$$

where $W(\mathbf{F})_{matrix}$ is the energy potential of matrix material that has been widely adopted in the description of hyperelastic matrix materials, see [29–31] and references therein, for Neo-Hookean material of incompressible type,

$$W_{matrix}(\mathbf{F}) = \kappa(\mathbf{F} \cdot \mathbf{F} - 3), \quad (6.13)$$

in which κ is the material parameter and should be multiplied with a factor 1/2 when κ incorporates the meaning of shear modulus. Then, $W(\varepsilon_1, \varepsilon_2)_{fiber\ extension}$ contributes to the fiber response regarding stretch, and such contribution may be demonstrated by using the Green-Lagrange strain in the quadratic form

$$W_{fiber\ extension}(\varepsilon_1, \varepsilon_2) = \frac{1}{2}E_1\varepsilon_1^2 + \frac{1}{2}E_2\varepsilon_2^2, \quad (6.14)$$

where E_i are stretch stiffness of fiber, strain ε_i can be presented using Eq. (6.6) with

$$\varepsilon_1 = \frac{1}{2}(\lambda^2 - 1) = \frac{1}{2}(\mathbf{FL} \cdot \mathbf{FL} - \mathbf{1}) \text{ and } \varepsilon_2 = \frac{1}{2}(\mu^2 - 1) = \frac{1}{2}(\mathbf{FM} \cdot \mathbf{FM} - \mathbf{1}). \quad (6.15)$$

To proceed, $W(\mathbf{g}_1, \mathbf{g}_2)_{fiber \ bending/twist}$ illustrates the bending and twisting contribution to the strain energy of FRC regarding the dot product of geodesic curvature, which has been considered as the fibers' bending energy potential of Spencer and Soldatos type [32] that the contributions of bending strain energy are entirely dependent on the geodesic curvature of fibers via the computation of the second-order gradient of continuum deformation. The concept of bending-contributed strain energy has been widely postulated and adopted in the associated studies (see, [24, 33–37]). Further, the computation of second-order gradient deformations necessitates the adherence to frame indifference, which remains applicable in the context of finite elastic deformations of general continuum bodies [38–40] and hyperelasticity of biological tissue [41]. Hence, the concept of bending strain energy is adopted without further proof in the present study, and the $W(\mathbf{g}_1, \mathbf{g}_2)_{fiber \ bending/twist}$ might be written as [25–28]

$$W_{fiber \ bending/twist}(\mathbf{g}_1, \mathbf{g}_2) = \frac{1}{2}C_1\mathbf{g}_1 \cdot \mathbf{g}_1 + \frac{1}{2}C_2\mathbf{g}_2 \cdot \mathbf{g}_2 + \frac{1}{2}T\mathbf{g}_1 \cdot \mathbf{g}_2, \quad (6.16)$$

where C_i represents the bending stiffness of the fiber and T is the torsional stiffness of fiber, which is, in general, independent of the gradient of deformation. Eventually, the constraint of bulk incompressibility furnishes the strain energy potential as

$$\begin{aligned} U(\mathbf{F}, \varepsilon_i, \mathbf{g}_i, p) &= \kappa(\mathbf{F} \cdot \mathbf{F} - 3) + \frac{1}{2}E_1\varepsilon_1^2 + \frac{1}{2}E_2\varepsilon_2^2 + \frac{1}{2}C_1\mathbf{g}_1 \cdot \mathbf{g}_1 + \quad (6.17) \\ &\quad \frac{1}{2}C_2\mathbf{g}_2 \cdot \mathbf{g}_2 + \frac{1}{2}T\mathbf{g}_1 \cdot \mathbf{g}_2 - p(J - 1), \end{aligned}$$

where J is the determinant of \mathbf{F} and p is Lagrange multiplier (a constitutive indeterminate parameter). Such constraint derives from the consideration that, for engineering material, volume changes in material deformation is a costly process (see, also, [29, 31]).

6.3 Equilibrium

A wealth of literature (see, for instance, [42–45]) has well-established the framework of variational principles in second-gradient finite elasticity. Hence, we derive the Euler equilibrium equations and loading conditions through the variational framework in this section. The potential energy of FRC occupying domain B is presented as [23]

$$E = \int_B U(\mathbf{F}, \varepsilon_i, \mathbf{g}_i, p) dV, \quad (6.18)$$

and it is assumed that, in reaction to virtual power \dot{E} , the fiber composites equilibrium may be balanced by the virtual load P [22], which is

$$\dot{E} = P, \quad (6.19)$$

where the superposed dot means the variational derivative to ϵ , say, a parameter that identifies configurations of the surface. The variation of energy that is conserved to a virtual load emphasizes on determining the equilibrium equation by minimizing the potential energy, i.e., deriving the Euler-Lagrange equation. Hence, the primary work is to compute [27]

$$\dot{E} = \int_B \dot{U}(\mathbf{F}, \varepsilon_i, \mathbf{g}_i, p) dV. \quad (6.20)$$

6.3.1 Variational formulation

The variational framework of E necessitates the computation of

$$\begin{aligned} \dot{U}(\mathbf{F}, \varepsilon_i, \mathbf{g}_i, p) &= \dot{W}_{matrix}(\mathbf{F}) + \dot{W}_{fiber\ extension}(\varepsilon_1, \varepsilon_2) + \\ &\quad \dot{W}_{fiber\ bending/twist}(\mathbf{g}_1, \mathbf{g}_2) - [p(J-1)] \\ &= U_{\mathbf{F}} \cdot \dot{\mathbf{F}} + U_{\varepsilon_i} \dot{\varepsilon}_i + U_{\mathbf{g}_i} \cdot \dot{\mathbf{g}}_i - [p(J-1)], \end{aligned} \quad (6.21)$$

where subscript \mathbf{F} , ε_i , \mathbf{g}_i denote partial derivative, and

$$\dot{\mathbf{F}} = \dot{\mathbf{a}}_{\alpha} \otimes \mathbf{X}^{\alpha} = \mathbf{u}_{,\alpha} \otimes \mathbf{X}^{\alpha}, \quad \because \dot{\mathbf{X}}^{\alpha} = 0, \quad (6.22)$$

in which $\mathbf{u} = \dot{\mathbf{r}}$ is called virtual displacement, i.e., the variation of position vector \mathbf{r} . Under this principle,

$$U_{\mathbf{F}} \cdot \dot{\mathbf{F}} = 2\kappa \mathbf{F} \cdot \dot{\mathbf{F}} = 2\kappa (\mathbf{a}_\alpha \otimes \mathbf{X}^\alpha) \cdot (\mathbf{u}_{,\beta} \otimes \mathbf{X}^\beta) = 2\kappa A^{\alpha\lambda} \mathbf{a}_\alpha \cdot \mathbf{u}_{,\lambda}, \quad (6.23)$$

it can be deduced that $A^{\alpha\beta} = \mathbf{X}^\alpha \cdot \mathbf{X}^\beta = L^\alpha L^\beta + M^\alpha M^\beta$ when orthogonal basis \mathbf{X}^α , \mathbf{X}^β coincide with fiber tangents \mathbf{L} and \mathbf{M} , respectively. After some algebra, $\dot{W}(\varepsilon_1, \varepsilon_2)_{fiber\ extension}$ is calculated as

$$\dot{W}_{fiber\ extension}(\varepsilon_1, \varepsilon_2) = \left\{ \begin{array}{l} [\frac{E_1}{2}(a_{\alpha\beta}L_\alpha L_\beta - 1)L_\lambda L_j + \\ \frac{E_2}{2}(a_{\alpha\beta}M_\alpha M_\beta - 1)M_\lambda M_j] \end{array} \right\} \mathbf{a}_j \cdot \mathbf{u}_{,\lambda}. \quad (6.24)$$

Regarding $\dot{W}(\mathbf{g}_1, \mathbf{g}_2)_{fiber\ bending/twist}$, we compute

$$U_{\mathbf{g}_i} \cdot \dot{\mathbf{g}}_i = C_1 \mathbf{g}_1 \cdot \dot{\mathbf{g}}_1 + C_2 \mathbf{g}_2 \cdot \dot{\mathbf{g}}_2 + \frac{T}{2} (\mathbf{g}_1 \cdot \dot{\mathbf{g}}_2 + \mathbf{g}_2 \cdot \dot{\mathbf{g}}_1), \quad (6.25)$$

where

$$\dot{\mathbf{g}}_i = [\nabla \mathbf{F}(\mathbf{D} \otimes \mathbf{D})]^\cdot = (\nabla \mathbf{F})^\cdot (\mathbf{D} \otimes \mathbf{D}), \quad (6.26)$$

here, $i = 1, 2$ and index $i = 1$ corresponds to fiber direction vector $\mathbf{D} = \mathbf{L}$, and index $i = 2$ means $\mathbf{D} = \mathbf{M}$. Invoking Eq. (6.11), we have

$$\begin{aligned} (\nabla \mathbf{F})^\cdot &= [(\mathbf{a}_{\alpha,\beta} - \bar{\Gamma}_{\alpha\beta}^\gamma \mathbf{a}_\gamma) \otimes \mathbf{X}^\alpha \otimes \mathbf{X}^\beta]^\cdot \\ &= [(\mathbf{a}_{\alpha,\beta})^\cdot - (\bar{\Gamma}_{\alpha\beta}^\gamma)^\cdot \mathbf{a}_\gamma - \bar{\Gamma}_{\alpha\beta}^\gamma (\mathbf{a}_\gamma)^\cdot] \otimes \mathbf{X}^\alpha \otimes \mathbf{X}^\beta, \end{aligned} \quad (6.27)$$

where we apply Eq. (6.10) to express

$$(\mathbf{a}_{\alpha,\beta})^\cdot = (\mathbf{u}_{,\alpha})_{,\beta} = \mathbf{u}_{;\alpha\beta} + \Gamma_{\alpha\beta}^\lambda \mathbf{u}_{,\lambda}, \quad (6.28)$$

in which $(\mathbf{a}_\alpha)^\cdot = \mathbf{u}_{,\alpha}$, while $(\bar{\Gamma}_{\alpha\beta}^\gamma)^\cdot = 0$ due to initial configuration of FRC. The substitution of Eq. (6.28) into Eq. (6.27) furnishes

$$(\nabla \mathbf{F})^\cdot = [\mathbf{u}_{;\alpha\beta} + (\Gamma_{\alpha\beta}^\lambda - \bar{\Gamma}_{\alpha\beta}^\lambda) \mathbf{u}_{,\lambda}] \otimes \mathbf{X}^\alpha \otimes \mathbf{X}^\beta. \quad (6.29)$$

Thus, we figure out $\dot{\mathbf{g}}_i$ from Eq. (6.8) that

$$\begin{aligned} \dot{\mathbf{g}}_i &= \left\{ [\mathbf{u}_{;\alpha\beta} + (\Gamma_{\alpha\beta}^\lambda - \bar{\Gamma}_{\alpha\beta}^\lambda) \mathbf{u}_{,\lambda}] \otimes \mathbf{X}^\alpha \otimes \mathbf{X}^\beta \right\} (\mathbf{D} \otimes \mathbf{D}) \\ &= [\mathbf{u}_{;\alpha\beta} + (\Gamma_{\alpha\beta}^\lambda - \bar{\Gamma}_{\alpha\beta}^\lambda) \mathbf{u}_{,\lambda}] D^\alpha D^\beta \end{aligned} \quad (6.30)$$

and invoking Eq. (6.9) and Eq. (6.10), we obtain

$$\begin{aligned}
\mathbf{g}_i \cdot \dot{\mathbf{g}}_i &= [(\mathbf{a}_{\mu;\eta} + (\Gamma_{\mu\eta}^\gamma - \bar{\Gamma}_{\mu\eta}^\gamma)\mathbf{a}_\gamma)D^\mu D^\eta \cdot [\mathbf{u}_{;\alpha\beta} + (\Gamma_{\alpha\beta}^\lambda - \bar{\Gamma}_{\alpha\beta}^\lambda)\mathbf{u}_{,\lambda}]D^\alpha D^\beta \\
&= [(b_{\mu\eta}\mathbf{n} + (\Gamma_{\mu\eta}^\gamma - \bar{\Gamma}_{\mu\eta}^\gamma)\mathbf{a}_\gamma) \cdot [\mathbf{u}_{;\alpha\beta} + (\Gamma_{\alpha\beta}^\lambda - \bar{\Gamma}_{\alpha\beta}^\lambda)\mathbf{u}_{,\lambda}]D^\alpha D^\beta D^\mu D^\eta \\
&= [(b_{\mu\eta}\mathbf{n} + (\Gamma_{\mu\eta}^\gamma - \bar{\Gamma}_{\mu\eta}^\gamma)\mathbf{a}_\gamma)(\Gamma_{\alpha\beta}^\lambda - \bar{\Gamma}_{\alpha\beta}^\lambda)D^\alpha D^\beta D^\mu D^\eta \cdot \mathbf{u}_{,\lambda} + \\
&\quad [(b_{\mu\eta}\mathbf{n} + (\Gamma_{\mu\eta}^\gamma - \bar{\Gamma}_{\mu\eta}^\gamma)\mathbf{a}_\gamma)D^\alpha D^\beta D^\mu D^\eta \cdot \mathbf{u}_{;\alpha\beta}
\end{aligned} \tag{6.31}$$

Hence, it can be derived that

$$\begin{aligned}
\mathbf{g}_1 \cdot \dot{\mathbf{g}}_1 &= [(b_{\mu\eta}\mathbf{n} + (\Gamma_{\mu\eta}^\gamma - \bar{\Gamma}_{\mu\eta}^\gamma)\mathbf{a}_\gamma)(\Gamma_{\alpha\beta}^\lambda - \bar{\Gamma}_{\alpha\beta}^\lambda)L^\alpha L^\beta L^\mu L^\eta \cdot \mathbf{u}_{,\lambda} + \\
&\quad [(b_{\mu\eta}\mathbf{n} + (\Gamma_{\mu\eta}^\gamma - \bar{\Gamma}_{\mu\eta}^\gamma)\mathbf{a}_\gamma)L^\alpha L^\beta L^\mu L^\eta \cdot \mathbf{u}_{;\alpha\beta} \\
\mathbf{g}_2 \cdot \dot{\mathbf{g}}_2 &= [(b_{\mu\eta}\mathbf{n} + (\Gamma_{\mu\eta}^\gamma - \bar{\Gamma}_{\mu\eta}^\gamma)\mathbf{a}_\gamma)(\Gamma_{\alpha\beta}^\lambda - \bar{\Gamma}_{\alpha\beta}^\lambda)M^\alpha M^\beta M^\mu M^\eta \cdot \mathbf{u}_{,\lambda} + \\
&\quad [(b_{\mu\eta}\mathbf{n} + (\Gamma_{\mu\eta}^\gamma - \bar{\Gamma}_{\mu\eta}^\gamma)\mathbf{a}_\gamma)M^\alpha M^\beta M^\mu M^\eta \cdot \mathbf{u}_{;\alpha\beta} \\
\mathbf{g}_1 \cdot \dot{\mathbf{g}}_2 &= [(b_{\mu\eta}\mathbf{n} + (\Gamma_{\mu\eta}^\gamma - \bar{\Gamma}_{\mu\eta}^\gamma)\mathbf{a}_\gamma)(\Gamma_{\alpha\beta}^\lambda - \bar{\Gamma}_{\alpha\beta}^\lambda)M^\alpha M^\beta L^\mu L^\eta \cdot \mathbf{u}_{,\lambda} + \\
&\quad [(b_{\mu\eta}\mathbf{n} + (\Gamma_{\mu\eta}^\gamma - \bar{\Gamma}_{\mu\eta}^\gamma)\mathbf{a}_\gamma)M^\alpha M^\beta L^\mu L^\eta \cdot \mathbf{u}_{;\alpha\beta} \\
\mathbf{g}_2 \cdot \dot{\mathbf{g}}_1 &= [(b_{\mu\eta}\mathbf{n} + (\Gamma_{\mu\eta}^\gamma - \bar{\Gamma}_{\mu\eta}^\gamma)\mathbf{a}_\gamma)(\Gamma_{\alpha\beta}^\lambda - \bar{\Gamma}_{\alpha\beta}^\lambda)L^\alpha L^\beta M^\mu M^\eta \cdot \mathbf{u}_{,\lambda} + \\
&\quad [(b_{\mu\eta}\mathbf{n} + (\Gamma_{\mu\eta}^\gamma - \bar{\Gamma}_{\mu\eta}^\gamma)\mathbf{a}_\gamma)L^\alpha L^\beta M^\mu M^\eta \cdot \mathbf{u}_{;\alpha\beta}.
\end{aligned} \tag{6.32}$$

To make $\dot{U}(\mathbf{F}, \varepsilon_i, \mathbf{g}_i, p)$ explicit in the variational form, we calculate

$$[p(J - 1)] = p\dot{J}, \tag{6.33}$$

where $J = \sqrt{\frac{a}{A}}$ [22] is the area dilatation and

$$\dot{J} = J_{\mathbf{F}} \cdot \dot{\mathbf{F}} = \mathbf{F}^* \cdot \dot{\mathbf{F}} = J(\mathbf{a}^\alpha \otimes \mathbf{X}_\alpha) \cdot \dot{\mathbf{F}} = J\mathbf{a}^\lambda \cdot \mathbf{u}_{,\lambda}, \tag{6.34}$$

where \mathbf{F}^* is adjugate of \mathbf{F} .

6.3.2 Euler equilibrium equation

Eqs. (6.20, 6.21) contribute to the virtual work statement

$$\dot{E} = \int_B \left\{ \begin{array}{l} \dot{W}_{matrix}(\mathbf{F}) + \dot{W}_{fiber\ extension}(\varepsilon_1, \varepsilon_2) + \dot{W}_{fiber\ bending/twist}(\mathbf{g}_1, \mathbf{g}_2) - \\ [p(J - 1)] \end{array} \right\} dV, \tag{6.35}$$

Here, the substitution of Eqs. (6.23, 6.24), (6.32-6.34) into Eq. (6.35) renders a bilinear form in terms of $\mathbf{u}_{,\lambda}$ and $\mathbf{u}_{;\alpha\beta}$, which is

$$\dot{E} = \int_B \left\{ \begin{array}{l} 2\kappa A^{\alpha\lambda} \mathbf{a}_\alpha \cdot \mathbf{u}_{,\lambda} + \\ \left[\frac{E_1}{2} (a_{\alpha\beta} L_\alpha L_\beta - 1) L_\lambda L_j + \frac{E_2}{2} (a_{\alpha\beta} M_\alpha M_\beta - 1) M_\lambda M_j \right] \mathbf{a}_j \cdot \mathbf{u}_{,\lambda} + \\ \left\{ \begin{array}{l} [(b_{\mu\eta} \mathbf{n} + (\Gamma_{\mu\eta}^\gamma - \bar{\Gamma}_{\mu\eta}^\gamma) \mathbf{a}_\gamma) (\Gamma_{\alpha\beta}^\lambda - \bar{\Gamma}_{\alpha\beta}^\lambda) \cdot \mathbf{u}_{,\lambda} + \\ [(b_{\mu\eta} \mathbf{n} + (\Gamma_{\mu\eta}^\gamma - \bar{\Gamma}_{\mu\eta}^\gamma) \mathbf{a}_\gamma) \cdot \mathbf{u}_{;\alpha\beta} \end{array} \right\} * \\ (C_1 L^\alpha L^\beta L^\mu L^\eta + C_2 M^\alpha M^\beta M^\mu M^\eta + \\ \frac{T}{2} M^\alpha M^\beta L^\mu L^\eta + \frac{T}{2} L^\alpha L^\beta M^\mu M^\eta) - p J \mathbf{a}^\lambda \cdot \mathbf{u}_{,\lambda} \end{array} \right\} dV. \quad (6.36)$$

Eq. (6.36) may be further arranged into the form of [22, 27, 28]

$$\dot{E} = \int_B (\varphi^\lambda \cdot \mathbf{u}_{,\lambda} + \psi^{\lambda\beta} \cdot \mathbf{u}_{;\lambda\beta}) dV, \quad (6.37)$$

where

$$\begin{aligned} \varphi^\lambda &= 2\kappa A^{\gamma\lambda} \mathbf{a}_\gamma + \left[\frac{E_1}{2} (a_{\alpha\beta} L_\alpha L_\beta - 1) L_\lambda L_\gamma + \frac{E_2}{2} (a_{\alpha\beta} M_\alpha M_\beta - 1) M_\lambda M_\gamma \right] \mathbf{a}_\gamma + \\ &\quad \left\{ \begin{array}{l} [(b_{\mu\eta} \mathbf{n} + (\Gamma_{\mu\eta}^\gamma - \bar{\Gamma}_{\mu\eta}^\gamma) \mathbf{a}_\gamma) (\Gamma_{\alpha\beta}^\lambda - \bar{\Gamma}_{\alpha\beta}^\lambda) (C_1 L^\alpha L^\beta L^\mu L^\eta + \\ C_2 M^\alpha M^\beta M^\mu M^\eta + \frac{T}{2} M^\alpha M^\beta L^\mu L^\eta + \frac{T}{2} L^\alpha L^\beta M^\mu M^\eta) \end{array} \right\} - \\ &\quad p J \mathbf{a}^\lambda \text{ and} \quad (6.38) \\ \psi^{\lambda\beta} &= \left\{ \begin{array}{l} [(b_{\mu\eta} \mathbf{n} + (\Gamma_{\mu\eta}^\gamma - \bar{\Gamma}_{\mu\eta}^\gamma) \mathbf{a}_\gamma) (C_1 L^\lambda L^\beta L^\mu L^\eta + C_2 M^\lambda M^\beta M^\mu M^\eta + \\ \frac{T}{2} M^\lambda M^\beta L^\mu L^\eta + \frac{T}{2} L^\lambda L^\beta M^\mu M^\eta) \end{array} \right\}. \end{aligned}$$

For the sake of conciseness, we invoke the treatments in [22, 27, 28, 46, 47] to clarify the tangential and normal components in Eq. (6.38), we write

$$\varphi^\lambda = \varphi^{\gamma\lambda} \mathbf{a}_\gamma + \varphi^\lambda \mathbf{n} \text{ and } \psi^{\lambda\beta} = \psi^{\lambda\beta\gamma} \mathbf{a}_\gamma + \psi^{\lambda\beta} \mathbf{n}, \quad (6.39)$$

where

$$\begin{aligned}
\varphi^{\gamma\lambda} &= 2\kappa A^{\gamma\lambda} + \frac{E_1}{2}(a_{\alpha\beta}L_\alpha L_\beta - 1)L_\lambda L_\gamma + \frac{E_2}{2}(a_{\alpha\beta}M_\alpha M_\beta - 1)M_\lambda M_\gamma + \\
&\quad \left[\begin{array}{c} (\Gamma_{\mu\eta}^\gamma - \bar{\Gamma}_{\mu\eta}^\gamma)(\Gamma_{\alpha\beta}^\lambda - \bar{\Gamma}_{\alpha\beta}^\lambda)(C_1 L^\alpha L^\beta L^\mu L^\eta + C_2 M^\alpha M^\beta M^\mu M^\eta + \\ \frac{T}{2}M^\alpha M^\beta L^\mu L^\eta + \frac{T}{2}L^\alpha L^\beta M^\mu M^\eta) \end{array} \right] - \\
&\quad pJ a^{\gamma\lambda}, \tag{6.40} \\
\varphi^\lambda &= \left[\begin{array}{c} b_{\mu\eta}(\Gamma_{\alpha\beta}^\lambda - \bar{\Gamma}_{\alpha\beta}^\lambda)(C_1 L^\alpha L^\beta L^\mu L^\eta + C_2 M^\alpha M^\beta M^\mu M^\eta + \\ \frac{T}{2}M^\alpha M^\beta L^\mu L^\eta + \frac{T}{2}L^\alpha L^\beta M^\mu M^\eta) \end{array} \right], \\
\psi^{\lambda\beta\gamma} &= \left[\begin{array}{c} (\Gamma_{\mu\eta}^\gamma - \bar{\Gamma}_{\mu\eta}^\gamma)(C_1 L^\lambda L^\beta L^\mu L^\eta + C_2 M^\lambda M^\beta M^\mu M^\eta + \\ \frac{T}{2}M^\lambda M^\beta L^\mu L^\eta + \frac{T}{2}L^\lambda L^\beta M^\mu M^\eta) \end{array} \right], \text{ and} \\
\psi^{\lambda\beta} &= b_{\mu\eta}(C_1 L^\lambda L^\beta L^\mu L^\eta + C_2 M^\lambda M^\beta M^\mu M^\eta + \frac{T}{2}M^\lambda M^\beta L^\mu L^\eta + \frac{T}{2}L^\lambda L^\beta M^\mu M^\eta).
\end{aligned}$$

To establish equilibrium equations, the Eq. (6.37) may be rearranged using integral by part and divergence theorem, yielding

$$\dot{E} = \int_B (\varphi^\lambda \cdot \mathbf{u}_{,\lambda} + \psi^{\lambda\beta} \cdot \mathbf{u}_{,\lambda\beta}) dV = \int_B (\varphi^\lambda - \psi_{;\beta}^{\lambda\beta}) \cdot \mathbf{u}_{,\lambda} dV + \int_{\partial B} \psi^{\lambda\beta} \cdot \mathbf{u}_{,\lambda} v_\beta dS. \tag{6.41}$$

Hence, in the absence of external loads, the Euler-Lagrange equation can be obtained with

$$(\varphi^\lambda - \psi_{;\beta}^{\lambda\beta})_{;\lambda} = 0. \tag{6.42}$$

Substituting Eq. (6.39) into Eq. (6.42) and project the resulting equation onto tangential and normal components, yielding the normal equilibrium

$$(\varphi^\lambda - \psi^{\lambda\beta\gamma} b_{\gamma\beta} - \psi_{;\beta}^{\lambda\beta})_{;\lambda} + b_{\gamma\lambda}(\varphi^{\gamma\lambda} - \psi_{;\beta}^{\lambda\beta\gamma} + \psi^{\lambda\beta} b_{\beta\epsilon} a^{\epsilon\gamma}) = 0 \tag{6.43}$$

and tangential equilibrium

$$(\varphi^{\gamma\lambda} - \psi_{;\beta}^{\lambda\beta\gamma} + \psi^{\lambda\beta} b_{\beta\epsilon} a^{\epsilon\gamma})_{;\lambda} + (\psi^{\lambda\beta\gamma} b_{\gamma\beta} + \psi_{;\beta}^{\lambda\beta} - \varphi^\lambda) b_\lambda^\gamma = 0. \tag{6.44}$$

By invoking Eq. (6.40), Eq. (6.9) and $\mathbf{a}^\varepsilon = a^{\varepsilon\gamma}\mathbf{a}_\gamma$, Eq. (6.43, 6.44) transform into normal shape equation

$$\begin{aligned}
0 = & 2\kappa A^{\alpha\lambda}b_{\alpha\lambda} + \left[\frac{E_1}{2}(a_{\alpha\beta}L_\alpha L_\beta - 1)L_\lambda L_j + \frac{E_2}{2}(a_{\alpha\beta}M_\alpha M_\beta - 1)M_\lambda M_j \right] b_{j\lambda} + \\
& \left\{ \begin{array}{l} (\Gamma_{\mu\eta}^\gamma)b_{\gamma\lambda}\Gamma_{\alpha\beta}^\lambda + (b_{\mu\eta}\Gamma_{\alpha\beta}^\lambda)_{;\lambda} - b_{\mu\eta;\beta\alpha} + b_{\mu\eta}b_{\varepsilon\beta}a^{\varepsilon\gamma}b_{\gamma\alpha} - \\ (\Gamma_{\mu\eta}^\gamma)_{;\beta}b_{\gamma\alpha} - [(\Gamma_{\mu\eta}^\gamma)b_{\gamma\beta}]_{;\alpha} \end{array} \right\} * \quad (6.45) \\
& (C_1 L^\alpha L^\beta L^\mu L^\eta + C_2 M^\alpha M^\beta M^\mu M^\eta + \frac{T}{2}M^\alpha M^\beta L^\mu L^\eta + \frac{T}{2}L^\alpha L^\beta M^\mu M^\eta) - \\
& pJa^{\lambda\mu}b_{\mu\lambda}
\end{aligned}$$

and tangential shape equations

$$\begin{aligned}
0 = & \left\{ \begin{array}{l} [-b_{\mu\eta}b_{\varepsilon\lambda}a^{\varepsilon\gamma} + (\Gamma_{\mu\eta}^\gamma)_{;\lambda}]\Gamma_{\alpha\beta}^\lambda + (\Gamma_{\mu\eta}^\gamma)(\Gamma_{\alpha\beta}^\lambda)_{;\lambda} + \\ b_{\mu\eta;\beta}b_{\varepsilon\alpha}a^{\varepsilon\gamma} + (b_{\mu\eta}b_{\varepsilon\beta}a^{\varepsilon\gamma})_{;\alpha} - (\Gamma_{\mu\eta}^\gamma)_{;\beta\alpha} + (\Gamma_{\mu\eta}^\xi)b_{\xi\beta}b_{\varepsilon\alpha}a^{\varepsilon\gamma} \end{array} \right\} * \quad (6.46) \\
& (C_1 L^\alpha L^\beta L^\mu L^\eta + C_2 M^\alpha M^\beta M^\mu M^\eta + \frac{T}{2}M^\alpha M^\beta L^\mu L^\eta + \frac{T}{2}L^\alpha L^\beta M^\mu M^\eta) - \\
& (pJa^{\gamma\beta})_{;\beta}
\end{aligned}$$

where

$$(pJa^{\gamma\beta})_{;\beta} = p_{,\beta}a^{\gamma\beta}, \because a = 1 = \det(\mathbf{F}) \text{ (incompressibility)}. \quad (6.47)$$

It should be noted that, in the presence of virtual loads in reaction to virtual power \dot{E} , virtual load P (see Eq. (6.19)) represents lateral pressure applied onto the FRC surface [48], theoretically, the P might be applied to the left-hand side of Eq. (6.45), shown as

$$\begin{aligned}
P = & 2\kappa A^{\alpha\lambda}b_{\alpha\lambda} + \left[\frac{E_1}{2}(a_{\alpha\beta}L_\alpha L_\beta - 1)L_\lambda L_j + \frac{E_2}{2}(a_{\alpha\beta}M_\alpha M_\beta - 1)M_\lambda M_j \right] b_{j\lambda} + \\
& \left\{ \begin{array}{l} (\Gamma_{\mu\eta}^\gamma)b_{\gamma\lambda}\Gamma_{\alpha\beta}^\lambda + (b_{\mu\eta}\Gamma_{\alpha\beta}^\lambda)_{;\lambda} - b_{\mu\eta;\beta\alpha} + b_{\mu\eta}b_{\varepsilon\beta}a^{\varepsilon\gamma}b_{\gamma\alpha} - \\ (\Gamma_{\mu\eta}^\gamma)_{;\beta}b_{\gamma\alpha} - [(\Gamma_{\mu\eta}^\gamma)b_{\gamma\beta}]_{;\alpha} \end{array} \right\} * \quad (6.48) \\
& (C_1 L^\alpha L^\beta L^\mu L^\eta + C_2 M^\alpha M^\beta M^\mu M^\eta + \frac{T}{2}M^\alpha M^\beta L^\mu L^\eta + \frac{T}{2}L^\alpha L^\beta M^\mu M^\eta) - \\
& pJa^{\lambda\mu}b_{\mu\lambda}
\end{aligned}$$

6.4 Model implementation and Boundary condition

In this section, we express the proposed model using Cartesian coordinates to make the proposed model explicit for the sake of simulation, and the numerical simulation results will be illustrated in the following sections. To implement the proposed model, we present a material position in a deformed FRC domain ω as

$$\mathbf{r} = \chi_k \mathbf{e}^k, \quad (6.49)$$

where $\{\mathbf{e}^k\}$ is contravariant basis for 3-dimensional Cartesian coordinate in the deformed configuration (the index can be lowered down because it is framed in the orthogonal Cartesian coordinate), so k takes the values in $\{1, 2, 3\}$, χ_k are corresponding components. Likewise, for the material position of the initially undeformed fiber composite, we present $\mathbf{X} = X_k \mathbf{E}^k$, where X_k are components of reference coordinate, $\{\mathbf{E}^k\}$ are orthogonal basis configured in reference coordinate. On the deformed fiber composite surface, the introduction of curvilinear coordinates θ^α on FRC surface gives rise to: $\theta^A \equiv X^A \equiv X_A$ under reference configuration (i.e., undeformed FRC) while $\mathbf{r} = \theta^\alpha \mathbf{e}_\alpha = \chi_\alpha \mathbf{e}^\alpha$ in the current configuration. In the view of continuum mechanics, the unit fibers' trajectories, whenever they are stretched or not, are assumed to be straight. Hence, by taking the derivative, we can compute the natural bases configuring fibers' trajectories in reference and current configurations, which are respectively

$$\mathbf{A}_i = \frac{\partial X_k \mathbf{E}^k}{\partial \theta^i} = \mathbf{E}^i \quad \text{and} \quad \mathbf{a}_i = \frac{\partial \chi_k \mathbf{e}^k}{\partial \theta^i} = \chi_{k,i} \mathbf{e}^k. \quad (6.50)$$

Then, we can deduce the surface metric of reference and current configuration as

$$A_{ij} = \delta_{ij} \quad \text{and} \quad a_{ij} = \chi_{m,i} \chi_{k,j} \delta_{km}, \quad (6.51)$$

where δ^{km} is the Kronecker delta. Then, Gauss and Weingarten equations (Eq. 6.9) necessitate the computation of normal vector

$$\mathbf{n} = \varepsilon^{kmn} \frac{\chi_{k,1} \chi_{m,2}}{\sqrt{a}} \mathbf{e}^n, \quad (6.52)$$

in which ε^{kmn} is Levi-Civita symbol, and

$$a = \det(a_{ij}) = a_{11}a_{22} - a_{12}a_{21}, \quad (6.53)$$

obeying $a = 1$ due to the constraint of incompressibility, in which

$$a^{11} = \frac{a_{22}}{a}, \quad a^{22} = \frac{a_{11}}{a}, \quad a^{12} = a^{21} = -\frac{a_{12}}{a} \quad \therefore a^{ij} = (a_{ij})^{-1}. \quad (6.54)$$

To make the curvature components explicit, we proceed to compute

$$A_{i,j} = \mathbf{E}_{i,j}^i = 0 \quad \text{and} \quad \mathbf{a}_{i,j} = \chi_{k,ij} \mathbf{e}^k, \quad (6.55)$$

then Eqs. (6.52, 6.55) furnish the expression of curvature components

$$b_{\alpha\beta} = \mathbf{n} \cdot \mathbf{a}_{\alpha,\beta} = \varepsilon^{nkm} \frac{\chi_{n,\alpha\beta} \chi_{k,1} \chi_{m,2}}{\sqrt{a}}. \quad (6.56)$$

Additionally, Christoffel symbols $\bar{\Gamma}_{i,j}^k = \mathbf{A}_{i,j} \cdot \mathbf{E}^k = 0$ in reference configuration, while $\Gamma_{i,j}^k = \mathbf{a}_{i,j} \cdot \mathbf{a}^k$ in deformed configuration. Apply relations (Eqs. (6.49-56)) to equilibrium equations Eqs. (6.46, 6.48), and after some algebra, we obtain a system of 4th order PDEs with 4 unknowns χ_1, χ_2, χ_3 , and p to be solved numerically. The numerical process of solving 4th-order PDEs is implemented via the open-resource packages FEniCS [49, 50], and the solving method and treatments can be found in [11, 19–21] that emphasizes solving the system of 4th-order PDEs. The algebra procedures expressing the PDEs are refrained for the sake of brevity.

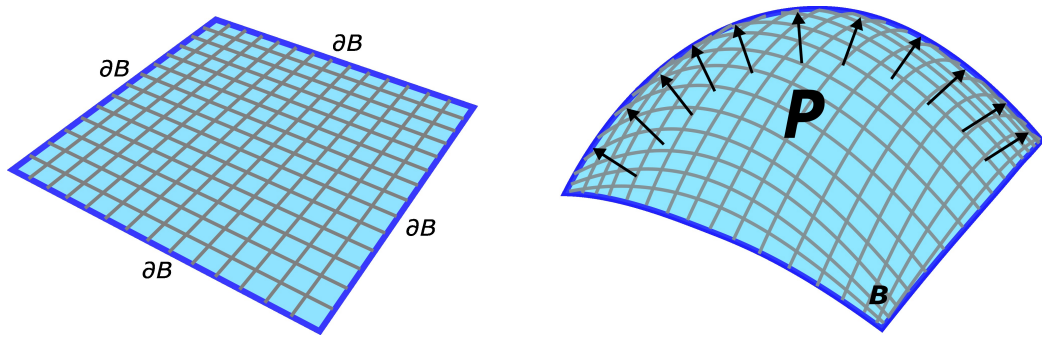


Figure 6.3: The illustration of boundary conditions: fixed boundaries ∂B and lateral pressure P applied on the domain B .

The boundary conditions of the simulation are portrayed in Figure 6.3, where the boundaries ∂B are fixed by applying $\chi_3 = 0$ and χ_1, χ_2 are clamped to their values X_1, X_2 in the initial configuration. Further, the lateral pressure P is applied on the rectangular FRC sheet surface, and no external in-plane loading is applied on the fiber-composite surface.

To illustrate and understand the theoretical results properly, the simulated results are expressed in initial and current configurations involving the the coordinate X_1, X_2, X_3 and χ_1, χ_2, χ_3 , shown in Figure 6.4. The χ_1, χ_2, χ_3 represent deformed material positions with respect to X_1, X_2, X_3 that configure initial material positions.

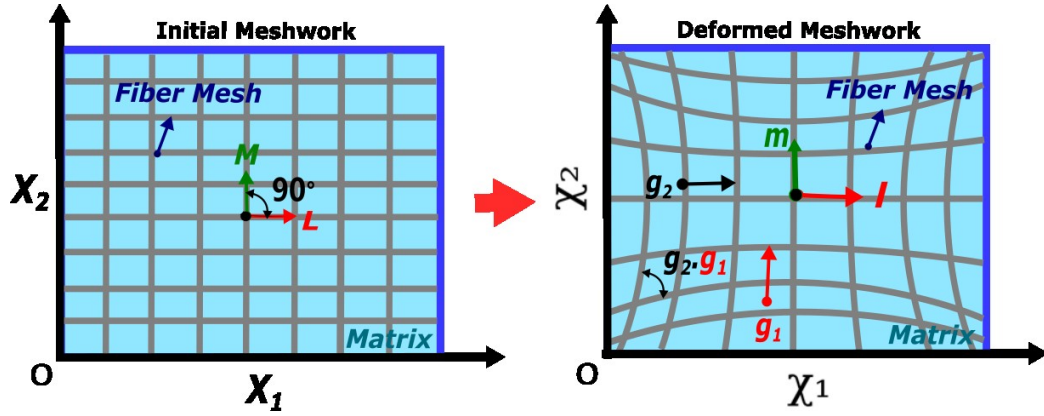


Figure 6.4: Coordinate expression in initial and current configurations: X_1, X_2, X_3 for initial configuration and χ_1, χ_2, χ_3 for current configuration (X_3 and χ_3 are normal to the $X_1 - X_2$ and $\chi_1 - \chi_2$ plane, respectively).

6.5 Results and Discussion

In this section, we theoretically analyze the matrix material deformation, meshwork deformation, and kinematics differences between the matrix material and meshwork, aimed at explaining the deformation of woven fabric, the damage pattern of the fabric-reinforced cementitious matrix (FRCM), and the shaping of bamboo fabric-PLA composite, through which the validity and adaptivity of the proposed model can be illustrated.

Since the kinematics of fiber extension, flexure, and twist have been built into

the proposed model, it is not trivial to unveil their crucial role in manipulating the mechanical performance of fiber meshwork via the simulation results. Hence, we theoretically investigate the kinematics of the fiber units to illustrate the role of the fiber units' deformation in determining the overall deformation of the meshwork.

6.5.1 Matrix material deformation

Figure 6.5(a) illustrates the matrix material's out-of-plane deformation, and it is apparent that the application of lateral pressure P results in out-of-plane deflection for the matrix material of FRC. In addition to the out-of-plane deformation response under lateral pressure, the matrix experiences concurrent in-plane deformation, as illustrated in Figure 6.5(b). It is observed that the material particles migrate toward the edges of the domain due to the lateral pressure, particularly in the diagonal direction, leading to the most substantial in-plane deformation (0.6) occurring along the diagonal direction of the domain. Conversely, the material located at the center of the FRC exhibits weak in-plane displacement because of the surface tension equilibrium there.

Furthermore, upon comparing Figure 6.5(b) and Figure 6.5(c), it is evident that the maximum in-plane deformation (0.6) surpasses the magnitude of the out-of-plane deformation (0.14) by a factor of 4.3. This discrepancy underscores the composite sheet's remarkable deformability in the plane (when $P/C_i = 1/3$). The substantial difference between in-plane and out-of-plane deformations arises from the pure out-of-plane deflection representing the material's response to flexural effects, and the in-plane deformation underlies the matrix material's ability to simultaneously undergo flexure and extension.

To elucidate the influence of FRC size and shape on the in-plane deformation, Figure 6.6 investigates the in-plane deformations of FRC with dimensions of 5×5 , 10×10 , and 10×5 when subjected to $P/C_i = 1/3$. Figure 6.6(a) and (b) illustrate that a larger domain size (10×10) leads to a greater in-plane deformation in the diagonal direction

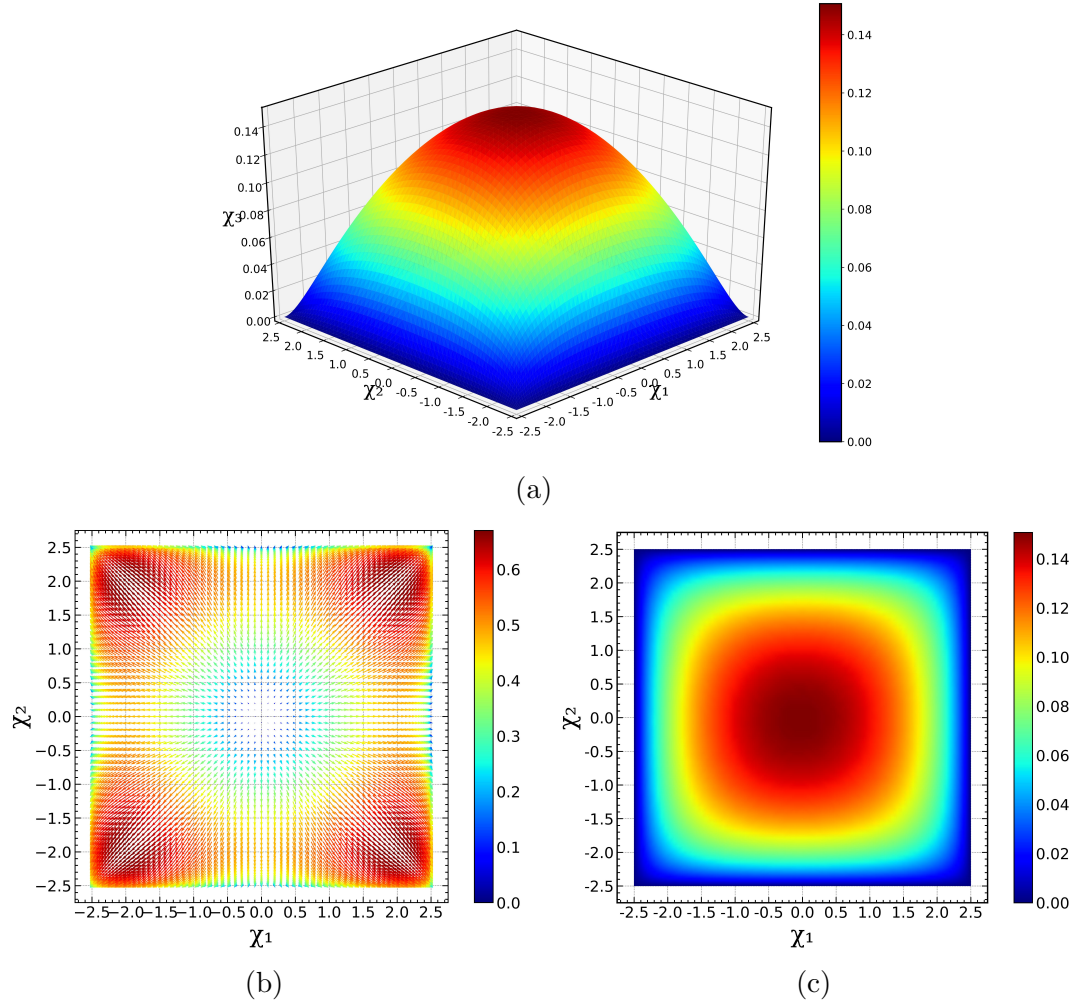


Figure 6.5: Deformations of the fiber-reinforced composite subjected to $\kappa = 1\text{Mpa}$, $E_i = 2\text{Mpa}$, $C_i = 3\text{Mpa}$, $T = 3\text{Mpa}$, $P = 1\text{Mpa}$: (a) out-of-plane deflection of the matrix material, (b) in-plane material displacement vector field, (c) top view of (a).

(1.2 compared to 0.6) for square-shaped FRC. Nevertheless, the transition from a square to a rectangular domain results in alterations in the deformation distribution: instead of the high in-plane deformation located around four corners (Figure 6.6(a) and Figure 6.6(b)), Figure 6.6(c) covers the peak in-plane deformation on the tips of the corners while the areas of peak deformation are reduced in comparison to Figure 6.6(a) and Figure 6.6(b). Although the area of Figure 6.6(c) domain is less than that of Figure 6.6(b), and its peak deformation (3.5) located at the corners exceeds the peaking value (1.2) in Figure 6.6(b) due to the transition of domain shape to a

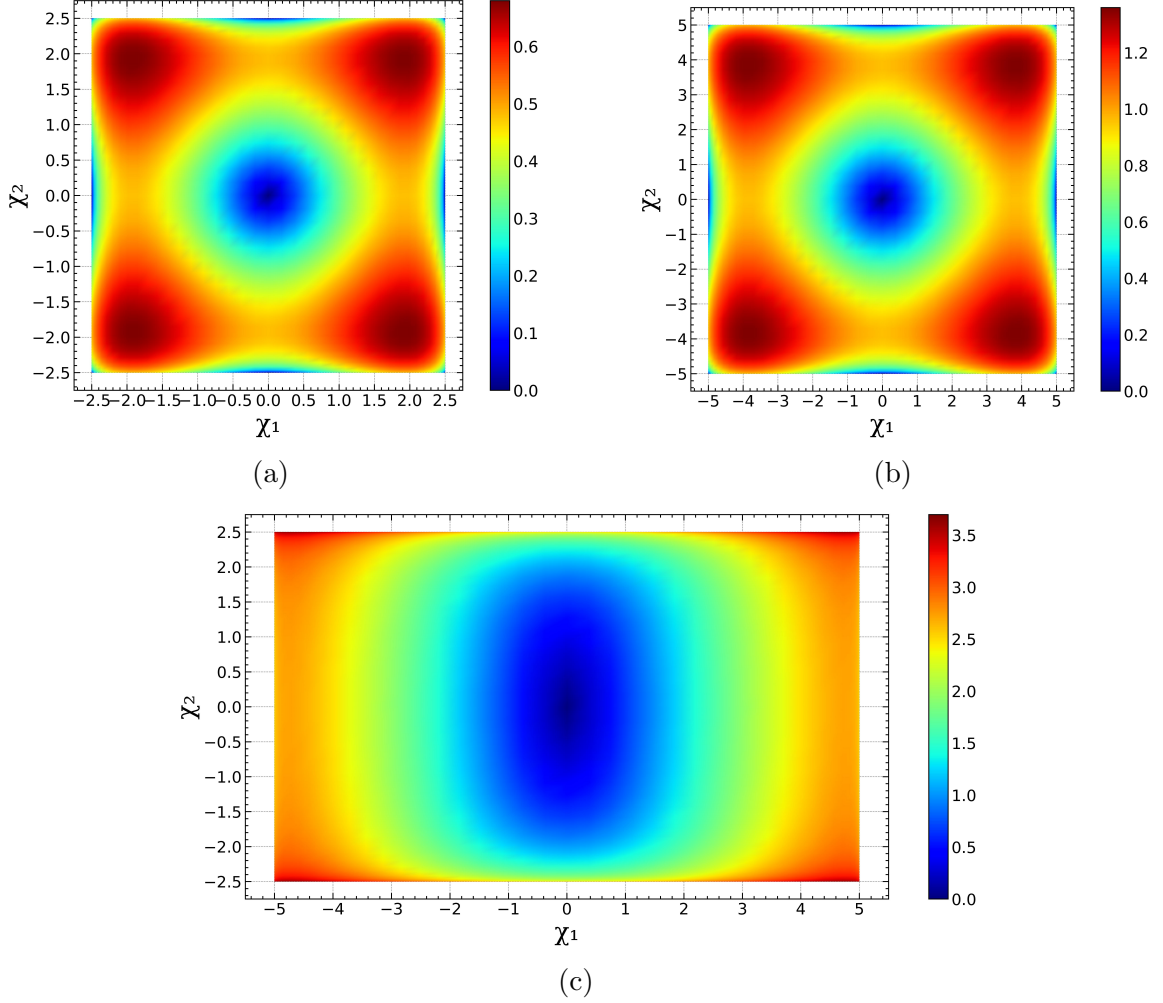


Figure 6.6: Size/shape effects on the in-plane deformation of the matrix material subjected to $\kappa = 1Mpa$, $E_i = 2Mpa$, $C_i = 3Mpa$, $T = 3Mpa$, $P = 3Mpa$: (a) 5×5 square, (b) 10×10 square, (c) 10×5 rectangular.

rectangle. It is concluded that, for FRC of the same shape, the boundaries of FRC confine the maximum in-plane deformation via the smaller size of the domain, while the change in the shape of the FRC can alter the distribution of in-plane deformation.

Figure 6.7 illustrates the full-scale deformation of FRC under the increasing lateral pressures P ($\kappa = 1Mpa$, $E_i = 2Mpa$, $C_i = 3Mpa$, $T = 3Mpa$). Notably, by invoking Figure 6.6, Figure 6.7 indicates that the central region of the FRC is dominated by the out-of-plane deformation, while in-plane displacement is constrained by the domain edges. To be precise, it is apparent that an increase in the lateral pressure results in a

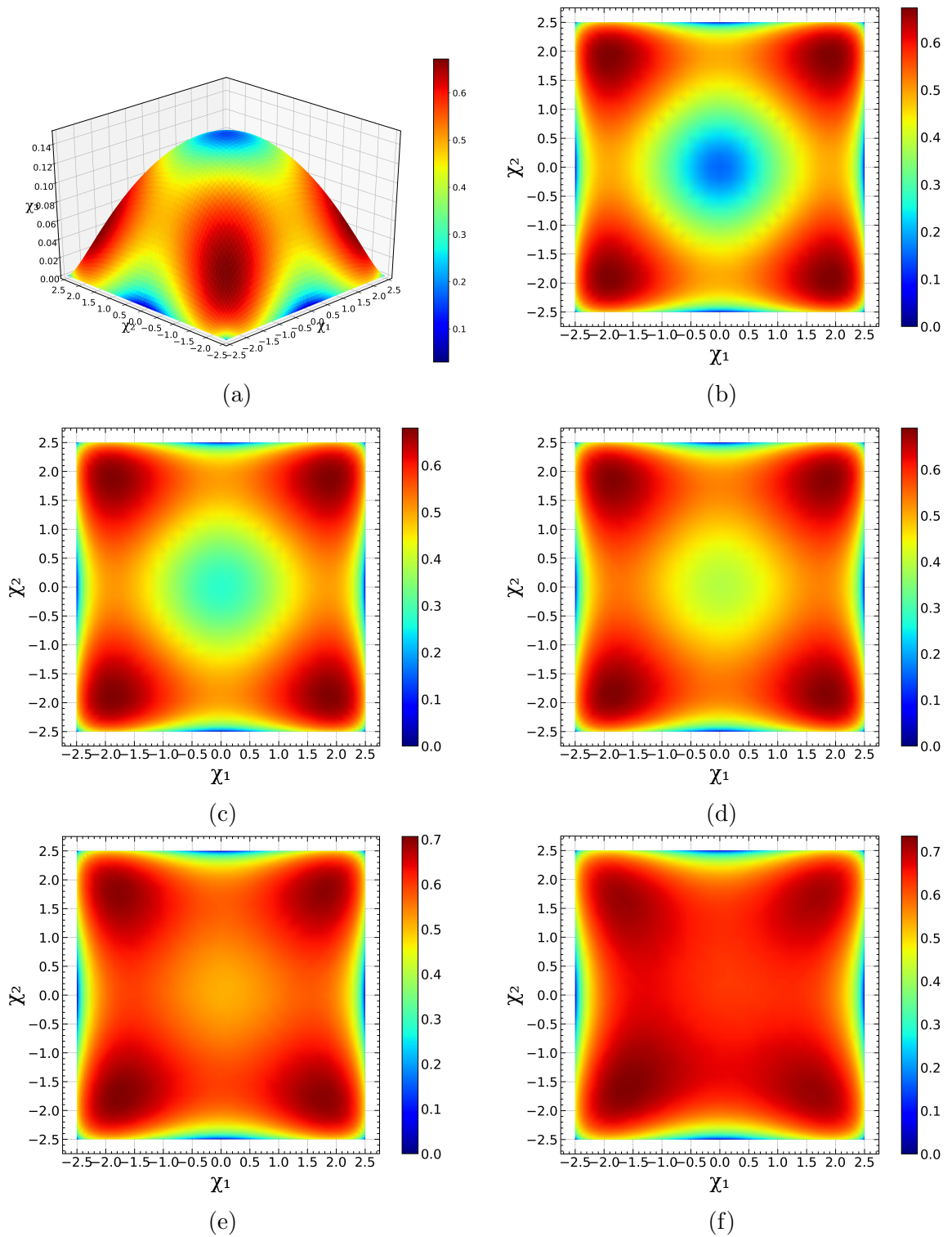


Figure 6.7: The material displacements of the matrix subjected to increasing lateral pressures: (a) $P/C_i = 1/3$ (3D view), (b) $P/C_i = 1/3$, (c) $P/C_i = 1$, (d) $P/C_i = 5/3$, (e) $P/C_i = 7/3$, (f) $P/C_i = 3$.

greater maximum deformation, evident from the transition from 0.6 in Figure 6.7(b) to 0.7 in Figure 6.7(f). In particular, there is a substantial increase in deformation at the center of the domain, transitioning from 0.1 in Figure 6.7(b) to 0.6 in Figure 6.7(f). This notable increase in deformation can be attributed to the dominant influence of the lateral pressure at the center of the domain. In contrast, it is observed that deformations occurring in the vicinity of the four corners of the domain exhibit a modest increase, progressing from 0.6 to 0.7. This weak increase in deformation is primarily contributed by the weak out-of-plane deflections in those regions and in-plane deformation is confined by the boundaries (illustrated in Figure 6.6(a) and Figure 6.6(b)). It is noteworthy that the out-of-plane material displacement remains unrestricted except for the occurrence of material damage.

In Figure 6.8, the distribution of Green-Lagrange strain intensity across the domain is depicted, highlighting the strain peaks in the hinterland of the domain (0.6) and the vicinity of the FRC boundaries (-0.4). The peaking strain inside the domain is invoked by the stretching and out-of-plane shear effects on the FRC surface while the strain concentration (-0.4) is induced by the shrinking/bending effects in the vicinity of boundaries. Of particular significance is the reinforcement of strain at the four corners, resulting from the combination of strains (ε_1 and ε_2). This strain concentration induces material points to migrate toward the corners of the domain, as visualized in Figure 6.5(b), which is fundamentally attributed to the fact that strain represents the rate of deformation, consequently dictating the direction of displacement.

6.5.2 Fiber meshwork deformation

To comprehensively comprehend the underlying mechanisms of deformation between matrix and fiber meshwork of fiber-reinforced composites, a detailed examination of the fiber units and fiber network deformation becomes imperative, and the associations between the micro deformations of fiber and the overall deformation of meshwork remain to be unveiled. Hence, the proceeding emphasis should be placed

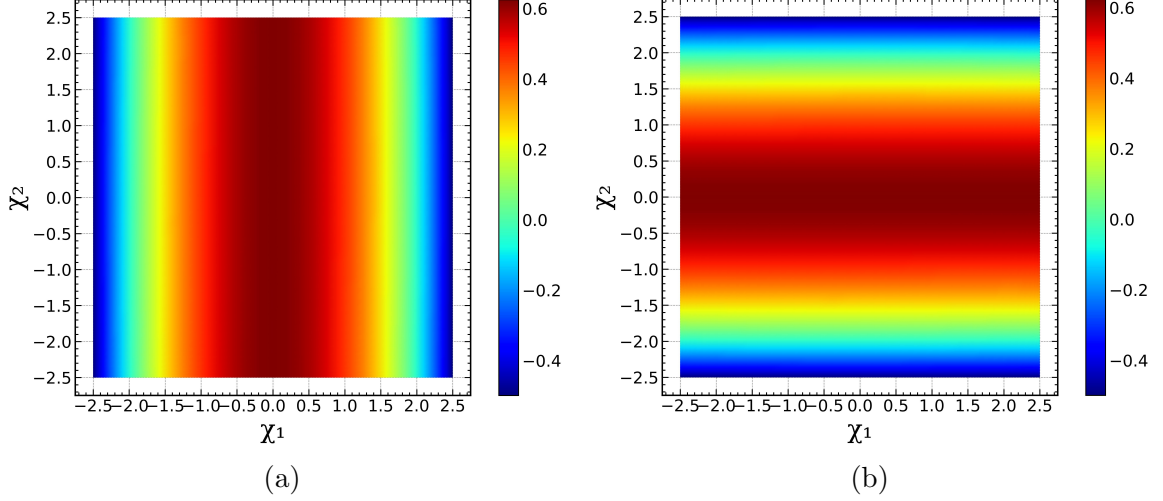


Figure 6.8: Green-Lagrange strain distribution of the matrix material over the domain ($\kappa = 1\text{Mpa}$, $E_i = 2\text{Mpa}$, $C_i = 3\text{Mpa}$, $T = 3\text{Mpa}$, $P = 1\text{Mpa}$): (a) ε_1 , (b) ε_2 .

on investigating the unit fiber kinematics and the meshwork deformation, and this pursuit is predicated on the widely held belief that the microstructures nestled within the matrix material exert a dominant influence over the overall mechanical responses, as substantiated in [51–54].

For the convenience of delivering the discussion, we understand the i th unit fiber \mathbf{L}^i and \mathbf{M}^i as microstructure in bi-direction, and the corresponding microstructure deformations of extension are understood as $\lambda\mathbf{L}^i$ and $\mu\mathbf{M}^i$, and $\mathbf{g}_i^1, \mathbf{g}_i^2$ for flexure, as illustrated in Figure 6.9 below. The main concept is to illustrate the microstructure deformation determining the overall extension and flexure of a single fiber. Within this configuration, Figure 6.10 illustrates the extension of individual fiber units through the calculation of $\lambda\mathbf{l} = \mathbf{F}\mathbf{L}$ and $\mu\mathbf{m} = \mathbf{F}\mathbf{M}$. It reveals that the fiber pieces experience significant elongation (1.4) at the central region of the material domain while undergoing localized contraction (0.2) near the boundaries. The deformed length of a fiber unit is theoretically 1.4 times its initial length at maximum, a result of local stretching, while the fiber unit length can be dramatically reduced to one-fifth of its original length. The local extension of the fiber unit is dominated by both in-plane and out-of-plane deformations when subjected to lateral pressure, and the bending

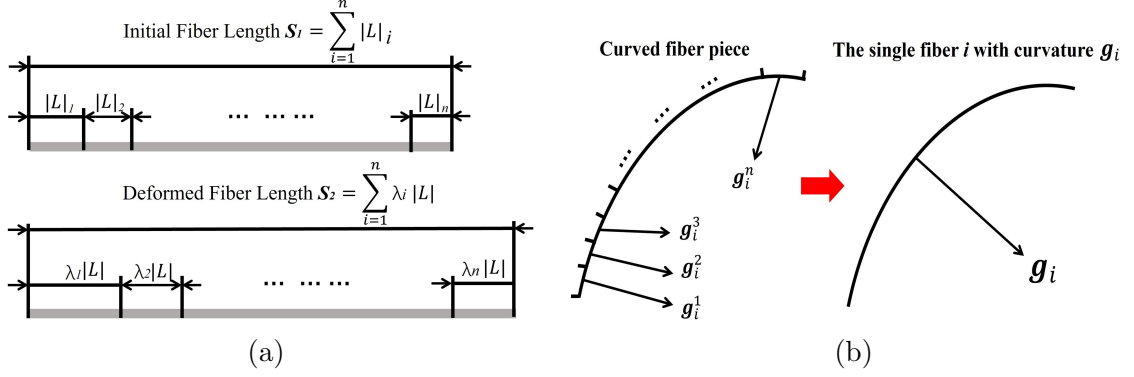


Figure 6.9: The illustration of fiber unit deformation determines the overall fiber deformation: (a) The mechanism of the elongated \mathbf{L} determines the elongation of a single fiber; (b) The mechanism of the curved \mathbf{L} determines the overall flexure of a single fiber.

effects induce the shrinking of fiber units in the vicinity of the boundaries. Notably, a larger “red” area featuring a larger amount of stretched fiber units, as indicated by the expanded red region in the central part of Figure 6.10(a) and (b), suggests that the most stretched fibers are situated near the domain’s central section.

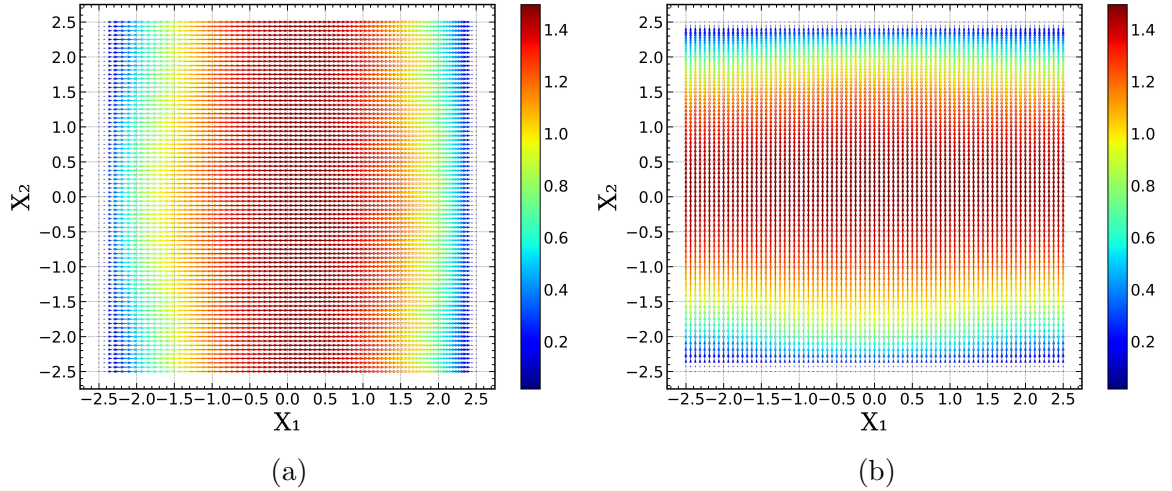


Figure 6.10: Distribution of deformed fiber unit over the domain ($\kappa = 1Mpa$, $E_i = 2Mpa$, $C_i = 3Mpa$, $T = 3Mpa$, $P = 12Mpa$): (a) Deformed \mathbf{L} ; (b) Deformed \mathbf{M} .

To theoretically validate the role of microstructure extensions in determining the overall stretching of fibers, we analyze the extension ratios of fibers by sampling the lengths of 5 unidirectional deformed fibers, as exemplified in Figure 6.11(a). As observed in Figure 6.11(b), under fixed lateral pressure, Fiber 4 exhibits the largest

length due to its central positioning within the FRC. This phenomenon is consistent with Figure 6.10 that the central region contains more stretched fiber units (as indicated by the larger red zones in Figure 6.10), which underscores the critical role played by the microstructure of fiber deformation in determining the overall extension response of the fibers. Additionally, Figure 6.11(b) demonstrates that the increasing lateral pressures result in increased lengths for all the sampled fibers. It is noteworthy that the fiber extension exhibits the J-shaped loading-extension response characteristic of hyperelastic materials [19, 20], which serves as a key indicator in the fabrication and analysis of synthetic composites [55, 56]. The geodesic curvature of fiber units,

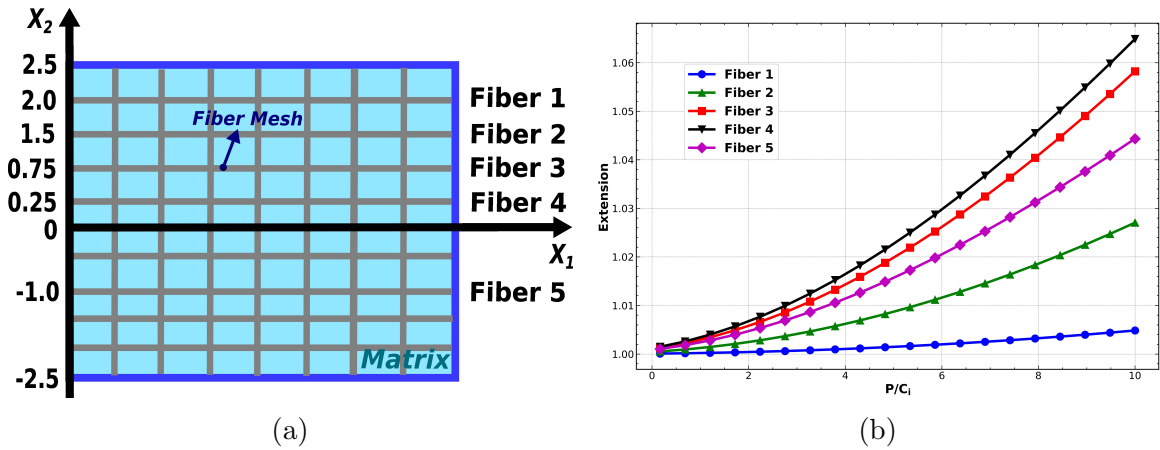


Figure 6.11: Fiber extension under increasing lateral pressures: (a) The locations of the sampled fibers; (b) The comparison of fiber extension.

denoted as \mathbf{g}_1 and \mathbf{g}_2 , are illustrated in Figure 6.12 to elucidate the bending and twisting characteristics of the fiber units across the domain. In Figure 6.12(a) and (b), it is evident that the geodesic curvature peaks along the domain's boundaries, while it is weak within the central region. This observation underscores the fact that fiber pieces experience significant curvature near the boundaries due to the bending effects, whereas they exhibit reduced curvature in the central zone of the domain because of extension. Notably, Figure 6.12(c) reveals the intersections between \mathbf{g}_1 and \mathbf{g}_2 , particularly intensified along the diagonal direction of the domain. The intersections suggest the presence of fiber twisting as illustrated in Figure 6.12(d), where the

intersections of \mathbf{g}_1 and \mathbf{g}_2 are indicative of fiber twisting in the diagonal direction of the domain. The deformations of fiber units (extension, flexure, and twist in Figure

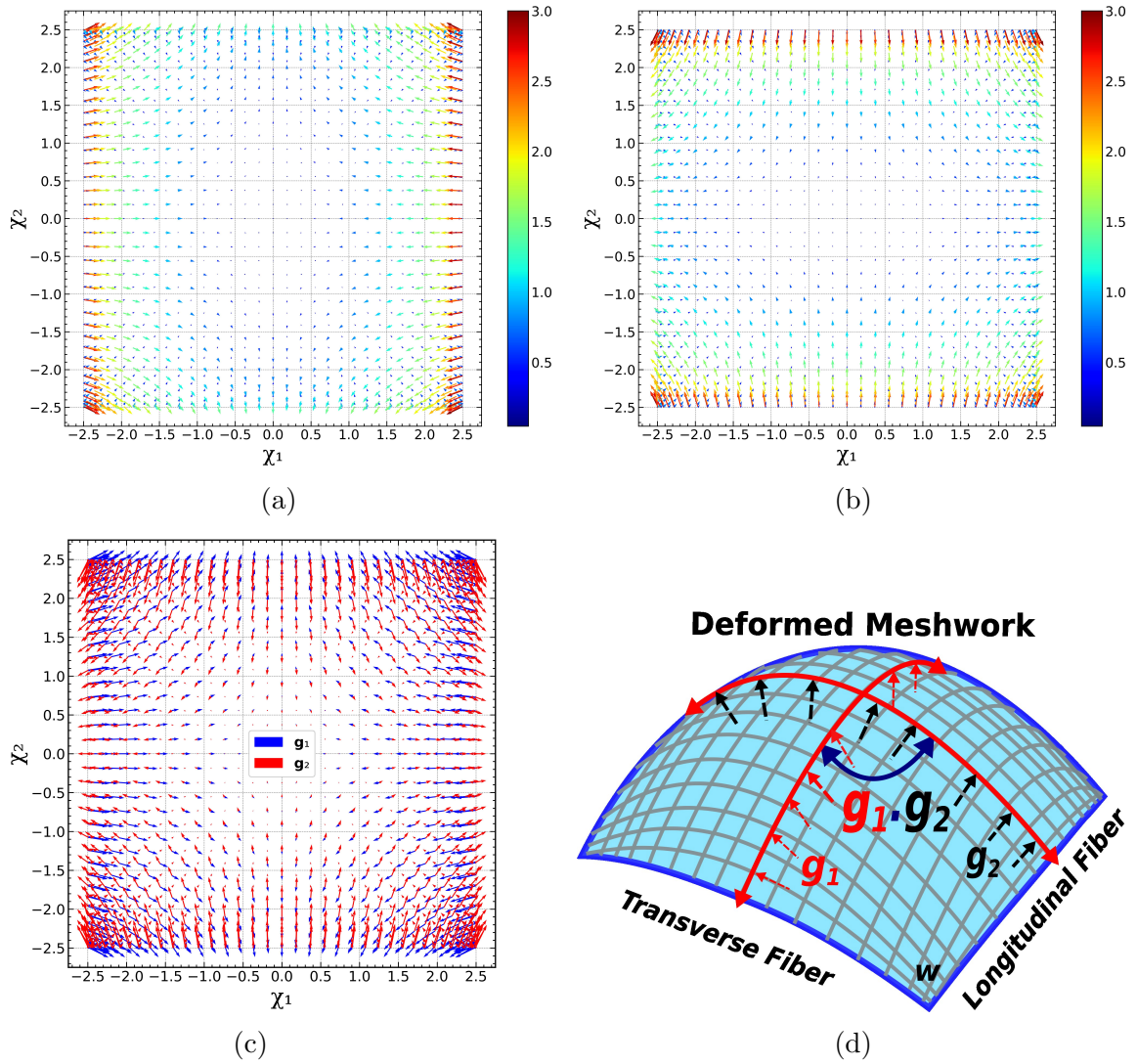


Figure 6.12: Distributions of unit fibers' geodesic curvature \mathbf{g}_1 and \mathbf{g}_2 ($\kappa = 1Mpa$, $E_i = 2Mpa$, $C_i = 3Mpa$, $T = 3Mpa$, $P = 3Mpa$): (a) \mathbf{g}_1 ; (b) \mathbf{g}_2 ; (c) \mathbf{g}_1 and \mathbf{g}_2 intersection; (d) The illustration of intersections between \mathbf{g}_1 and \mathbf{g}_2 .

6.10 and Figure 6.12) ultimately cultivate the overall deformation of the network, as exemplified in Figure 6.13(a). Figure 6.13(a) phenomenologically portrays the transformation of the grid structure into parallelograms, predominantly along the diagonal direction. This transformation is believed to be a collective work of both the extension of fiber units (as indicated in Figure 6.10) and their torsional deformations (Figure

6.12(c)). By comparing Figure 6.13(b) and Figure 6.13(c), it is noteworthy that the grid enlargement in the central section and the shrink in the vicinity of boundaries derive from the stretching and shrinking of fiber units, respectively (see, Figure 6.10), underlying the microstructure deformation of fibers determined the overall extension of the meshwork.

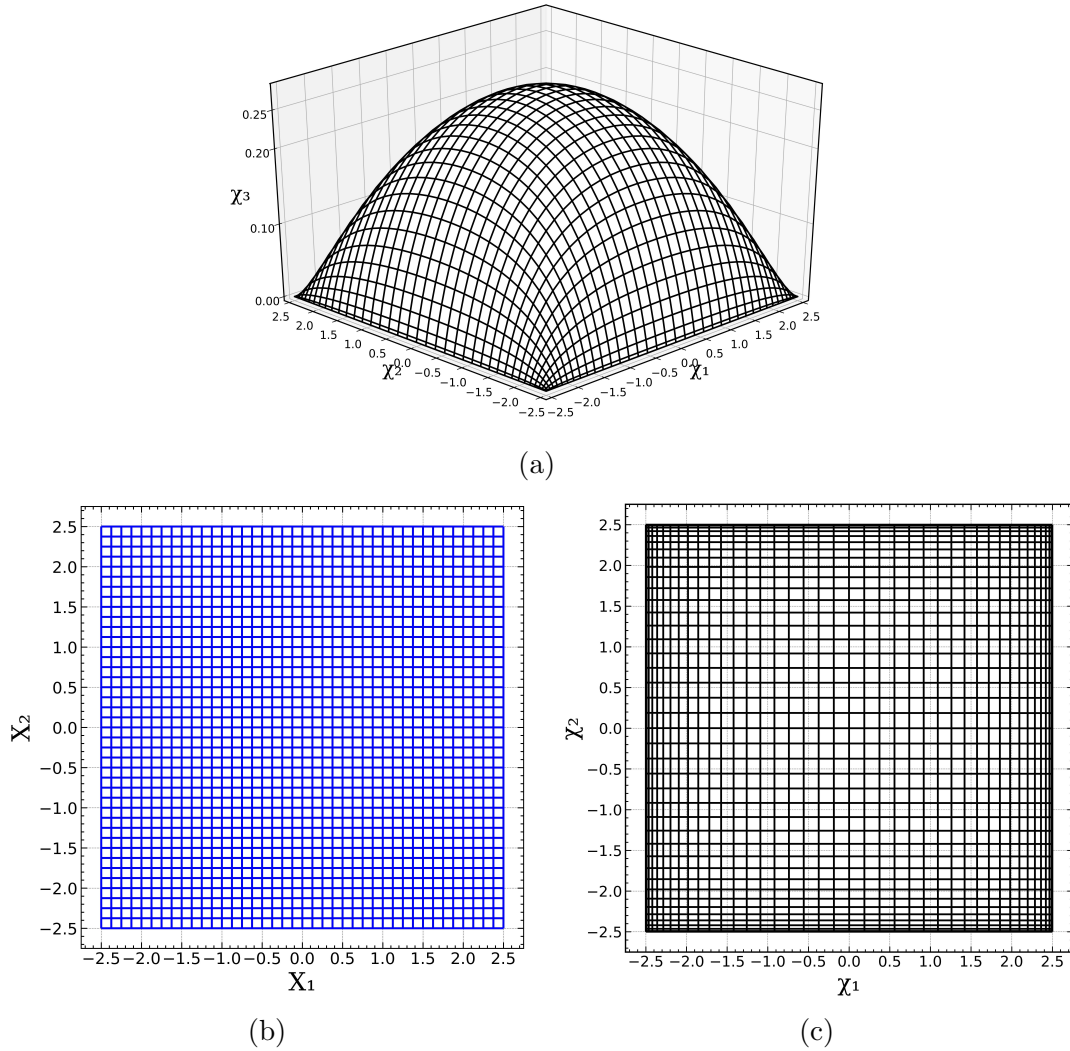


Figure 6.13: Geometry comparison between the initial meshwork and deformed meshwork ($\kappa = 1Mpa$, $E_i = 2Mpa$, $C_i = 3Mpa$, $T = 3Mpa$, $P = 3Mpa$): (a) deformed meshwork, (b) initial meshwork, (c) top view of (a).

To validate the theoretical results of fiber mesh deformation, Figure 6.14 provides comparisons by invoking the theoretical and experimental deformation results

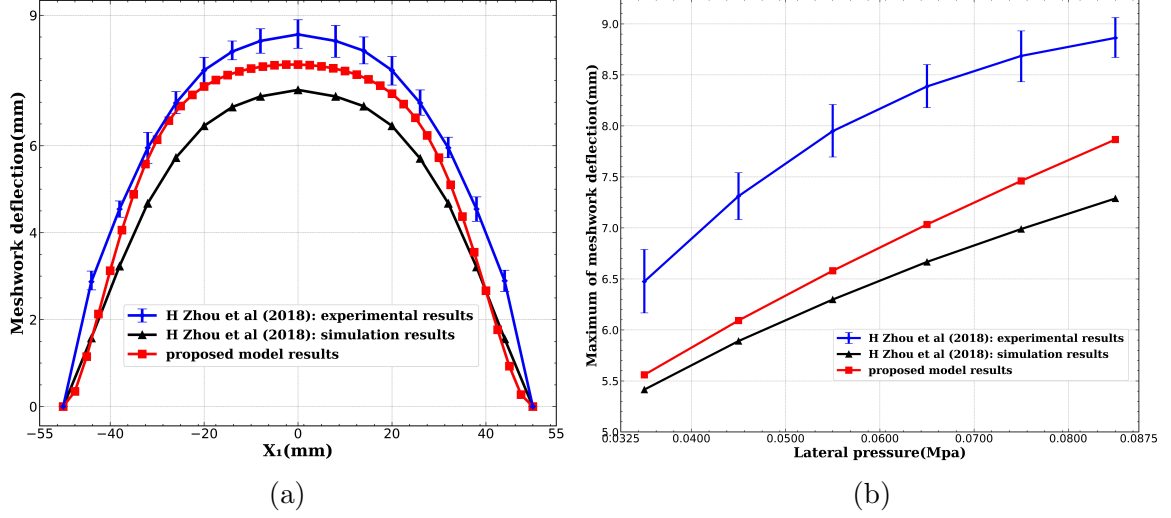


Figure 6.14: Comparison of the meshwork deformation between proposed model results and the out-of-plane deflection results in [57] (bidirectional reinforcements case): (a) profile of meshwork ($\kappa = 0.24Mpa$, $E_i = 9.64Mpa$, $C_i = 5Mpa$, $T = 1Mpa$, $P = 0.085Mpa$.), (b) peaking values of the out-of-plane deformation subjected to increasing lateral pressures ($\kappa = 0.24Mpa$, $E_i = 9.64Mpa$, $C_i = 5Mpa$, $T = 1Mpa$, $P = 0.035 - 0.085Mpa$).

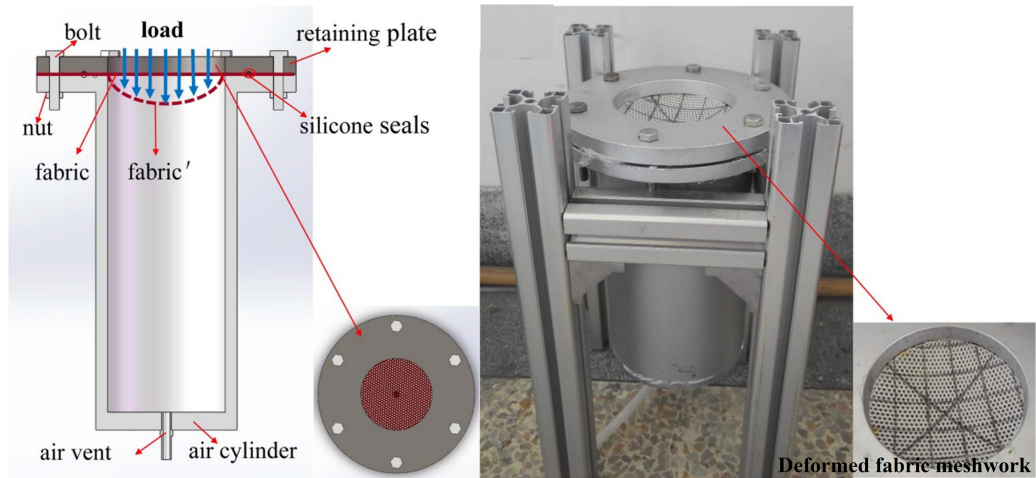
of bi-directional meshwork deformation in [57]. Figure 6.14(a) demonstrates both the proposed model and fabric meshwork perform dome-like profiles when subjected to lateral pressure despite the slight local curvature difference. In addition, Figure 6.14(b) indicates a larger lateral pressure results in intensified out-of-plane deformation for both the proposed model meshwork and fabric network, despite the differences in peaking values. The differences regarding the profile and peaking deflection might derive from that the results of the proposed model account for the effects of matrix material while the cited results are based on testing pure fabric meshwork; Our model describes the rectangular domain while the cited work demonstrates the circular domain; Our model is capable of theoretically describing the in-plane deformation which is critical in demonstrating the profile of meshwork while the [57] merely measures the out-of-plane deflection and stress; Despite the utilization of the same extension modulus $9.64Mpa$ in [57], the under-defined bending and twisting stiffness in [57] hedge to obtain more accurate results quantitatively. Furthermore, the experiment and mea-

surement settings of [57] are invoked in Figure 6.15, where the lateral pressure on the fabric meshwork is applied by the negative pressure of the air while maintaining the edge of meshwork fixed, showing the boundary condition of the proposed model aligns with the cited work, i.e., the applied lateral pressure is normal to the material surface at pointwise while maintaining the boundary clamped. Hence, it is concluded from the experimental setting and the invoked out-of-plane results that our proposed model might still predict the trend of out-of-plane deformation of fiber meshwork despite the scarcity of in-house experimental results.

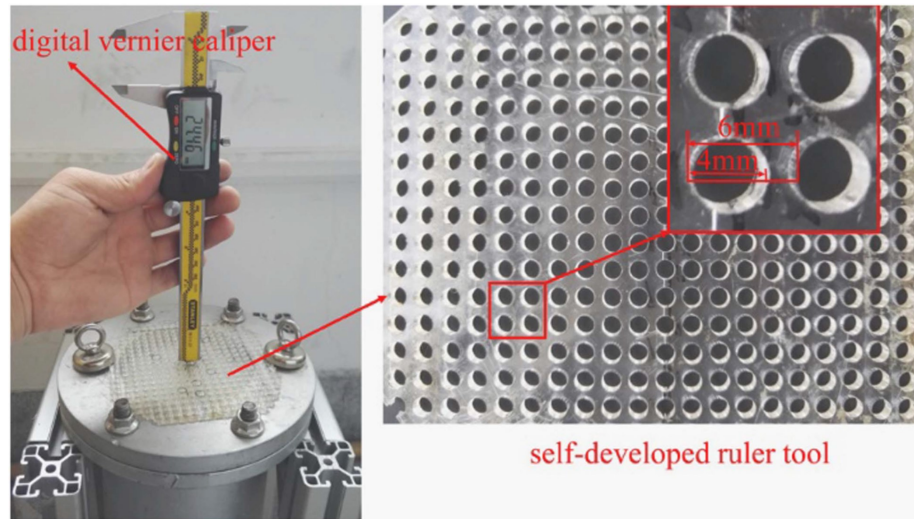
6.5.3 Fiber-reinforced composite deformation

In this section, the demonstrated deformation of matrix material and fiber meshwork are collectively illustrated to analyze the kinematics differences between the matrix material and meshwork in the FRC, and the validity of the model analysis is evidenced by invoking the damage pattern of the construction material and shaping process of fabric-reinforced material.

Within this aim, Figure 6.16 demonstrates the overall deformation of FRC subjected to lateral pressure, it is noteworthy that the corners of matrix material experience significant deformation, and the grids in there are found to be dramatically distorted/sheared, resulting in the rectangular grid's transition to parallelogram and the meshwork is locally curved on the FRC surface. The dramatic matrix material deformation and meshwork geometry transition address the vulnerability of material/reinforcement damage or instability in the diagonal direction of the domain. In particular, it is observed in Figure 6.16(b) that the matrix material at the central region of the domain undergoes weak in-plane displacement while the grids of the embedded meshwork in the same region experience enlargement. This underlying disparity in kinematics between the matrix material and the embedded meshwork highlights the potential for dislocation/split within the central section of the domain. To qualitatively verify the vulnerability of damage, the damage patterns of the



(a)



(b)

Figure 6.15: Experimental configuration on testing and measuring the woven fabric deformation in [57]: (a) the sketch of the deformation tester (left) and real tester (right), where the fabric edges are clamped by the bolts, nuts and retaining plate. The plate has a hole of radius of 50mm to expose the fabric to the air inside the cylinder container. Then, the lateral pressure is induced by the vacuum pumper connected at the cylinder container bottom and a pressure gauge is utilized to monitor the lateral pressure. In addition, the O-type silicone seal is applied to maintain the pressure. (b) the ruler and positioner for measuring the fabric meshwork out-of-plane deformation, and more details can be found in [57].

fabric-reinforced cementitious matrix (FRCM) subjected to in-plane and out-of-plane loadings [58] are invoked in Figure 6.17 and the corresponding experimental configurations are shown in Figure 6.18. In [58], the damage patterns include cracks and

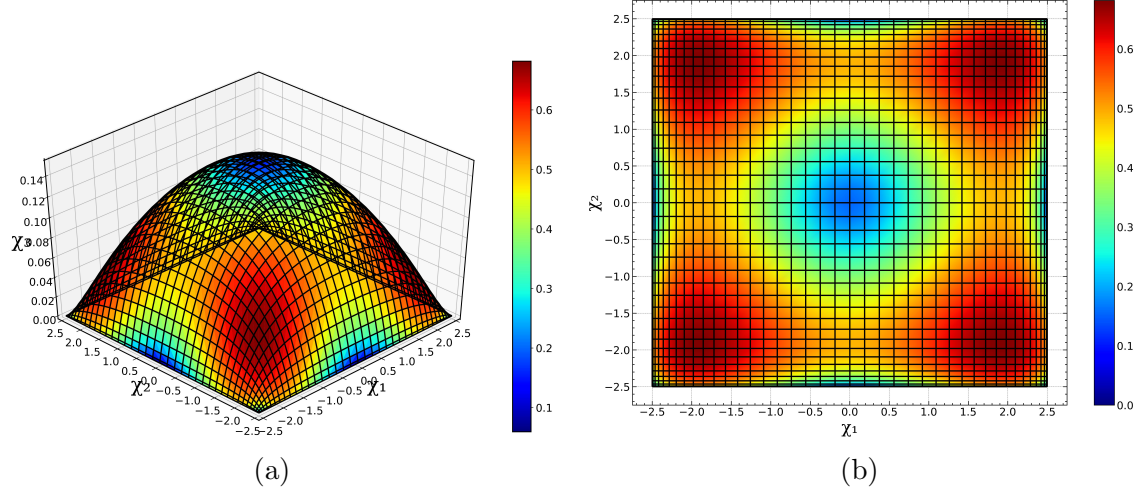
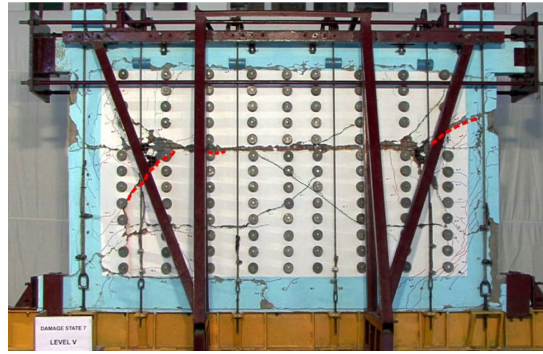


Figure 6.16: Fiber-reinforced composite deformation ($\kappa = 1Mpa$, $E_i = 2Mpa$, $C_i = 3Mpa$, $T = 3Mpa$, $P = 1Mpa$): (a) side view of 3-dimensional deformation, (b) top view of (a).

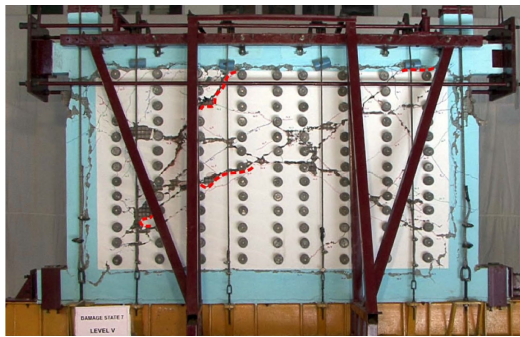
spalling of the matrix material, and the breaking of fabric reinforcement. In addition, these damage phenomena are particularly observed in the diagonal direction of the matrix material as shown in Figure 6.17 from which the diagonal and horizontal splits (indicated by red dashed lines) are illustrated. In detail, the study describes the split damage patterns observed in rectangular FRCM as “the fabrics ruptured along the diagonal cracks”, which exhibit a high alignment to the large diagonal deformation results in the diagonal direction in Figure 6.16 and the discussed dislocation potentials, and additional proof regarding the failure pattern can be found in [59, 60].

Further efforts in evidencing the theoretical results have been given to explain the observed horizontal split in Figure 6.17(c) and concentrated stresses at the corners of the matrix material of FRCM specimens mentioned in [58], shown in Figure 6.19, where the simulated Lagrange strain and meshwork deformation are presented. It is found that the meshwork is observed to shrink and the matrix material in the vicinity of boundaries is undergoing compressing strains, indicating the substantial compression effects might result in the horizontal split of matrix material and fabric reinforcement in Figure 6.17(c). In addition, the superimposed ε_1 and ε_2 in the vicinity of domain corners highlights the observed intensified stress at the corners of

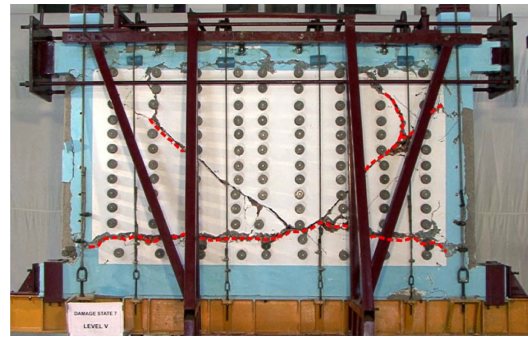
the domain (discussed in [58] and reference therein).



(a)



(b)



(c)

Figure 6.17: Damage pattern of FRCM specimens fabricated using different modes of fabric application [58]: (a) DA_{0-90} , (b) SA_{0-90} , (c) DA_{45} where D means direct, S presents sandwich, A for anchored, the subscript number represents the angle of fiber orientation. The fabric is mounted on the matrix/infill material with mechanical anchors in the vicinity of the blue zone and fabric ruptures are marked by dash lines.

The validity of the proposed model might be additionally located in qualitatively describing the reshaping process of bamboo fabric-PLA composites, as illustrated in Figure 6.20, The comparability between the proposed model results and the reshaping process of bamboo fabric-PLA composites is attributed to despite the bamboo fabric-PLA composite laminate domain being circular (the proposed model investigates rectangular cases), the laminate is subjected to lateral pressure on the surface induced by the contact from hemispherical dies while maintaining the fixed edges, which aligns to the boundary condition in the proposed model. In addition, the fabric reinforcement of laminate shows its alignment with the proposed model regarding the

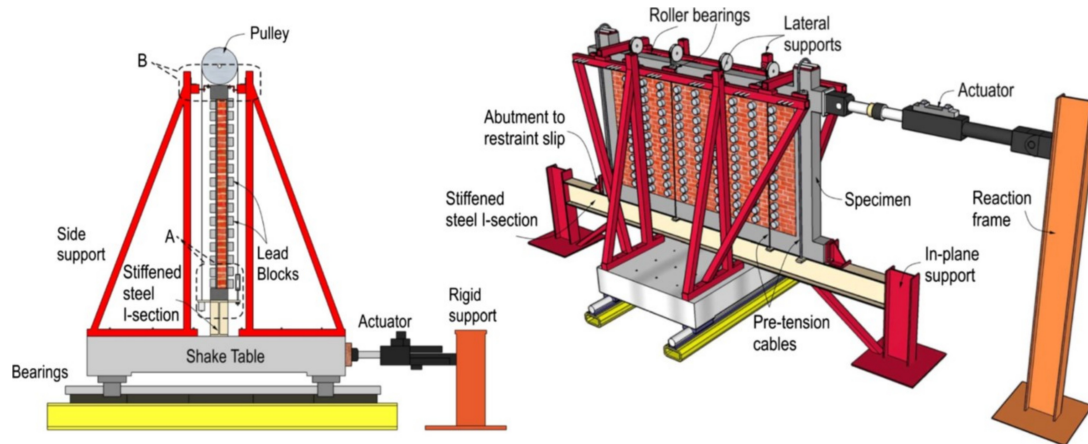


Figure 6.18: Experimental setting on testing the out-of-plane performance of FRCM [58]: The left image is the side view of the right graph, in which the motion of the shake table is used for inducing the out-of-plane loading, and the side supports provide lateral supports for the specimen. The FRCM specimens are further positioned and fixed with abutment restraint slips and pre-tension cables near the boundaries, which align with the proposed model's boundary conditions in a clamped manner.

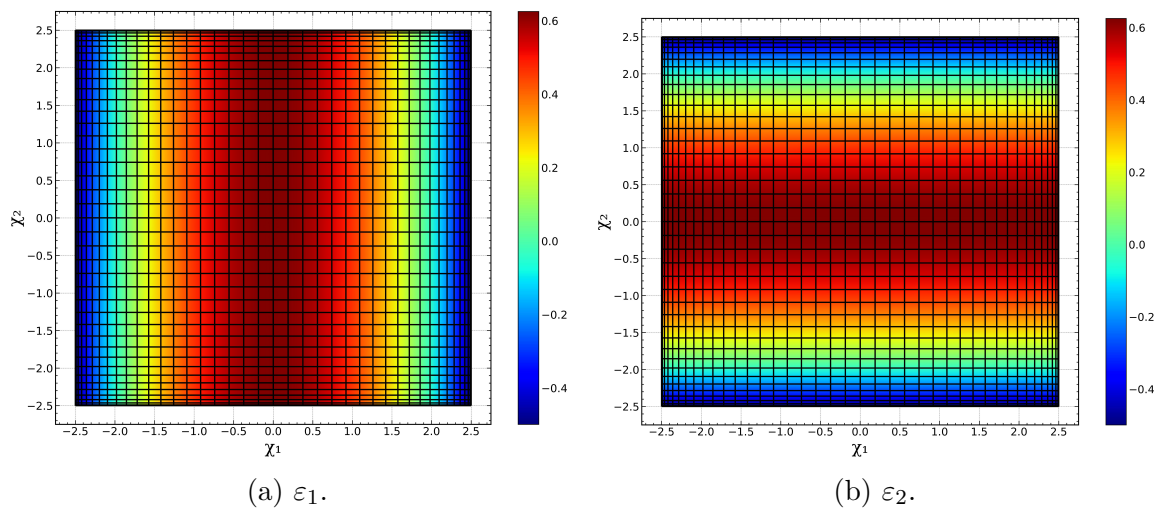
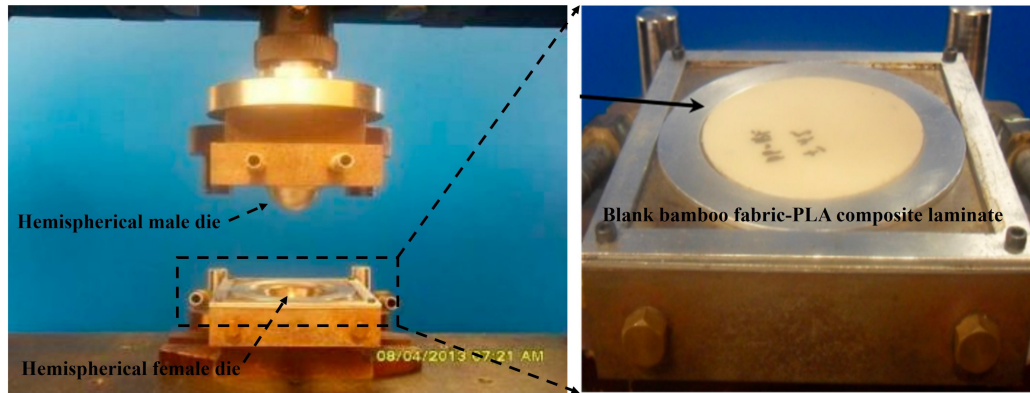


Figure 6.19: Green-Lagrange strain and meshwork deformation of fiber-reinforced composite over the domain ($\kappa = 1Mpa$, $E_i = 2Mpa$, $C_i = 3Mpa$, $T = 3Mpa$, $P = 1Mpa$).

bidirectional distributed fabric reinforcements. More importantly, as shown in Figure 6.16(a) and Figure 6.20(c), the dome-like theoretical result aligns with the profile of the deformed fabric-PLA composite, and it is apparent that the grids situated in the central region of the domain undergo enlargement (Figure 6.16(b) VS Figure 6.20(c)), while grids in the vicinity of the boundaries experience shrinkage (Figure 6.16(b) VS

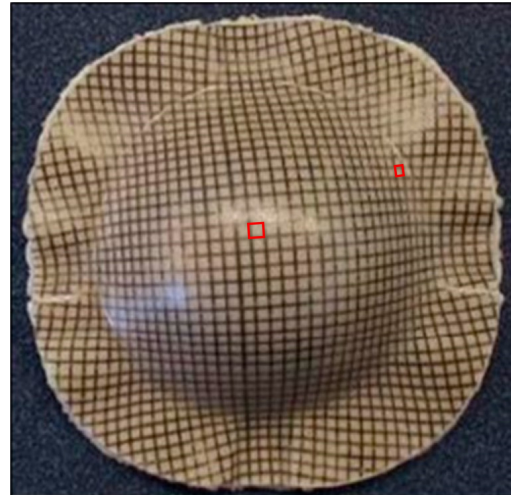
Figure 6.20(c)). Hence, these findings collectively showcase a high phenomenological agreement of the proposed model results in Figure 6.16.



(a)



(b)



(c)

Figure 6.20: Experimental configuration on shaping bamboo fabric-PLA composites [61]: (a) the blank PLA composite is placed on the top surface of the hemispherical female die surface to be reshaped by the male die, (b) the male and female die are matching to form the dome-like bamboo fabric-PLA composites, (c) the obtained dome-like bamboo fabric-PLA composites with the enlarged grids in the hinterland and shrunk grids in the vicinity of boundaries.

6.6 Conclusion

We propose a continuum model aiming to achieve comprehensive descriptions and understandings of three-dimensional deformation in fiber-reinforced materials. The

model-building approach involves incorporating an elastomeric matrix material by using the Neo-Hookean hyperelastic material model, then considering the bidirectional fiber meshwork as the reinforcement. The kinematics of the reinforcing fibers are configured by computing their positions and kinematics vector fields, which facilitate the derivation and integration of the first-order and second-order gradients of deformation into the continuum models. The formulation process is implemented within the framework of differential geometry on FRC surfaces and variational principles, resulting in the derivation of the Euler equilibrium equation and admissible loading conditions while accounting for the constraint of material incompressibility. By projecting the Euler equilibrium equations onto three-dimensional Euclidean coordinates, a system of PDEs is obtained and then solved numerically using a custom-built FEM procedure to illustrate the mechanical response of the elastomeric composite. Research attention is particularly dedicated to the characterization of three-dimensional deformation, the kinematics of microstructures (extension, flexure, and twist of fiber pieces), and the mechanism of microstructure that determines the overall deformation of the meshwork.

The simulation results phenomenologically illustrate that the matrix material of FRC undergoes concurrent three-dimensional deformations when subjected to lateral pressures, resulting in the maximum in-plane deformations occurring in the diagonal direction of FRC while the center of the domain exhibits weak in-plane deformation. In particular, the matrix is more deformable in the plane as indicated by the in-plane deformation exceeds the out-of-plane deformation significantly, and the in-plane deformation of matrix material shows a high dependency on the domain shape/size. Notably, the simulated deformations of fiber pieces reasonably predict the overall deformations of fiber meshwork, showing the embedded microstructures of fiber determine the overall deformation of fiber meshwork. Impressively, the mechanical responses of the fibers exhibit clear J-shaped loading-extension relations, which are in alignment with the strain-stiffening behaviors observed in fiber-reinforced composites

and synthetic materials. More importantly, these characterizations reasonably and qualitatively explain and validate the deformation of fibrous materials, such as the shaping of bamboo fabric-PLA composites and woven fabric, as well as the damage patterns observed in fabrics used for strengthening cementitious matrices.

The proposed model offers reasonable and comprehensive descriptions of elastomeric composite deformation, potential damage patterns in fiber meshworks, and the deformations of fibers and fibrous meshworks. Therefore, it is advisable to consider these theoretical estimations before fabricating elastomeric composites. This approach can assist in achieving high-quality fiber-reinforced composites while effectively minimizing the costs associated with design and fabrication processes.

References

- [1] A. C. Pipkin, "Stress analysis for fiber-reinforced materials," *Advances in Applied Mechanics*, vol. 19, C 1979, ISSN: 00652156. DOI: 10.1016/S0065-2156(08)70308-9.
- [2] F. J. Lockett, "Deformations of fibre-reinforced materials: A. j. m. spencer clarendon press: Oxford university press (1972), £3.00," 1973. [Online]. Available: <https://api.semanticscholar.org/CorpusID:139003333>.
- [3] D. K. Rajak, D. D. Pagar, P. L. Menezes, and E. Linul, *Fiber-reinforced polymer composites: Manufacturing, properties, and applications*, 2019. DOI: 10.3390/polym11101667.
- [4] D. Myung *et al.*, "Biomimetic strain hardening in interpenetrating polymer network hydrogels," *Polymer*, vol. 48, 18 2007, ISSN: 00323861. DOI: 10.1016/j.polymer.2007.06.070.
- [5] R. E. Shadwick, "Mechanical design in arteries," *Journal of Experimental Biology*, vol. 202, 23 1999, ISSN: 00220949. DOI: 10.1242/jeb.202.23.3305.
- [6] Y. Ma, X. Feng, J. A. Rogers, Y. Huang, and Y. Zhang, *Design and application of 'j-shaped' stress-strain behavior in stretchable electronics: A review*, 2017. DOI: 10.1039/c7lc00289k.
- [7] R. V. Martinez *et al.*, "Robotic tentacles with three-dimensional mobility based on flexible elastomers," *Advanced Materials*, vol. 25, 2 2013, ISSN: 09359648. DOI: 10.1002/adma.201203002.
- [8] A. Gupta, G. K. Meena, and V. Singhal, "Strengthening of autoclaved aerated concrete (aac) masonry wallettes with fabric reinforced cementitious matrix for in-plane shear and out-of-plane loads," *Structures*, vol. 51, 2023, ISSN: 23520124. DOI: 10.1016/j.istruc.2023.03.099.
- [9] Y. Wang, C. Gregory, and M. A. Minor, "Improving mechanical properties of molded silicone rubber for soft robotics through fabric compositing," *Soft Robotics*, vol. 5, 3 2018, ISSN: 21695180. DOI: 10.1089/soro.2017.0035.
- [10] B. Yan *et al.*, "Duplicating dynamic strain-stiffening behavior and nanomechanics of biological tissues in a synthetic self-healing flexible network hydrogel," *ACS Nano*, vol. 11, 11 2017, ISSN: 1936086X. DOI: 10.1021/acsnano.7b05109.
- [11] C. I. Kim and M. Zeidi, "Gradient elasticity theory for fiber composites with fibers resistant to extension and flexure," *International Journal of Engineering Science*, vol. 131, 2018, ISSN: 00207225. DOI: 10.1016/j.ijengsci.2018.06.002.
- [12] J. F. Mulhern, T. G. Rogers, and A. J. Spencer, "A continuum theory of a plastic-elastic fibre-reinforced material," *International Journal of Engineering Science*, vol. 7, 2 1969, ISSN: 00207225. DOI: 10.1016/0020-7225(69)90053-6.

- [13] A. C. Pipkin and T. G. Rogers, “Plane deformations of incompressible fiber-reinforced materials,” *Journal of Applied Mechanics, Transactions ASME*, vol. 38, 3 1971, ISSN: 15289036. DOI: 10.1115/1.3408866.
- [14] D. J. Steigmann, “Theory of elastic solids reinforced with fibers resistant to extension, flexure and twist,” *International Journal of Non-Linear Mechanics*, vol. 47, 7 2012, ISSN: 00207462. DOI: 10.1016/j.ijnonlinmec.2012.04.007.
- [15] D. J. Steigmann and F. dell’Isola, “Mechanical response of fabric sheets to three-dimensional bending, twisting, and stretching,” *Acta Mechanica Sinica/Lixue Xuebao*, vol. 31, 3 2015, ISSN: 16143116. DOI: 10.1007/s10409-015-0413-x.
- [16] M. Cuomo, F. dell’Isola, and L. Greco, “Simplified analysis of a generalized bias test for fabrics with two families of inextensible fibres,” *Zeitschrift für Angewandte Mathematik und Physik*, vol. 67, 3 2016, ISSN: 00442275. DOI: 10.1007/s00033-016-0653-z.
- [17] F. dell’Isola, M. Cuomo, L. Greco, and A. D. Corte, “Bias extension test for pantographic sheets: Numerical simulations based on second gradient shear energies,” *Journal of Engineering Mathematics*, vol. 103, 1 2017, ISSN: 15732703. DOI: 10.1007/s10665-016-9865-7.
- [18] F. Dell’Isola, A. D. Corte, L. Greco, and A. Luongo, “Plane bias extension test for a continuum with two inextensible families of fibers: A variational treatment with lagrange multipliers and a perturbation solution,” *International Journal of Solids and Structures*, vol. 81, 2016, ISSN: 00207683. DOI: 10.1016/j.ijsolstr.2015.08.029.
- [19] S. Islam, D. Zhalmuratova, H. J. Chung, and C. I. Kim, “A model for hyperelastic materials reinforced with fibers resistance to extension and flexure,” *International Journal of Solids and Structures*, vol. 193-194, 2020, ISSN: 00207683. DOI: 10.1016/j.ijsolstr.2020.02.036.
- [20] S. Islam, S. E. S. Bolouri, and C. I. Kim, “Mechanics of hyperelastic composites reinforced with nonlinear elastic fibrous materials in finite plane elastostatics,” *International Journal of Engineering Science*, vol. 165, 2021, ISSN: 00207225. DOI: 10.1016/j.ijengsci.2021.103491.
- [21] M. H. Rahman, S. Yang, and C. I. Kim, “A third gradient-based continuum model for the mechanics of continua reinforced with extensible bidirectional fibers resistant to flexure,” *Continuum Mechanics and Thermodynamics*, vol. 35, 2 2023, ISSN: 14320959. DOI: 10.1007/s00161-023-01198-9.
- [22] D. J. Steigmann, “Equilibrium of elastic lattice shells,” *Journal of Engineering Mathematics*, vol. 109, 1 2018, ISSN: 15732703. DOI: 10.1007/s10665-017-9905-y.
- [23] F. dell’Isola and D. Steigmann, “A two-dimensional gradient-elasticity theory for woven fabrics,” *Journal of Elasticity*, vol. 118, 1 2015, ISSN: 15732681. DOI: 10.1007/s10659-014-9478-1.

- [24] D. J. Steigmann and F. dell’Isola, “Mechanical response of fabric sheets to three-dimensional bending, twisting, and stretching,” *Acta Mechanica Sinica/Lixue Xuebao*, vol. 31, pp. 373–382, 3 Jun. 2015, ISSN: 16143116. DOI: 10.1007/s10409-015-0413-x.
- [25] I. Giorgio, R. Grygoruk, F. Dell’Isola, and D. J. Steigmann, “Pattern formation in the three-dimensional deformations of fibered sheets,” *Mechanics Research Communications*, vol. 69, 2015, ISSN: 00936413. DOI: 10.1016/j.mechrescom.2015.08.005.
- [26] I. Giorgio, A. D. Corte, F. dell’Isola, and D. J. Steigmann, “Buckling modes in pantographic lattices,” *Comptes Rendus - Mecanique*, vol. 344, 7 2016, ISSN: 16310721. DOI: 10.1016/j.crme.2016.02.009.
- [27] D. J. Steigmann, “Continuum theory for elastic sheets formed by inextensible crossed elasticae,” *International Journal of Non-Linear Mechanics*, vol. 106, 2018, ISSN: 00207462. DOI: 10.1016/j.ijnonlinmec.2018.03.012.
- [28] I. Giorgio, F. dell’Isola, and D. J. Steigmann, “Edge effects in hyper nets,” *Comptes Rendus - Mecanique*, vol. 347, 2 2019, ISSN: 16310721. DOI: 10.1016/j.crme.2019.01.003.
- [29] R. Ogden, “Non-linear elastic deformations,” *Engineering Analysis with Boundary Elements*, vol. 1, 2 1984, ISSN: 09557997. DOI: 10.1016/0955-7997(84)90049-3.
- [30] D. J. Steigmann, “Invariants of the stretch tensors and their application to finite elasticity theory,” *Mathematics and Mechanics of Solids*, vol. 7, 4 2002, ISSN: 10812865. DOI: 10.1177/108128028481.
- [31] D. J. Steigmann, *Finite elasticity theory*. Oxford University Press, Dec. 2017, pp. 1–184, ISBN: 9780191746536. DOI: 10.1093/oso/9780198567783.001.0001.
- [32] A. J. Spencer and K. P. Soldatos, “Finite deformations of fibre-reinforced elastic solids with fibre bending stiffness,” *International Journal of Non-Linear Mechanics*, vol. 42, 2 2007, ISSN: 00207462. DOI: 10.1016/j.ijnonlinmec.2007.02.015.
- [33] C. I. Kim, “Superposed incremental deformations of an elastic solid reinforced with fibers resistant to extension and flexure,” *Advances in Materials Science and Engineering*, vol. 2018, 2018, ISSN: 16878442. DOI: 10.1155/2018/6501985.
- [34] C. I. Kim, “Strain-gradient elasticity theory for the mechanics of fiber composites subjected to finite plane deformations: Comprehensive analysis,” *Multiscale Science and Engineering*, vol. 1, 2 2019, ISSN: 2524-4515. DOI: 10.1007/s42493-019-00015-3.
- [35] M. Zeidi and C. I. Kim, “Finite plane deformations of elastic solids reinforced with fibers resistant to flexure: Complete solution,” *Archive of Applied Mechanics*, vol. 88, 5 2018, ISSN: 14320681. DOI: 10.1007/s00419-018-1344-3.

- [36] M. Zeidi and C. I. Kim, “Mechanics of fiber composites with fibers resistant to extension and flexure,” *Mathematics and Mechanics of Solids*, vol. 24, 1 2019, ISSN: 17413028. DOI: 10.1177/1081286517728543.
- [37] M. Zeidi and C. I. Kim, “Mechanics of an elastic solid reinforced with bidirectional fiber in finite plane elastostatics: Complete analysis,” *Continuum Mechanics and Thermodynamics*, vol. 30, 3 2018, ISSN: 09351175. DOI: 10.1007/s00161-018-0623-0.
- [38] R. S. Rivlin, “Constitutive equation for a fiber-reinforced lamina,” in *IUTAM Symposium on Anisotropy, Inhomogeneity and Nonlinearity in Solid Mechanics*, D. F. Parker and A. H. England, Eds., Dordrecht: Springer Netherlands, 1995, pp. 379–384, ISBN: 978-94-015-8494-4.
- [39] A. J. M. A. J. M. Spencer, *Deformations of fibre-reinforced materials* (Oxford science research papers). Clarendon Press, 1972. [Online]. Available: <https://cir.nii.ac.jp/crid/1130282268887032192>.
- [40] A. J. Spencer and K. P. Soldatos, “Finite deformations of fibre-reinforced elastic solids with fibre bending stiffness,” *International Journal of Non-Linear Mechanics*, vol. 42, pp. 355–368, 2 Mar. 2007, ISSN: 00207462. DOI: 10.1016/j.ijnonlinmec.2007.02.015.
- [41] G. A. Holzapfel and R. W. Ogden, *Mechanics of biological tissue*. 2006. DOI: 10.1007/3-540-31184-X.
- [42] R. A. Toupin, “Theories of elasticity with couple-stress,” *Archive for Rational Mechanics and Analysis*, vol. 17, 2 1964, ISSN: 00039527. DOI: 10.1007/BF00253050.
- [43] W. T. Koiter, “Couple stresses in the theory of elasticity, i and ii,” *Proceedings of the Koninklijke Nederlandse Akademie van Wetenschappen, Series B*, vol. 67, 1964.
- [44] R. D. Mindlin and H. F. Tiersten, “Effects of couple-stresses in linear elasticity,” *Archive for Rational Mechanics and Analysis*, vol. 11, 1 1962, ISSN: 00039527. DOI: 10.1007/BF00253946.
- [45] P. Germain, “The method of virtual power in continuum mechanics. part 2: Microstructure,” *SIAM Journal on Applied Mathematics*, vol. 25, pp. 556–575, 3 Nov. 1973, ISSN: 0036-1399. DOI: 10.1137/0125053.
- [46] D. J. Steigmann, “Mechanics and physics of lipid bilayers,” in 2018, vol. 577. DOI: 10.1007/978-3-319-56348-0_1.
- [47] D. J. Steigmann, “A model for lipid membranes with tilt and distension based on three-dimensional liquid crystal theory,” *International Journal of Non-Linear Mechanics*, vol. 56, 2013, ISSN: 00207462. DOI: 10.1016/j.ijnonlinmec.2013.02.006.
- [48] A. Agrawal and D. J. Steigmann, “Boundary-value problems in the theory of lipid membranes,” *Continuum Mechanics and Thermodynamics*, vol. 21, 1 2009, ISSN: 09351175. DOI: 10.1007/s00161-009-0102-8.

- [49] A. Logg and G. N. Wells, “Dolfin: Automated finite element computing,” *ACM Transactions on Mathematical Software*, vol. 37, 2 2010, ISSN: 00983500. DOI: 10.1145/1731022.1731030.
- [50] A. Logg, G. N. Wells, and J. Hake, “Dolfin: A c++/python finite element library,” in 2012, vol. 84. DOI: 10.1007/978-3-642-23099-8_10.
- [51] S. W. Hahm and D. Y. Khang, “Crystallization and microstructure-dependent elastic moduli of ferroelectric p(vdf-trfe) thin films,” *Soft Matter*, vol. 6, 22 2010, ISSN: 1744683X. DOI: 10.1039/c0sm00350f.
- [52] J. Monecke, “Microstructure dependence of material properties of composites,” *physica status solidi (b)*, vol. 154, 2 1989, ISSN: 15213951. DOI: 10.1002/pssb.2221540239.
- [53] F. Moravec and M. Holeček, “Microstructure-dependent nonlinear viscoelasticity due to extracellular flow within cellular structures,” *International Journal of Solids and Structures*, vol. 47, 14-15 2010, ISSN: 00207683. DOI: 10.1016/j.ijsolstr.2010.03.024.
- [54] P. Germain, “The method of virtual power in continuum mechanics. part 2: Microstructure,” *SIAM Journal on Applied Mathematics*, vol. 25, 3 1973, ISSN: 0036-1399. DOI: 10.1137/0125053.
- [55] Y. C. Fung, “Structure and stress-strain relationship of soft tissues,” *Integrative and Comparative Biology*, vol. 24, 1 1984, ISSN: 15407063. DOI: 10.1093/icb/24.1.13.
- [56] M. Vatankhah-Varnosfaderani *et al.*, “Mimicking biological stress–strain behaviour with synthetic elastomers,” *Nature*, vol. 549, 7673 2017, ISSN: 14764687. DOI: 10.1038/nature23673.
- [57] H. Zhou, X. Xiao, K. Qian, K. Zhang, and D. Zhang, “Numerical and experimental analyses of out-of-plane deformation of triaxial woven fabric,” *Materials Research Express*, vol. 5, 5 2018, ISSN: 20531591. DOI: 10.1088/2053-1591/aac0d2.
- [58] S. L. Sagar, V. Singhal, and D. C. Rai, “In-plane and out-of-plane behavior of masonry-infilled rc frames strengthened with fabric-reinforced cementitious matrix,” *Journal of Composites for Construction*, vol. 23, 1 2019, ISSN: 1090-0268. DOI: 10.1061/(asce)cc.1943-5614.0000905.
- [59] G. Magenes and G. M. Calvi, “In-plane seismic response of brick masonry walls,” *Earthquake Engineering and Structural Dynamics*, vol. 26, 11 1997, ISSN: 00988847. DOI: 10.1002/(SICI)1096-9845(199711)26:11<1091::AID-EQE693>3.0.CO;2-6.
- [60] N. Ismail and J. M. Ingham, “In-plane and out-of-plane testing of unreinforced masonry walls strengthened using polymer textile reinforced mortar,” *Engineering Structures*, vol. 118, 2016, ISSN: 18737323. DOI: 10.1016/j.engstruct.2016.03.041.

- [61] M. R. N. Fazita, K. Jayaraman, and D. Bhattacharyya, "Formability analysis of bamboo fabric reinforced poly (lactic) acid composites," *Materials*, vol. 9, 7 2016, ISSN: 19961944. DOI: 10.3390/ma9070539.

Chapter 7

Conclusions and Future Work

7.1 Conclusions

This thesis sets out to study the hyperelasticity of lipid membranes and fiber-reinforced composite material by incorporating associated factors into the well-established strain energy potential and illustrating the resulting simulation/analytical results. This involves considering the lipid membrane strain energy is non-uniformly distributed over the lipid membrane, the presence of intra-surface viscous flow on the lipid membrane surface, and the fiber-reinforced composite performs concurrent three-dimensional deformations subjected to out-of-plane loadings. The emphasis is placed on demonstrating the morphologies of lipid membranes to understand the cell functioning process and analyze the mechanical performance of fiber-reinforced composites which are widely used in various industries and engineering fields.

The studying approaches include respectively assimilating the strain energy contributions of lipid membrane non-uniformity and surface distension into the Canham-Helfrich model, and building the strain energy potential of fiber composite by using the Neo-Hookean hyperelastic model for the matrix material while accommodating fiber kinematics. To derive the constitutive relations on the material surface and establish equilibrium equations, differential geometry is utilized to present the material position on the surface of the deformed lipid bilayer and fiber-reinforced composite, enabling the computation of the surface metric, covariant/contravariant derivative

on the surface, as well as the gradient of deformation. To derive the Euler-Lagrange equation describing the mechanics of hyperelastic material, the variational framework is implemented on the furnished strain energy potential, where the equilibrium equations and admissible boundary conditions are formulated to demonstrate the physical behavior of hyperelastic material. Through the implementation of the proposed models, the formulated equilibrium equations and boundary conditions are projected onto the Cartesian coordinate and a system of PDEs is obtained and then solved numerically/analytically. In particular, the non-linear equilibrium equations of lipid membranes are linearized and solved analytically to demonstrate the “small” deformation of lipid membranes. Aiming at validating the refined Helfrich model of the lipid membrane, the obtained numerical simulation results and analytical results are evidenced by the established theoretical results and experimental results, suggesting the capability of the refined lipid membrane model in describing cell morphogenesis, such as the off-centered lipid membrane morphology induced by being treated under 14 days of storage in a liquid medium, the multiple peak morphology of abnormal cell membranes (burr cell) commonly observed in uremia and chronic kidney disease. Further, the phenomenological consistency of the obtained theoretical results regarding the descriptions of lipid membrane morphology might assist in understanding cell physiology and pathology. In addition, the MD simulation approach is applied in the study of viscous effects on the surface distension of lipid membranes, where the MD simulation results prohibit a high consistency to the results obtained from the proposed model. As for the study of fiber composite, the proposed three-dimensional model of fiber-reinforced composite comprehensively describes the fiber composite deformation subjected to out-of-plane loadings by evidencing numerical results with the experimental results of the damage pattern of FRCM specimens, shaping process of bamboo fabric-PLA meshwork, and the out-of-plane deformation of woven fabric. It is specifically summarised: Chapter 3 and Chapter 4 investigate the non-uniformity of lipid membranes while respectively focusing on describing different cellular cases

(Chapter 3 mainly for protein-membrane interaction, Chapter 4 for cell inflammation). Chapter 5 emphasizes studying the viscous effects on the surface distension of lipid membranes. Chapter 6 proposed a three-dimensional model describing the mechanics of fiber-reinforced composite film.

In Chapters 3 and 4, two sets of complete analytical solutions are presented to describe the mechanical responses of non-uniform lipid membranes subjected to protein-membrane interactions and local inflammations, respectively. Emphasis is placed on deriving the rigorous and sufficiently general linear theory of lipid membranes to accommodate the complex nature of non-uniform membrane morphology undergoing substrate-interaction force and lateral pressure. As such, a series of more general forms of the energy potential of the Helfrich type are proposed depending explicitly on the surface coordinates. In this regard, the non-uniformity of the lipid membrane is formulated into the equilibrium equations by introducing the coordinate-dependent functions, where the corresponding linear shape equations are formulated, and the normal shape equation is homogeneous for protein-membrane interaction problem while it is inhomogeneous for local inflammation case. Within the Monge parameterization, the formulated non-linear shape equations are transformed into PDEs and linearized, then, the corresponding complete analytical solutions are achieved within the prescription of superposed incremental deformations. To illustrate the morphological transition of a non-uniform lipid membrane, the boundary conditions of the existing non-linear model are reformulated in the present context to accommodate the obtained analytical solutions in describing lipid membrane morphology. Consequently, a wealth of examples that portray the evolutions of the membrane in response to applied substrate-interaction force (for circular membrane patches) and lateral pressures (for circular and rectangular membrane patches) are elucidated.

The results of Chapter 3 (the protein-membrane interaction case) suggest that the resulting deformation fields (in the cases of energy distribution functions define the lipid membrane as circumferentially and radially non-uniform) demonstrate clear

signs of coordinate dependency of the non-uniform lipid membrane, showing that the descriptions of the non-uniform responses of membranes are intrinsically dependent on the augmented strain energy potential which is explicitly determined by the surface coordinates. The key findings are: the analytical solutions of the proposed linear model demonstrate reasonable agreement with those obtained from the non-linear analysis, e.g., the linear theory and non-linear theory tend to coincide when the lipid membrane is subjected to small deformation; The superposition of analytical solutions from linear shape equations remains valid for the present application, i.e., the analytical solution of the combined non-uniform energy distribution cases may be obtained by superimposing the analytical results of the circumferentially and radially non-uniform membrane cases, respectively; The non-linear solution promisingly predicts the off-centered biconcave morphology of lipid membranes and the multiple peak formations of abnormal cell membranes (burr cell), which are commonly observed in uremia and chronic disease.

In Chapter 4 (membrane inflammation case), the effects of cell inflammation on non-uniform lipid membranes are investigated, in which the radial and circumferential non-uniformity of lipid membranes are illustrated by the analytical solution of the linear theory of lipid membrane. The key findings include the lateral pressure effects can be generally equivalent to the bending effects on the lipid membrane deformation at specific values while maintaining the non-uniformity of the lipid membrane. In addition, the analytical solution of linear theory phenomenologically assimilates the sequences of discocyte-stomatocyte morphology in cell membranes and the off-centered biconcave discoid formation of a red blood cell. It is also found that the superimposed analytical solution remains valid in describing the combined non-uniform cases of membrane inflammation (discussed in Chapter 3). Particularly, the combination manner of analytical solutions further suggests that a more general class of membrane morphology transition may be characterized by the superposition of different types of analytical solutions in describing membrane non-uniformity and so may accommo-

date a wide range of phenomenologically relevant problems. It can be deduced that the potential application of investigating the inflammation effects on the non-uniform lipid membranes might be in the conformation analyses of membranes associated with the compromised membrane-skeleton connections and/or lateral diffusion processes.

Unlike Chapter 3 and Chapter 4 which study the non-uniformity of lipid membranes, Chapter 5 sheds light on studying the effects of viscous flow on surface distension of lipid membrane. In there, the surface distension and morphological transitions of lipid bilayer membranes are jointly investigated through the continuum-based model and CGMD simulation. To incorporate the effects of intra-membrane viscosity and thickness distension into the strain energy, the classic Helfrich-type model is reformulated into the framework of a crystal thin film which is deduced from the three-dimensional liquid crystal theory. Then, the variational framework and Monge representations are utilized to derive the tangential and normal shape equations of the lipid membranes in the presence of viscous stress, and the resulting system of PDEs is solved numerically. To validate the proposed model, the problems of membrane inflammation and membrane-protein interaction are demonstrated. In addition, MD simulations are implemented to further evidence the results obtained from the proposed continuum model. It is found that viscous flow might result in the off-centered membrane morphology and, at the same time, increase/reduce the membrane thickness by compressing and stretching the membrane on the membrane surface. In the case of membrane-protein interactions, the acting interaction force gives rise to local bending effects in the vicinity of the inner boundary and, hence, reduces the membrane thickness. Further, the proposed continuum model may provide quantitative descriptions for the highly curved morphology and the associated thickness reduction of the membrane when NPCs interact with the nuclear envelope. More importantly, despite the MD simulation and the continuum modeling approaches being two distinct approaches (with different constitutive backgrounds) in the lipid membrane studies, they show high consistency in predicting both the membranes' deformation and thick-

ness dilation except for the particular cases when the MD results showcase high fluctuations at the molecular scale. The difference between the results obtained from the proposed continuum model and MD simulation may derive from the fact that the MD simulation can identify the intermediate structures with tilted lipid molecules whereas the proposed continuum model describes the membranes' substructure as essentially non-tilted lipids. Further research in this respect is certainly of more practical interest yet is beyond the scope of the proposed study.

The highlight of Chapter 6 is located in proposing a continuum model that reasonably and comprehensively describes the concurrent three-dimensional deformation of fiber-reinforced composites. In there, the kinematics of the reinforcing fibers are configured by computing their positions and vector fields, which involves the derivation and integration of the first-order and second-order gradients of deformation into the continuum models. The formulation process is implemented within the framework of differential geometry on fiber composite surface and variational principles, resulting in the derivation of the Euler equilibrium equation and the establishment of admissible boundary conditions while maintaining the material incompressibility. By projecting the Euler equilibrium equation onto three-dimensional Euclidean coordinates, a system of PDEs is obtained and then solved numerically using a custom-built FEM procedure to illustrate the mechanical response of the elastomeric composite. Research attention is dedicated to the characterization of various aspects of fiber-reinforced composites, including the in-plane and out-of-plane deformation, strain distribution, and the deformations of fiber and fiber meshwork. Considering the scarcity of available data at the microscopic scale, particular attention has been given to investigating the microstructure deformation of fibers to understand the underlying mechanisms behind the overall mechanical deformation of fiber composite. These characterizations are reasonably explained and validated by the results of fibrous material deformation, such as the shaping of bamboo fabric-PLA composites and woven fabric, as well as the damage patterns observed in fabrics used for strengthening ce-

mentitious matrices. Further, the simulated deformations of fiber units accurately predict the overall deformation of individual fiber and fiber meshwork, showing the embedded microstructure does determine the mechanical performance of fiber composite materials. Additionally, the mechanical responses of the fibers exhibit clear J-shaped loading-extension relations, which are in alignment with the strain-stiffening behaviors observed in fiber-reinforced composites.

This dissertation has been one of the first attempts to comprehensively examine two distinct types of hyperelastic materials, i.e., lipid membrane and fiber-reinforced composite, aiming at advancing the understanding of the commonality of hyperelastic material, particularly in the cases of subjecting to out-of-plane loadings. The primary study approach is to solve the proposed models numerically/analytically and examine the theoretical results with simulation results and experimental results in the current literature. Chapters 3 and 4 theoretically reveal the critical role of the non-uniform morphology of lipid membranes (subjected to protein-membrane interaction, and cell inflammation, respectively) in the cellular function implementation and associated biological status. Chapter 5 demonstrates the effects of viscous flow on the membrane surface distension in the cases of protein-membrane interaction and cell inflammation, respectively. Given the experience of studying lipid membrane deformation, Chapter 6 develops a three-dimensional model that offers reasonable and comprehensive descriptions of elastomeric composite deformation which are evidenced by the potential damage patterns in fiber meshworks, and the deformations of fibers and fibrous meshwork, especially unveiling the mechanism of the fiber microstructure determines the overall deformation of fiber meshwork. The thesis theoretically highlights that hyperelastic materials (e.g., lipid membrane and fiber composite) are concurrently deformable in three dimensions (i.e., out-of-plane deformation for lipid membrane while three-dimensional deformation for fiber composite), which can significantly extend our knowledge of hyperelasticity in investigating biological and engineering materials.

7.2 Future Work

For lipid membrane theory, the proceeding works include investigating the surface distension of lipid membranes subjected to protein-membrane interaction and cell inflammation without considering the viscous effects. This study can be achieved by assimilating the dimension-reduced liquid-crystal theory into the lipid membrane theory, hence, the associated equilibrium equations can be formulated and numerically solved in the studying approach discussed in Chapter 5. The motivation is that despite the viscosity-coupled cases of membrane-protein interaction and cell inflammation being investigated, the static effects of membrane-protein interaction and cell inflammation on membrane surface distension are still lacking. Further, the MD simulation can be utilized to simulate the membrane deformation and surface distension without applying the viscous flow.

Regarding the proposed three-dimensional fiber-reinforced composite theory in Chapter 6, the proposed model can be further refined by introducing the computation of the higher-order gradient of deformation utilized to describe the fiber kinematics embedded in a matrix material. The motivation for the incorporation derives from that the higher-order gradient theories can explain complicated phenomena such as buckling and internal resonance, while accounting for singularities and explaining local response phenomena within the material, such as the generation of shear band and the local shear stresses. It is also believed that the linear theory remains applicable to the three-dimensional fiber-reinforced composite model, underlying a wealth of problems framed in the “small deformation” of fiber composite to be completed in the future.

Bibliography

- [1] M. Shahzad, A. Kamran, M. Z. Siddiqui, and M. Farhan, “Mechanical characterization and fe modelling of a hyperelastic material,” *Materials Research*, vol. 18, 5 2015, ISSN: 19805373. DOI: 10.1590/1516-1439.320414.
- [2] G. Chagnon, M. Rebouah, and D. Favier, *Hyperelastic energy densities for soft biological tissues: A review*, 2015. DOI: 10.1007/s10659-014-9508-z.
- [3] I. Major and M. Major, “Application of hyperelastic materials in a composite hollow brick for assessing the reduction of dynamic loads - numerical analysis,” vol. 585, 2019. DOI: 10.1088/1757-899X/585/1/012031.
- [4] W. Noll, “Materially uniform simple bodies with inhomogeneities,” *Archive for Rational Mechanics and Analysis*, vol. 27, 1 1967, ISSN: 00039527. DOI: 10.1007/BF00276433.
- [5] Y. Ma, X. Feng, J. A. Rogers, Y. Huang, and Y. Zhang, *Design and application of 'j-shaped' stress-strain behavior in stretchable electronics: A review*, 2017. DOI: 10.1039/c7lc00289k.
- [6] A. A. Abbasi, M. T. Ahmadian, A. Alizadeh, and S. Tarighi, “Application of hyperelastic models in mechanical properties prediction of mouse oocyte and embryo cells at large deformations,” *Scientia Iranica*, vol. 25, 2B 2018, ISSN: 23453605. DOI: 10.24200/sci.2017.4321.
- [7] W. Helfrich, “Elastic properties of lipid bilayers: Theory and possible experiments,” *Zeitschrift fur Naturforschung - Section C Journal of Biosciences*, vol. 28, pp. 693–703, 11-12 Dec. 1973, ISSN: 18657125. DOI: 10.1515/znc-1973-11-1209.
- [8] Z. Liu and C. il Kim, “Deformation analysis of lipid membranes subjected to general forms of intra-membrane viscous flow and interactions with an elliptical-cross-section substrate,” *Scientific Reports*, vol. 10, 1 2020, ISSN: 20452322. DOI: 10.1038/s41598-019-57179-z.
- [9] W. Yao and C. I. Kim, “A lipid membrane morphology subjected to intra-membrane viscosity and membrane thickness dilation,” *Continuum Mechanics and Thermodynamics*, vol. 35, 2 2023, ISSN: 14320959. DOI: 10.1007/s00161-023-01204-0.
- [10] W. Yao and C. I. Kim, “Deformation analysis of nonuniform lipid membrane subjected to local inflammations,” *Mathematics and Mechanics of Complex Systems*, vol. 9, 2 2021, ISSN: 23253444. DOI: 10.2140/MEMOCS.2021.9.203.

- [11] M. Zeidi and C. I. Kim, “The effects of intra-membrane viscosity on lipid membrane morphology: Complete analytical solution,” *Scientific Reports*, vol. 8, 1 2018, ISSN: 20452322. DOI: 10.1038/s41598-018-31251-6.
- [12] T. Belay, K. C. Il, and P. Schiavone, “Mechanics of a lipid bilayer subjected to thickness distension and membrane budding,” *Mathematics and Mechanics of Solids*, vol. 23, 1 2018, ISSN: 17413028. DOI: 10.1177/1081286516666136.
- [13] W. Yao and C. I. Kim, *An analysis of lipid membrane morphology in the presence of coordinate-dependent non-uniformity*, 2021. DOI: 10.1177/1081286520939162.
- [14] S. K. Melly, L. Liu, Y. Liu, and J. Leng, *A review on material models for isotropic hyperelasticity*, 2021. DOI: 10.1002/msd2.12013.
- [15] S. L. Veatch and S. L. Keller, “Organization in lipid membranes containing cholesterol,” *Physical Review Letters*, vol. 89, 26 2002, ISSN: 10797114. DOI: 10.1103/PhysRevLett.89.268101.
- [16] B. B. Diaz-Rohrer, K. R. Levental, K. Simons, and I. Levental, “Membrane raft association is a determinant of plasma membrane localization,” *Proceedings of the National Academy of Sciences of the United States of America*, vol. 111, 23 2014, ISSN: 10916490. DOI: 10.1073/pnas.1404582111.
- [17] H. I. Ingólfsson *et al.*, “Lipid organization of the plasma membrane,” *Journal of the American Chemical Society*, vol. 136, 41 2014, ISSN: 15205126. DOI: 10.1021/ja507832e.
- [18] I. Ermilova, “Modeling of biomembranes: From computational toxicology to simulations of neurodegenerative diseases,” Ph.D. dissertation, Department of Materials and Environmental Chemistry, Stockholm University, 2019. DOI: 10.13140/RG.2.2.24409.57447.
- [19] A. M. Seddon, D. Casey, R. V. Law, A. Gee, R. H. Templer, and O. Ces, “Drug interactions with lipid membranes,” *Chemical Society Reviews*, vol. 38, 9 2009, ISSN: 14604744. DOI: 10.1039/b813853m.
- [20] H. Alimohamadi, A. S. Smith, R. B. Nowak, V. M. Fowler, and P. Rangamani, “Non-uniform distribution of myosin-mediated forces governs red blood cell membrane curvature through tension modulation,” *PLoS Computational Biology*, vol. 16, 5 2020, ISSN: 15537358. DOI: 10.1371/journal.pcbi.1007890.
- [21] B. Alberts, A. Johnson, J. Lewis, M. Raff, K. Roberts, and P. Walter, *Molecular Biology of the Cell*. W.W. Norton Company, Dec. 2007. DOI: 10.1201/9780203833445.
- [22] P. Paumard, “The atp synthase is involved in generating mitochondrial cristae morphology,” *EMBO Journal*, vol. 21, 3 2002, ISSN: 02614189. DOI: 10.1093/emboj/21.3.221.
- [23] S. Aimon, A. Callan-Jones, A. Berthaud, M. Pinot, G. E. Toombes, and P. Bassereau, “Membrane shape modulates transmembrane protein distribution,” *Developmental Cell*, vol. 28, 2 2014, ISSN: 15345807. DOI: 10.1016/j.devcel.2013.12.012.

- [24] S. Vanni, H. Hirose, H. Barelli, B. Antonny, and R. Gautier, *A sub-nanometre view of how membrane curvature and composition modulate lipid packing and protein recruitment*, 2014. DOI: 10.1038/ncomms5916.
- [25] M. Pribil *et al.*, “Fine-tuning of photosynthesis requires curvature thylakoid1-mediated thylakoid plasticity,” *Plant Physiology*, vol. 176, 3 2018, ISSN: 15322548. DOI: 10.1104/pp.17.00863.
- [26] K. V. Pinigin, P. I. Kuzmin, S. A. Akimov, and T. R. Galimzyanov, “Additional contributions to elastic energy of lipid membranes: Tilt-curvature coupling and curvature gradient,” *Physical Review E*, vol. 102, 4 2020, ISSN: 24700053. DOI: 10.1103/PhysRevE.102.042406.
- [27] C. P. Chng, Y. Sadovsky, K. J. Hsia, and C. Huang, “Curvature-regulated lipid membrane softening of nano-vesicles,” *Extreme Mechanics Letters*, vol. 43, 2021, ISSN: 23524316. DOI: 10.1016/j.eml.2021.101174.
- [28] S. Zhang, J. Li, G. Lykotrafitis, G. Bao, and S. Suresh, “Size-dependent endocytosis of nanoparticles,” *Advanced Materials*, vol. 21, 4 2009, ISSN: 09359648. DOI: 10.1002/adma.200801393.
- [29] A. U. Andar, R. R. Hood, W. N. Vreeland, D. L. Devoe, and P. W. Swaan, “Microfluidic preparation of liposomes to determine particle size influence on cellular uptake mechanisms,” *Pharmaceutical Research*, vol. 31, 2 2014, ISSN: 07248741. DOI: 10.1007/s11095-013-1171-8.
- [30] Y. Takechi-Haraya, Y. Goda, and K. Sakai-Kato, “Control of liposomal penetration into three-dimensional multicellular tumor spheroids by modulating liposomal membrane rigidity,” *Molecular Pharmaceutics*, vol. 14, 6 2017, ISSN: 15438392. DOI: 10.1021/acs.molpharmaceut.7b00051.
- [31] X. Yi, X. Shi, and H. Gao, “Cellular uptake of elastic nanoparticles,” *Physical Review Letters*, vol. 107, 9 2011, ISSN: 10797114. DOI: 10.1103/PhysRevLett.107.098101.
- [32] Y. Hui *et al.*, *Role of nanoparticle mechanical properties in cancer drug delivery*, 2019. DOI: 10.1021/acsnano.9b03924.
- [33] I. Liguori *et al.*, *Oxidative stress, aging, and diseases*, 2018. DOI: 10.2147/CIA.S158513.
- [34] J. Emerit, M. Edeas, and F. Bricaire, *Neurodegenerative diseases and oxidative stress*, 2004. DOI: 10.1016/j.biopha.2003.11.004.
- [35] R. A. Floyd, R. A. Towner, T. He, K. Hensley, and K. R. Maples, “Translational research involving oxidative stress and diseases of aging,” *Free Radical Biology and Medicine*, vol. 51, 5 2011, ISSN: 08915849. DOI: 10.1016/j.freeradbiomed.2011.04.014.
- [36] B. Xu, S. L. Chen, Y. Zhang, B. Li, Q. Yuan, and W. Gan, “Evaluating the cross-membrane dynamics of a charged molecule on lipid films with different surface curvature,” *Journal of Colloid and Interface Science*, vol. 610, 2022, ISSN: 10957103. DOI: 10.1016/j.jcis.2021.12.015.

- [37] H. T. McMahon and E. Boucrot, “Membrane curvature at a glance,” *Journal of Cell Science*, vol. 128, 6 2015, ISSN: 14779137. DOI: 10.1242/jcs.114454.
- [38] E. D. Alba, S. Weiler, and N. Tjandra, “Solution structure of human saposin c: Ph-dependent interaction with phospholipid vesicles,” *Biochemistry*, vol. 42, 50 2003, ISSN: 00062960. DOI: 10.1021/bi0301338.
- [39] A. Darmoise, P. Maschmeyer, and F. Winau, “The immunological functions of saposins,” in 2010, vol. 105. DOI: 10.1016/S0065-2776(10)05002-9.
- [40] C. A. Hawkins, E. D. Alba, and N. Tjandra, “Solution structure of human saposin c in a detergent environment,” *Journal of Molecular Biology*, vol. 346, 5 2005, ISSN: 00222836. DOI: 10.1016/j.jmb.2004.12.045.
- [41] A. Falco, R. M. Medina-Gali, J. A. Poveda, M. Bello-Perez, B. Novoa, and J. A. Encinar, “Antiviral activity of a turbot (*scophthalmus maximus*) nk-lysin peptide by inhibition of low-ph virus-induced membrane fusion,” *Marine Drugs*, vol. 17, 2 2019, ISSN: 16603397. DOI: 10.3390/md17020087.
- [42] S. I. Sandin, D. M. Gravano, C. J. Randolph, M. Sharma, and E. de Alba, “Engineering of saposin c protein chimeras for enhanced cytotoxicity and optimized liposome binding capability,” *Pharmaceutics*, vol. 13, 4 2021, ISSN: 19994923. DOI: 10.3390/pharmaceutics13040583.
- [43] A. Flayhan, H. D. Mertens, Y. Ural-Blimke, M. M. Molledo, D. I. Svergun, and C. Löw, “Saposin lipid nanoparticles: A highly versatile and modular tool for membrane protein research,” *Structure*, vol. 26, 2 2018, ISSN: 18784186. DOI: 10.1016/j.str.2018.01.007.
- [44] R. A. Villanueva, Y. Rouillé, and J. Dubuisson, *Interactions between virus proteins and host cell membranes during the viral life cycle*, 2005. DOI: 10.1016/S0074-7696(05)45006-8.
- [45] M. F. Brown, “Curvature forces in membrane lipid-protein interactions,” *Biochemistry*, vol. 51, 49 2012, ISSN: 00062960. DOI: 10.1021/bi301332v.
- [46] T. Baumgart, B. R. Capraro, C. Zhu, and S. L. Das, “Thermodynamics and mechanics of membrane curvature generation and sensing by proteins and lipids,” *Annual Review of Physical Chemistry*, vol. 62, 2011, ISSN: 0066426X. DOI: 10.1146/annurev.physchem.012809.103450.
- [47] R. Parthasarathy and J. T. Groves, *Curvature and spatial organization in biological membranes*, 2007. DOI: 10.1039/b608631d.
- [48] B. Božič, S. L. Das, and S. Svetina, “Sorting of integral membrane proteins mediated by curvature-dependent protein-lipid bilayer interaction,” *Soft Matter*, vol. 11, 12 2015, ISSN: 17446848. DOI: 10.1039/c4sm02289k.
- [49] B. G. Tenchov, “Nonuniform lipid distribution in membranes,” *Progress in Surface Science*, vol. 20, 4 1985, ISSN: 00796816. DOI: 10.1016/0079-6816(85)90014-0.

- [50] R. C. Capeta, J. A. Poveda, and L. M. Loura, “Non-uniform membrane probe distribution in resonance energy transfer: Application to protein-lipid selectivity,” vol. 16, 2006. DOI: 10.1007/s10895-005-0036-x.
- [51] M. Staykova, D. P. Holmes, C. Read, and H. A. Stone, “Mechanics of surface area regulation in cells examined with confined lipid membranes,” *Proceedings of the National Academy of Sciences of the United States of America*, vol. 108, 22 2011, ISSN: 00278424. DOI: 10.1073/pnas.1102358108.
- [52] H. Alimohamadi, A. S. Smith, R. B. Nowak, V. M. Fowler, and P. Ranganmani, “Non-uniform distribution of myosin-mediated forces governs red blood cell membrane curvature through tension modulation,” *PLoS Computational Biology*, vol. 16, 5 2020, ISSN: 15537358. DOI: 10.1371/journal.pcbi.1007890.
- [53] H. Elliott *et al.*, “Myosin ii controls cellular branching morphogenesis and migration in three dimensions by minimizing cell-surface curvature,” *Nature Cell Biology*, vol. 17, 2 2015, ISSN: 14764679. DOI: 10.1038/ncb3092.
- [54] S. Singer and G. L. Nicolson, “The fluid mosaic model of the structure of cell membranes: Cell membranes are viewed as two-dimensional solutions of oriented globular proteins and lipids,” *Science*, vol. 175, 4023 1972.
- [55] H. A. Faizi, R. Dimova, and P. M. Vlahovska, “Viscosity of fluid membranes measured from vesicle deformation,” *bioRxiv*, 2021.
- [56] T. T. Hormel, S. Q. Kurihara, M. K. Brennan, M. C. Wozniak, and R. Parthasarathy, “Measuring lipid membrane viscosity using rotational and translational probe diffusion,” *Physical Review Letters*, vol. 112, 18 2014, ISSN: 10797114. DOI: 10.1103/PhysRevLett.112.188101.
- [57] E. A. Evans and R. M. Hochmuth, “Membrane viscoelasticity,” *Biophysical Journal*, vol. 16, 1 1976, ISSN: 00063495. DOI: 10.1016/S0006-3495(76)85658-5.
- [58] P. M. Vlahovska, “Nonequilibrium dynamics of lipid membranes: Deformation and stability in electric fields,” in 2010, vol. 12. DOI: 10.1016/B978-0-12-381266-7.00005-5.
- [59] M. E. Cerf, *Developmental programming and glucolipotoxicity: Insights on beta cell inflammation and diabetes*, 2020. DOI: 10.3390/metabo10110444.
- [60] R. Sanwlani and L. Gangoda, *Role of extracellular vesicles in cell death and inflammation*, 2021. DOI: 10.3390/cells10102663.
- [61] E. Nader, M. Romana, and P. Connes, *The red blood cell—inflammation vicious circle in sickle cell disease*, 2020. DOI: 10.3389/fimmu.2020.00454.
- [62] J. Schumann, “Does plasma membrane lipid composition impact the mirna-mediated regulation of vascular inflammation?” *Medical Hypotheses*, vol. 88, 2016, ISSN: 15322777. DOI: 10.1016/j.mehy.2016.01.012.
- [63] G. Battineni, G. G. Sagaro, N. Chintalapudi, F. Amenta, D. Tomassoni, and S. K. Tayebati, “Impact of obesity-induced inflammation on cardiovascular diseases (cvd),” *International Journal of Molecular Sciences*, vol. 22, 9 2021, ISSN: 14220067. DOI: 10.3390/ijms22094798.

- [64] T. V. Rohm, D. T. Meier, J. M. Olefsky, and M. Y. Donath, *Inflammation in obesity, diabetes, and related disorders*, 2022. DOI: 10.1016/j.immuni.2021.12.013.
- [65] N. Singh, D. Baby, J. Rajguru, P. Patil, S. Thakkannavar, and V. Pujari, “Inflammation and cancer,” *Annals of African Medicine*, vol. 18, 3 2019, ISSN: 09755764. DOI: 10.4103/aam.aam_56_18.
- [66] J. Ngo, C. Osto, F. Villalobos, and O. S. Shirihai, “Mitochondrial heterogeneity in metabolic diseases,” *Biology*, vol. 10, 9 Sep. 2021, ISSN: 20797737. DOI: 10.3390/biology10090927.
- [67] M. Parilla and S. Gurbuxani, *Red cell morphology in sickle cell disease*, 2020. DOI: 10.1182/BLOOD.2020007602.
- [68] Y. Wu, Y. Niu, F. Lv, W. Gao, and X. Shen, “Morphology classification of circulating tumor cells could be a predictor of recurrent disease in patients with non-small cell lung cancer after surgery,” *Journal of Clinical Oncology*, vol. 38, 15_{suppl} 2020, ISSN: 0732-183X. DOI: 10.1200/jco.2020.38.15_suppl.e15530.
- [69] A. Jamali *et al.*, “Intravital multiphoton microscopy of the ocular surface: Alterations in conventional dendritic cell morphology and kinetics in dry eye disease,” *Frontiers in Immunology*, vol. 11, 2020, ISSN: 16643224. DOI: 10.3389/fimmu.2020.00742.
- [70] R. J. Bevan, T. R. Hughes, P. A. Williams, M. A. Good, B. P. Morgan, and J. E. Morgan, “Retinal ganglion cell degeneration correlates with hippocampal spine loss in experimental alzheimer’s disease,” *Acta Neuropathologica Communications*, vol. 8, 1 2020, ISSN: 20515960. DOI: 10.1186/s40478-020-01094-2.
- [71] Z. Zhang *et al.*, “Morphology-based prediction of cancer cell migration using an artificial neural network and a random decision forest,” *Integrative Biology (United Kingdom)*, vol. 10, 12 2018, ISSN: 17579708. DOI: 10.1039/c8ib00106e.
- [72] M. Fujitani *et al.*, “Morphology-based non-invasive quantitative prediction of the differentiation status of neural stem cells,” *Journal of Bioscience and Bioengineering*, vol. 124, 3 2017, ISSN: 13474421. DOI: 10.1016/j.jbiosc.2017.04.006.
- [73] D. Chen, J. P. Dunkers, W. Losert, and S. Sarkar, “Early time-point cell morphology classifiers successfully predict human bone marrow stromal cell differentiation modulated by fiber density in nanofiber scaffolds,” *Biomaterials*, vol. 274, 2021, ISSN: 18785905. DOI: 10.1016/j.biomaterials.2021.120812.
- [74] B. A. Lewis and D. M. Engelman, *Lipid bilayer thickness varies linearly with acyl chain length in fluid phosphatidylcholine vesicles*, 1983. DOI: 10.1016/S0022-2836(83)80007-2.
- [75] W. Rawicz, K. C. Olbrich, T. McIntosh, D. Needham, and E. A. Evans, “Effect of chain length and unsaturation on elasticity of lipid bilayers,” *Biophysical Journal*, vol. 79, 1 2000, ISSN: 00063495. DOI: 10.1016/S0006-3495(00)76295-3.

- [76] J. Frallicciardi, J. Melcr, P. Siginou, S. J. Marrink, and B. Poolman, “Membrane thickness, lipid phase and sterol type are determining factors in the permeability of membranes to small solutes,” *Nature Communications*, vol. 13, 1 2022, ISSN: 20411723. DOI: 10.1038/s41467-022-29272-x.
- [77] L. B. Li, I. Vorobyov, and T. W. Allen, “The role of membrane thickness in charged protein-lipid interactions,” *Biochimica et Biophysica Acta - Biomembranes*, vol. 1818, pp. 135–145, 2 Feb. 2012, ISSN: 00052736. DOI: 10.1016/j.bbamem.2011.10.026.
- [78] X. Liao and P. K. Purohit, “Kinetics of self-assembly of inclusions due to lipid membrane thickness interactions,” *Soft Matter*, vol. 17, 9 2021, ISSN: 17446848. DOI: 10.1039/d0sm01752c.
- [79] B. E. Uygun, T. Bou-Akl, M. Albanna, and H. W. Matthew, “Membrane thickness is an important variable in membrane scaffolds: Influence of chitosan membrane structure on the behavior of cells,” *Acta Biomaterialia*, vol. 6, 6 2010, ISSN: 17427061. DOI: 10.1016/j.actbio.2009.11.018.
- [80] A. Anishkin, S. H. Loukin, J. Teng, and C. Kung, *Feeling the hidden mechanical forces in lipid bilayer is an original sense*, 2014. DOI: 10.1073/pnas.1313364111.
- [81] O. S. Andersen and R. E. Koeppe, *Bilayer thickness and membrane protein function: An energetic perspective*, 2007. DOI: 10.1146/annurev.biophys.36.040306.132643.
- [82] J. A. Lundbæk, S. A. Collingwood, H. I. Ingólfsson, R. Kapoor, and O. S. Andersen, *Lipid bilayer regulation of membrane protein function: Gramicidin channels as molecular force probes*, 2010. DOI: 10.1098/rsif.2009.0443.
- [83] A. R. Battle, P. Ridone, N. Bavi, Y. Nakayama, Y. A. Nikolaev, and B. Martinac, *Lipid-protein interactions: Lessons learned from stress*, 2015. DOI: 10.1016/j.bbamem.2015.04.012.
- [84] H. Träuble and D. H. Haynes, “The volume change in lipid bilayer lamellae at the crystalline-liquid crystalline phase transition,” *Chemistry and Physics of Lipids*, vol. 7, 4 1971, ISSN: 00093084. DOI: 10.1016/0009-3084(71)90010-7.
- [85] H. W. Huang, “Deformation free energy of bilayer membrane and its effect on gramicidin channel lifetime,” *Biophysical Journal*, vol. 50, 6 1986, ISSN: 00063495. DOI: 10.1016/S0006-3495(86)83550-0.
- [86] N. Dan, P. Pincus, and S. A. Safran, *Membrane-induced interactions between inclusions*, 1993. DOI: 10.1021/la00035a005.
- [87] R. Phillips, T. Ursell, P. Wiggins, and P. Sens, *Emerging roles for lipids in shaping membrane-protein function*, 2009. DOI: 10.1038/nature08147.
- [88] I. M. Alarifi, *A comprehensive review on advancements of elastomers for engineering applications*, 2023. DOI: 10.1016/j.aiepr.2023.05.001.

- [89] S. R. Lavoie, P. Millereau, C. Creton, R. Long, and T. Tang, “A continuum model for progressive damage in tough multinetwork elastomers,” *Journal of the Mechanics and Physics of Solids*, vol. 125, 2019, ISSN: 00225096. DOI: 10.1016/j.jmps.2019.01.001.
- [90] Y. Zhang, C. Xuan, Y. Jiang, and Y. Huo, “Continuum mechanical modeling of liquid crystal elastomers as dissipative ordered solids,” *Journal of the Mechanics and Physics of Solids*, vol. 126, 2019, ISSN: 00225096. DOI: 10.1016/j.jmps.2019.02.018.
- [91] A. Ricker and P. Wriggers, *Systematic fitting and comparison of hyperelastic continuum models for elastomers*, 2023. DOI: 10.1007/s11831-022-09865-x.
- [92] H. Darijani and R. Naghdabadi, “Hyperelastic materials behavior modeling using consistent strain energy density functions,” *Acta Mechanica*, vol. 213, 3-4 2010, ISSN: 00015970. DOI: 10.1007/s00707-009-0239-3.
- [93] R. Ogden, “Non-linear elastic deformations,” *Engineering Analysis with Boundary Elements*, vol. 1, 2 1984, ISSN: 09557997. DOI: 10.1016/0955-7997(84)90049-3.
- [94] A. Anssari-Benam and A. Bucchi, “A generalised neo-hookean strain energy function for application to the finite deformation of elastomers,” *International Journal of Non-Linear Mechanics*, vol. 128, 2021, ISSN: 00207462. DOI: 10.1016/j.ijnonlinmec.2020.103626.
- [95] M. C. Boyce and E. M. Arruda, “Swelling and mechanical stretching of elastomeric materials,” *Mathematics and Mechanics of Solids*, vol. 6, 6 2001, ISSN: 10812865. DOI: 10.1177/108128650100600605.
- [96] L. Bokobza and M. Kolodziej, “On the use of carbon nanotubes as reinforcing fillers for elastomeric materials,” *Polymer International*, vol. 55, 9 2006, ISSN: 09598103. DOI: 10.1002/pi.2064.
- [97] D. J. Steigmann, “Fluid films with curvature elasticity,” *Archive for Rational Mechanics and Analysis*, vol. 150, 2 1999, ISSN: 00039527. DOI: 10.1007/s002050050183.
- [98] D. J. Steigmann, “On the relationship between the cosserat and kirchhoff-love theories of elastic shells,” *Mathematics and Mechanics of Solids*, vol. 4, 3 1999, ISSN: 10812865. DOI: 10.1177/108128659900400301.
- [99] C. Goodbrake and D. J. Steigmann, “Mechanics of an elastic membrane infused with a liquid,” *International Journal of Mechanical Sciences*, vol. 149, 2018, ISSN: 00207403. DOI: 10.1016/j.ijmecsci.2017.07.062.
- [100] I. Sokolnikoff, *Tensor Analysis: Theory and Applications* (Applied mathematics series). Wiley, 1951. [Online]. Available: https://books.google.ca/books?id=q_pQAAAAMAAJ.
- [101] P. B. Canham, “The minimum energy of bending as a possible explanation of the biconcave shape of the human red blood cell,” *Journal of Theoretical Biology*, vol. 26, 1 1970, ISSN: 10958541. DOI: 10.1016/S0022-5193(70)80032-7.

- [102] W. Helfrich, “Elastic properties of lipid bilayers: Theory and possible experiments,” *Zeitschrift fur Naturforschung - Section C Journal of Biosciences*, vol. 28, 11-12 1973, ISSN: 18657125. DOI: 10.1515/znc-1973-11-1209.
- [103] B. Seguin and E. Fried, “Microphysical derivation of the canham-helfrich free-energy density,” *Journal of Mathematical Biology*, vol. 68, 3 2014, ISSN: 14321416. DOI: 10.1007/s00285-013-0647-9.
- [104] A. Kossa, M. T. Valentine, and R. M. McMeeking, “Analysis of the compressible, isotropic, neo-hookean hyperelastic model,” *Meccanica*, vol. 58, 1 2023, ISSN: 15729648. DOI: 10.1007/s11012-022-01633-2.
- [105] L. V. Chernomordik and M. M. Kozlov, *Mechanics of membrane fusion*, Jul. 2008. DOI: 10.1038/nsmb.1455.
- [106] M. Lenz, S. Morlot, and A. Roux, *Mechanical requirements for membrane fission: Common facts from various examples*, 2009. DOI: 10.1016/j.febslet.2009.11.012.
- [107] J. E. Rothman, “The machinery and principles of vesicle transport in the cell,” *Nature medicine*, vol. 8, no. 10, pp. 1059–1062, 2002. DOI: <https://doi.org/10.1038/nm770>.
- [108] A. Agrawal and D. J. Steigmann, “Coexistent fluid-phase equilibria in biomembranes with bending elasticity,” *Journal of Elasticity*, vol. 93, 1 2008, ISSN: 03743535. DOI: 10.1007/s10659-008-9165-1.
- [109] A. Agrawal and D. J. Steigmann, “Boundary-value problems in the theory of lipid membranes,” *Continuum Mechanics and Thermodynamics*, vol. 21, pp. 57–82, 1 Jun. 2009, ISSN: 09351175. DOI: 10.1007/s00161-009-0102-8.
- [110] D. J. Steigmann, “Mechanics and physics of lipid bilayers,” *The role of mechanics in the study of lipid bilayers*, pp. 1–61, 2018. [Online]. Available: https://link.springer.com/chapter/10.1007/978-3-319-56348-0_1.
- [111] T. Belay, C. I. Kim, and P. Schiavone, “Analytical solution of lipid membrane morphology subjected to boundary forces on the edges of rectangular membranes,” *Continuum Mechanics and Thermodynamics*, vol. 28, 1-2 2016, ISSN: 09351175. DOI: 10.1007/s00161-015-0426-5.
- [112] E. Gorter and F. Grendel, “On bimolecular layers of lipoids on the chromocytes of the blood,” *Journal of Experimental Medicine*, vol. 41, 4 1925, ISSN: 15409538. DOI: 10.1084/jem.41.4.439.
- [113] J. D. Robertson, “The ultrastructure of cell membranes and their derivatives,” *Biochemical Society symposium*, vol. 16, pp. 3–43, 1959. [Online]. Available: <https://api.semanticscholar.org/CorpusID:7814193>.
- [114] P. M. Naghdi, “On a variational theorem in elasticity and its application to shell theory,” *Journal of Applied Mechanics, Transactions ASME*, vol. 31, 4 1964, ISSN: 15289036. DOI: 10.1115/1.3629726.

- [115] M. E. Gurtin, “The linear theory of elasticity,” in *Linear Theories of Elasticity and Thermoelasticity: Linear and Nonlinear Theories of Rods, Plates, and Shells*, C. Truesdell, Ed. Berlin, Heidelberg: Springer Berlin Heidelberg, 1973, pp. 1–295, ISBN: 978-3-662-39776-3. DOI: 10.1007/978-3-662-39776-3_1. [Online]. Available: https://doi.org/10.1007/978-3-662-39776-3_1.
- [116] W. Helfrich, “Elastic properties of lipid bilayers: Theory and possible experiments,” *Zeitschrift fur Naturforschung - Section C Journal of Biosciences*, vol. 28, 11-12 1973, ISSN: 18657125. DOI: 10.1515/znc-1973-11-1209.
- [117] T. Belay, K. C. Il, and P. Schiavone, “Mechanics of a lipid bilayer subjected to thickness distension and membrane budding,” *Mathematics and Mechanics of Solids*, vol. 23, 1 2018, ISSN: 17413028. DOI: 10.1177/1081286516666136.
- [118] T. Belay, C. I. Kim, and P. Schiavone, “Bud formation of lipid membranes in response to the surface diffusion of transmembrane proteins and line tension,” *Mathematics and Mechanics of Solids*, vol. 22, 11 2017, ISSN: 17413028. DOI: 10.1177/1081286516657684.
- [119] M. Zeidi and C. I. Kim, “Notes on superposed incremental deformations in the mechanics of lipid membranes,” *Mathematics and Mechanics of Solids*, vol. 24, 1 2019, ISSN: 17413028. DOI: 10.1177/1081286517734608.
- [120] C. I. Kim, “A discussion on the mechanics of lipid membranes: Lagrange multipliers and a singular substrate,” *Zeitschrift fur Angewandte Mathematik und Physik*, vol. 68, 4 2017, ISSN: 00442275. DOI: 10.1007/s00033-017-0825-5.
- [121] A. Agrawal and D. J. Steigmann, “Modeling protein-mediated morphology in biomembranes,” *Biomechanics and Modeling in Mechanobiology*, vol. 8, 5 2009, ISSN: 16177959. DOI: 10.1007/s10237-008-0143-0.
- [122] N. Walani, J. Torres, and A. Agrawal, “Anisotropic spontaneous curvatures in lipid membranes,” *Physical Review E - Statistical, Nonlinear, and Soft Matter Physics*, vol. 89, 6 2014, ISSN: 15502376. DOI: 10.1103/PhysRevE.89.062715.
- [123] P. Rangamani, A. Agrawal, K. K. Mandadapu, G. Oster, and D. J. Steigmann, “Interaction between surface shape and intra-surface viscous flow on lipid membranes,” *Biomechanics and Modeling in Mechanobiology*, vol. 12, 4 2013, ISSN: 16177959. DOI: 10.1007/s10237-012-0447-y.
- [124] D. J. Steigmann, “Fluid films with curvature elasticity,” *Archive for Rational Mechanics and Analysis*, vol. 150, 2 1999, ISSN: 00039527. DOI: 10.1007/s002050050183.
- [125] D. J. Steigmann, “On the relationship between the cosserat and kirchhoff-love theories of elastic shells,” *Mathematics and Mechanics of Solids*, vol. 4, 3 1999, ISSN: 10812865. DOI: 10.1177/108128659900400301.
- [126] M. Zeidi and C. I. Kim, “The effects of intra-membrane viscosity on lipid membrane morphology: Complete analytical solution,” *Scientific Reports*, vol. 8, 1 2018, ISSN: 20452322. DOI: 10.1038/s41598-018-31251-6.

- [127] D. J. Steigmann, “A model for lipid membranes with tilt and distension based on three-dimensional liquid crystal theory,” *International Journal of Non-Linear Mechanics*, vol. 56, 2013, ISSN: 00207462. DOI: 10.1016/j.ijnonlinmec.2013.02.006.
- [128] P. Rangamani and D. J. Steigmann, “Variable tilt on lipid membranes,” *Proceedings of the Royal Society A: Mathematical, Physical and Engineering Sciences*, vol. 470, 2172 2014, ISSN: 14712946. DOI: 10.1098/rspa.2014.0463.
- [129] C. I. Kim and D. J. Steigmann, “Distension-induced gradient capillarity in lipid membranes,” *Continuum Mechanics and Thermodynamics*, vol. 27, 4-5 2015, ISSN: 09351175. DOI: 10.1007/s00161-014-0333-1.
- [130] J. L. Ericksen, “Conservation laws for liquid crystals,” *Transactions of the Society of Rheology*, vol. 5, 1 1961, ISSN: 0038-0032. DOI: 10.1122/1.548883.
- [131] J. L. Ericksen, “Hydrostatic theory of liquid crystals,” *Archive for Rational Mechanics and Analysis*, vol. 9, 1 1962, ISSN: 00039527. DOI: 10.1007/BF00253358.
- [132] J. Ericksen, “Equilibrium theory of liquid crystals,” in 1976. DOI: 10.1016/b978-0-12-025002-8.50012-9.
- [133] A. Agrawal and D. J. Steigmann, “A model for surface diffusion of transmembrane proteins on lipid bilayers,” *Zeitschrift fur Angewandte Mathematik und Physik*, vol. 62, 3 2011, ISSN: 00442275. DOI: 10.1007/s00033-011-0132-5.
- [134] A. Mahapatra, D. Saintillan, and P. Rangamani, “Transport phenomena in fluid films with curvature elasticity,” *Journal of Fluid Mechanics*, 2020, ISSN: 14697645. DOI: 10.1017/jfm.2020.711.
- [135] R. C. Capeta, J. A. Poveda, and L. M. Loura, “Non-uniform membrane probe distribution in resonance energy transfer: Application to protein-lipid selectivity,” vol. 16, 2006. DOI: 10.1007/s10895-005-0036-x.
- [136] D. Kabaso *et al.*, “Attachment of rod-like (bar) proteins and membrane shape,” *Mini Reviews in Medicinal Chemistry*, vol. 11, 4 2011, ISSN: 13895575. DOI: 10.2174/138955711795305353.
- [137] R. Ogden, “Non-linear elastic deformations,” *Engineering Analysis with Boundary Elements*, vol. 1, 2 1984, ISSN: 09557997. DOI: 10.1016/0955-7997(84)90049-3.
- [138] D. J. Steigmann, *Finite elasticity theory*. 2017. DOI: 10.1093/oso/9780198567783.001.0001.
- [139] K. I. Tsubota, S. Wada, and H. Liu, “Elastic behavior of a red blood cell with the membrane’s nonuniform natural state: Equilibrium shape, motion transition under shear flow, and elongation during tank-treading motion,” *Biomechanics and Modeling in Mechanobiology*, vol. 13, 4 2014, ISSN: 16177940. DOI: 10.1007/s10237-013-0530-z.

- [140] B. Blasi, A. D'Alessandro, N. Ramundo, and L. Zolla, "Red blood cell storage and cell morphology," *Transfusion Medicine*, vol. 22, 2 2012, ISSN: 09587578. DOI: 10.1111/j.1365-3148.2012.01139.x.
- [141] N. M. Geekiyanage *et al.*, "A coarse-grained red blood cell membrane model to study stomatocyte-discocyteechinocyte morphologies," *PLoS ONE*, vol. 14, 4 Apr. 2019, ISSN: 19326203. DOI: 10.1371/journal.pone.0215447.
- [142] C. Spier, "Wintrobe's atlas of clinical hematology," *American Journal of Surgical Pathology*, vol. 32, 9 2008, ISSN: 0147-5185. DOI: 10.1097/pas.0b013e31816955c5.
- [143] I. S. Sokolnikoff and M. J. Walker, "Tensor analysis: Theory and applications," *American Journal of Physics*, vol. 20, 4 1952, ISSN: 0002-9505. DOI: 10.1119/1.1933186.
- [144] R. M. Hochmuth and R. E. Waugh, "Erythrocyte membrane elasticity and viscosity," *Annual Review of Physiology*, vol. Vol. 49, 1987, ISSN: 00664278. DOI: 10.1146/annurev.ph.49.030187.001233.
- [145] I. Derényi, F. Jülicher, and J. Prost, "Erratum: Formation and interaction of membrane tubes [phys. rev. lett.prltao0031-9007 88, 238101 (2002)]," *Phys. Rev. Lett.*, vol. 89, p. 209901, 20 2002. DOI: 10.1103/PhysRevLett.89.209901. [Online]. Available: <https://link.aps.org/doi/10.1103/PhysRevLett.89.209901>.
- [146] K. J. V. Vliet and P. Hinterdorfer, "Probing drug-cell interactions," *Nano Today*, vol. 1, 3 2006, ISSN: 17480132. DOI: 10.1016/S1748-0132(06)70076-7.
- [147] P. G. Gallagher, *Red cells red cell membrane disorders*, 2005. [Online]. Available: <http://ashpublications.org/hematology/article-pdf/2005/1/13/645048/013.pdf>.
- [148] L. Blanc and L. C. Wolfe, "Chapter 7 - general considerations of hemolytic diseases, red cell membrane, and enzyme defects," in *Lanzkowsky's Manual of Pediatric Hematology and Oncology (Seventh Edition)*, J. D. Fish, J. M. Lipton, and P. Lanzkowsky, Eds., Seventh Edition, Academic Press, 2022, pp. 125–149, ISBN: 978-0-12-821671-2. DOI: <https://doi.org/10.1016/B978-0-12-821671-2.00030-1>. [Online]. Available: <https://www.sciencedirect.com/science/article/pii/B9780128216712000301>.
- [149] A. M. Mathai, "A handbook of generalized special functions for statistical and physical sciences," 1993. [Online]. Available: <https://api.semanticscholar.org/CorpusID:118403333>.
- [150] J. B. Seaborn, *Hypergeometric functions and their applications*. Springer Science & Business Media, 2013, vol. 8. DOI: <https://doi.org/10.1007/978-1-4757-5443-8>.
- [151] A. Escudero *et al.*, "Effect of dietary (n-9), (n-6) and (n-3) fatty acids on membrane lipid composition and morphology of rat erythrocytes," *Biochimica et Biophysica Acta - Lipids and Lipid Metabolism*, vol. 1394, 1 1998, ISSN: 00052760. DOI: 10.1016/S0005-2760(98)00095-2.

- [152] H. W. Lim, M. Wortis, and R. Mukhopadhyay, “Stomatocyte-discocyte-echinocyte sequence of the human red blood cell: Evidence for the bilayer-couple hypothesis from membrane mechanics,” *Proceedings of the National Academy of Sciences of the United States of America*, vol. 99, 26 2002, ISSN: 00278424. DOI: 10.1073/pnas.202617299.
- [153] S. Muñoz, J. L. Sebastián, M. Sancho, and G. Álvarez, “Elastic energy of the discocyte-stomatocyte transformation,” *Biochimica et Biophysica Acta - Biomembranes*, vol. 1838, 3 2014, ISSN: 00052736. DOI: 10.1016/j.bbamem.2013.10.020.
- [154] C. A. Galán, A. Mulero, and F. Cuadros, “Calculation of the surface tension and the surface energy of lennard-jones fluids from the radial distribution function in the liquid phase,” *Molecular Physics*, vol. 103, 4 2005, ISSN: 00268976. DOI: 10.1080/00268970512331317372.
- [155] T. D. Gurkov and P. A. Kralchevsky, “Surface tension and surface energy of curved interfaces and membranes,” *Colloids and Surfaces*, vol. 47, C 1990, ISSN: 01666622. DOI: 10.1016/0166-6622(90)80061-8.
- [156] W. Helfrich, “Elastic properties of lipid bilayers: Theory and possible experiments,” *Zeitschrift für Naturforschung c*, vol. 28, no. 11-12, pp. 693–703, 1973. DOI: 10.1515/znc-1973-11-1209.
- [157] E. A. Evans and R. Skalak, *Mechanics and thermodynamics of biomembranes*. 2018. DOI: 10.1201/9781351074339.
- [158] T. W. Secomb and R. Skalak, “Surface flow of viscoelastic membranes in viscous fluids,” *Quarterly Journal of Mechanics and Applied Mathematics*, vol. 35, 2 1982, ISSN: 00335614. DOI: 10.1093/qjmam/35.2.233.
- [159] U. Seifert, “Configurations of fluid membranes and vesicles,” *Advances in Physics*, vol. 46, 1 1997, ISSN: 14606976. DOI: 10.1080/00018739700101488.
- [160] M. Jarić, U. Seifert, W. Wintz, and M. Wortis, “Vesicular instabilities: The prolate-to-oblate transition and other shape instabilities of fluid bilayer membranes,” *Physical Review E*, vol. 52, no. 6, p. 6623, 1995. DOI: 10.1103/physreve.52.6623.
- [161] E. Gorter and F. Grendel, “On bimolecular layers of lipoids on the chromocytes of the blood,” *Journal of Experimental Medicine*, vol. 41, 4 1925, ISSN: 15409538. DOI: 10.1084/jem.41.4.439.
- [162] J. D. Robertson, “The ultrastructure of cell membranes and their derivatives.,” *Biochemical Society symposium*, vol. 16, pp. 3–43, 1959. [Online]. Available: <https://api.semanticscholar.org/CorpusID:7814193>.
- [163] P. M. Naghdi, “On a variational theorem in elasticity and its application to shell theory,” *Journal of Applied Mechanics, Transactions ASME*, vol. 31, 4 1964, ISSN: 15289036. DOI: 10.1115/1.3629726.
- [164] P. M. Naghdi, “The theory of shells and plates,” in 1973. DOI: 10.1007/978-3-662-39776-3_5.

- [165] T. Belay, C. I. Kim, and P. Schiavone, “Mechanics of a lipid bilayer subjected to thickness distension and membrane budding,” *Mathematics and Mechanics of Solids*, vol. 23, 1 2018, ISSN: 17413028. DOI: 10.1177/1081286516666136.
- [166] T. Belay, C. I. Kim, and P. Schiavone, “Bud formation of lipid membranes in response to the surface diffusion of transmembrane proteins and line tension,” *Mathematics and Mechanics of Solids*, vol. 22, 11 2017, ISSN: 17413028. DOI: 10.1177/1081286516657684.
- [167] A. Agrawal and D. J. Steigmann, “Boundary-value problems in the theory of lipid membranes,” *Continuum Mechanics and Thermodynamics*, vol. 21, 1 2009, ISSN: 09351175. DOI: 10.1007/s00161-009-0102-8.
- [168] T. Belay, C. I. Kim, and P. Schiavone, “Interaction-induced morphological transitions of lipid membranes in contact with an elliptical cross section of a rigid substrate,” *Journal of Applied Mechanics, Transactions ASME*, vol. 83, 1 2016, ISSN: 15289036. DOI: 10.1115/1.4031485.
- [169] A. Agrawal and D. J. Steigmann, “Coexistent fluid-phase equilibria in biomembranes with bending elasticity,” *Journal of Elasticity*, vol. 93, 1 2008, ISSN: 03743535. DOI: 10.1007/s10659-008-9165-1.
- [170] A. Agrawal and D. J. Steigmann, “Modeling protein-mediated morphology in biomembranes,” *Biomechanics and Modeling in Mechanobiology*, vol. 8, 5 2009, ISSN: 16177959. DOI: 10.1007/s10237-008-0143-0.
- [171] K. I. Tsubota, S. Wada, and H. Liu, “Elastic behavior of a red blood cell with the membrane’s nonuniform natural state: Equilibrium shape, motion transition under shear flow, and elongation during tank-treading motion,” *Biomechanics and Modeling in Mechanobiology*, vol. 13, pp. 735–746, 4 2014, ISSN: 16177940. DOI: 10.1007/s10237-013-0530-z.
- [172] B. Blasi, A. D’Alessandro, N. Ramundo, and L. Zolla, “Red blood cell storage and cell morphology,” *Transfusion Medicine*, vol. 22, 2 2012, ISSN: 09587578. DOI: 10.1111/j.1365-3148.2012.01139.x.
- [173] K. J. V. Vliet and P. Hinterdorfer, “Probing drug-cell interactions,” *Nano Today*, vol. 1, 3 2006, ISSN: 17480132. DOI: 10.1016/S1748-0132(06)70076-7.
- [174] E. A. Evans, “Bending resistance and chemically induced moments in membrane bilayers,” *Biophysical Journal*, vol. 14, 12 1974, ISSN: 00063495. DOI: 10.1016/S0006-3495(74)85959-X.
- [175] P. B. Canham, “The minimum energy of bending as a possible explanation of the biconcave shape of the human red blood cell,” *Journal of Theoretical Biology*, vol. 26, 1 1970, ISSN: 10958541. DOI: 10.1016/S0022-5193(70)80032-7.
- [176] P. Rangamani, A. Agrawal, K. K. Mandadapu, G. Oster, and D. J. Steigmann, “Interaction between surface shape and intra-surface viscous flow on lipid membranes,” *Biomechanics and Modeling in Mechanobiology*, vol. 12, pp. 833–845, 4 Aug. 2013, ISSN: 16177959. DOI: 10.1007/s10237-012-0447-y.

- [177] M. Zeidi and C. I. Kim, “The effects of intra-membrane viscosity on lipid membrane morphology: Complete analytical solution,” *Scientific Reports*, vol. 8, 1 2018, ISSN: 20452322. DOI: 10.1038/s41598-018-31251-6.
- [178] Z. Liu and C. il Kim, “Deformation analysis of lipid membranes subjected to general forms of intra-membrane viscous flow and interactions with an elliptical-cross-section substrate,” *Scientific Reports*, vol. 10, 1 2020, ISSN: 20452322. DOI: 10.1038/s41598-019-57179-z.
- [179] W. Yao and C. I. Kim, “An analysis of lipid membrane morphology in the presence of coordinate-dependent non-uniformity,” *Mathematics and Mechanics of Solids*, vol. 26, no. 1, pp. 45–61, 2021. DOI: 10.1177/1081286520939162.
- [180] M. Zeidi and C. I. Kim, “Notes on superposed incremental deformations in the mechanics of lipid membranes,” *Mathematics and Mechanics of Solids*, vol. 24, 1 2019, ISSN: 17413028. DOI: 10.1177/1081286517734608.
- [181] C. I. Kim, “A discussion on the mechanics of lipid membranes: Lagrange multipliers and a singular substrate,” *Zeitschrift für Angewandte Mathematik und Physik*, vol. 68, 4 2017, ISSN: 00442275. DOI: 10.1007/s00033-017-0825-5.
- [182] T. Belay, C. I. Kim, and P. Schiavone, “Analytical solution of lipid membrane morphology subjected to boundary forces on the edges of rectangular membranes,” *Continuum Mechanics and Thermodynamics*, vol. 28, 1-2 2016, ISSN: 09351175. DOI: 10.1007/s00161-015-0426-5.
- [183] P. F. Franck *et al.*, “Uncoupling of the membrane skeleton from the lipid bilayer. the cause of accelerated phospholipid flip-flop leading to an enhanced procoagulant activity of sickled cells,” *Journal of Clinical Investigation*, vol. 75, 1 1985, ISSN: 00219738. DOI: 10.1172/JCI111672.
- [184] W. C. Hwang and R. E. Waugh, “Energy of dissociation of lipid bilayer from the membrane skeleton of red blood cells,” *Biophysical Journal*, vol. 72, 6 1997, ISSN: 00063495. DOI: 10.1016/S0006-3495(97)78910-0.
- [185] D. Allan and P. Raval, “Some morphological consequences of uncoupling the lipid bilayer from the plasma membrane skeleton in intact erythrocytes,” *Biomedica Biochimica Acta*, vol. 42, 11-12 1983, ISSN: 0232766X.
- [186] H. J. Müller and H. J. Galla, “Pressure variation of the lateral diffusion in lipid bilayer membranes,” *BBA - Biomembranes*, vol. 733, 2 1983, ISSN: 00052736. DOI: 10.1016/0005-2736(83)90535-7.
- [187] P. G. Saffman and M. Delbrueck, “Brownian motion in biological membranes,” *Proceedings of the National Academy of Sciences of the United States of America*, vol. 72, 8 1975, ISSN: 00278424. DOI: 10.1073/pnas.72.8.3111.
- [188] S. T. Mohyud-Din, M. A. Noor, and K. I. Noor, “Modified variation of parameters method for second-order integro-differential equations and coupled systems,” *World Applied Sciences Journal*, vol. 6, pp. 1139–1146, 8 2009, ISSN: 1818-4952.

- [189] M. A. Noor, S. T. Mohyud-Din, and A. Waheed, "Variation of parameters method for solving fifth-order boundary value problems," *Applied Mathematics and Information Sciences*, vol. 2, 2 2008, ISSN: 19350090.
- [190] A. Escudero *et al.*, "Effect of dietary (n-9), (n-6) and (n-3) fatty acids on membrane lipid composition and morphology of rat erythrocytes," *Biochimica et Biophysica Acta - Lipids and Lipid Metabolism*, vol. 1394, 1 1998, ISSN: 00052760. DOI: 10.1016/S0005-2760(98)00095-2.
- [191] M. Girasole, A. Cricenti, R. Generosi, A. Congiu-Castellano, G. Boumis, and G. Amiconi, "Artificially induced unusual shape of erythrocytes: Anatomic force microscopy study," *Journal of Microscopy*, vol. 204, 1 2001, ISSN: 00222720. DOI: 10.1046/j.1365-2818.2001.00937.x.
- [192] C. I. Kim and D. J. Steigmann, "Distension-induced gradient capillarity in lipid membranes," *Continuum Mechanics and Thermodynamics*, vol. 27, 4-5 2015, ISSN: 09351175. DOI: 10.1007/s00161-014-0333-1.
- [193] D. J. Steigmann, "On the relationship between the cosserat and kirchhoff-love theories of elastic shells," *Mathematics and Mechanics of Solids*, vol. 4, 3 1999, ISSN: 10812865. DOI: 10.1177/108128659900400301.
- [194] D. J. Steigmann, "Fluid films with curvature elasticity," *Archive for Rational Mechanics and Analysis*, vol. 150, 2 1999, ISSN: 00039527. DOI: 10.1007/s002050050183.
- [195] R. M. Hochmuth and R. E. Waugh, "Erythrocyte membrane elasticity and viscosity," *Annual Review of Physiology*, vol. Vol. 49, 1987, ISSN: 00664278. DOI: 10.1146/annurev.ph.49.030187.001233.
- [196] I. Derényi, F. Jülicher, and J. Prost, "Formation and interaction of membrane tubes," *Physical Review Letters*, vol. 88, 23 2002, ISSN: 10797114. DOI: 10.1103/PhysRevLett.88.238101.
- [197] "Interaction between surface shape and intra-surface viscous flow on lipid membranes," *Biomechanics and Modeling in Mechanobiology*, vol. 12, pp. 833–845, 4 Aug. 2013, ISSN: 16177959. DOI: 10.1007/s10237-012-0447-y.
- [198] P. Rangamani and D. J. Steigmann, "Variable tilt on lipid membranes," *Proceedings of the Royal Society A: Mathematical, Physical and Engineering Sciences*, vol. 470, 2172 2014, ISSN: 14712946. DOI: 10.1098/rspa.2014.0463.
- [199] N. M. Geekiyanage *et al.*, "A coarse-grained red blood cell membrane model to study stomatocyte-discocyteechinocyte morphologies," *PLoS ONE*, vol. 14, 4 2019, ISSN: 19326203. DOI: 10.1371/journal.pone.0215447.
- [200] G. Lim, M. Wortis, and R. Mukhopadhyay, *Stomatocyte-discocyte-echinocyte sequence of the human red blood cell: Evidence for the bilayer-couple hypothesis from membrane mechanics*, 2002. [Online]. Available: www.pnas.org/cgi/doi/10.1073/pnas.202617299.

- [201] S. Muñoz, J. L. Sebastián, M. Sancho, and G. Álvarez, “Elastic energy of the discocyte-stomatocyte transformation,” *Biochimica et Biophysica Acta - Biomembranes*, vol. 1838, 3 2014, ISSN: 00052736. DOI: 10.1016/j.bbamem.2013.10.020.
- [202] U. Seifert and R. Lipowsky, “Chapter 8 - morphology of vesicles,” in *Structure and Dynamics of Membranes*, ser. Handbook of Biological Physics, R. Lipowsky and E. Sackmann, Eds., vol. 1, North-Holland, 1995, pp. 403–463. DOI: [https://doi.org/10.1016/S1383-8121\(06\)80025-4](https://doi.org/10.1016/S1383-8121(06)80025-4). [Online]. Available: <https://www.sciencedirect.com/science/article/pii/S1383812106800254>.
- [203] G. Cevc and H. Richardsen, “Lipid vesicles and membrane fusion,” *Advanced Drug Delivery Reviews*, vol. 38, 3 1999, ISSN: 0169409X. DOI: 10.1016/S0169-409X(99)00030-7.
- [204] J. Yoo, M. B. Jackson, and Q. Cui, “A comparison of coarse-grained and continuum models for membrane bending in lipid bilayer fusion pores,” *Biophysical Journal*, vol. 104, 4 2013, ISSN: 00063495. DOI: 10.1016/j.bpj.2012.12.043.
- [205] S. P. Fu, Z. Peng, H. Yuan, R. Kfoury, and Y. N. Young, “Lennard-jones type pair-potential method for coarse-grained lipid bilayer membrane simulations in lammps,” *Computer Physics Communications*, vol. 210, 2017, ISSN: 00104655. DOI: 10.1016/j.cpc.2016.09.018.
- [206] I. Hanasaki, J. H. Walther, S. Kawano, and P. Koumoutsakos, “Coarse-grained molecular dynamics simulations of shear-induced instabilities of lipid bilayer membranes in water,” *Physical Review E - Statistical, Nonlinear, and Soft Matter Physics*, vol. 82, 5 Nov. 2010, ISSN: 15393755. DOI: 10.1103/PhysRevE.82.051602.
- [207] W. Helfrich, “Elastic properties of lipid bilayers: Theory and possible experiments,” *Zeitschrift fur Naturforschung - Section C Journal of Biosciences*, vol. 28, 11-12 1973, ISSN: 18657125. DOI: 10.1515/znc-1973-11-1209.
- [208] A. Agrawal and D. J. Steigmann, “Boundary-value problems in the theory of lipid membranes,” *Continuum Mechanics and Thermodynamics*, vol. 21, 1 2009, ISSN: 09351175. DOI: 10.1007/s00161-009-0102-8.
- [209] W. Yao and C. I. Kim, *An analysis of lipid membrane morphology in the presence of coordinate-dependent non-uniformity*, 2021. DOI: 10.1177/1081286520939162.
- [210] T. Belay, C. I. Kim, and P. Schiavone, “Bud formation of lipid membranes in response to the surface diffusion of transmembrane proteins and line tension,” *Mathematics and Mechanics of Solids*, vol. 22, 11 2017, ISSN: 17413028. DOI: 10.1177/1081286516657684.
- [211] P. Rangamani, A. Agrawal, K. K. Mandadapu, G. Oster, and D. J. Steigmann, “Interaction between surface shape and intra-surface viscous flow on lipid membranes,” *Biomechanics and Modeling in Mechanobiology*, vol. 12, pp. 833–845, 4 Aug. 2013, ISSN: 16177959. DOI: 10.1007/s10237-012-0447-y.

- [212] M. Zeidi and C. I. Kim, “The effects of intra-membrane viscosity on lipid membrane morphology: Complete analytical solution,” *Scientific Reports*, vol. 8, 1 2018, ISSN: 20452322. DOI: 10.1038/s41598-018-31251-6.
- [213] C. I. Kim and D. J. Steigmann, “Distension-induced gradient capillarity in lipid membranes,” *Continuum Mechanics and Thermodynamics*, vol. 27, 4-5 2015, ISSN: 09351175. DOI: 10.1007/s00161-014-0333-1.
- [214] J. Frallicciardi, J. Melcr, P. Siginou, S. J. Marrink, and B. Poolman, “Membrane thickness, lipid phase and sterol type are determining factors in the permeability of membranes to small solutes,” *Nature Communications*, vol. 13, 1 2022, ISSN: 20411723. DOI: 10.1038/s41467-022-29272-x.
- [215] X. Liao and P. K. Purohit, “Kinetics of self-assembly of inclusions due to lipid membrane thickness interactions,” *Soft Matter*, vol. 17, 9 2021, ISSN: 17446848. DOI: 10.1039/d0sm01752c.
- [216] A. Shrestha, O. Kahraman, and C. A. Haselwandter, “Regulation of membrane proteins through local heterogeneity in lipid bilayer thickness,” *Physical Review E*, vol. 102, 6 2020, ISSN: 24700053. DOI: 10.1103/PhysRevE.102.060401.
- [217] B. A. Camley, C. Esposito, T. Baumgart, and F. L. Brown, “Lipid bilayer domain fluctuations as a probe of membrane viscosity,” *Biophysical Journal*, vol. 99, 6 2010, ISSN: 15420086. DOI: 10.1016/j.bpj.2010.07.007.
- [218] M. Nagao, E. G. Kelley, R. Ashkar, R. Bradbury, and P. D. Butler, “Probing elastic and viscous properties of phospholipid bilayers using neutron spin echo spectroscopy,” *Journal of Physical Chemistry Letters*, vol. 8, 19 2017, ISSN: 19487185. DOI: 10.1021/acs.jpcllett.7b01830.
- [219] E. G. Kelley, P. D. Butler, R. Ashkar, R. Bradbury, and M. Nagao, “Scaling relationships for the elastic moduli and viscosity of mixed lipid membranes,” *Proceedings of the National Academy of Sciences of the United States of America*, vol. 117, 38 2020, ISSN: 10916490. DOI: 10.1073/pnas.2008789117.
- [220] M. Nagao *et al.*, “Relationship between viscosity and acyl tail dynamics in lipid bilayers,” *Physical Review Letters*, vol. 127, 7 2021, ISSN: 10797114. DOI: 10.1103/PhysRevLett.127.078102.
- [221] A. E. Cohen and Z. Shi, “Do cell membranes flow like honey or jiggle like jello?” *BioEssays*, vol. 42, 1 2020, ISSN: 15211878. DOI: 10.1002/bies.201900142.
- [222] A. L. L. Roux, X. Quiroga, N. Walani, M. Arroyo, and P. Roca-Cusachs, *The plasma membrane as a mechanochemical transducer*, 2019. DOI: 10.1098/rstb.2018.0221.
- [223] R. Illukkumbura, T. Bland, and N. W. Goehring, *Patterning and polarization of cells by intracellular flows*, 2020. DOI: 10.1016/j.ceb.2019.10.005.
- [224] A. Agrawal and D. J. Steigmann, “Modeling protein-mediated morphology in biomembranes,” *Biomechanics and Modeling in Mechanobiology*, vol. 8, pp. 371–379, 5 Oct. 2009, ISSN: 16177959. DOI: 10.1007/s10237-008-0143-0.

- [225] A. Agrawal and D. J. Steigmann, “A model for surface diffusion of transmembrane proteins on lipid bilayers,” *Zeitschrift für Angewandte Mathematik und Physik*, vol. 62, 3 2011, ISSN: 00442275. DOI: 10.1007/s00033-011-0132-5.
- [226] D. J. Steigmann and A. Agrawal, “Electromechanics of polarized lipid bilayers,” *Mathematics and Mechanics of Complex Systems*, vol. 4, pp. 31–54, 1 2016, ISSN: 23253444. DOI: 10.2140/memocs.2016.4.31.
- [227] R. A. Sauer and R. A. Sauer, *The role of mechanics in the study of lipid bilayers*, D. J. Steigmann, Ed. Springer, 2018, vol. 577, ISBN: 9783319563473.
- [228] P. Rangamani, A. Benjamini, A. Agrawal, B. Smit, D. J. Steigmann, and G. Oster, “Small scale membrane mechanics,” *Biomechanics and Modeling in Mechanobiology*, vol. 13, 4 2014, ISSN: 16177940. DOI: 10.1007/s10237-013-0528-6.
- [229] T. Belay, C. I. Kim, and P. Schiavone, “Mechanics of a lipid bilayer subjected to thickness distension and membrane budding,” *Mathematics and Mechanics of Solids*, vol. 23, pp. 67–84, 1 Jan. 2018, ISSN: 17413028. DOI: 10.1177/1081286516666136.
- [230] D. J. Steigmann, “A model for lipid membranes with tilt and distension based on three-dimensional liquid crystal theory,” *International Journal of Non-Linear Mechanics*, vol. 56, 2013, ISSN: 00207462. DOI: 10.1016/j.ijnonlinmec.2013.02.006.
- [231] D. Steigmann, E. Baesu, R. E. Rudd, J. Belak, and M. McElfresh, “On the variational theory of cell-membrane equilibria,” *Interfaces and Free Boundaries*, vol. 5, 4 2003, ISSN: 14639963. DOI: 10.4171/IFB/83.
- [232] W. Yao and C. I. Kim, “Deformation analysis of nonuniform lipid membrane subjected to local inflammations,” *Mathematics and Mechanics of Complex Systems*, vol. 9, 2 2021, ISSN: 23253444. DOI: 10.2140/MEMOCS.2021.9.203.
- [233] R. Aris, *Vectors, tensors, and the basic equations of fluid mechanics*, 1989.
- [234] B. Blasi, A. D’Alessandro, N. Ramundo, and L. Zolla, “Red blood cell storage and cell morphology,” *Transfusion Medicine*, vol. 22, 2 2012, ISSN: 09587578. DOI: 10.1111/j.1365-3148.2012.01139.x.
- [235] S. J. Marrink, H. J. Risselada, S. Yefimov, D. P. Tieleman, and A. H. D. Vries, “The martini force field: Coarse grained model for biomolecular simulations,” *Journal of Physical Chemistry B*, vol. 111, 27 2007, ISSN: 15206106. DOI: 10.1021/jp071097f.
- [236] A. M. Herrera-Rodríguez, V. Miletić, C. Aponte-Santamaría, and F. Gräter, “Molecular dynamics simulations of molecules in uniform flow,” *Biophysical Journal*, vol. 116, 9 2019, ISSN: 15420086. DOI: 10.1016/j.bpj.2018.12.025.
- [237] A. Kadoura, A. Salama, and S. Sun, “Switching between the nvt and npt ensembles using the reweighting and reconstruction scheme,” vol. 51, 2015. DOI: 10.1016/j.procs.2015.05.309.

- [238] S. Buchoux, “Fatslim: A fast and robust software to analyze md simulations of membranes,” *Bioinformatics*, vol. 33, 1 2017, ISSN: 14602059. DOI: 10.1093/bioinformatics/btw563.
- [239] R. Höller, F. Libisch, and C. Hellmich, “A membrane theory for circular graphene sheets, based on a hyperelastic material model for large deformations,” *Mechanics of Advanced Materials and Structures*, pp. 1–11, 2020, ISSN: 15376532. DOI: 10.1080/15376494.2020.1785598.
- [240] A. F. Bitbol, N. Puff, Y. Sakuma, M. Imai, J. B. Fournier, and M. I. Angelova, “Lipid membrane deformation in response to a local ph modification: Theory and experiments,” *Soft Matter*, vol. 8, 22 2012, ISSN: 1744683X. DOI: 10.1039/c2sm25519g.
- [241] H. W. Huang, “Deformation free energy of bilayer membrane and its effect on gramicidin channel lifetime,” *Biophysical Journal*, vol. 50, 6 1986, ISSN: 00063495. DOI: 10.1016/S0006-3495(86)83550-0.
- [242] N. Dan, P. Pincus, and S. A. Safran, *Membrane-induced interactions between inclusions*, 1993. DOI: 10.1021/la00035a005.
- [243] O. S. Andersen and R. E. Koeppe, *Bilayer thickness and membrane protein function: An energetic perspective*, 2007. DOI: 10.1146/annurev.biophys.36.040306.132643.
- [244] R. Phillips, T. Ursell, P. Wiggins, and P. Sens, *Emerging roles for lipids in shaping membrane-protein function*, 2009. DOI: 10.1038/nature08147.
- [245] A. Shrestha, O. Kahraman, and C. A. Haselwandter, “Mechanochemical coupling of lipid organization and protein function through membrane thickness deformations,” *Physical Review E*, vol. 105, 5 2022, ISSN: 24700053. DOI: 10.1103/PhysRevE.105.054410.
- [246] B. W. Peeters, A. C. Piët, and M. Fornerod, “Generating membrane curvature at the nuclear pore: A lipid point of view,” *Cells*, vol. 11, 3 2022, ISSN: 20734409. DOI: 10.3390/cells11030469.
- [247] A. C. Pipkin, “Stress analysis for fiber-reinforced materials,” *Advances in Applied Mechanics*, vol. 19, C 1979, ISSN: 00652156. DOI: 10.1016/S0065-2156(08)70308-9.
- [248] F. J. Lockett, “Deformations of fibre-reinforced materials: A. j. m. spencer clarendon press: Oxford university press (1972), £3-00,” 1973. [Online]. Available: <https://api.semanticscholar.org/CorpusID:139003333>.
- [249] D. K. Rajak, D. D. Pagar, P. L. Menezes, and E. Linul, *Fiber-reinforced polymer composites: Manufacturing, properties, and applications*, 2019. DOI: 10.3390/polym11101667.
- [250] D. Myung *et al.*, “Biomimetic strain hardening in interpenetrating polymer network hydrogels,” *Polymer*, vol. 48, 18 2007, ISSN: 00323861. DOI: 10.1016/j.polymer.2007.06.070.

- [251] R. E. Shadwick, “Mechanical design in arteries,” *Journal of Experimental Biology*, vol. 202, 23 1999, ISSN: 00220949. DOI: 10.1242/jeb.202.23.3305.
- [252] Y. Ma, X. Feng, J. A. Rogers, Y. Huang, and Y. Zhang, *Design and application of 'j-shaped' stress-strain behavior in stretchable electronics: A review*, 2017. DOI: 10.1039/c7lc00289k.
- [253] R. V. Martinez *et al.*, “Robotic tentacles with three-dimensional mobility based on flexible elastomers,” *Advanced Materials*, vol. 25, 2 2013, ISSN: 09359648. DOI: 10.1002/adma.201203002.
- [254] A. Gupta, G. K. Meena, and V. Singhal, “Strengthening of autoclaved aerated concrete (aac) masonry wallettes with fabric reinforced cementitious matrix for in-plane shear and out-of-plane loads,” *Structures*, vol. 51, 2023, ISSN: 23520124. DOI: 10.1016/j.istruc.2023.03.099.
- [255] Y. Wang, C. Gregory, and M. A. Minor, “Improving mechanical properties of molded silicone rubber for soft robotics through fabric compositing,” *Soft Robotics*, vol. 5, 3 2018, ISSN: 21695180. DOI: 10.1089/soro.2017.0035.
- [256] B. Yan *et al.*, “Duplicating dynamic strain-stiffening behavior and nanomechanics of biological tissues in a synthetic self-healing flexible network hydrogel,” *ACS Nano*, vol. 11, 11 2017, ISSN: 1936086X. DOI: 10.1021/acsnano.7b05109.
- [257] C. I. Kim and M. Zeidi, “Gradient elasticity theory for fiber composites with fibers resistant to extension and flexure,” *International Journal of Engineering Science*, vol. 131, 2018, ISSN: 00207225. DOI: 10.1016/j.ijengsci.2018.06.002.
- [258] J. F. Mulhern, T. G. Rogers, and A. J. Spencer, “A continuum theory of a plastic-elastic fibre-reinforced material,” *International Journal of Engineering Science*, vol. 7, 2 1969, ISSN: 00207225. DOI: 10.1016/0020-7225(69)90053-6.
- [259] A. C. Pipkin and T. G. Rogers, “Plane deformations of incompressible fiber-reinforced materials,” *Journal of Applied Mechanics, Transactions ASME*, vol. 38, 3 1971, ISSN: 15289036. DOI: 10.1115/1.3408866.
- [260] D. J. Steigmann, “Theory of elastic solids reinforced with fibers resistant to extension, flexure and twist,” *International Journal of Non-Linear Mechanics*, vol. 47, 7 2012, ISSN: 00207462. DOI: 10.1016/j.ijnonlinmec.2012.04.007.
- [261] D. J. Steigmann and F. dell’Isola, “Mechanical response of fabric sheets to three-dimensional bending, twisting, and stretching,” *Acta Mechanica Sinica/Lixue Xuebao*, vol. 31, 3 2015, ISSN: 16143116. DOI: 10.1007/s10409-015-0413-x.
- [262] M. Cuomo, F. dell’Isola, and L. Greco, “Simplified analysis of a generalized bias test for fabrics with two families of inextensible fibres,” *Zeitschrift fur Angewandte Mathematik und Physik*, vol. 67, 3 2016, ISSN: 00442275. DOI: 10.1007/s00033-016-0653-z.

- [263] F. dell’Isola, M. Cuomo, L. Greco, and A. D. Corte, “Bias extension test for pantographic sheets: Numerical simulations based on second gradient shear energies,” *Journal of Engineering Mathematics*, vol. 103, 1 2017, ISSN: 15732703. DOI: 10.1007/s10665-016-9865-7.
- [264] F. Dell’Isola, A. D. Corte, L. Greco, and A. Luongo, “Plane bias extension test for a continuum with two inextensible families of fibers: A variational treatment with lagrange multipliers and a perturbation solution,” *International Journal of Solids and Structures*, vol. 81, 2016, ISSN: 00207683. DOI: 10.1016/j.ijsolstr.2015.08.029.
- [265] S. Islam, D. Zhalmuratova, H. J. Chung, and C. I. Kim, “A model for hyperelastic materials reinforced with fibers resistance to extension and flexure,” *International Journal of Solids and Structures*, vol. 193-194, 2020, ISSN: 00207683. DOI: 10.1016/j.ijsolstr.2020.02.036.
- [266] S. Islam, S. E. S. Bolouri, and C. I. Kim, “Mechanics of hyperelastic composites reinforced with nonlinear elastic fibrous materials in finite plane elastostatics,” *International Journal of Engineering Science*, vol. 165, 2021, ISSN: 00207225. DOI: 10.1016/j.ijengsci.2021.103491.
- [267] M. H. Rahman, S. Yang, and C. I. Kim, “A third gradient-based continuum model for the mechanics of continua reinforced with extensible bidirectional fibers resistant to flexure,” *Continuum Mechanics and Thermodynamics*, vol. 35, 2 2023, ISSN: 14320959. DOI: 10.1007/s00161-023-01198-9.
- [268] A. Logg and G. N. Wells, “Dolfin: Automated finite element computing,” *ACM Transactions on Mathematical Software*, vol. 37, 2 2010, ISSN: 00983500. DOI: 10.1145/1731022.1731030.
- [269] A. Logg, G. N. Wells, and J. Hake, “Dolfin: A c++/python finite element library,” in 2012, vol. 84. DOI: 10.1007/978-3-642-23099-8_10.
- [270] H. Zhou, X. Xiao, K. Qian, K. Zhang, and D. Zhang, “Numerical and experimental analyses of out-of-plane deformation of triaxial woven fabric,” *Materials Research Express*, vol. 5, 5 2018, ISSN: 20531591. DOI: 10.1088/2053-1591/aac0d2.
- [271] S. L. Sagar, V. Singhal, and D. C. Rai, “In-plane and out-of-plane behavior of masonry-infilled rc frames strengthened with fabric-reinforced cementitious matrix,” *Journal of Composites for Construction*, vol. 23, 1 2019, ISSN: 1090-0268. DOI: 10.1061/(asce)cc.1943-5614.0000905.
- [272] G. Magenes and G. M. Calvi, “In-plane seismic response of brick masonry walls,” *Earthquake Engineering and Structural Dynamics*, vol. 26, 11 1997, ISSN: 00988847. DOI: 10.1002/(SICI)1096-9845(199711)26:11<1091::AID-EQE693>3.0.CO;2-6.
- [273] N. Ismail and J. M. Ingham, “In-plane and out-of-plane testing of unreinforced masonry walls strengthened using polymer textile reinforced mortar,” *Engineering Structures*, vol. 118, 2016, ISSN: 18737323. DOI: 10.1016/j.engstruct.2016.03.041.

- [274] S. W. Hahm and D. Y. Khang, “Crystallization and microstructure-dependent elastic moduli of ferroelectric p(vdf-trfe) thin films,” *Soft Matter*, vol. 6, 22 2010, ISSN: 1744683X. DOI: 10.1039/c0sm00350f.
- [275] J. Monecke, “Microstructure dependence of material properties of composites,” *physica status solidi (b)*, vol. 154, 2 1989, ISSN: 15213951. DOI: 10.1002/pssb.2221540239.
- [276] F. Moravec and M. Holeček, “Microstructure-dependent nonlinear viscoelasticity due to extracellular flow within cellular structures,” *International Journal of Solids and Structures*, vol. 47, 14-15 2010, ISSN: 00207683. DOI: 10.1016/j.ijsolstr.2010.03.024.
- [277] P. Germain, “The method of virtual power in continuum mechanics. part 2: Microstructure,” *SIAM Journal on Applied Mathematics*, vol. 25, 3 1973, ISSN: 0036-1399. DOI: 10.1137/0125053.
- [278] M. R. N. Fazita, K. Jayaraman, and D. Bhattacharyya, “Formability analysis of bamboo fabric reinforced poly (lactic) acid composites,” *Materials*, vol. 9, 7 2016, ISSN: 19961944. DOI: 10.3390/ma9070539.
- [279] D. J. Steigmann and F. dell’Isola, “Mechanical response of fabric sheets to three-dimensional bending, twisting, and stretching,” *Acta Mechanica Sinica/Lixue Xuebao*, vol. 31, pp. 373–382, 3 Jun. 2015, ISSN: 16143116. DOI: 10.1007/s10409-015-0413-x.
- [280] A. J. Spencer and K. P. Soldatos, “Finite deformations of fibre-reinforced elastic solids with fibre bending stiffness,” *International Journal of Non-Linear Mechanics*, vol. 42, 2 2007, ISSN: 00207462. DOI: 10.1016/j.ijnonlinmec.2007.02.015.
- [281] C. I. Kim, “Superposed incremental deformations of an elastic solid reinforced with fibers resistant to extension and flexure,” *Advances in Materials Science and Engineering*, vol. 2018, 2018, ISSN: 16878442. DOI: 10.1155/2018/6501985.
- [282] C. I. Kim, “Strain-gradient elasticity theory for the mechanics of fiber composites subjected to finite plane deformations: Comprehensive analysis,” *Multiscale Science and Engineering*, vol. 1, 2 2019, ISSN: 2524-4515. DOI: 10.1007/s42493-019-00015-3.
- [283] M. Zeidi and C. I. Kim, “Finite plane deformations of elastic solids reinforced with fibers resistant to flexure: Complete solution,” *Archive of Applied Mechanics*, vol. 88, 5 2018, ISSN: 14320681. DOI: 10.1007/s00419-018-1344-3.
- [284] M. Zeidi and C. I. Kim, “Mechanics of fiber composites with fibers resistant to extension and flexure,” *Mathematics and Mechanics of Solids*, vol. 24, 1 2019, ISSN: 17413028. DOI: 10.1177/1081286517728543.
- [285] M. Zeidi and C. I. Kim, “Mechanics of an elastic solid reinforced with bidirectional fiber in finite plane elastostatics: Complete analysis,” *Continuum Mechanics and Thermodynamics*, vol. 30, 3 2018, ISSN: 09351175. DOI: 10.1007/s00161-018-0623-0.

- [286] R. S. Rivlin, “Constitutive equation for a fiber-reinforced lamina,” in *IUTAM Symposium on Anisotropy, Inhomogeneity and Nonlinearity in Solid Mechanics*, D. F. Parker and A. H. England, Eds., Dordrecht: Springer Netherlands, 1995, pp. 379–384, ISBN: 978-94-015-8494-4.
- [287] A. J. M. A. J. M. Spencer, *Deformations of fibre-reinforced materials* (Oxford science research papers). Clarendon Press, 1972. [Online]. Available: <https://cir.nii.ac.jp/crid/1130282268887032192>.
- [288] A. J. Spencer and K. P. Soldatos, “Finite deformations of fibre-reinforced elastic solids with fibre bending stiffness,” *International Journal of Non-Linear Mechanics*, vol. 42, pp. 355–368, 2 Mar. 2007, ISSN: 00207462. DOI: 10.1016/j.ijnonlinmec.2007.02.015.
- [289] G. A. Holzapfel and R. W. Ogden, *Mechanics of biological tissue*. 2006. DOI: 10.1007/3-540-31184-X.
- [290] R Ogden, “Non-linear elastic deformations,” *Engineering Analysis with Boundary Elements*, vol. 1, 2 1984, ISSN: 09557997. DOI: 10.1016/0955-7997(84)90049-3.
- [291] D. J. Steigmann, “Invariants of the stretch tensors and their application to finite elasticity theory,” *Mathematics and Mechanics of Solids*, vol. 7, 4 2002, ISSN: 10812865. DOI: 10.1177/108128028481.
- [292] D. J. Steigmann, *Finite elasticity theory*. Oxford University Press, Dec. 2017, pp. 1–184, ISBN: 9780191746536. DOI: 10.1093/oso/9780198567783.001.0001.
- [293] R. A. Toupin, “Theories of elasticity with couple-stress,” *Archive for Rational Mechanics and Analysis*, vol. 17, 2 1964, ISSN: 00039527. DOI: 10.1007/BF00253050.
- [294] W. T. Koiter, “Couple stresses in the theory of elasticity, i and ii,” *Proceedings of the Koninklijke Nederlandse Akademie van Wetenschappen, Series B*, vol. 67, 1964.
- [295] R. D. Mindlin and H. F. Tiersten, “Effects of couple-stresses in linear elasticity,” *Archive for Rational Mechanics and Analysis*, vol. 11, 1 1962, ISSN: 00039527. DOI: 10.1007/BF00253946.
- [296] P. Germain, “The method of virtual power in continuum mechanics. part 2: Microstructure,” *SIAM Journal on Applied Mathematics*, vol. 25, pp. 556–575, 3 Nov. 1973, ISSN: 0036-1399. DOI: 10.1137/0125053.
- [297] D. J. Steigmann, “Mechanics and physics of lipid bilayers,” in 2018, vol. 577. DOI: 10.1007/978-3-319-56348-0_1.
- [298] D. J. Steigmann, “A model for lipid membranes with tilt and distension based on three-dimensional liquid crystal theory,” *International Journal of Non-Linear Mechanics*, vol. 56, 2013, ISSN: 00207462. DOI: 10.1016/j.ijnonlinmec.2013.02.006.

- [299] F. dell’Isola and D. Steigmann, “A two-dimensional gradient-elasticity theory for woven fabrics,” *Journal of Elasticity*, vol. 118, 1 2015, ISSN: 15732681. DOI: 10.1007/s10659-014-9478-1.
- [300] Y. C. Fung, “Structure and stress-strain relationship of soft tissues,” *Integrative and Comparative Biology*, vol. 24, 1 1984, ISSN: 15407063. DOI: 10.1093/icb/24.1.13.
- [301] M. Vatankehah-Varnosfaderani *et al.*, “Mimicking biological stress–strain behaviour with synthetic elastomers,” *Nature*, vol. 549, 7673 2017, ISSN: 14764687. DOI: 10.1038/nature23673.
- [302] F. dell’Isola and D. Steigmann, “A two-dimensional gradient-elasticity theory for woven fabrics,” *Journal of Elasticity*, vol. 118, 1 2015, ISSN: 15732681. DOI: 10.1007/s10659-014-9478-1.
- [303] I. Giorgio, R. Grygoruk, F. Dell’Isola, and D. J. Steigmann, “Pattern formation in the three-dimensional deformations of fibered sheets,” *Mechanics Research Communications*, vol. 69, 2015, ISSN: 00936413. DOI: 10.1016/j.mechrescom.2015.08.005.
- [304] I. Giorgio, A. D. Corte, F. dell’Isola, and D. J. Steigmann, “Buckling modes in pantographic lattices,” *Comptes Rendus - Mecanique*, vol. 344, 7 2016, ISSN: 16310721. DOI: 10.1016/j.crme.2016.02.009.
- [305] D. J. Steigmann, “Equilibrium of elastic lattice shells,” *Journal of Engineering Mathematics*, vol. 109, 1 2018, ISSN: 15732703. DOI: 10.1007/s10665-017-9905-y.
- [306] D. J. Steigmann, “Continuum theory for elastic sheets formed by inextensible crossed elasticae,” *International Journal of Non-Linear Mechanics*, vol. 106, 2018, ISSN: 00207462. DOI: 10.1016/j.ijnonlinmec.2018.03.012.
- [307] I. Giorgio, F. dell’Isola, and D. J. Steigmann, “Edge effects in hyper nets,” *Comptes Rendus - Mecanique*, vol. 347, 2 2019, ISSN: 16310721. DOI: 10.1016/j.crme.2019.01.003.
- [308] A. Agrawal and D. J. Steigmann, “Boundary-value problems in the theory of lipid membranes,” *Continuum Mechanics and Thermodynamics*, vol. 21, 1 2009, ISSN: 09351175. DOI: 10.1007/s00161-009-0102-8.